UNIVERSITAT POLITÈCNICA DE VALÈNCIA

Departamento de Máquinas y Motores Térmicos

Doctoral Thesis

Experimental study of oil coking problem and contribution to the modelling of heat transfer in turbochargers

---

Presented by: Ms. Yuly Tatiana Rodríguez Usaquén
Supervised by: Dr. Andrés Omar Tiseira Izaguirre

in fulfilment of the requisites for the degree of

Doctor of Philosophy

Valencia, January 2019

Ph.D. Thesis

Experimental study of oil coking problem and contribution to the modelling of heat transfer in turbochargers

AUTHORS

Presented by: Ms. Yuly Tatiana Rodríguez Usaquén
Supervised by: Dr. Andrés Omar Tiseira Izaguirre

PhD ASSESSORS

Dr. Ricardo Vinuesa Motilva
Dr. Sergio Lavagnoli
Dr. Francisco Vera García

DEFENSE COMMITTEE

Chairman: Dr. José Manuel Lujan Martinez
Secretary: Dr. Pedro Acisclo Rodriguez Aumente
Vocal: Dr. Ricardo Vinuesa Motilva

Valencia, January 2019

Experimental study of oil coking problem and contribution to the modelling of heat transfer in turbochargers

Yuly Tatiana Rodríguez Usaquén

Abstract

The automotive industry represents one of the most important sectors in the world. Given its socio-economic influence, research is aimed at reducing fuel consumption and emissions. Turbochargers provide several benefits including increased power for a given engine size, improved fuel economy and reduced emissions. The turbocharger is an important piece for the new generation of engines that must comply with the Euro 6 or in the U.S. Tier 3 vehicle emissions and fuel standard program. As more effort is made to increase efficiencies and reduce emissions, the complexity of the system increases. The high rotational speeds, pulsating flow conditions and high temperature differences between working fluids (exhaust gases, compressed air, lubricating oil, coolant fluids) make the turbo-charging a challenging task. Numerical simulation opens a range of possibilities to study the performance, efficiency and design of components in the turbocharger, but requires continued accuracy refinements.

In this thesis, a great effort has been made to improve the overall understanding of the different physical phenomena that occur inside the turbocharger. Both, experimental and modelling efforts have been made to understand the thermal behaviour of the turbocharger under engine start/stop conditions. After state-of-the-art review of thermal studies and heat transfer simulation codes, this work presents an extensive experimental testing campaign that includes a thermal characterization of the turbocharger in stationary and transient conditions. Subsequently, several turbochargers were measured to assess the consequences that degraded oils can generate in the bearing system during endurance tests of oil-coking.

To minimize the possibilities of coke formation, some theoretical studies were done. First, a 1D turbocharger model was used in GT-Power^{TM} for a detailed study of the temperature rise in the central housing during an engine hot-stop. The simulated cooling strategies aims to find an optimal in terms of minimizing extra energy consumption per K housing temperature reduction. After, a 2D radial model is proposed as improvement of an existing one-dimensional model developed at CMT - Universitat Politècnica de València. Aiming for a low computational cost, the radial model was developed to be compatible with fast one-dimensional engine simulations. Later, a detailed solution of heat fluxes was made by means of CFD using a 3D design of the turbocharger's central housing. The 3D model improved the results when temperature of the bearings/shaft is required. Additionally, thermal properties within the turbocharger can be obtained and therefore a reduction of the experimental tasks in the thermo-hydraulic test bench. Both 2D and 3D models were validated using experimental data, demonstrating predictive accuracy improvements on the results of previous models.

Resumen

La industria automotriz representa uno de los sectores más importantes del mundo. Dada su influencia socioeconómica, la investigación está destinada a reducir el consumo de combustible y las emisiones. Los turbocompresores ofrecen varios beneficios, entre ellos, mayor potencia para un tamaño de motor determinado, mejor economía de combustible y reducción de emisiones. El turbocompresor es una pieza importante para la nueva generación de motores que deben cumplir con la normativa Euro 6 o en el programa estándar de emisiones y combustible de los EE. UU. Tier 3. A medida que se hacen más esfuerzos para aumentar la eficiencia y reducir las emisiones, la complejidad del sistema aumenta. Las altas velocidades de rotación, las condiciones de flujo pulsante y las altas diferencias de temperatura entre los fluidos de trabajo (gases de escape, aire comprimido, aceite lubricante, fluidos refrigerantes) hacen que la turbocarga sea una tarea desafiante. La simulación numérica abre un rango de posibilidades para estudiar el rendimiento, la eficiencia y el diseño de los componentes en el turbocompresor, pero requiere continuos refinamientos de precisión. En esta tesis, se ha hecho un gran esfuerzo para mejorar la comprensión global de los diferentes fenómenos físicos que ocurren al interior del turbocompresor. Se han hecho esfuerzos experimentales y de modelado para comprender el comportamiento térmico del turbocompresor en condiciones de arranque/parada del motor. Luego de una revisión de los estudios térmicos y de los códigos de simulación de transferencia de calor, éste trabajo presenta una extensa campaña de pruebas experimentales que incluye una caracterización térmica del turbocompresor en condiciones estacionarias y transitorias. Posteriormente, se midieron varios turbocompresores para evaluar las consecuencias que los aceites degradados pueden generar en el sistema de rodamientos durante pruebas de resistencia de coque de aceite. Para minimizar las posibilidades de formación de coque, se realizaron algunos estudios teóricos. En primer lugar, se usó un modelo de turbocompresor 1D en GT-Power^{TM} para un estudio detallado del aumento de temperatura de la carcasa central del turbocompresor durante un paro en caliente del motor. Las estrategias de enfriamiento simuladas apuntan a encontrar un óptimo en términos de minimizae el consumo de energía extra por reducción de la temperatura de la carcasa en Kelvin. Posteriormente, se propone un modelo radial 2D como mejora de un modelo unidimensional existente desarrollado en la CMT - Universitat Politècnica de València. Con el objetivo de conseguir un bajo costo computacional, el modelo radial 2D se desarrolló para ser compatible con simulaciones unidimensionales rápidas de motor. Después, se realizó una solución detallada de los flujos de calor mediante CFD utilizando un diseño 3D de la carcasa central del turbocompresor. El modelo 3D mejora los resultados cuando se requiere la temperatura de los cojinetes/eje. Además, con ésta campaña de CFD se pueden obtener propiedades térmicas dentro del turbocompresor y, por lo tanto, una reducción de las tareas experimentales en el banco de pruebas termohidráulico.

Ambos modelos 2D y 3D fueron validados utilizando datos experimentales, demostrando mejoras de precisión de predicción sobre los resultados de modelos anteriores.

Resum

La indústria automotriu representa un dels sectors més importants del món. Donada la seua influència socioeconòmica, la investigació està destinada a reduir el consum de combustible i les emissions. Els turbocompressors oferixen diversos beneficis, entre ells, major potència per a una grandària de motor determinat, millor economia de combustible i reducció d'emissions. El turbocompressor és una peça important per a la nova generació de motors que han de complir amb la normativa Euro 6 o en el programa estàndard d'emissions i combustible dels EE. UU. Tier 3. A mesura que es fan més esforços per a augmentar l'eficiència i reduir les emissions, la complexitat del sistema augmenta. Les altes velocitats de rotació, les condicions de flux polsen-te i les altes diferències de temperatura entre els fluids de treball (gasos de fuga, aire comprimit, oli lubricant, fluids refrigerants) fan que la turbocarga siga una tasca desafiador. La simulació numèrica obri un rang de possibilitats per a estudiar el rendiment, l'eficiència i el disseny dels components en el turbocompressor, però requerix continus refinaments de precisión.

En aquesta tesi, s'ha fet un gran esforç per a millorar la comprensió global dels diferents fenòmens físics que ocorren a l'interior del turbocompressor. S'han fet esforços experimentals i de modelatge per a comprendre el comportament tèrmic del turbocompressor en condicions d'arranque/parada del motor. Després d'una revisió dels estudis tèrmics i dels codis de simulació de transferència de calor, este treball presenta una extensa campanya de proves experimentals que inclou una caracterització tèrmica del turbocompressor en condicions estacionàries i transitòries. Posteriorment, es van mesurar uns quants turbocompressors per a avaluar les conseqüències que els olis degradats poden generar en el sistema de rodaments durant proves de resistència de coc d'aceite.

Per a minimitzar les possibilitats de formació de coc, es van realitzar alguns estudis teòrics. En primer lloc, es va usar un model de turbocompressor 1D en GT- Power ^{TM} per a un estudi detallat de l'augment de temperatura de la carcassa central del turbocompressor durant una desocupació en calent del motor. Les estratègies de refredament simulades apunten a trobar un òptim en termes de minimizae el consum d'energia extra per reducció de la temperatura de la carcassa en Kelvin. Posteriorment, es proposa un model radial 2D com a millora d'un model unidimensional existent desenrotllat en la CMT - Universitat Politècnica de València. Amb l'objectiu d'aconseguir un baix cost computacional, el model radial 2D es va desenrotllar per a ser compatible amb simulacions unidimensionals ràpides de motor. Después, es va realitzar una solució detallada dels fluxos de calor per mitjà de CFD utilitzant un disseny 3D de la carcassa central del turbocompressor. El model 3D millora els resultats quan es requerix la temperatura dels cojinetes/eje. A més, amb esta campanya de CFD es poden obtindre propietats tèrmiques dins del turbocompressor i, per tant, una reducció de les tasques experimentals en el banc de proves termohidráulico.

Ambdós models 2D i 3D van ser validats utilitzant dades experimentals, demostrant millores de precisió de predicció sobre els resultats de models anteriores.

List of publications

The following papers are the basis of this thesis and have been published as follows:

- "Fast 2-D Heat Transfer Model for Computing Internal Temperatures in Automotive Turbochargers" by Serrano, Tiseira, García-Cuevas, Rodriguez Usaquen, and Mijotte [1].
- "Adaptation of a 1-D tool to study transient thermal in turbocharger bearing housing" by Serrano, Tiseira, García-Cuevas, and Rodríguez Usaquen [2].
- "A methodology to study oil-coking problem in small turbochargers" by Serrano, Tiseira, García-Cuevas, Rodriguez Usaquen, and Mijotte [3].
- "Fast 3-D heat transfer model for computing internal temperatures in the bearing housing of automotive turbochargers" by Gil, García-Cuevas, Tiseira, and Rodriguez Usaquen [4].

Division of work between authors

These publications have been produced in collaboration with other researchers, being the author signatures in order of seniority. The author of this Thesis helped with the experimental measurements, performed results post-processing and developed the models presented here. Methodologies and results discussions were conducted in collaboration with Prof. Serrano, as well as with the rest of co-authors.

A mi familia,
con amor.

Don't find fault, find a remedy.
- Henry Ford

Acknowledgements

First of all, I want to thank to the whole CMT-Motores Térmicos team for giving me the opportunity of being part of it and to “Apoyo para la investigación y Desarrollo (PAID)” grant for doctoral studies (FPI-2016-S2-1354). I extend a sincere acknowledgement to Polytechnic University of Valencia, human resources and all staff that have contributed to the successful completion of my research.

I would like to thank those fellow graduate students who have successfully obtained their PhD title during these years, specially Lucia Royo, Luis Miguel García-Cuevas and Artem Dombrowsky. Also, my special acknowledgements are for Guillermo Miró, Vicente Boronat and Alex Hernandez for their contribution in the experimental process and their patience with the testing demands.

My sincere gratitude to professor Jose Ramón Serrano, who has done all the best to guide the project used for the realization of my thesis. I also express gratitude to my thesis supervisor, professor Andres Tiseira for the guidance throughout these years.

I would like to thank people from BMW group Steyr - Austria; Mr. Dworschak, Giulio Bertulin and all the simulation team ZM-E-23 that did everything possible for me to have such an excellent experience. I was very fortunate to work in such experienced and knowledgeable team.

Besides, I feel emotionally in debt with Carlos Brocal for being the best support for me, being away from home. In addition, I want to thank my friends who have given me their unconditional friendship during these years; specially Darling Trujillo, Cata Ortiz, Sol Rodriguez, Andrés Aguillón, Nati Acosta, Oferman González and all wonderful people who have added a part in one way or another in the development of this thesis.

Finally, I would like to thank my parents, my brother and Andrzej for their support and encouragement throughout this experience. Thank you all for the love and patience through these years of hard work, for the advices which motivated me and gave me strength to conclude with this Thesis.

Contents

List of Figures

List of Tables

Nomenclature

$\dot{W}$	Power [kW]
$\dot{m}$	Mass flow rate [kg/s]
A	Area [m^2]
A_G	Geometric Area [m^2]
C	Heat capacity [J/K]
c	Massive heat capacitance [J/kgK]
C_p	Specific heat [J/kgK]
D_C	Discharge Coefficient
$e_{axialload}$	Axial load
$e_{radialbearing}$	Constant for the radial bearing effect
$e_{thrustbearing}$	Constant for the thrust bearing effect
F	Form factor [-]
g	Gravity [m/s^2]
G_r	Grashof number
h	Convective heat transfer coefficient
I	Identity Matrix
K	Conductance term, conductance matrix
k	Fluid conductivity
L	Length [m]
M	Conductance terms submatrix
N	Rotational speed [rpm]
N_u	Nusselt number
P	Power [kW]
P_r	Prandtl number
Q	Heat flux [W/m^2]
r	Radius
R_a	Rayleigh number
R_e	Reynolds number
T	Temperature [°C]
t	Specific time [s]
t_f	Time where maximum temperature in the central node is reached [s]
t_i	Time when engine stops [s]
t_n	Time step [s]
V	Volume
y	Heat flux fraction

ACEA European Automobile Manufacturers Association

API American Petroleum Institute

ASTM American Society for Testing and Materials

BH Bearing Housing

C Compressor side

CAD Computer Aided Design

CFD Computational Fluid Dynamic

CHT Computational Heat Transfer

CMT Centro de Motores Termicos

CO2 Carbon Dioxide

D Diameter

DI Direct Injection

E Engine

ECU Electronic Control Unit

EGR Exhaust Gas Recirculation

FEM Finite Element Method

FL Full Load

FN Normal Force

FRB Floating Ring Bearing

FTIR Fourier Transform Infrared Spectroscopy

H1 Turbine backplate node

H2 Central housing node

H3 Compressor backplate node

H4 Internal metal node close to the turbine backplate

H5 Internal metal node at the center of the central housing

H6 Internal metal node close to the compressor backplate

H7 Bearing node close to the turbine backplate

H8 Bearing node at the center of the central housing

H9 Bearing node close to the compressor backplate

HTHS High Temperature High Shear

HTM Heat Transfer Model

IC Internal Combustion

ILSAC International Lubricants Standardization and Approval Committee

IT Inlet Turbine

KV Kinematic Viscosity

L Distance between nodes [m]

NOx Nitrogen Oxides

O1 Oil node, before the shaft

O2 Oil node, after friction losses

O3 Oil node, before the last heat flux term

Obox Oil mean temperature between nodes

OD	Outlet Diffusor
OEM	Original Equipment Manufacturer
OI	Oil Inlet
OO	Oil Outlet
OP	Operating Point
OT	Outlet Turbine
PAO	Polyalphaolefin Oils
PMEP	Pumping Mean Effective Pressure
PS	Power Shaft
PXI	PCI eXtensions for Instrumentation
S1	Shaft node, turbine side
S2	Shaft node, central
S3	Shaft node, compressor side
SAE	Society of Automotive Engineers
SFC	Specific Fuel Consumption
SMA	Semi-Major Axis
ST	Steady
T	Turbine side
TAN	Total Acid Number
TBN	Total Base Number
TEOST	Thermo-oxidation Engine Oil Simulation Test
THD	Thermohydrodynamic Analysis
TIT	Turbine Inlet Temperature
TR	Transient
VGT	Variable Geometry Turbocharger
VNT	Variable Nozzle Turbine

Greek Symbols

β	Coefficient of thermal expansion
Δ	Increment
ϵ	Eccentricity
η	Efficiency
Λ	Axial force [N]
λ	Thermal conductivity [W/mK]
μ	Dynamic viscosity [Pa s]
ν	Kinematic viscosity [m^2/s]
Ω	Power [kW]
ϕ	Power factor
ρ	Density [kg/m^3]

Subscripts

∞	fluid
$axial$	Axial
bc	Temperature boundary condition
C	Compressor
$c,size$	Coolant pump size
$Cond$	Conduction
$Conv$	Convection

Cs	Compressor isentropic
e	External radius
i	Internal radius
iC	Inlet Compressor
ij	Interaction between two adjacent nodes
iT	Inlet Turbine
$mech$	Mechanical
$o,size$	Oil pump size
oC	Outlet Compressor
oil	Oil
oT	Outlet Turbine
p	Constant pressure
Rad	Radiation
S	Shaft
s	Surface
st	Steady
T	Turbine
Ts	Turbine isentropic
$wallturb$	Wall turbine
x	Unknown temperature

CHAPTER 1

Introduction

Contents

Figures

1.1 Background

Only to consider the history of the turbocharger as a machine to boost pressure in the cylinders of an automotive engine, an important implementation occurs in 1952 when a petrol engine with turbocharger was used for the first time to compete in the 500 miles of Indianapolis. The first commercial automobile in production equipped with a turbocharged engine was the Oldsmobile Cutlass Jet fire of 1962 that mounted a turbo Garrett TO-3 coupled to a V8 petrol engine.

The reliability problems of supercharged engine vehicles, made their use restricted for years to the competition. In Formula 1, they reached their maximum development. This ERA is known as the "ERA of Turbo". It started with Renault in 1977 with a small V6 engine of 1500cc that yielded a production of more than 1000 hp. The evolution of these engines during this time allowed supercharged engines to reach the sales catalogues of all manufacturers as robust and high performance vehicles. The improvement in productive processes and materials, as well as the advances in research, have allowed beginning to join auto-ignited internal combustion engines with turbochargers in light vehicles.

Nowadays, the objective of the industry is defined by the concept of eco-cars. Vehicle manufacturers add energy-efficient technologies such as turbochargers to their products to meet increasingly stringent emission standards for light-duty vehicles. Using a smaller, turbocharged engine can lower fuel consumption by 2 to 6% [5]. Consequently, money is saved and the impact on the environment is reduced.

Turbochargers boost the power of smaller engines. However, in a highly compacted engine the heat transmission is an important point to consider due to high temperatures reached between the compressor (admission) and the turbine (manifold) on a very short length as shown in Figure 1.1.

Turbo-charging system always works with a large temperature gradient due to the high gas exhaust temperature regardless of the type of fuel [6, 7]. Diesel, natural gas and petrol engines generate high temperatures in the turbocharger inlet turbine. On the compressor side, the pressure and the inlet temperature are at ambient conditions. Therefore, the thermal load can be very important between each component. Unfortunately, this difference can damage the turbocharger as result of heat concentrations in certain parts of the turbocharger [8]. In addition, the temperature change caused by a sudden load change from accelerating at full load to zero and back to full load causes temperature changes of several hundred degrees within seconds on the turbocharger exhaust side leading to high thermal stress and eventually fatigue.

Severe and transient working conditions worsen wear in the turbocharger. Strategies such as start/stop are an easy and low-cost solution for fuel saving however, this action can damage the performance of the turbocharger system due to the shut-down of the lubrication and cooling systems.

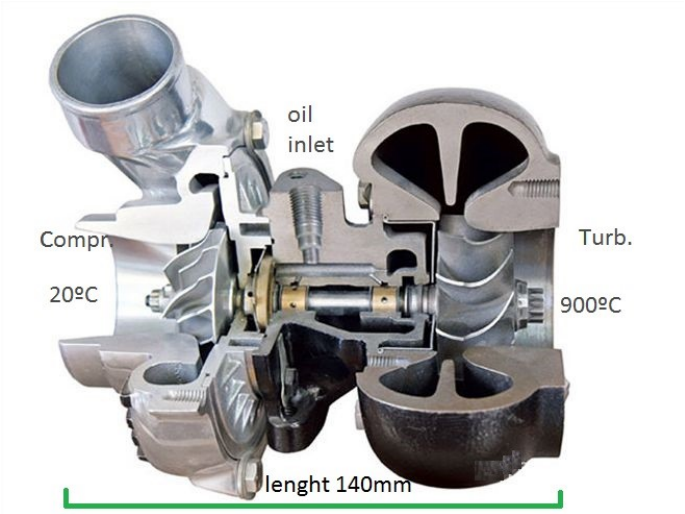

Figure 1.1: Turbocharger compressor, turbine and central housing

The cooling and lubrication circuits, as well as the clamping components, the bearings and the shaft are located in the central housing of the turbocharger. The turbocharger rotates at speeds of up to 250,000 rpm and the lubrication system is used to keep the bearings and shaft in operation, avoiding metal-to-metal contact. The oil film inside serves as a shock absorber to help stabilize the turbine wheel assembly, compressor wheel and shaft. This lubrication is done thanks to the engine oil circulation. The lubrication system has a pressurized inlet orifice and an ambient-pressure outlet. The oil working temperature is usually 90 ºC. If the supercharging system is at a high working temperature, it is necessary to cool down. When the engine stops, the lubrication and cooling systems stop. This action makes it impossible to evacuate the heat. Therefore, the heat through the metal of central housing increases the temperature of the oil trapped in the turbocharger that can lead to the oil degradation or generation of oil coking (solid residue created when oil undergoes severe oxidative and thermal breakdown at extreme engine temperatures).

The lubrication system is very important to preserve the turbocharger's operation. A lubricant in service is subjected to a wide range of work that can degrade the oil base and additives [9, 10, 11]. Heat, air, incompatible gasses, humidity, internal or external contamination, combustion processes, the radiation and the unnoticed mixture with a different fluid influence such factors. For instance, after engine stops it may happen that the by-products of the combustion, which are deposited in the lubricant act as corrosive agents when combined with the water that condenses on the walls due to a low temperature during the immediate start-up.

The thermal damage to the turbocharger may be noticeable after it has occurred. If the thermal load of the oil is too large, the oil may degrade and produce coke. Deposits of oil coking cause an obstruction of the lubrication lines and bearings thus reducing the oil flow [12]. This reduction in the flow leads to a loss of bearing load capacity and cooling performance.

The lubrication system has been defined as a system that dissipates heat and lubricates the important components of the turbocharger. Therefore, it must always be in good operating condition to preserve the life of the turbocharger and prevent breakages [13]. Any type of problem with the lubrication system can cause an irreversible problem in the machine. These types of problems are impossible to repair.

Currently, engine manufacturers allocate a lot of effort to make improvements in areas that were taken of lesser importance, such as heat transfer and thermal damage caused by severe operating conditions. Improvements in the turbocharger play a key role in future engine developments.

1.2 Motivation

The evolution of diesel engines has highlighted the fragility of the turbo-charging system and the attention that should be paid to the lubrication system. Nowadays, engineers work to adapt an improvement to the bearings [14, 15], to the materials used in the turbine and central housing [16, 17, 18], as well to carry out systematic studies of the heat transfer processes in the turbochargers.

Although it is known that heat transmission varies depending on the geometrical characteristics of each turbocharger, useful tools are needed to help studying thermal processes. The best geometry is determined in the design process according to the working temperatures of each of the turbochargers.

Some experimental and modelling studies are based on turbocharger heat transfer processes. Thermal studies with experimental tools are made with turbochargers of a size that allow easily to introduce temperature sensors. This type of turbochargers are used in the aeronautical or naval industry. However, in the case of automotive engines the turbochargers are small and the temperature gradients are significant, especially on the turbine side. The importance of thermal control knowledge can prevent a destructive impact on rotating components, such as the shaft, bearings and wheels of the turbine and compressor.

Strategies for low consumption and pollution reduction may deteriorate systems, such as the turbocharger. Consequently, it is important to study any type of situation that leads to the risk of oil deterioration at different points of engine operation. Currently there are few studies of oil coking applied directly in turbochargers.

Studies of oil properties in laboratories and correlations with the engine components can be found. However, the determination of consequences of contaminated oils have directly on the performance of the engine and the supercharging is a process that needs to be studied in detail. Any problem in the oil supply or in its characteristics is harmful to the turbocharger bearing and shaft balance and should be avoided.

On the other hand, engineers need tools that ensure their designs will work well on the first prototype. Hence, contribution of predictive models in the turbocharger is imperative due to the cost that experimental studies require. Heat transfer, mechanical losses and non-steady behaviour were corrected with relative ease in the past, but today turbochargers and engines are becoming smaller and these effects are increasingly important. This is where multi-physics and high-fidelity simulations are beneficial[19, 20].

Notable modelling efforts have been made to obtain greater accuracy while maintaining low computational cost, with very smart approaches for heat transfer, mechanical losses and unsteady performance modelling. Nevertheless, simulation models are needed to calculate the thermal evolution of the components when new strategies such as start/stop are used. Calculation problems are found in simulation models when the engine speed is reduced to zero.

1.3 Objectives

The main objective of this thesis is to contribute to a better knowledge of heat transmission, internal temperature gradients and its relation with the oil degradation and coke formation for turbochargers used in automotive engines of up to 2 litters. This main objective can be divided into two aspects: The experimental evaluation of oil coking and theoretical modelling of heat transfer.

In order to understand and evaluate the damage due to oil coking inside the turbocharger during engine start/stops is necessary to comply with the following principles:

- To perform an experimental characterization of the temperature gradients in the turbocharger.
- To make an initial analysis on fresh oil to define the reference baseline.
- To evaluate the designs of turbine housings to see the thermal impact over the central housing and bearing system.
- To provide a criterion to quantify the coking level at the end of an endurance test.

- To analyse the effect of oil coking on selected key parameters by means of experiments on engine test bench.
- To study the influence that engine operating points, oil soot content, oil oxidation have on the performance of the turbocharger and the engine.

A constant evolution of the current numerical methods is necessary since the level of refinement of the engine is constantly increasing. In this thesis, the theoretical objectives are based on:

- To improve an existing 1D simulation tool developed in the CMT department for heat transfer evaluation in the turbocharger.

Although the existing 1D model produces good results when computing the turbine outlet temperature, this model focuses on the axial heat transfer paths and lack the capability of producing detailed results about the internal thermal behaviour of the turbocharger. The new mathematical model must be able to predict the internal temperatures of the turbocharger for steady and transient conditions. Within this objective, an experimental process must be linked to the model. The experimental study contemplates the adaptation of embedded thermocouples inside the turbocharger to validate the model at different parts of the machine (compressor, central housing, turbine, shaft and bearings).

1.4 Methodology

The methodology used in this work has been firstly focused on the literature review of heat transmission in automotive turbochargers and is shown in Chapter 2. This chapter includes experimental thermal studies and mathematical models developed to compute heat transfer in the turbocharger or its components. In addition, a review of oil tribology in IC engines and lubrication in the turbocharger is presented.

Chapter 3 has been dedicated to the experimental campaigns performed in turbochargers. A detailed methodology has been developed to analyze oil-coking influence in turbocharger during engine start/stops. Two main tasks are performed:

- A thermal characterization is performed to define the maximum level of temperature in different parts of the bearing system. This thermal characterization serves as baseline reference for the endurance tests of oil coking. The calibration of engine speed, fuel consumption and engine cycle conditions before to start endurance tests are obtained in this part. A complementary study using a thermal decoupled turbine housing is

carried out during the thermal characterization. These thermal decoupled tests allow to evaluate the effects that the turbine volute has with the temperatures in turbocharger's central housing.

- Several endurance tests of oil coking are carried out using two different multi-grade aged oils. In total fourteen turbochargers are measured using these contaminated oils. An engine-independent lubrication system is used for this purpose to better control of lubrication and oil properties, independently of the engine oil pump. The conditions of lubrication are representative in terms of pressure, temperature and flow rate. The treatment of the instantaneous measured variables from their acquisition, post-processing and analysis is presented.

Chapter 4 focuses on the study of heat transfer through simulations with an existing 1D-model of turbocharger and the cross-analysis of experimental results of oil coking. First, several combinations of cooling strategies in order to find the optimum one in terms of minimizing extra energy consumption per K of housing temperature reduction are simulated. These simulations are highly valuable to study the temperature rise of the central housing of an automotive turbocharger after a hot-stop process. Subsequently, a cross-analysis of different techniques used to quantify the effect that the engine operating point, the soot content and the oil oxidation level have on the performance of the turbocharger and the robustness of the machine is presented. The correlations found between the techniques used are shown.

Chapter 5 presents a study of the thermal characteristics in turbochargers by means of a radial and 3D heat transfer models. The proposed models have been developed using VBA interface and commercial code ANSYS CFX respectively. The calibration and validation for both models are presented in the last section of this chapter. The results of the models can be used to study heat exchanges inside the turbocharger and the effects on its performance under engine start/stop conditions. An improvement in the temperature prediction of the previous 1D heat transfer model is achieved.

Chapter 6 summarizes the main findings and contributions of this Ph.D. dissertation, presenting the main conclusions obtained at experimental and modelling level as well as recommendations for improvements and future work.

1.5 References

[5] National Research Council (U.S.) *Assessment of fuel economy technologies for light-duty vehicles*. Ed. by C. on the Assessment of Technologies for Improving Light-Duty Vehicle Fuel Economy. National Academies Press, 2011, p. 217. ISBN: 9780309156073 (cit. on p. 2).

[6] V. Simon, G. Oberholz, and M. Mayer. "Exhaust gas temperature 1050 ° C An engineering challenge". In: *BorgWarner TurboSystems Academy* (2000), pp. 1–12 (cit. on pp. 2, 112, 125).

[7] K. Matsumoto, Y. Jinnai, M. Tojo, N. Hayashi, and S. Ibaraki. *Development of Compact and High-performance Turbocharger for 1050°C Exhaust Gas*. Tech. rep. September. Mitsubishi Heavy Industries, Ltd. Technical Review, 2008, pp. 1–5 (cit. on pp. 2, 23).

[8] M. Comerais, P. Chesse, and J.-F. Hetet. "Turbocharger Heat Transfer Modeling Under Steady and Transient Conditions". In: *International Journal of Thermodynamics* 12.4 (2009), pp. 193–202. URL: http://dergipark.ulakbim.gov.tr/eoguijt/article/view/1034000257/1034000237 (cit. on pp. 2, 17, 19, 21).

[9] J. Addison and W. Needelman. "Diesel Engine Lubricant Contamination and Wear". In: *Pall Corporation Engwear* (1986), p. 12 (cit. on p. 3).

[10] M. Stark, J. Wilkinson, P. Lee, J. Lindsay Smith, R. Taylor, and S. Chung. "The Degradation of Lubricants in Gasoline Engines: Lubricant Flow and Degradation in the Piston Assembly". In: *Tribology and Interface Engineering Series* 48 (2005), pp. 779–786. ISSN: 1572-3364. DOI: 10.1016/S0167-8922(05)80079-3. URL: https://www.sciencedirect.com/science/article/pii/S0167892205800793 (cit. on p. 3).

[11] M. J. Plumley, V. Wong, and T. Martins. "Oil Degradation in a Diesel Engine with Dual-Loop Lubricating System". In: *Tribology Transactions* 61.4 (2018), pp. 596–603. ISSN: 1040-2004. DOI: 10.1080/10402004.2017.1378396. URL: https://www.tandfonline.com/doi/full/10.1080/10402004.2017.1378396 (cit. on p. 3).

[12] T. W. Selby. "Turbocharger Deposits and Engine Deposits – A Duality : Correlative Bench Test Studies of Turbocharger Deposits Shut-down". In: *TAE Esslingen Conference* (2010), pp. 1–12 (cit. on p. 4).

[13] J Galindo, J. R. Serrano, V Dolz, and M. A. Lopez. "Behavior of an IC Engine Turbocharger in Critical Condition of Lubrication". In: *SAE International Journal Engines* 6.2 (2013), pp. 797–805. ISSN: 19463936. DOI: 10.4271/2013-01-0921 (cit. on pp. 4, 14, 38).

[14] C. Mitchell, C. Schaefer, O. Graf-Goller, P. Solfrank, and M. Scheidt. “Rolling Bearings in Turbochargers A Real Bargain with Regard to CO2 Emissions”. In: *10th Schaeffler Symposium - Solving the Powertrain Puzzle*. USA: Schaeffler Technologies AG & Co. KG, 2014, pp. 1–10 (cit. on p. 4).

[15] D. Zeppei, S. Koch, and A. Rohi. “Ball Bearing Technology for Passenger Car Turbochargers”. In: *Motortechnische Zeitschrift - Springer* 77.11/2016 (2016), pp. 26–31 (cit. on pp. 4, 29, 164).

[16] M Burkinshaw and D Blacker. *The high temperature tribological performance of turbocharger wastegate materials*. Tech. rep. 2014, pp. 289–298. DOI: 10.1016/B978-0-081000-33-5.50024-X. URL: https://ac.els-cdn.com/B978008100033550024X/3-s2.0-B978008100033550024X-main.pdf?{_}tid=1fea6f38-770e-48f5-91f1-0b794611d337{\&}acdnat=1537525468{_}9d68c108414b330d1f43f88a121f9ffc (cit. on p. 4).

[17] F. Zhang, Q. Zhu, D. Li, Y. He, and X. Xu. “Semi-solid moulding technology in making automotive turbocharge compressor wheels”. In: *International Journal of Computational Materials Science and Surface Engineering* 6.3/4 (2016), p. 204. ISSN: 1753-3465. DOI: 10.1504/IJCMSSE.2016.081684. URL: http://www.inderscience.com/link.php?id=81684 (cit. on p. 4).

[18] A. Chinchilla, M. Burkinshaw, M. Lindsay, D. Proprentner, and B. Shollock. *The tribological performance of coated and non-coated materials in high temperature environments*. Tech. rep. 2018 (cit. on p. 4).

[19] M. Schmitt, C. E. Frouzakis Tomboulides, G. Ananias, Y. M. Wright, and K. Boulouchos. “Direct numerical simulation of multiple cycles in a valve/piston assembly”. In: *Physics of Fluids* 26.3 (2014). ISSN: 10897666. DOI: 10.1063/1.4868279 (cit. on p. 5).

[20] R. Vinuesa, P. S. Negi, M. Atzori, A. Hanifi, D. S. Henningson, and P. Schlatter. “Turbulent boundary layers around wing sections up to Rec=1,000,000”. In: *International Journal of Heat and Fluid Flow* 72.April (2018), pp. 86–99. ISSN: 0142727X. DOI: 10.1016/j.ijheatfluidflow.2018.04.017 (cit. on p. 5).

CHAPTER 2

Literature review

Contents

Figures

2.1 Current status of the turbocharger

THE automotive industry represents one of the most important sectors at global level. Given its socio-economic influence, research is aimed at reducing fuel consumption and emissions [21, 22, 23]. Development of techniques are carried out to improve the behaviour of each engine component.

Turbochargers provide several benefits including increased power for a given engine size, improved fuel economy and reduced emissions [24]. The Engine Segment has benefited from the growth in turbocharger demand around the world for both combustion and hybrid propulsion systems [25, 26]. The turbocharger is an important piece for the new generation of engines that must comply with Euro 6 standard [27] or in U.S. the Tier 3 Vehicle Emissions [28] and Fuel Standard Program [29].

The growing demand for products from original equipment manufacturers to offer light and low-power vehicles in addition to strict CO_2 emission regulations results in a high production of turbochargers. According to the classification by type of technology, Variable Geometry Turbochargers (VGT) are expected to grow rapidly and exhibit more than 8% of compound annual growth rate from 2017 to 2024 (Figure 2.1) [30]. These turbochargers are responsible for precise control of NOx and particulate emissions [31]. The increase in engine efficiency, reduction in lag time and cost effectiveness compared to counterparts makes it more attributable to growth.

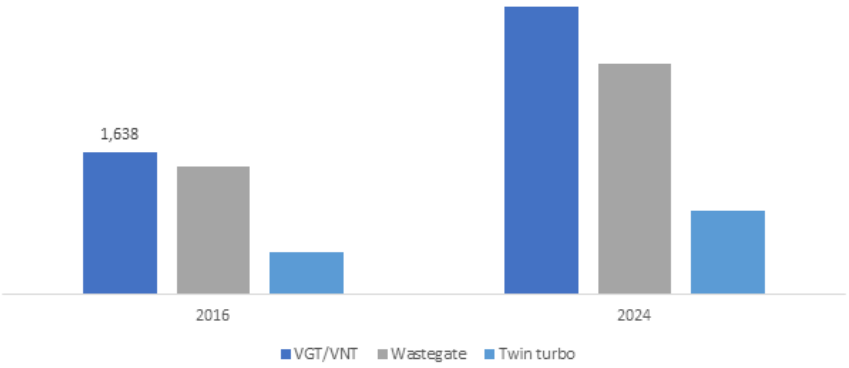

Figure 2.1: U.S. Automotive Turbocharger Market, By System, 2016 & 2024, (Thousand Units) [30]

As more effort is put into taking higher efficiencies and lower emissions [32], the role of the turbocharger becomes more and more important, increasing the

complexity of the system. As an example, two stage turbo-charging systems are used in more applications, to improve the trade-off between emissions and fuel consumption [33]. In literature, several studies about turbocharger endurance and loss of efficiency have been found. Serrano et al., study the robustness in various turbochargers with ingestion of different elements such as screws, sand or water on the compressor [34]. More over the behaviour of different parts of the turbocharger affecting its final performance is studied in detail, such as mechanical efficiency [35], computation of power friction losses due to journal bearing [36], and the examination of mechanical pre-load and bearing clearance to improve the rotor dynamic performance [37].

The requirements of customers have imposed a roadmap for turbochargers development that has resulted in a significant increase in thermal stability and more interest in the heat transfer phenomena. Thermal stability and the bearing system are basic requirements of the turbo-charging system and of the entire engine. Galindo et al. [13], studied the mechanical behaviour of turbochargers with intermittent stops of the lubricating oil flow, Polichronis et al., studied the whirl and frictional characteristics in floating ring bearings and ball bearings caused by vibrational modes and oil film instabilities[38], Bloch contributed widely to the research on faults in the bearings [39, 40] that affect the ability to withstand high temperatures.

Currently, new strategies are being studied such as start-stop systems that lead to mechanical failures of the bearing system, causing breakage of the lubrication film that leads to metal contact with the metal and degradation of the turbocharger. All these studies are leading to a significant improvement in the research activities as part of the engine-turbocharger development.

2.2 Experimental thermal studies in turbochargers

Thermal management becomes increasingly important for the required engine performance. Experimental measurements of heat transfer in turbochargers are necessary to generate data validation that help to characterize the turbocharger, improve mathematical models and correct turbine and compressor maps to have a better engine-turbocharger match. The measures are usually carried out under hot or cold test conditions. Hot measurements are the standard practice for turbocharger manufacturers to generate performance maps (diabatic maps) that include heat transfer and mechanical losses while cold measurements enable to resemble the adiabatic nature of the turbocharger decoupling the heat transfer from the mechanical losses [41]. Figure 2.2 shows a summary of experimental measurements for evaluation and assessment of heat transfer within the turbocharger.

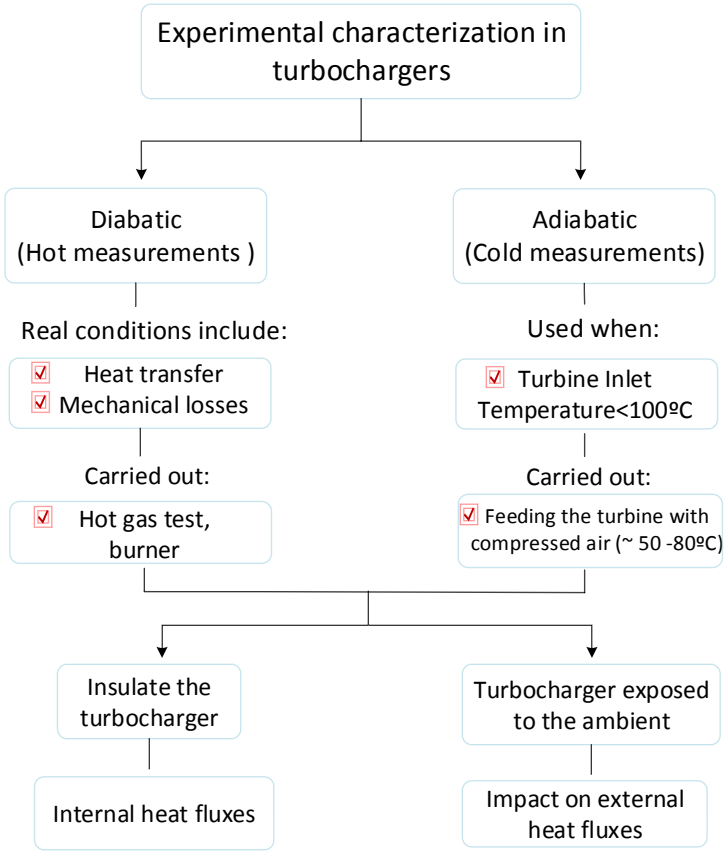

Figure 2.2: Experimental measurements for turbocharger characterization

Hot or cold measurements can be carried out in turbochargers isolated or exposed to the ambient conditions. For thermal characterization, it will depend on whether to analyse if internal or external heat fluxes.
Independent from the type of testing being conducted, instantaneous parameters are measured at different locations upstream and downstream of the turbine, compressor and in the oil. Common monitoring parameters for turbocharger performance are the mass flow rate of exhaust gas, air and oil, the inlet and outlet temperatures of the compressor and turbine side, the pressure in the oil, the pressure in both, compressor and turbine side, and the rotational speed [42, 43].

For any proposed problem, the desired result is always the implementation in the real world, therefore, experimental validation though expensive, is essential. Most thermal design and analysis codes need data for validation; but often the available data fall outside the range of actual engine operating conditions leading the need to interpolate and extrapolate disproportionately.

Szymko et al. [44] contribute to this area by providing extensive experimental data in a large range conditions of the turbine performance under pulsating flow. Jung et al. [45] conducted experimental tests in VGT turbochargers to determine the impact of heat transfer on performance maps for low and medium speed-load points typically excluded by turbocharger manufacturers. From the results, significant changes in the efficiency are visible at low speed conditions due to the increased compressor outlet temperature which leads to an important drop in performance. Experimental methodologies for the study of thermal behaviour of turbocharger in the compressor are proposed by Comerais et al. [46] demonstrating that the heat transfer from the turbine to the compressor has great influence on the compressor performances that need to take into account when the performance maps are used.

Different experimental studies have been carried out focusing on quantifying the effects of heat transfer on constant gas flow test rigs. Based on changes in temperature at the turbine inlet, results from Serrano et al [47] show that an appreciable deterioration of compressor efficiency due to a positive air mass flow rate is presented in low rotation speed ranges and high turbine inlet temperatures. Romagnoli et al.[48] show that the difference with the adiabatic conditions is considerable, especially at low compressor power. Chesse et al. [49] showed that the error in predicting the compressor power reaches 48% when heat transfer is excluded. Additional studies show that under adiabatic conditions the efficiency of the turbine differs considerably from the diabatic conditions particularly to a low pressure ratio of the turbine [50].

To fully understand the turbocharger operating range, it cannot be considered adiabatic and heat transfer effects have to be included [51, 52]. Further methods to characterize the turbocharger under steady and transient conditions are also proposed by Comerais et al. [8]. The data obtained and optimization methods applied were used to improve heat transfer prediction under steady state at diabatic and non-insulated conditions. Other experimental tests to characterize the complex heat transfer phenomena in the turbocharger body at different engine operating conditions are analysed by Shaaban et al. [53] showing that thermal energy is transferred to the compressor in all cases investigated and that the turbine is the most affected parameter followed by the engine volumetric efficiency. Romagnoli et al. [54] assess the impact of the engine on the temperature distribution in the compressor and turbine under diabatic conditions and from the study, a correlation that relates the compressor outlet temperature with the exhaust gas temperature is proposed.

Tanda et al.[55] explain that the increase of compressor power absorption with mass flow rate leads to a general reduction of heat transfer effects on the compressor efficiency. Basically, it is important that performance maps include any heat transfer that affects the experiments, otherwise there will be errors in the characterization of the turbocharger. Recently, correction models to improve the accuracy of performance turbine and compressor maps are proposed [56, 57].

The turbocharger accomplishes two things. It fills the cylinder bore with more air, and it causes turbulence in the cylinder. This latter effect greatly improves combustion. Thus, a turbocharger makes a diesel more powerful, lets it run cleaner, and gives it the potential to use less fuel.

Experimental procedures have been carried out to characterize thermal properties in the turbocharger. For example, Serrano et al. [58] use an array of thermocouples placed on five different external planes in the turbocharger and use a special thermohydraulic test rig to obtain conductive conductances. From this study, a proposed methodology to correct mechanical efficiency is implemented. Refined and tested methods are implemented in [59, 60, 61], including the external heat flow.

The evaluation of the different heat transfer conditions for the external surface of the turbocharger considering various speeds and loads of the engine is studied by Aghaali et al. [62]. The results show that changing convective heat transfer condition around the turbocharger affects the heat fluxes more noticeably than changing the radiation and conduction; although the heat transfer between the turbine and the bearing housing has not been measured, the authors conclude that internal heat transfer from the turbine to the bearing housing and from the bearing housing to the compressor are significant.

The high temperature of the turbocharger presents a challenge for the bearing system [63]. Recently, experimental tests have been conducted on gasoline engines to predict the consequences that lubricants can generate in the bearing system during severe hot stops [64]. Also, the thermodynamic effects are studied in the start-stop of the engine, where undesirable conditions for the operation of the bearings occur. It is known that if the engine shuts off immediately after a high power, the turbine and the turbine housing temperature rise to its upper limits, suddenly all the gas flow through the turbine stops and all the oil flowing through the central housing stops. This conditions produce damage due to overheating [38] or thermal stress that can settle in the form of coke or varnish in the turbocharger rotating assembly.
Experiments from Miyata et al. show that the amount of deposit formation is strongly dependent on temperature [64]. The authors conclude that the management of the temperature in the turbocharger is an effective way to prevent the formation of coke deposits, one of the main causes of failure turbochargers [40].

2.3 Turbocharger heat transfer models

Thermal management of engine components and subsystems is important not only for reduction of emissions in absolute terms, but also contribute to reduce emissions variability for different driving conditions [65]. Heat transfer modelling, as an integral part of numerical studies of internal combustion engines, is intended to help a manufacturer improve engine performance, predict thermal conditions and analyse thermal stress limits for the materials among others.

Thermal management solutions have grown over the last decade, automotive suppliers and researchers have developed and commercialized new heat transfer models that evaluate the progress of technology in IC engines to complement their growth in a cost effective way.

The solution of heat transfer has turned in complex models. The heat transfer phenomena in turbochargers is difficult to predict and engineers can not stablish a model that fits all solutions. The number of systems and subsystems in the engine, the different mechanisms of heat transfer that occur at the same time, the quick and unsteady changes inside the system make it a very challenging task. Different simple and complex models have been developed in recent years that improve the prediction of heat transfer phenomena in order to have more accurate performance maps that contribute to the turbocharger-engine match.

1D and 2D models. In literature it is possible to find models developed to predict the behaviour of the turbocharger under a wide range of operating conditions. For example, Galindo et al. [66] use a simple 1-D heat transfer model for predicting engine transient conditions and improve the thermal response in the turbo-charging system. Shaaban et al. [67] developed a software that implements a model based on regression equations that is able of simulating the performance of the turbocharger taking into account the heat transfer phenomena in compressor and turbine.

Different fast models for heat transfer have been presented [8, 54] in order to compute the thermal behavior of the turbocharger while performing one-dimensional simulations. However, these models lack the capability to produce results for the internal thermal state of the turbocharger. Romagnoli et al. [54] have developed and validated a heat transfer model for a range of engine speeds and loads. In this work, the temperatures of the turbine and the compressor housings have been measured in the engine, top and external side. The results show that the high temperature of the turbine housing causes the heat fluxes to be directed towards the surrounding environment.

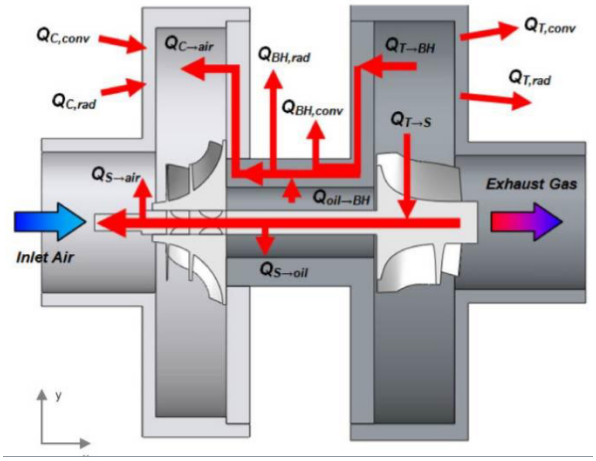

Figure 2.3: Main heat transfer paths [54]

Romagnoli et al. perform a simplification to describe the heat fluxes of the environment as shown in Figure 2.3, where the exhaust gases exchange heat by forced convection to the turbine housing and to the bearing housing (Qt/BH), dissipated heat by radiation ($Qt,_{rad}$) and free convection ($Qt,_{conv}$) to the environment; in the bearing housing heat is dissipated by forced convection to the oil ($Qoil/BH$), free convection ($QBH,_{conv}$) and through radiation ($QBH,_{rad}$) to the environment; in the compressor side, the air flows into the diffuser, where the gas is further heated up by forced convection to the back-plate (Qc/air), natural convection (Qc,conv) and radiation (Qc,rad). This is a good starting point to provide a qualitative and quantitative assessment of the heat transfer within a turbocharger. However, this can be true at constant load points for a range of engine speeds and loads. Under thermal transients the different mechanisms of heat transfer by convection, conduction and radiation, besides the quack and unsteady changes that occur within the system may differ from this correlation and should be studied in detail. With this thermal model proposed, the authors can obtain a good correlation for non-adiabatic efficiency of the compressor through multiple regression analysis.

Furthermore, models based on calibrated coefficients to provide an estimation of heat transfer or adiabatic efficiency are widely used. Luddecke et al. [68] propose a method to correct measurements of turbine efficiency taking into account heat transfer. The corrected characteristics are presented as a function of turbine pressure ratio and blade speed ratio. The model takes into account the conduction inside of the turbocharger but not external heat transfer between the test cell and the turbocharger. Besides, Aghaali et al [41] implement a turbocharger model considering heat transfer in GT-Power ^{TM}. Calibration

coefficients such as efficiency multipliers are used [69, 70]. The temperature estimation of turbocharger working fluids and walls under steady state are obtained.

In addition, calculations of the heat transfer from the external surfaces of the turbocharger have been made taking into account the different conduction, convection and radiation methods in the turbocharger [62]. The results show that changing the convection heat transfer condition around the turbocharger affects the heat fluxes more noticeably than the change in radiation and conduction. On the other hand, Burke et al. [71] have developed an initial lumped model of thermal capacity considering only turbine and compressor housings. From this model, seemingly a prediction of turbine and compressor outlet temperatures can be obtained under transient conditions with turbine inlet temperatures between 200°C and 800°C. However, high inaccuracies in predicting metal temperatures during warm-up is evidenced. The influences of heat transfer in the calculation of engine performance have been studied by the same authors arguing that heat transfer in the turbine always represents an important part of its enthalpy change and more relevant in the low torque region [72].

Heat transfer correction methods for turbocharger performance are found in literature, [73]. A significant improvement can be obtained in the prediction of the turbine's outlet temperature with a better calculation of the isentropic efficiency of the turbine using heat transfer models. Fast turbocharger heat transfer models can be used coupled with steady-state, 0D and 1D simulations to compute the internal and external heat fluxes, leading to better prediction of variables such as the turbine outlet temperature. These models interact with other phenomena: the exchange of heat to oil (changes in viscosity and friction losses); the exchange of heat with the gases (variation of the isentropic power of the turbine and its working point).

A global 1-D gas-dynamic code coupled with heat transfer and mechanical losses sub-models has been used to analyse hot pulsating flow conditions on the turbine side [74]. The results obtained show that an improvement of the temperature prediction in the compressor and turbine outlet can be obtained when the transfer model is activated. Also, an improvement in the results is seen regarding to mass flows, pressure ratios, outlet temperatures and turbocharger speed. Similarly, other models have been developed [8, 75, 76] focusing on the axial heat transfer paths. Although they produce good results when calculating the turbine's outlet temperature, they lack the ability to produce detailed results of the internal surface of the turbocharger. Therefore, the internal thermal state or phenomena such as oil degradation can not be easily predicted.

The internal thermal state of the turbocharger is a complex system containing different heat flows between compressor, turbine, bearing housing (shaft,

bearing, lubrication system) and environment. Porzig et al [77] conducted a study that clarifies the significance impact of the temperature in the shaft on overall bearing operating parameters.

Moreover, 2D thermal solutions in the turbocharger bearing system have been developed. San Andres and Kerth [78] use a two-dimensional model to perform thermohydrodynamic analysis (THD) on the bearing system. The lumped-parameter thermal model determines the effective temperature increase within the inner and outer film of the floating ring bearings. The resulting temperatures are used to set the viscosities of the internal and external film fluid and changes in operating clearances. This thermal model is represented by quasi-stationary state equations whose solution is a thermal energy balance coupled with a Newton-Raphson algorithm to solve iteratively and determine the general temperature increase in each film.

Another 2-D model is developed to predict the heat distribution in the turbine volute [79], in this work, several assumptions have been made. The volute of the turbine is considered as a 2-D flat plate and the internal area of the volute is assumed to be a converging nozzle. The thermal analysis performed uses three different values of heat transfer coefficients to simulate and observe the effect towards the efficiency of the turbine. The results show that the temperature difference between the inner and outer wall increases if there is an external forced convection flowing around the turbine volute.

To summarize, the use of 1D or coupled 1D-2D modelling approaches are used today in conjunction with the experimental performance maps to obtain the desired heat exchanges, since they are computationally cheaper than the full 3D models and less arduous than the experimental works. These modelling approaches are useful to improve existing numerical models or even help the development of more complex 3D models.

3D models. The increase in the level of complexity in the three-dimensional analysis brings improvements in each phase of the turbocharger design.

Some 3D models focus their study on aerodynamic or acoustic phenomena, looking for flow disturbance sources in either the compressor or the turbine side. Drewczynski et al. [80] use methods of load transfer that affect rotor blade stress and displacement levels during one period of rotation. Filsinger et al. [81] study the vibration behaviour of an axial turbocharger turbine by using an approach to unidirectional coupled Computational Fluid Dynamic-Finite Element Method (CFD-FEM) analysis.

Different authors have performed 3D studies to better understand the heat transfer phenomena in turbochargers and their implications. For example, analysis of heat transfer changing the materials of the turbine blade and assuming that the car runs at a higher speed can be found using a 3D model [82]. Matsumoto et al. perform 3D analysis of sliding mechanisms to evaluate the turbocharger design before prototyping [7]. Turbine wheel and turbine casing materials are studied to meet exhaust gas temperature requirements for turbochargers used in competition vehicles such as rally cars. The thermal analysis in that study shows that a similar nickel-based alloy and austenitic stainless steel are suitable for using in turbine wheel and turbine casing respectively when the exhaust temperatures exceed 1050 °C.

Integration of modern computational methods in the design cycle are done to understand the thermal behaviour of the turbochargers by offering an idea of the performance of the components and the system. Bet and Seider use a simulation approach with direct thermal fluid coupling (CFD/CHT) [83]. An overview of the simulation methodology for a water-cooled turbocharger and its closest environment is presented in Figure 2.4. The heat transfer from the exhaust side to the compressor can reduce the efficiency of the compressor and, therefore, directly influences the performance of the engine.

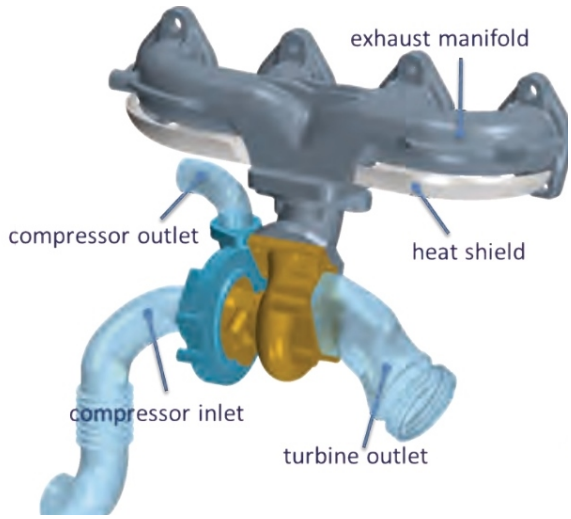

Figure 2.4: Sample of a 3D turbocharger model [83]

A coupling of the rotary assembly to the flow through the compressor and the turbine by means of a fluid body is done. Simulation approach with direct thermal- fluid-structure coupling (CFD/CHT) was chosen for the turbocharger

and its closer environment. The heat transfer coefficients and the ambient temperature were defined on the external surfaces of the turbocharger and the thermal shields to take thermal convection into account. A sample temperature contour plot is shown in Figure 2.5 for a discrete time step. These temperature profiles can give some indication of critical conditions for the structure of the turbocharger. With this model, authors explain that the short but sudden acceleration of the turbocharger does not immediately lead to critical temperatures.

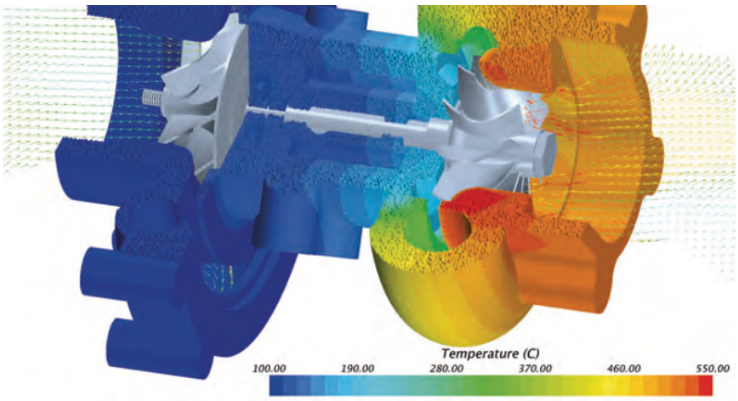

Figure 2.5: Temperature contours in turbocharger structure [83]

It is also possible to find studies of heat transfer in specific parts of the turcompressor. As an example, Zheng et al. use a solid fluid model to calculate the surface temperature distribution of the impeller compressor [84].For the numerical calculation in the fluid domain, a CFD code based on a 3D steady compressible finite volume scheme was used to solve the RANS equations in conservative formulation. The turbulence model is a standard k-epsilon model. A central scheme was used for spatial discretization while fourth-order Runge?Kutta scheme for the temporal discretization and conjugate heat transmission analysis technology was applied in the solid?fluid coupling calculation of the impeller temperature. Figure 2.6 shows the temperature distribution of the impeller surface obtained from solid-fluid coupling analysis for a pressure ratio of 3.4. It can be seen that the surface temperature of the impeller increases continuously from inlet to outlet (339 K to 389 K respectively).

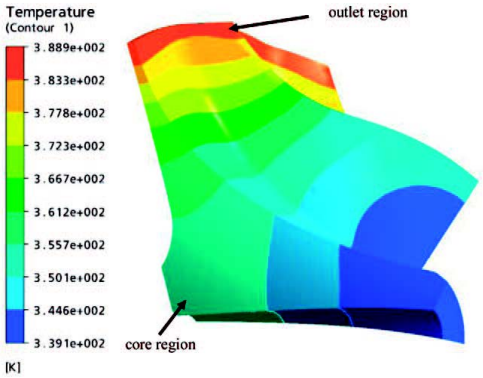

Figure 2.6: Temperature of compressor impeller surface for pressure ratio of 3.4 [84]

In their work, Zheng et al. show in Figure 2.7 the temperatures variation between the core and the outlet region. There can be seen that when the pressure ratio increases from 1.5 to 4.6, the outlet temperature of the compressor impeller increases from 318 to 432 K and from 313 to 379 K in the core region. By increasing the pressure ratio, the interaction of aerodynamics and heat transfer between the air and the impeller gets stronger. The authors from this work conclude that the stress caused by the centrifugal load has an important role at high pressure ratio.

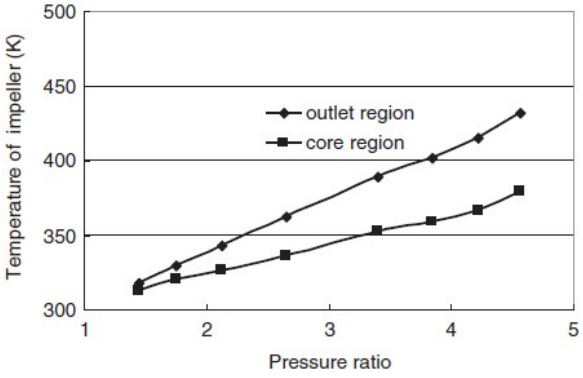

Figure 2.7: Compressor impeller temperature against pressure ratio [84]

In a more recent study, Zheng and Ding use the results of temperature distributions from previous work as boundary conditions in a three-dimensional finite element to analyse the impeller stress under different inlet conditions [85]. The effect of temperature is large for low inlet temperature, reaching 57% of the total equivalent stress, so it should be considered and also argue that the

temperature mainly affects the stress on the disk and the root of the blade. On the other hand, the effect of the pressure is small for the low inlet temperature but may be large enough for a high inlet temperature.

Furthermore, Burke et al. perform a 3D conjugate heat transfer analysis of the compressor in steady state using a simplified geometry and different assumptions [86]. In this study, the heat transfer to and from the model are not considered and the external boundary walls were set as adiabatic. The results show that assuming a single temperature for the compressor housing is not suitable for high speed conditions, since it is difficult to capture the reversal of heat transfer through the compression process. However, at lower speed the temperature of the compressor housing remains higher than the temperature of the gas, the heat flows are consistently from the housing to the gas and the model may be suitable for the temperature distribution on the compressor side. There have been further improvements in this model with regard to the phenomena of heat transfer [87]. Besides, Roclawski et al. have developed a model for studying the heat transfer in a high-pressure compressor of a two-stage turbocharger [88]. In this model, the heat transfer between the solid parts is assumed as an ideal contact using thermal boundary conditions. The numerical results show that the temperature distribution in the compressor wheel is uniform in the circumferential direction but in the radial direction, a gradient of 30 K can be present in operating points of high pressure ratio and high volumetric flow rate.

Simulation and analysis of fluid flow and heat transfer can be found in literature. De Vos et al. addresses the fluid flow phenomena present in the turbine housing using augmented Nusselt correlations to represent the heat transfer coefficients of the internal volute surface [89]. The results show a good prediction of the surface temperature under two measured operating conditions. Tomm et al. study the energy balance of a turbocharger with a complex 3D CAD model [90]. The main contribution in this work is the determination of the lumped mass elements and the thermal properties that can be implemented in a simplified 1D heat transfer model. Nevertheless, the heat transfer between the oil and the solid elements for this work needs a better correlation near the bearing, since there is almost 35% temperature difference with the results from the experiments.

Regarding to the bearing system, recent studies are presented. For instance, Deligant et al. use a CFD model to analyse the steady state performance of a turbocharger inner film based on the Gumbel boundary [36]. Also, Yin et al. have developed a 3D CFD method for support bearing analysis where cavitation and conjugate heat transfer are considered [91]. Recently, Li et al. have developed a 3D thermohydrodynamic (THD) model to analyse the mechanical and

thermal performance of the turbocharger rotor and floating rings [92]. In this study, experiments on a hot gas test bench heated up to 600 ° C and standard SAE 15W40 engine oil to lubricate the bearings have been used. The Figure 2.8 shows the temperature results obtained from the model. It can be seen that the temperature of the outer film on the turbine side is about 30 °C higher than the compressor and that as the rotor speed increases from 40 to 240 krpm, the temperature increases approximately 30-40 °C. It can also be observed that the temperatures in different solid parts of the floating ring bearing have a difference of 20-40 °C. The temperatures of the outer films have been measured at different rotor speeds. The bush temperatures (T9 and T10) measured have been used as boundary conditions in the numerical simulations.

This THD model of oil film is essential for high-speed oil film bearing. In this work, experiments are conducted to calibrate and thereafter validate the numerical simulation.However, some probes for temperature measuring points need to be arranged so as to ensure the accuracy of decoupled simulation boundaries. The Figure 2.9 shows the temperature distributions that are considerable in circumferential and axial directions. On the other hand, the authors note that solid parts play an important role in the THD analysis of the rotor bearing system, and therefore should not be treated as thermal insulation.

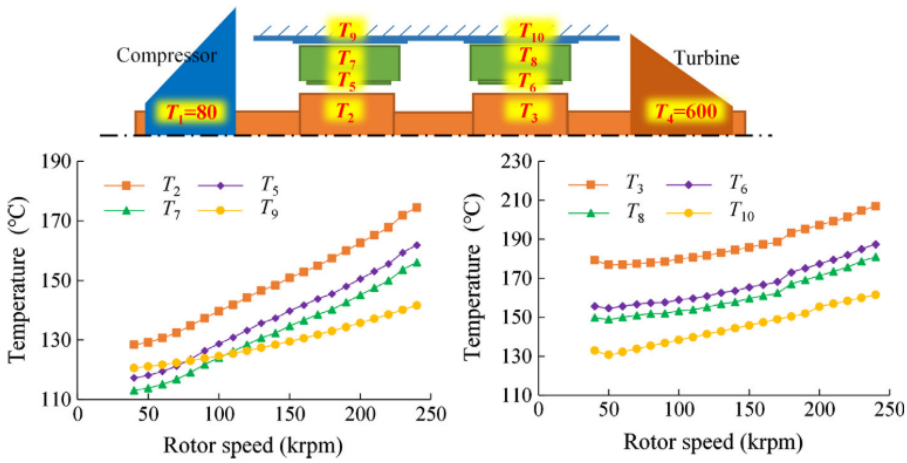

Figure 2.8: Temperatures of solid parts in the rotor system (steady state) [92]

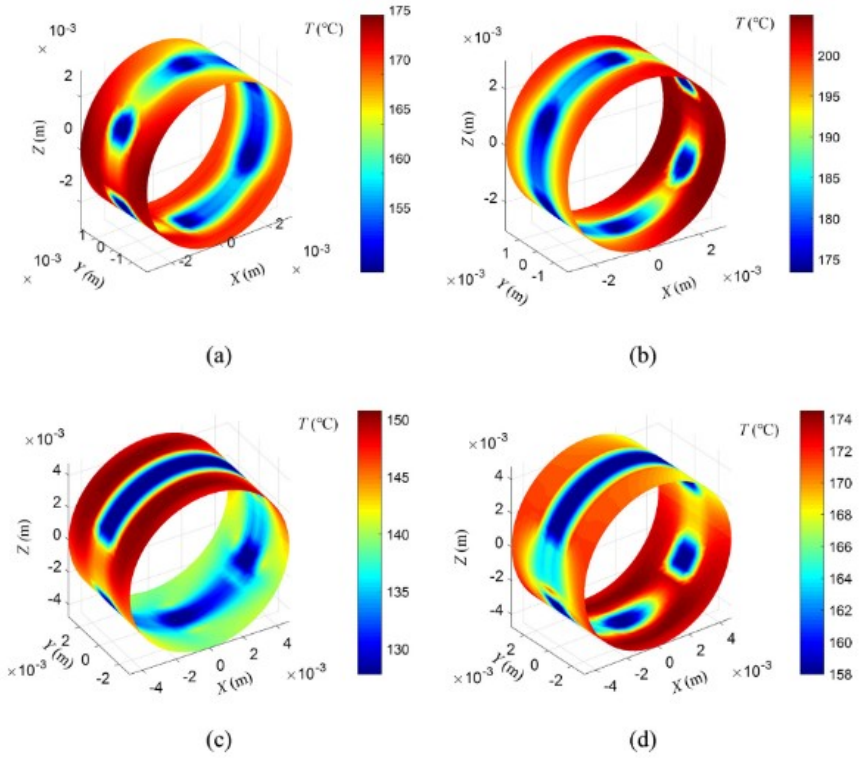

Figure 2.9: Transient thickness-averaged temperature fields at 240 krpm [92]

New analysis of oil film temperature, clearance and bearing profile that can change the stiffness and damping characteristics of sliding bearings are studied [93]. CFD analysis proposed by the authors considers a fully coupled fluid-structure interaction. For complete floating bushing designs, several hundred rotations of the rotor are required and the calculation time is in the range of 2 to 24 hours per speed. Nevertheless, the presented methodology proves to be a next level approach in the prediction of the simulation of turbochargers in the development process.

2.4 Tribology in IC engines

The oil is an element specially studied as it has influence on several parts of the engine systems. Lubricant quality testing helps minimize costly down-time and repairs, developing problems before they become.

Although tribology is not the main topic of this thesis, a special mention must be given because of its importance in terms of quality, composition, classification, control and maintenance in engines and turbochargers. Tribology has been observed as a science capable of influencing the behavior of IC engines and improving their efficiency [94, 95] always seeking to minimize energy consumption and maximizing the tribological behavior of the components [96, 97, 98]. Tribological characterization of high temperature materials used within turbochargers are studied in [99]. Extensive test and analysis is conducted to understand and validate the capabilities of such materials within turbocharger products. Of course, materials that find use within high temperature tribosystems are usually of high cost due to the high chemical composition[15, 100], which is required to provide oxidation stability and also affording sufficient mechanical characteristics.

Fundamentals of tribology. Tribology represents friction, and includes the sciences and technologies of relative moving surface interaction. The tribology is divided into three main areas of research and application: friction, wear and lubrication [101].

- **Friction:** It is considered that there are four types of friction; static, dynamic, interferential and adhesive. The classic way to define the phenomenon is using the coefficient of friction, which is defined as a ratio between the force “F” that is required for the movement and the normal force “FN” to the contact surface between the sliding bodies. Friction will depend on the roughness of the surface (micro-structure), mechanical factors (load conditions, type of movement, sliding speed) and on the properties of the material (physical properties, composition). Considering both the variables that affect the sliding system individually, as well as those external to the system result in a complex tribological system

- **Lubrication:** The purpose of the lubrication is to reduce the friction between two surfaces with relative movement that are in contact, heat dissipation among adjacent running surfaces (i.e in the bearing, shaft and bearing housing) and to reduce the wear thereby providing greater service life of a mechanical component. Within the tribology, lubrication is considered the only solution to the friction phenomenon.

  There are different regimes of lubrication based on the coefficient of friction and number of Hersey, these are the boundary lubrication, mixed, hydrodynamic and elastohydrodynamic. The regime of lubrication can be determined using the dimensionless film thickness ratio.

  All these regimes impact in a different way to the IC engine. Each of the tribological systems described above presents different and unique lubricant characteristics [102]. For example, bearings intended to reduce the friction on a shaft that rotates in its housing, are designed to operate with hydrodynamic lubrication with the usual operation conditions of the IC engines. [103]. The friction may increase or decrease as velocity or pressure is increased.

- **Wear:** It can be defined as the main consequence of friction in the tribological system, and cause of failures. Once wear begins in a metal surface, there are a number of effects on the different layers: the outermost layer is almost destroyed, the intermediate is slightly disfigured, and the internal one remains practically unchanged. All the operating processes of the lubricated system cause different mechanisms of wear and usually more than one involved, so it is difficult to determine which of them is the predominant. Therefore, it is not easy to find the solution to counteract the wear effects that these mechanisms produce.

  The phenomenon of wear can be responsible for catastrophic consequences in the engine, such as loss of performance, reduction of service life of its components or loss of efficiency.

  Although in the tribology, the phenomenon of lubrication could be considered as the most significant when it comes to modifying wear and its consequences [104], in the IC engines there are a number of boundary conditions that are also involved in the process of wear [105].

  To sum up Figure 2.10 describes the classic tribology described above.

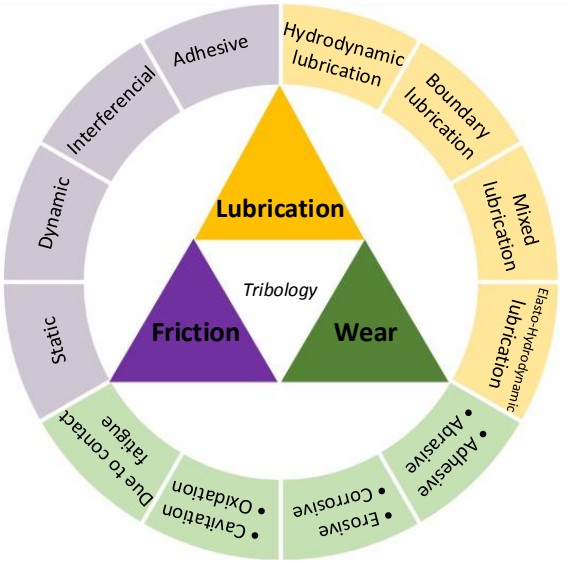

Figure 2.10: Fundamentals of tribology

Engine oil formulation. In IC engines the oils must perform the roles of lubrication, refrigeration, cleaning, neutralization, protection and sealing. Currently, liquid lubricants for engines are formulated with fluid bases from hydrocarbons and chemical additives. The components-base oils constitute 70 to 85 percent of the total, while additives round out the remaining 15 to 25 percent [106].

The hydrocarbons used for the bases of lubricating oils are paraffins, naphtenes and aromatics [102]. These lubricant bases provide a fluid layer to separate two movable surfaces, generating a hydrodynamic lubrication and thus reducing the friction between them. In addition, remove the heat and wear particles of the system. The additives, are comprised of dispersant, detergents, anti-wear additives, friction modifiers, antioxidants, anti-foam additives and corrosion inhibitors.

Several investigations in the field of lubricants are related to the additives and their properties [107, 108, 109] as well as with the “tribochemical” interactions between the surface and the lubricant due to the use of these additives [110, 111]. The base fluid acts as a carrier for these additives and keeps them in solution under normal working conditions. Moreover engine oil additives also include a viscosity index improver and a pour-point depressant. Figure 2.11 shows an example of the percentage distribution in the formulation of engine oils.

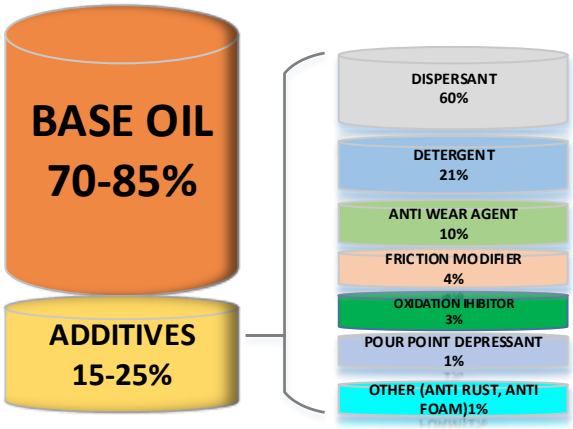

Figure 2.11: Engine oil formulation

Oil bases are divided into minerals and synthetic. The American Petroleum Institute (API) has categorized base oils into five categories (API 1509, Appendix E [112]) as shown in Table 2.1. The first three groups are refined from petroleum crude oil. Group IV base oils are full synthetic polyalphaolefin (PAO) oils. Group V is for all other base oils not included in Groups I to IV. Before all the additives are added to the mixture, lubricating oils begin as one or more of these five API groups.

Table 2.1: API base oil categories [113]

	API BASE OIL CATEGORIES				
	Base Oil Category	Sulfur (%)		Saturates (%)	Viscosity Index
Mineral	Group I (solvent refined)	>0.03	and/or	<90	80 to 120
Mineral	Group II (hydrotreated)	<0.03	and	>90	80 to 120
Mineral	Group III (hydrocracked)	<0.03	and	>90	>120
Synthetic	Group IV	PAO Synthetic Lubricants			
Synthetic	Group V	All other base oils not included in Groups I, II, III or IV			

As a matter of fact, the introduction of technological improvements, new designs and changes in the modes of operation in modern engines have to led the need to formulate high quality lubricants that are able to maintain their properties under any kind of situation. This has led to a parallel development of research in the field of additives to have lubricants of better performance

in terms of both life service and level of protection provided to the lubricated mechanisms.

Properties. Some of the fundamental properties of lubricating oils are viscosity, density, pour point, cloud point, flash point, and acidity/basicity. A brief description of them is presented below.

- **Viscosity:** It is one of the most important characteristics of the lubricating oils and can be expressed in two different ways: dynamic viscosity or kinematic viscosity. The viscosity is not a constant of the fluid and depends on several parameters being the most important the temperature and pressure [114, 115].

  In IC engines, the representative parameter of the viscosity variation of a lubricating oil with the temperature is the so-called viscosity index (IV). The bases behave as Newtonian liquids, but when adding polymeric chains as improver of the viscosity index, the oil behaves as non-Newtonian fluid, where high rates of shearing cause substantial decreases in viscosity, known as "shear-thinning effect". The higher the viscosity index, the lower the effect of temperature on the oil viscosity.

- **Density:** It is defined as the ratio between the mass and the volume of the element studied for a constant temperature. There is an equivalent measure from crude oil called API density, this is related to the specific weight so that an increase in density corresponds to a decrease in specific weight. The units are API degrees and can be calculated from the specific weight defined in the ASTM D1298 standard [116]. Both the specific weight and the API degrees refer to the volume unit measured at 60 °F or 15.6 °C, and it is possible to convert the density at any temperature to the reference density by means of tables.

- **Pour point:** It is the temperature below which the liquid loses its flow characteristics. This parameter presents a great importance for the behavior of the oil at very low temperatures, and is measured according to the standardized test described in the ASTM D97 [117].

- **Cloud point:** It is the temperature at which paraffins and other substances in solution begin to separate forming crystals under standardized test conditions, shown in the ASTM D2500 Standard [118]. The presence of solidified waxes thickens the oil and clogs fuel filters and injectors in engines.

- **Flash point:** It is a very important property for safety. It is the lowest temperature to which the oil emits enough vapours to ignite when applying

an external source of energy. It is usually expressed in Celsius degrees. In the case of automotive lubricants, the flashpoint is at levels that should not offer potential risk of inflammation, always above 200 °C according to the standards ASTM D93 [119] or ASTM D92 [120].

- **Acidity/basicity:** This property provides information on the degree of oil refining and additive. The acidity monitoring allows to evaluate the chemical changes experienced by the oil as a result of its oxidation and the combustion products. The parameter used for the measurement of acidity is the TAN (Total Acid Number), measured according to the standard ASTM D664 [121]. The basic oil reserve is usually expressed with the TBN parameter (Total Base Number), according to the ASTM D2896 Standard [122]. The capacity of the oils is measured to neutralize the acids from the combustion and the own oil oxidation due to high temperatures.

Classification. There are two main classification criteria for engine oils:

- Based on Viscosity (SAE)

  Kinematic viscosity measured at 100°C defines SAE degrees from 20 to 60 for rising levels of viscosity. Dynamic viscosity at low temperatures defines the SAE "W" degrees, from the initial "winter", from 0W to 25W on the basis of viscosity levels measured at temperatures from -35° to -5°C. The temperature represents the lowest possible temperature at which the engine can be started when lubricated with an oil of the corresponding SAE degree (i.e a 15W oil makes it possible to start the engine at up to -20°C). The minimum pumping temperature is the minimum temperature at which oil, in addition to allowing start up, can flow freely and lubricate the critical parts of the engine [123]. These oils are superimposing the two grades SAE: SAE XXWYY, being XX the degree of winter and YY the degree of summer.

- Based on Performance (API, ACEA, manufacturer's specifications)

  API Classification: API stands for "American Petroleum Institute". The SAE and ASTM "American Society for Testing and Materials" established the API service classification system to define the performance level of a given oil, unrelated in the main, to oil viscosity. The API requirements "S" for Spark Ignition (petrol) and "C" for Compression Ignition (diesel).

  ACEA Classification: ACEA stands for "European Auto-mobile Manufacturer's Association". This classification system is the European equivalent

of the APIsystem, but is stricter and has more severe requirements. Therefore oil that meets both API and ACEA specifications uses a better additive package than one that is designed to meet only API specifications. Unlike the API, ACEA has three main groups “A/B” for gasoline and light duty diesel engines, “C” for light duty three way catalyst and diesel particulate filter compatible oils and “E” for heavy duty diesel engines. The description of the A/B group has special interest in this thesis and is described in Table 2.2. Detailed information about oil sequences for service fill oils can be found in [124].

Table 2.2: ACEA gasoline and diesel engine oils classification[124]

A/B: Gasoline and Diesel Engine Oils - “High SAPS”	
A1/B1	Category is removed with these Oil Sequences.
A3/B3	Stable, stay-in-grade Engine Oil intended for use in Passenger Car & Light Duty Van Gasoline & Diesel Engines with extended drain intervals where specified by the Engine Manufacturer, and for severe operating conditions as defined by Engine Manufacturer
A3/B4	Stable, stay-in-grade Engine Oil intended for use at extended Drain Intervals in Passenger Car & Light Duty Van Gasoline & DI Diesel Engines, but also suitable for applications described under A3/B3.
A5/B5	Stable, stay-in-grade Engine Oil intended for use at extended Drain Intervals in Passenger Car & Light Duty Van Gasoline & Diesel Engines designed to be capable of using Low Viscosity Oils with HTHS Viscosity of 2.9 to 3.5 mPa.s. These Oils are unsuitable for use in certain Engines - consult vehicle- OEM’s owner’s manual/handbook in case of doubt

Control and maintenance. Several techniques have been developed to study engine oil wear at regular sampling intervals [125]. Engine oil undergoes degradation and has to be changed periodically. The oil change is usually done as part of a preventive maintenance program when the engine odometer reaches a given threshold.

Emerging technologies related to several sensors and wireless communication offer new opportunities to improve the efficiency of maintenance operation for automotive industry, in particular, the implementation of predictive maintenance. The key point of maintenance is to develop an algorithm that can analyse the state of degradation, level of contamination from engine wear, water vapour in the crankcase, acids and engine blow-by gasses to make preventive decisions. In a study for the application of predictive maintenance on an engine oil of a car, a new algorithm is proposed to determine the time of oil change through the analysis of its degradation level [126, 127].

Although most lubricants are formulated with anti oxidants to control oxidation, this degradation cannot be avoided. Consequently, this can lead to an increase in viscosity and varnish formation. This condition can occur even when the oils are not especially old or contaminated, as well as in synthetic lubricants and hydraulic fluids thermally resistant. This type of degraded oil can leave traces in the turbine shaft and bearings affecting the dynamics of the turbocharger [64, 128].

Recently a test rig designed by Siddaiah et al. proves to be a method to monitor wear and corrosion synergism in an oil medium, which can be in contaminated or uncontaminated conditions [129]. Nevertheless, future investigations in terms of oil life in correlation with the synergistic effects of wear and corrosion rates have to be made. On the other hand, while controlling temperature and using higher-quality base oils can help limit the degree and rate of oxidation, the eventual breakdown of the base oil molecules due to oxidative processes is inevitable. Fourier transform infrared spectroscopy (FTIR), measures the degree of infrared absorption in different parts of the infrared spectrum, this can be an excellent tool for pinpointing base oil oxidation.

Nonetheless, when the turbocharger deteriorates, the Engine Control Unit (ECU) can manage the turbocharger operation through VGT vane position [130] or waste-gate [131], offsetting the problem and reaching the required inlet pressure but hiding any degradation that may have the turbo-charging system. The evaluation of the oil performance within the turbocharger is difficult due to narrow access to the lubrication channels. In high temperature tribosystems such as variable geometry and wastegate mechanisms, turbine inlet temperature significantly affects tribological performance.

2.5 Lubrication in the turbocharger

Conditions of lubrication in the turbocharger must be representative in terms of pressure, temperature and flow rate of oil. Ensuring an optimum lubrication quality is essential to ensure the successful operation of the turbocharger and the engine as a whole; if the system deteriorates, a decrease in engine performance can reach up to 20% in power and torque [36].

A big part of the energy from the exhaust gases that move the turbine can be lost due to friction [132], generating heat fluxes that increase the temperature of the oil that might even break the turbocharger. Oil degradation can be promoted due to thermal loads, liquid, gas or solid contamination. A lubricant in service is subjected to a wide range of work that can degrade the oil base and additives. Heat, air, incompatible gasses, humidity, internal or external contamination, combustion processes, radiation and the unnoticed mixture with different fluids infers in such factors. For instance, the inclusion of combustion air increases the rate of elements that do not belong to the oil, such as soot particles, nitrogen oxides, air, etc., which lead to oxidation of the oil, one of the main mechanisms of lubricant degradation [133].

Oil degradation can form solid residues in static films on engine components. This is known as a coke phenomenon and in the lubricating circuit of turbocharger unit is a well-known issue that affects turbocharger efficiency and durability. The solid residue created when oil undergoes severe oxidative and thermal breakdown at extreme engine temperatures is a potential issue, and its prevention has been required in some engine oil specifications, through the inclusion of lubricant performance tests such as ASTM D6335 (Thermo-oxidation Engine Oil Simulation Test - TEOST 33C) in ILSAC specifications. Although a laboratory test is easier to run, it is more difficult to reproduce the actual mechanism of the coking phenomena [134].

Engine start-stop. A typical situation of oil thermal damage is produced during engine hot-stop, where oil flow is halted. In these cases, the turbine exchanges huge amounts of heat with the central housing as it cools down, increasing the temperature of the small amounts of oil trapped inside the turbocharger.

During the hot stops, metal-to-metal contact ensues and the bearing material wears faster than in the hydrodynamic regime. Since the start-stop engines are switched off and restarted very frequently, the bearings operate in a condition of mixed lubrication (with metal-to-metal contact) for much longer. Such conditions

require bearing materials with greatly enhanced anti-friction properties.

Engine hot stop and carbon build up failure produces blockage in the system of bearings [38]. For instance, Galindo et al. [13] study the mechanical behaviour of turbochargers with intermittent stops of the lubricating oil flow. The temporal lack of lubrication leads to wear of the bearings and final imbalance of the shaft very quickly. The turbocharger friction losses inside the bearings system is also dependent on the geometry of such bearings [132], so even when wearing might not finally break the turbocharger it could affect its mechanical efficiency.

Turbocharger failures. The thermal damage in the turbocharger might be noticed some time after it has been produced. If the oil thermal load is too big, it might degrade and produce coke leading to oil ducts and bearings clogging, thus reducing the oil flow. This reduction in oil flow leads to a loss of bearing loading capabilities and cooling performance, enabling mechanical wear and further thermal damage.

Common failing conditions in turbochargers are mostly achieve due to oil contamination which results in little particles of debris that engine parts have shed; thrust failure turning the boost up; excessive exhaust gas temperatures, oil delay, impact damage in compressor or turbine wheels. Tight tolerances in the turbocharger does not take much for bits of debris to block oil ways and reduce the oil flow [128]. High boost pressures and high rotational speeds make the material will shred. Excessive exhaust gas temperatures can range from a severely pitted turbine wheel to a bent turbine shaft, affecting other areas of the engine and leaving bits of aluminium piston melted onto the turbine wheel.

Some signs of oil delay failure can be material wipe out all over the shaft and blue colouring due to the high temperature that has been built by the heat. Failures that cause damage in compressor or turbine wheel [135] can be produced by anything from dust entering to large pieces of debris in the air system from previous failures or in turbine wheel by bits coming from the combustion chamber or the manifold itself.

On the other hand, carbon builds up due to lack of servicing and poor quality oils, which results in a gradual build-up of sludge in both the sump and all oil galleries of the engine. Inside the turbocharger there are some of the narrowest oil ways, some as small as 1mm in diameter, and when they become blocked failure can occur.

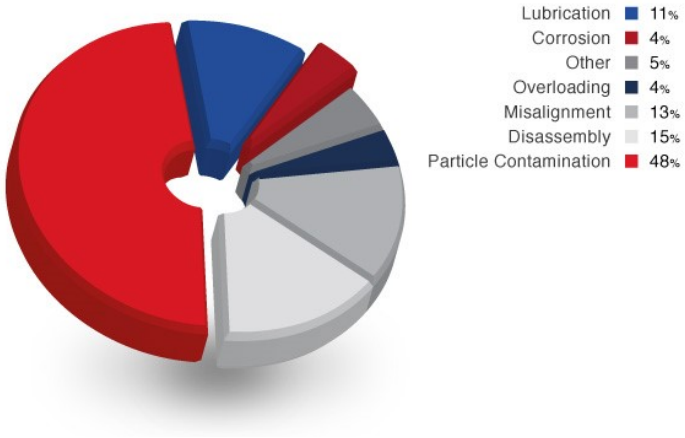

Figure 2.12: Causes of bearing failure [40]

To sump up, several investigations into bearing failures and a comprehensive study of lubrication are done by Bloch [39, 40] who shows that almost half of bearing failures are due to the contamination of oil particles that affect turbocharger efficiency as shown in Figure 2.12. Disassembly, misalignment and lubrication also contribute in large part to the bearing failures. A lower proportion of failures is attributed to corrosion, overloading and other factors.

2.6 References

[7] K. Matsumoto, Y. Jinnai, M. Tojo, N. Hayashi, and S. Ibaraki. *Development of Compact and High-performance Turbocharger for 1050°C Exhaust Gas*. Tech. rep. September. Mitsubishi Heavy Industries, Ltd. Technical Review, 2008, pp. 1–5 (cit. on pp. 2, 23).

[8] M. Comerais, P. Chesse, and J.-F. Hetet. "Turbocharger Heat Transfer Modeling Under Steady and Transient Conditions". In: *International Journal of Thermodynamics* 12.4 (2009), pp. 193–202. URL: http://dergipark.ulakbim.gov.tr/eoguijt/article/view/1034000257/1034000237 (cit. on pp. 2, 17, 19, 21).

[13] J Galindo, J. R. Serrano, V Dolz, and M. A. Lopez. "Behavior of an IC Engine Turbocharger in Critical Condition of Lubrication". In: *SAE International Journal Engines* 6.2 (2013), pp. 797–805. ISSN: 19463936. DOI: 10.4271/2013-01-0921 (cit. on pp. 4, 14, 38).

[15] D. Zeppei, S. Koch, and A. Rohi. "Ball Bearing Technology for Passenger Car Turbochargers". In: *Motortechnische Zeitschrift - Springer* 77.11/2016 (2016), pp. 26–31 (cit. on pp. 4, 29, 164).

[21] European Commission. *Reducing CO2 emissions from passenger cars | Climate Action*. 2018. URL: https://ec.europa.eu/clima/policies/transport/vehicles/cars{_}en (cit. on p. 13).

[22] J. H. Stock. "The Renewable Fuel Standard: A Path Forward". In: *Center On Global Energy Policy | Columbia Sipa* (2015). URL: https://scholar.harvard.edu/files/stock/files/renewable{_}fuel{_}standard.pdf (cit. on p. 13).

[23] The European Parliament and The Council of the European Union. "Amending Regulation (EC) No 443/2009 to define the modalities for reaching the 2020 target to reduce CO2 emissions from new passenger cars". In: *Official Journal of the European Union* (2014). URL: http://eur-lex.europa.eu/legal-content/EN/TXT/?uri=uriserv:OJ.L{_}.2014.103.01.0015.01.ENG (cit. on p. 13).

[24] N Watson and M. S Janota. *Turbocharging the Internal Combustion Engine*. 1st edition. London and Basingstoke: The macmillan press LTD, 1982, p. 595. ISBN: 978-1-349-04024-7. DOI: 10.1007/978-1-349-04024-7. URL: https://link.springer.com/content/pdf/bfm{\%}3A978-1-349-04024-7{\%}2F1.pdf (cit. on p. 13).

[25] T. Grissom. "Turbocharging for Improved Engine Performance & Reduced CO2 Emissions Turbocharging for Improved Engine". In: *BWTS* (2013) (cit. on p. 13).

[26] B. Padhiyar and P Sharma. “Application of hybrid turbocharger to improve performance of engine”. In: *IJEET* 1 (Apr. 2014), pp. 1–2014 (cit. on p. 13).

[27] Williams Martin and Minjares Ray. “A technical summary of Euro 6/VI vehicle emission standards”. In: *The international council on clean transportation* (2016), p. 12. URL: https://www.theicct.org/sites/default/files/publications/ICCT{_}Euro6-VI{_}briefing{_}june2016.pdf (cit. on p. 13).

[28] United States Environmental Protection Agency. *Tier 3 Evap/OBD - Epa, Us of Transportation Office and Quality Air Division Compliance*. 2016. URL: https://www.epa.gov/sites/production/files/2016-12/documents/tier3-evap-obd-summary.pdf (cit. on p. 13).

[29] United States Environmental Protection Agency. *Renewable Fuel Standard Program: Standards for 2018 and BiomassBased Diesel Volume for 2019, 40 CFR Part 80*. 2017. URL: https://www.gpo.gov/fdsys/pkg/FR-2017-12-12/pdf/2017-26426.pdf (cit. on p. 13).

[30] Global Market Insights Inc. *Automotive Turbochargers Market Size, Growth Potential, Price Trends, Competitive Market Share and Forecast, 2017 – 2024*. Tech. rep. Delaware: Global Market Insights, 2018, p. 300. DOI: GMI2463. URL: https://www.gminsights.com/methodology/detail/automotive-turbocharger-market (cit. on p. 13).

[31] A. J. Feneley, A. Pesiridis, and A. M. Andwari. “Variable Geometry Turbocharger Technologies for Exhaust Energy Recovery and Boosting A Review”. In: *Renewable and Sustainable Energy Reviews* 71 (2017), pp. 959–975. ISSN: 1364-0321. DOI: 10.1016/J.RSER.2016.12.125. URL: https://www.sciencedirect.com/science/article/pii/S1364032116311807 (cit. on p. 13).

[32] W. Knecht. “Diesel engine development in view of reduced emission standards”. In: *Energy* 33.2 (2008), pp. 264–271. ISSN: 03605442. DOI: 10.1016/j.energy.2007.10.003 (cit. on p. 13).

[33] E. Watel, A. Pagot, P. Pacaud, and J.-c. Schmitt. “Matching and Evaluating Methods for Euro 6 and Efficient Two-stage Turbocharging Diesel Engine”. In: *SAE Technical Paper* (2010). DOI: 10.4271/2010-01-1229. URL: http://dx.doi.org/10.4271/2010-01-1229 (cit. on p. 14).

[34] J. Serrano, B. Tormos, K. Gargar, and F. Bouffaud. “Study of the Effects on Turbocharger Performance Generated by the Presence of Foreign Objects at the Compressor Intake”. In: *Experimental Techniques* 37.2 (2013), pp. 30–40. ISSN: 07328818. DOI: 10.1111/j.1747-1567.2011

.00795.x. URL: http://doi.wiley.com/10.1111/j.1747-1567.2011.00795.x (cit. on p. 14).

[35] F. Payri, J. R. Serrano, P. Olmeda, A. Paez, and F. Vidal. "Experimental Methodology to Characterize Mechanical Losses in Small Turbochargers". In: *Volume 5: Industrial and Cogeneration; Microturbines and Small Turbomachinery; Oil and Gas Applications; Wind Turbine Technology*. ASME, 2010, pp. 413–423. ISBN: 978-0-7918-4400-7. DOI: 10.1115/GT2010-22815. URL: http://proceedings.asmedigitalcollection.asme.org/proceeding.aspx?articleid=1609171 (cit. on p. 14).

[36] M. Deligant, P. Podevin, and G. Descombes. "CFD model for turbocharger journal bearing performances". In: *Applied Thermal Engineering* 31.5 (2011), pp. 811–819. ISSN: 13594311. DOI: 10.1016/j.applthermaleng.2010.10.030 (cit. on pp. 14, 26, 37).

[37] K. Sim, Y.-B. Lee, and T. H. Kim. "Effects of Mechanical Preload and Bearing Clearance on Rotordynamic Performance of Lobed Gas Foil Bearings for Oil-Free Turbochargers". In: *Tribology Transactions* 56.2 (2013), pp. 224–235. ISSN: 1040-2004. DOI: 10.1080/10402004.2012.737502. URL: http://www.tandfonline.com/doi/abs/10.1080/10402004.2012.737502 (cit. on p. 14).

[38] D. Polichronis, R. Evaggelos, G. Alcibiades, G. Elias, and P. Apostolos. "Turbocharger Lubrication - Lubricant Behavior and Factors That Cause Turbocharger Failure". In: *International Journal of Automotive Engineering and Technologies* 2.1 (2013), pp. 40–54 (cit. on pp. 14, 18, 38).

[39] H. P. Bloch and A. R. Budris. *Pump user's handbook : life extension*. 2nd ed. Fairmont Press, 2006, p. 477. ISBN: 0849391792 (cit. on pp. 14, 39).

[40] H. P. Bloch. "Bearing Isolators: An Expert Guide". In: *AESSEAL* (). URL: http://www.aesseal.com/en/resources/academy/bearing-isolators (cit. on pp. 14, 18, 39).

[41] H. Aghaali. "On-Engine Turbocharger Performance Considering Heat Transfer". PhD thesis. KTH Royal Institute of Technology, 2012. ISBN: 978-91-7501-332-9. URL: http://kth.diva-portal.org/smash/get/diva2:524801/FULLTEXT01 (cit. on pp. 15, 20).

[42] J Galindo, J. M. Lujan, C Guardiola, and G. S. Lapuente. "A method for data consistency checking in compressor and variable-geometry turbine maps". In: *Proceedings of the Institution of Mechanical Engineers, Part D: Journal of Automobile Engineering* 220.10 (2006), pp. 1465–1473. ISSN: 0954-4070. DOI: 10.1243/09544070JAUTO82. URL: http://sdj.sagepub.com/lookup/10.1243/09544070JAUTO82 (cit. on p. 16).

[43] J. R. Serrano, F. J. Arnau, V Dolz, and P Piqueras. “Methodology for characterisation and simulation of turbocharged diesel engines combustion during transient operation. Part 1: Data acquisition and post-processing”. In: *Applied Thermal Engineering* 29 (2008), pp. 142–149. DOI: 10.1016/j.applthermaleng.2008.02.011. URL: http://ac.els-cdn.com/S135943110800077X/1-s2.0-S135943110800077X-main.pdf?{_}tid=57560138-4473-11e7-9693-00000aab0f26{\&}acdnat=1496064963{_}d2bc76947168411d6499a0e925e0ea77 (cit. on p. 16).

[44] S. Szymko, R. F. Martinez-Botas, and K. R. Pullen. “Experimental Evaluation of Turbocharger Turbine Performance Under Pulsating Flow Conditions”. In: *Volume 6: Turbo Expo 2005, Parts A and B*. ASME, 2005, pp. 1447–1457. ISBN: 0-7918-4730-6. DOI: 10.1115/GT2005-68878. URL: http://proceedings.asmedigitalcollection.asme.org/proceeding.aspx?articleid=1585493 (cit. on p. 16).

[45] M. Jung, R. G. Ford, K. Glover, N. Collings, U. Christen, and M. J. Watts. “Parameterization and Transient Validation of a Variable Geometry Turbocharger for Mean-Value Modeling at Low and Medium Speed-Load Points”. In: 2002. DOI: 10.4271/2002-01-2729. URL: http://papers.sae.org/2002-01-2729/ (cit. on p. 16).

[46] M. Cormerais, J. F. Hetet, P. Chesse, and A. Maiboom. “Heat Transfer Analysis in a Turbocharger Compressor: Modeling and Experiments”. In: 2006. DOI: 10.4271/2006-01-0023. URL: http://papers.sae.org/2006-01-0023/ (cit. on p. 16).

[47] J Serrano, C Guardiola, V Dolz, A. Tiseira, and C Cervelló. “Experimental Study of the Turbine Inlet Gas Temperature Influence on Turbocharger Performance”. In: *SAE World Congress & Exhibition*. Apr. 2007 (cit. on p. 16).

[48] A. Romagnoli and M.-B. Ricardo. “Heat Transfer on a Turbocharger Under Constant Load Points”. In: *ASME Turbo Expo 2009: Power for Land, Sea, and Air*. Jan. 2009 (cit. on p. 16).

[49] P. Chesse, D. Chalet, and X. Tauzia. “Impact of the Heat Transfer on the Performance Calculations of Automotive Turbocharger Compressor”. In: *Oil & Gas Science and Technology* 66 (Sept. 2011), pp.791–800 (cit. on p. 16).

[50] N. Baines, K. D. Wygant, and A. Dris. “The Analysis of Heat Transfer in Automotive Turbochargers”. In: *Journal of Engineering for Gas Turbines and Power* 132.4 (2010), p. 042301. ISSN: 07424795. DOI: 10.1115/1.3204586. URL: http://gasturbinespower.asmedigitalcollection.asme.org/article.aspx?articleid=1474996 (cit. on p. 16).

[51] M. V. Casey and T. M. Fesich. “The Efficiency of Turbocharger Compressors With Diabatic Flows”. In: *Journal of Engineering for Gas Turbines and Power* 132.7 (2010), p. 072302. ISSN: 07424795. DOI: 10.1115/1.4000300. URL: http://gasturbinespower.asmedigitalcollection.asme.org/article.aspx?articleid=1428499 (cit. on p. 17).

[52] A. Sidorow and R. Isermann. “Physical and experimental modeling of turbochargers with thermodynamic approach for calculation of virtual sensors”. In: *The International Federation of Automatic Control Rueil-Malmaison* (2012). DOI: 10.3182/20121023-3-FR-4025.00064 (cit. on p. 17).

[53] S. Shaaban and J. Seume. “Impact of Turbocharger Non-Adiabatic Operation on Engine Volumetric Efficiency and Turbo Lag”. In: *International Journal of Rotating Machinery* 2012 (2012), pp. 1–11. ISSN: 1023-621X. DOI: 10.1155/2012/625453 (cit. on p. 17).

[54] A Romagnoli and R Martinez-Botas. “Heat Transfer Analysis in a Turbocharger Turbine: An Experimental And Computational Evaluation”. In: *Applied Thermal Engineering* 38.May 2012 (2012), pp. 58–77 (cit. on pp. 17, 19, 20).

[55] G. Tanda, S. Marelli, G. Marmorato, and M. Capobianco. “An experimental investigation of internal heat transfer in an automotive turbocharger compressor”. In: *Applied Energy* 193 (2017), pp. 531–539. ISSN: 0306-2619. DOI: 10.1016/J.APENERGY.2017.02.053. URL: https://www.sciencedirect.com/science/article/pii/S0306261917301812?via{\%}3Dihub (cit. on p. 17).

[56] S. Marelli, G. Marmorato, and M. Capobianco. “Evaluation of heat transfer effects in small turbochargers by theoretical model and its experimental validation”. In: *Energy* 112 (2016), pp. 264–272. ISSN: 03605442. DOI: 10.1016/j.energy.2016.06.067. URL: http://linkinghub.elsevier.com/retrieve/pii/S0360544216308416 (cit. on p. 17).

[57] S. Marelli, S. Gandolfi, and M. Capobianco. “Heat Transfer Effect on Performance Map of a Turbocharger Turbine for Automotive Application”. In: *SAE international United States*. 2017. DOI: 10.4271/2017-01-1036. URL: http://papers.sae.org/2017-01-1036/ (cit. on p. 17).

[58] J R Serrano; P Olmeda; APaez; F Vidal. “An experimental procedure to determine heat transfer properties of turbochargers”. In: *Measurement Science and Technology* 21 (2010), p. 14. DOI: 10.1088/0957-0233/21/3/035109. URL: http://iopscience.iop.org/article/10.1088/0957-0233/21/3/035109/pdf (cit. on pp. 17, 64).

[59] P. Olmeda, V. Dolz, F. J. Arnau, and M. a. Reyes-Belmonte. “Determination of heat flows inside turbochargers by means of a one dimensional lumped model”. In: *Mathematical and Computer Modelling* 57 (2013), pp. 1847–1852. ISSN: 08957177. DOI: 10.1016/j.mcm.2011.11.078 (cit. on pp. 17, 64).

[60] J. Serrano, P. Olmeda, F. Arnau, M. Reyes-Belmonte, and A. Lefebvre. “Importance of Heat Transfer Phenomena in Small Turbochargers for Passenger Car Applications”. In: *SAE International Journal of Engines* 6 (2013), pp. 716–728. ISSN: 19463936. DOI: 10.4271/2013-01-0576. URL: http://www.scopus.com/inward/record.url?eid=2-s2.0-84878797944{\&}partnerID=tZOtx3y1 (cit. on p. 17).

[61] F. Payri, P. Olmeda, F. J. Arnau, A. Dombrovsky, and L. Smith. “External heat losses in small turbochargers: Model and experiments”. In: *Energy* 71 (2014), pp. 534–546. ISSN: 03605442. DOI: 10.1016/j.energy.2014.04.096 (cit. on pp. 17, 145, 149, 155).

[62] H. Aghaali, H.-E. Angstrom, and J. R. Serrano. “Evaluation of different heat transfer conditions on an automotive turbocharger”. In: *International J of Engine Research* 16.2 (2015), pp. 137–151. DOI: 10.1177/1468087414524755 (cit. on pp. 17, 21).

[63] B. Sirakov and M. Casey. “Evaluation of Heat Transfer Effects on Turbocharger Performance”. In: *Journal of Turbomachinery* 135.2 (2012), p. 021011. ISSN: 0889-504X. DOI: 10.1115/1.4006608. URL: http://turbomachinery.asmedigitalcollection.asme.org/article.aspx?doi=10.1115/1.4006608 (cit. on p. 18).

[64] I. Miyata, S. Hirano, M. Tanada, and K. Fujimoto. “Mechanism of Turbocharger Coking in Gasoline Engines”. In: *SAE International* JSAE 20159223 (2015), pp. 1–15. DOI: 10.4271/2015-01-2029 (cit. on pp. 18, 36, 144, 183, 184).

[65] S. Osborne, J. Kopinsky, S. Norton, A. Sutherland, D. Lancaster, E. Nielsen, A. Isenstadt, and J. German. “Automotive Thermal Management Technology”. In: *The international council on clean transportation* (2016), p. 16. URL: https://www3.epa.gov/otaq/climate/regs-light-duty.htm{\#}2017-2025. (cit. on p. 19).

[66] J. Galindo, J. Lujan, J. Serrano, V. Dolz, and S. Guilain. “Description of a heat transfer model suitable to calculate transient processes of turbocharged diesel engines with one-dimensional gas-dynamic codes”. In: *Applied Thermal Engineering* 26.1 (2006), pp. 66–76. ISSN: 13594311. DOI: 10.1016/j.applthermaleng.2005.04.010 (cit. on p. 19).

[67] S Shaaban, J. Seume, R Berndt, H Pucher, and H. Linnhoff. “Part-load Performance Prediction of Turbocharged Engines”. In: *8th International Conference on Turbochargers and Turbocharging* (Dec. 2006), pp. 131–144. DOI: 10.1016/B978-1-84569-174-5.50013-0 (cit. on p. 19).

[68] B. Luddecke, D. Filsinger, and M. Bargende. “On wide mapping of a mixed flow turbine with regard to compressor heat flows during turbocharger testing”. In: *10th International Conference on Turbochargers and Turbocharging*. International Conference on Turbochargers and Turbocharging, 10. Oxford: Elsevier, 2012, pp. 185–202. ISBN: 978-085-709-209-0. DOI: 10.1533/9780857096135.4a.185. URL: http://linkinghub.elsevier.com/retrieve/pii/B9780857092090500157 (cit. on p. 20).

[69] H. Aghaali and H.-E. Angstrom. “Improving Turbocharged Engine Simulation by Including Heat Transfer in the Turbocharger”. In: *SAE 2012 World Congress & Exhibition*. SAE International, 2012. DOI: 10.4271/2012-01-0703. URL: http://papers.sae.org/2012-01-0703/ (cit. on p. 21).

[70] H. Aghaali and H.-E. Angstrom. “Temperature Estimation of Turbocharger Working Fluids and Walls under Different Engine Loads and Heat Transfer Conditions”. In: *11th International Conference on Engines & Vehicles*. SAE Internationa, 2013. DOI: 10.4271/2013-24-0123. URL: http://papers.sae.org/2013-24-0123/ (cit. on p. 21).

[71] R. D. Burke. “Analysis and Modeling of the Transient Thermal Behavior of Automotive Turbochargers”. In: *Journal of Engineering for Gas Turbines and Power* 136.10 (2014). ISSN: 0742-4795. DOI: 10.1115/1.4027290. URL: http://gasturbinespower.asmedigitalcollection.asme.org/article.aspx?doi=10.1115/1.4027290 (cit. on pp. 21, 113).

[72] R. Burke, C. Vagg, D. Chalet, and P. Chesse. “Heat transfer in turbocharger turbines under steady, pulsating and transient conditions”. In: *International Journal of Heat and Fluid Flow* 52 (2015), pp. 185–197. ISSN: 0142727X. DOI: 10.1016/j.ijheatfluidflow.2015.01.004 (cit. on p. 21).

[73] M. Schinnerl, J. Seume, J. Ehrhard, and M. Bogner. “Heat Transfer Correction Methods for Turbocharger Performance Measurements”. In: *Journal of Engineering for Gas Turbines and Power* 139.2 (2016), p. 022602. ISSN: 0742-4795. DOI: 10.1115/1.4034234. URL: http://gasturbinespower.asmedigitalcollection.asme.org/article.aspx?doi=10.1115/1.4034234 (cit. on p. 21).

[74] J. R. Serrano, F. J. Arnau, R. Novella, and M. Á. Reyes-belmonte. “A Procedure to Achieve 1D Predictive Modeling of Turbochargers under Hot and Pulsating Flow Conditions at the Turbine Inlet”. In: *SAE Technical Paper* 2014-01-10.February 2016 (2014). ISSN: 0148-7191. DOI: 10.4271/2014-01-1080 (cit. on p. 21).

[75] R. D. Burke, P. Olmeda, F. J. Arnau, and M. Reyes-Belmonte. “Modelling of turbocharger heat transfer under stationary and transient engine operating conditions”. In: *Institution of Mechanical Engineers - 11th International Conference on Turbochargers and Turbocharging*. Woodhead Publishing Limited, 2014, pp. 103–112. ISBN: 9780081000335. URL: http://www.scopus.com/inward/record.url?eid=2-s2.0-84933526285{\&}partnerID=tZOtx3y1 (cit. on pp. 21, 114, 145, 169).

[76] J. R. Serrano, P. Olmeda, F. J. Arnau, A. Dombrovsky, and L. Smith. “Analysis and Methodology to Characterize Heat Transfer Phenomena in Automotive Turbochargers”. In: *Journal of Engineering for Gas Turbines and Power* 137.GTP–14–1352 (2015), pp. 1–11. DOI: 10.1115/1.4028261 (cit. on pp. 21, 113, 145, 169).

[77] D. Porzig, H. Raetz, H. Schwarze, and J. Seume. “Thermal analysis of small high-speed floating-ring journal bearings”. In: *11th International Conference on Turbochargers and Turbocharging* (2014), pp. 421–436. DOI: 10.1533/9781000342.421. URL: http://linkinghub.elsevier.com/retrieve/pii/B9780081000335500342 (cit. on p. 22).

[78] L San Andrés and J Kerth. “Thermal effects on the performance of floating ring bearings for turbochargers”. In: *Proceedings of the Institution of Mechanical Engineers, Part J: Journal of Engineering Tribology* 218.5 (2004), pp. 437–450. ISSN: 1350-6501. DOI: 10.1243/1350650042128067. URL: http://pij.sagepub.com/lookup/doi/10.1243/13506500421 28067 (cit. on p. 22).

[79] I. A. Mohd, S Rajoo, and A. N. Darus. “Heat Distribution Study on Turbocharger Turbine’s Volute”. In: *Jurnal Mekanikal* 35 (2012), pp. 63–81. URL: http://mech.utm.my/wp-content/uploads/2017/01/6-Heat-Distribution-Study-onTurbocharger-Turbines-Volute{_}revised{_}version.pdf (cit. on p. 22).

[80] M Drewczynski and R Rzadkowski. “A stress analysis of a compressor blade in partially blocked inlet condition”. In: *Proceedings of the Institution of Mechanical Engineers, Part G: Journal of Aerospace Engineering* 230.5 (2016), pp. 934–952. DOI: 10.1177/0954410015601149. URL: http://journals.sagepub.com/doi/10.1177/0954410015601149 (cit. on p. 22).

[81] D. Filsinger, J. Szwedowicz, and O. Schafer. “Approach to Unidirectional Coupled CFD–FEM Analysis of Axial Turbocharger Turbine Blades”. In: *Journal of Turbomachinery* 124.1 (2002), p. 125. ISSN: 0889504X. DOI: 10.1115/1.1415035. URL: http://turbomachinery.asmedigitalcollection.asme.org/article.aspx?articleid=1466279 (cit. on p. 22).

[82] S. M. Shafi, V Ramakrishna, and S Rajasekhar. “Thermal Analysis of Turbocharger by Varying Materials”. In: *International Journal and Magazne of engineering, technology, management and research* 2 (2015), pp. 1840–1844. ISSN: 2348-4845. URL: http://www.ijmetmr.com/olddecember2015/ShaikMohammedShafi-VVRamakrishna-SRajasekhar-A-111.pdf (cit. on p. 23).

[83] F. Bet and G. Sieder. “Dynamic Simulating Systems - Multi-disciplinary design exploration unleashing simulation”. In: *Computational Thermal Management of Transient Turbocharger Operation* (), pp. 1–56. URL: www.cd-adapco.com/magazine (cit. on pp. 23, 24).

[84] X. Zheng, L. Jin, T. Du, B. Gan, F. Liu, and H. Qian. “Effect of temperature on the strength of a centrifugal compressor impeller for a turbocharger”. In: *Proceedings of the Institution of Mechanical Engineers, Part C: Journal of Mechanical Engineering Science* 227.5 (2013), pp. 896–904. ISSN: 09544062. DOI: 10.1177/0954406212454966 (cit. on pp. 24, 25).

[85] X. Zheng and C. Ding. “Effect of temperature and pressure on stress of impeller in axial-centrifugal combined compressor”. In: *Advances in Mechanical Engineering* 8.6 (2016), pp. 1–11. ISSN: 16878140. DOI: 10.1177/1687814016653547 (cit. on p. 25).

[86] R. Burke, C. Copeland, and T. Duda. “Investigation into the Assumptions for Lumped Capacitance Modelling of Turbocharger Heat Transfer”. In: *University of Bath* (2014) (cit. on p. 26).

[87] R. D. Burke, C. D. Copeland, T. Duda, and M. A. Rayes-Belmote. “Lumped Capacitance and Three-Dimensional Computational Fluid Dynamics Conjugate Heat Transfer Modeling of an Automotive Turbocharger”. In: *Journal of Engineering for Gas Turbines and Power* 138.9 (2016), p. 092602. ISSN: 0742-4795. DOI: 10.1115/1.4032663. URL: http://gasturbinespower.asmedigitalcollection.asme.org/article.aspx?doi=10.1115/1.4032663 (cit. on p. 26).

[88] H. Roclawski, C. Oberste-brandenburg, and M. Böhle. “Conjugate Heat Transfer Analysis of a Centrifugal Compressor for Turbocharger Applications”. In: *International Symposium on Transport Phenomena and Dynamics of Rotating Machinery*. Hawaii, Honolulu, 2016, pp. 1–7 (cit. on p. 26).

[89] S. De Vos, K. Haehndel, T. Frank, F. Christel, and S. Abanteriba. “The Development of Turbine Volute Surface Temperature Models for 3D CFD Vehicle Thermal Management Simulations: Part 3: Exhaust Radial Turbine Volute Systems”. In: *SAE International Journal of Passenger Cars - Mechanical Systems* 7.2 (2014), pp. 2014–01–0648. ISSN: 1946-4002. DOI: 10.4271/2014-01-0648. URL: http://papers.sae.org/2014-01-0648/ (cit. on p. 26).

[90] U. Tomm, S. Weiske, A. Coksen, Y. Rafaa, and S. Münz. “Validation of a Heat Transfer Prediction Approach Inside Turbochargers and its Application on Turbocharged Engine Performance Analysis”. In: *Volume 8: Microturbines, Turbochargers and Small Turbomachines; Steam Turbines*. Charlotte: ASME, 2017, V008T26A003. ISBN: 978-0-7918-5095-4. DOI: 10.1115/GT2017-63195 (cit. on p. 26).

[91] Y. Song and C.-w. Gu. “Development and Validation of a Three-Dimensional Computational Fluid Dynamics Analysis for Journal Bearings Considering Cavitation and Conjugate Heat Transfer”. In: *Journal of Engineering for Gas Turbines and Power* 137.12 (2015), p. 122502. ISSN: 0742-4795. DOI: 10.1115/1.4030633. URL: http://gasturbinespower.asmedigitalcollection.asme.org/article.aspx?doi=10.1115/1.4030633 (cit. on p. 26).

[92] Y. Li, F. Liang, Y. Zhou, S. Ding, F. Du, M. Zhou, J. Bi, and Y. Cai. “Numerical and experimental investigation on thermohydrodynamic performance of turbocharger rotor-bearing system”. In: *Applied Thermal Engineering* 121 (2017), pp. 27–38. ISSN: 1359-4311. DOI: 10.1016/J.APPLTHERMALENG.2017.04.041. URL: https://www.sciencedirect.com/science/article/pii/S1359431117323724 (cit. on pp. 27, 28).

[93] S Bukovnik, G Offner, A Diemath, and L Smolik. “Turbocharger Dynamic Analysis: Advanced Design Simulation in Time Domain Using CFD Predicted Thermal Boundary Conditions”. In: *Technische Mechanik* 37 (2017), pp. 2–5. DOI: 10.24352/UB.OVGU-2017-117. URL: http://www.uni-magdeburg.de/ifme/zeitschrift{_}tm/2017{_}Heft2{_}5/32{_}Bukovnik.pdf (cit. on p. 28).

[94] B. Karpuschewski, F. Welzel, K. Risse, M. Schorgel, S. Kreter, and M. Putz. “Potentials for Improving Efficiency of Combustion Engines due to Cylinder Liner Surface Engineering”. In: *Procedia CIRP* 46 (2016), pp. 258–265. ISSN: 2212-8271. DOI: 10.1016/j.procir.2016.04.025. URL: www.sciencedirect.com (cit. on p. 29).

[95] V. W. Wong and S. C. Tung. “Overview of automotive engine friction and reduction trends–Effects of surface, material, and lubricant-additive technologies”. In: *Friction* 4.1 (2016), pp. 1–28. DOI: 10.1007/s40544-0

16-0107-9. URL: http://link.springer.com/10.1007/s40544-016-0107-9 (cit. on p. 29).

[96] M. Ahmed Ali and H. Xianjun. “Improving the tribological behavior of internal combustion engines via the addition of nanoparticles to engine oils”. In: 4 (2015), 347–358 (cit. on p. 29).

[97] S. Milojevic, R. Pesic, and D. Taranovic. “Determination of Losses Related to Friction within the Reciprocating Compressors – Influences of Tribological Optimization of Piston and Cylinder”. In: *13th International Conference on Accomplishments in Mechanical and Industrial Engineering DEMI*. Banja Luka, 2017, pp. 1–6 (cit. on p. 29).

[98] N. J. Morris, R. Rahmani, and H. Rahnejat. “A hydrodynamic flow analysis for optimal positioning of surface textures”. In: *Proceedings of the Institution of Mechanical Engineers, Part J: Journal of Engineering Tribology* 231.9 (2017), pp. 1140–1150. DOI: 10.1177/1350650117709672. URL: http://journals.sagepub.com/doi/10.1177/1350650117709672 (cit. on p. 29).

[99] M Burkinshawa and D Blackerb. “The high temperature tribological performance of turbocharger wastegate materials”. In: *11th International Conference on Turbochargers and Turbocharging: 13-14 May 2014: 13-14 May 2014*. Vol. 1384. Elsevier. 2014, p. 289 (cit. on p. 29).

[100] K. Bobzin and T. Brogelmann. “Minimizing Frictional Losses in Crankshaft Bearings of Automobile Powertrain by Diamond-like Carbon Coatings under Elasto-hydrodynamic Lubrication”. In: *Surface and Coatings Technology* 290 (2016), pp. 100–109. ISSN: 0257-8972. DOI: 10.1016/J.SURFCOAT.2015.08.064. URL: https://www.sciencedirect.com/science/article/pii/S0257897215302383 (cit. on p. 29).

[101] G. W. Stachowiak and A. W. Batchelor. *Engineering tribology*. 3rd ed. Elsevier Butterworth-Heinemann, 2006, p. 832. ISBN: 978-0-7506-7836-0. DOI: https://doi.org/10.1016/B978-0-7506-7836-0.X5000-7 (cit. on p. 29).

[102] C. M. Taylor. *Engine tribology*. Elsevier, 1993, p. 301. ISBN: 9780080875903 (cit. on pp. 30, 31).

[103] J. Frene, D. Nicolas, B. Degueurce, D. Berthe, and M. Godet. *Hydrodynamic lubrication : bearings and thrust bearings*. Elsevier, 1997, p. 470. ISBN: 9780080534312 (cit. on p. 30).

[104] A. Roslan, A. S. Ibrahem, and A. Hadi. “Metal additives composition and its effect on lubricant characteristic”. In: *AIP Conference Proceedings*. Vol. 1774. 040001. American Institute of Physics, 2016. DOI: 10.1063/1.4965083. URL: https://doi.org/10.1063/1.4965083https://doi.org/10.1063/1.4965083 (cit. on p. 30).

[105] M. M. Maru and D. K. Tanaka. “Consideration of Stribeck Diagram Parameters in the Investigation on Consideration of Stribeck Diagram Parameters in the Investigation on Wear and Friction Behavior in Lubricated Sliding”. In: *Journal of the Brazilian Society of Mechanical Science & Eng.* XXIX.1 (2007), p. 8. DOI: 10.1590/S1678-58782007000100009. URL: http://www.scielo.br/pdf/jbsmse/v29n1/a09v29n1 (cit. on p. 30).

[106] A. J. Caines, R. F. Haycock, and J. E. Hillier. *Automotive lubricants reference book*. Second edition. Pennsylvania: Professional Engineering Pub, 2004, p. 737. ISBN: 9781860584718 (cit. on p. 31).

[107] P. J. Blau. “The significance and use of the friction coefficient”. In: *Tribology International* 34.9 (2001), pp. 585–591. DOI: 10.1016/S0301-679X(01)00050-0. URL: https://www.sciencedirect.com/science/article/pii/S0301679X01000500 (cit. on p. 31).

[108] M. Ichiro. “Molecular Science of Lubricant Additives”. In: *Applied Sciences* 7.April (2017). DOI: 10.3390 (cit. on p. 31).

[109] M. Laad and V. K. S. Jatti. “Titanium oxide nanoparticles as additives in engine oil”. In: *Journal of King Saud University - Engineering Sciences* 30.2 (2018), pp. 116–122. DOI: 10.1016/J.JKSUES.2016.01.008. URL: https://www.sciencedirect.com/science/article/pii/S101836391600012X (cit. on p. 31).

[110] P. Andersson, J. Tamminen, and C.-E. Sandstrom. *Piston ring tribology A literature survey*. Ed. by Maini Manninen. Espoo, Finland, 2002, p. 108. ISBN: 951–38–6107–4. URL: https://www.vtt.fi/inf/pdf/tiedotteet/2002/T2178.pdf (cit. on p. 31).

[111] C. J. James. “Analysis of parasitic losses in heavy duty diesel engines”. PhD thesis. Massachusetts Institute of Technology, 2012, p. 131. DOI: 1721.1/74921. URL: https://dspace.mit.edu/handle/1721.1/74921 (cit. on p. 31).

[112] American Petroleum Institute. *Annex E—Api Base Oil Interchangeability Guidelines For Passenger Car Motor Oils And Diesel Engine Oils E.1 General*. 2015. URL: http://www.api.org/{~}/media/files/certification/engine-oil-diesel/publications/anne-rev-03-25-15.pdf?la=en (cit. on p. 32).

[113] Noria Corporation. *Understanding the Differences in Base Oil Groups*. Tech. rep. Machinery Lubrication, 2012. URL: https://www.machinerylubrication.com/Read/29113/base-oil-groups (visited on 07/02/2018) (cit. on p. 32).

[114] D. S. Viswanath. *Viscosity of liquids : theory, estimation, experiment, and data*. Springer, 2007, p. 660. ISBN: 1402054815 (cit. on p. 33).

[115] P. J. Shayler, A. J. Allen, D. K. W. Leong, I Pegg, A. J. Brown, and J.-C. Dumenil. "Characterising Lubricating Oil Viscosity to Describe Effects on Engine Friction". In: *JSAE/SAE International Fuels & Lubricants Meeting*. United States: SAE international, 2007. DOI: 10.4271/2007-01-1984. URL: http://papers.sae.org/2007-01-1984/ (cit. on p. 33).

[116] ASTM International. "Standard Test Method for Density, Relative Density, or API Gravity of Crude Petroleum and Liquid Petroleum Products by Hydrometer Method". In: *ASTM* D1298.July (2017). DOI: 10.1520/D1298-12BR17. URL: https://compass.astm.org/download/D1298.11799.pdf (cit. on p. 33).

[117] ASTM International. "Standard Test Method for Pour Point of Petroleum Products". In: *ASTM* D97.December (2017). DOI: 10.1520/D0097-17B. URL: https://compass.astm.org/download/D97.4665.pdf (cit. on p. 33).

[118] ASTM International. "Standard Test Method for Cloud Point of Petroleum Products and Liquid Fuels". In: *ASTM* D2500.January 2018 (2017). DOI: 10.1520/D2500-17A. URL: https://compass.astm.org/download/D2500.35295.pdf (cit. on p. 33).

[119] ASTM International. "Standard Test Methods for Flash Point by Pensky-Martens Closed Cup Tester". In: *ASTM* D93 (2016). DOI: 10.1520/D0093-16A. URL: https://compass.astm.org/download/D93.36165.pdf (cit. on p. 34).

[120] ASTM International. "Standard Test Method for Flash and Fire Points by Clevelenad Open Cup Tester". In: *ASTM* D92 (2016). DOI: 10.1520/D0092-16B. URL: https://compass.astm.org/download/D92.4457.pdf (cit. on p. 34).

[121] ASTM International. "Standard Test Method for Acid Number of Petroleum Products by Potentiometric Titration". In: *ASTM* D664.December (2017). DOI: 10.1520/D0664-17A. URL: https://compass.astm.org/download/D664.20424.pdf (cit. on p. 34).

[122] ASTM International. “Standard Test Method for Base Number of Petroleum Products by Potentiometric Perchloric Acid Titration 1”. In: *ASTM* D2896.December (2015). DOI: 10.1520/D2896-15. URL: https://compass.astm.org/download/D2896.31866.pdf (cit. on p. 34).

[123] SAE Standard. *Engine Oil Viscosity Classification (J300 Ground Vehicle Standard)*. Tech. rep. USA: SAE, 2015. URL: https://saemobilus.sae.org/content/J300{_}201501/{\#}datasets (cit. on p. 34).

[124] ACEA Oil Sequences. *Service Fill Engine Oils For Gasoline &Amp; Light Duty Diesel Engines (A/B Categories), Gasoline &Amp; Light Duty Diesel Engines With Exhaust Aftertreatment Devices (C Categories), And Heavy Duty Diesel Engines (E Categories)*. Tech. rep. ACEA, 2016, p. 14. URL: https://www.acea.be/uploads/news{_}documents/ACEA{_}European{_}oil{_}sequences{_}2016{_}update.pdf (cit. on p. 35).

[125] P. Sharma and P. Jayaswal. “Wear Rate Measurement (Ic Engine) Using Lubricant Oil Testing Method”. In: *IJREAS International Journal of Research in Engineering & Applied Sciences* 2.22 (2012). ISSN: 2249-3905. URL: http://www.euroasiapub.org (cit. on p. 35).

[126] H. B. Jun, D. Kiritsis, M. Gambera, and P. Xirouchakis. “Predictive algorithm to determine the suitable time to change automotive engine oil”. In: *Computers and Industrial Engineering* 51.4 (2006), pp. 671–683. ISSN: 03608352. DOI: 10.1016/j.cie.2006.06.017 (cit. on p. 36).

[127] H.-B. Jun, F. L. Conte, D. Kiritsis, and P. Xirouchakis. “A Predictive Algorithm for Estimating the Quality of Vehicle Engine Oil”. In: *International Journal of Industrial Engineering* 15.4 (2008), pp. 386–396 (cit. on p. 36).

[128] D Deng, F. Shi, L. Begin, I Du, and General Motors. “The Effect of Oil Debris in Turbocharger Journal Bearings on SubSynchronous NVH”. In: *SAE International* 2015-01-12.April (2015). DOI: 10.4271/2015-01-1285 (cit. on pp. 36, 38, 165, 176).

[129] A. Siddaiah, Z. Khan, R. Ramachandran, and P. Menezes. “Performance Analysis of Retrofitted Tribo-Corrosion Test Rig for Monitoring In Situ Oil Conditions”. In: *Materials* 10.10 (2017), p. 1145. DOI: 10.3390/ma10101145. URL: http://www.mdpi.com/1996-1944/10/10/1145 (cit. on p. 36).

[130] J Black, P. G. Eastwood, K Tufail, T Winstanley, Y Hardalupas, and A. M. K. P. Taylor. “The Effect of VGT Vane Control on Pumping Losses during Full-Load Transient Operation of a Common-Rail Diesel Engine”. In: *SAE Naples Section* 2007-24-0063 (2007). DOI: 10.4271/2007-24-0063 (cit. on p. 36).

[131] M. Ghazikhani, M. Davarpanah, and S. A. M. Shaegh. "An experimental study on the effects of different opening ranges of waste-gate on the exhaust soot emission of a turbo-charged DI diesel engine". In: *Energy Conversion and Management* 49.10 (2008), pp. 2563–2569. ISSN: 01968904. DOI: 10.1016/j.enconman.2008.05.012 (cit. on p. 36).

[132] J. R. Serrano, P. Olmeda, A. Tiseira, L. M. Garcia-Cuevas, and A. Lefebvre. "Theoretical and experimental study of mechanical losses inautomotive turbochargers". In: *Energy* 55 (2013), pp. 888–898. ISSN: 03605442. DOI: 10.1016/j.energy.2013.04.042. URL: http://dx.doi.org/10.1016/j.energy.2013.04.042 (cit. on pp. 37, 38, 155).

[133] F. Owrang, H. Mattsson, J. Olsson, and J. Pedersen. "Investigation of oxidation of a mineral and a synthetic engine oil". In: *Thermochimica Acta* 413.1-2 (2004), pp. 241–248. ISSN: 00406031. DOI: 10.1016/j.tca.2003.09.016 (cit. on p. 37).

[134] K. Yang, K. A. Fletcher, J. P. Styer, W. Y. Lam, and G. H. Guinther. "Engine Oil Components Effects on Turbocharger Protection and the Relevance of the TEOST 33C Test for Gasoline Turbocharger Deposit Protection". In: *SAE International Journal of Fuels and Lubricants* 10.3 (2017), pp. 2017–01–2341. DOI: 10.4271/2017-01-2341. URL: http://papers.sae.org/2017-01-2341/ (cit. on p. 37).

[135] M. F. Moreira. "Failure analysis in aluminium turbocharger wheels". In: *Engineering Failure Analysis* 61 (2016), pp. 108–118. ISSN: 13506307. DOI: 10.1016/j.engfailanal.2015.11.024. URL: http://dx.doi.org/10.1016/j.engfailanal.2015.11.024 (cit. on p. 38).

CHAPTER 3

Experimental tests

Contents

Figures

Tables

3.1 Introduction

THE study of heat transfer in automotive turbochargers helps to evaluate and understand some of turbocharger damages which may affect the engine performance. Bearings clogged, damages in the shaft, oil coke formation and other failures are because of high temperatures inside the turbocharger in a different engine operating conditions to which the cars are exposed daily. In this chapter, a description of the thermal characterization and oil coking tests in turbochargers is presented.

- section 3.2 describes the engine test bench set-up used for all experimental campaign. It includes description of the engine, specifications of the turbocharger units used and description of the lubrication system.
- section 3.3 describes the sensors location in the turbocharger and test bench; also the engine hot stop duty cycle used for turbocharger thermal characterization and endurance tests of oil coking is presented.
- section 3.4 presents the thermal characterization procedure done in the fully instrumented turbocharger and the evaluation of heat transfer effect by using a normal and thermal decoupled turbine housing.
- section 3.5 presents the endurance tests of oil coking in turbochargers. The test procedure employed, the influence factors with contaminated oils at different levels soot and oxidation and the inspection criteria used to study the oil coking problem in turbochargers are described.

3.2 Experimental set-up

The experimental work carried out is focused on the thermal characterization of turbocharger and the endurance tests of oil coking to see the impact that degraded oils have in the performance of the turbocharger and bearing system under engine hot-stop conditions.

In this section, the experimental facilities used to characterize non-water cooled automotive turbochargers are described in detail. Then, the experimental campaign used to globally study the oil coking phenomena is presented.

3.2.1 General description of the experimental test cell

The studies required to achieve the general objective in this thesis contemplate several experiments. The most important part has been done using an engine test bench. This singular facility consists of three main components named as follows:

- An internal combustion engine (E)
- Turbocharger Units (T)
- An independent lubrication system (L)

The IC diesel engine characteristics are presented in subsection 3.2.2. The most interesting engine variables are: torque, speed, fuel consumption and air flow at the inlet. Temperature and pressure sensors are installed in the main engine components. The engine is placed in a test bench with an asynchronous dynamometer. Different driving cycles can be simulated in the dynamometer. In this thesis an engine hot stop cycle will be used for the whole test campaign. A PXI system let the control sensors and actuators in the engine through Electronic Control Unit (ECU) and record them by using the data collection device.

First, a fully instrumented turbocharger is used for thermal characterization. Afterwards, twelve turbochargers with the same characteristics are used for endurance test of coking. The probes location are described in subsection 3.3.2.

The independent lubrication system is one of the most important components, the oil can be provided only to the turbocharger system without the dependence of engine oil pump. The lubrication system is important especially in the endurance tests of coking where the oil used to feed the turbocharger has been intentionally contaminated. The schematic layout of experimental set-up is shown in Figure 3.1.

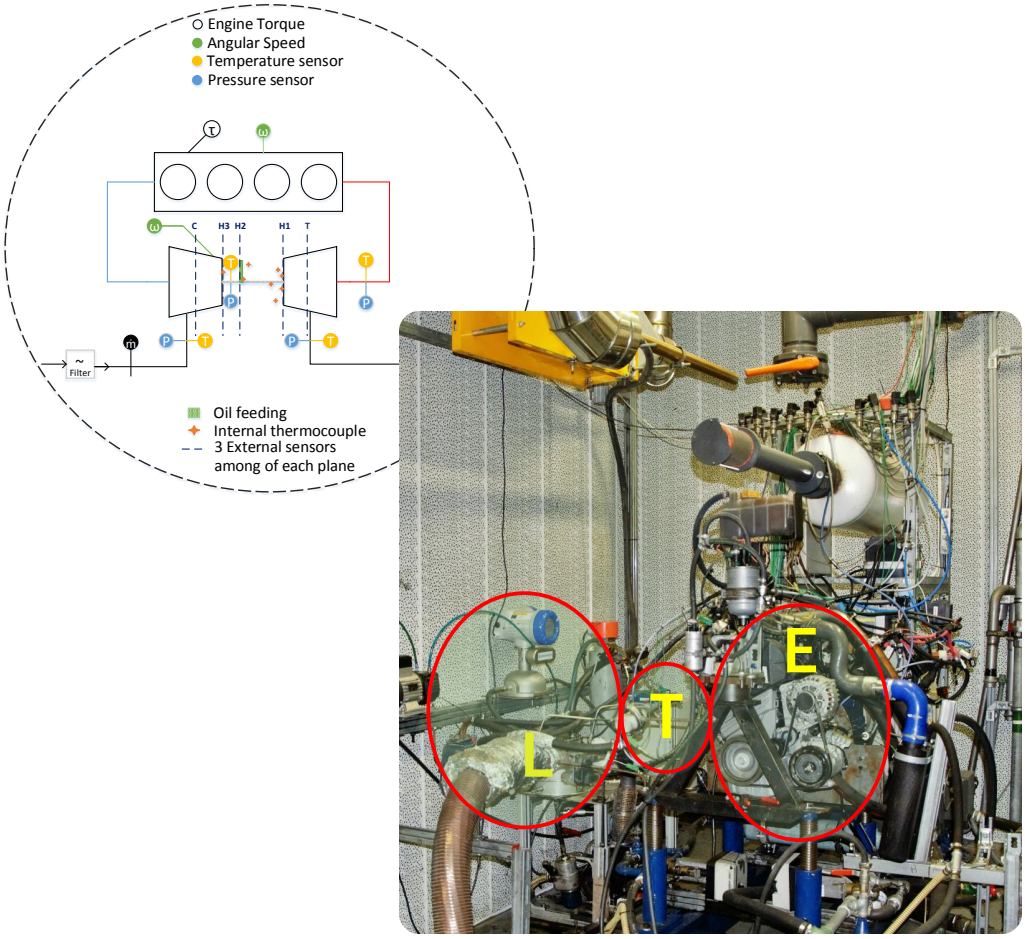

Figure 3.1: Schematic layout of experimental set-up

3.2.2 Description of the Diesel engine

The engine used for the tests is an in-line four-cylinder turbocharged diesel engine with a volumetric capacity of 1.5 litres, an engine torque of 260 Nm over a wide speed range from 1750 to 2500 rpm. The engine is a high power version with variable geometry turbocharger. The maximum power output varies depending on the emission standards. This engine complies with Euro 6 standards and has a power of 110 HP (81 kW).

The engine is placed in a test bench and is instrumented to measure torque, speed, temperature in the exhaust line , injected mass of fuel and mass flow in the intake line. For the turbocharger thermal characterization, fifteen engine operating points are used and listed in Table 3.1. Every engine operating

condition has a stabilization time of ten minutes and an equivalent deceleration time that corresponds to an engine hot stop cycle described in subsection 3.3.3. References to the operating points will be made throughout the whole document. These points of operation can be adapted according to the specifications of the

Table 3.1: Engine operating points

Speed	**Load [%]**					**Deceleration**
[rpm]	**100**	**75**	**50**	**33**	**25**	**time [s]**
1500	✓	✓		✓		10
1750	✓					10
2000	✓		✓			10
2500	✓	✓	✓		✓	10
2750	✓					10
3000	✓		✓			20
3500	✓		✓			30

research project by adding extra specific operating points (i.e scrubbing strategy for the EGR system, double supercharging transition regime)

3.2.3 Turbocharger specifications

In this section, a brief description of the turbocharger used in the experimental tests is given. Table 3.2 shows the main characteristics of the turbochargers used in the thermal characterization procedure and oil coking tests.

3.2.4 Independent lubrication system

An independent lubrication system is used for controlling oil flow, oil temperature, and oil pressure in the turbocharger, making it independently from the engine oil pump. The oil flow rate and pressure are controlled by means of an oil pump and a pressure control valve. The temperature is controlled by using an electrical heater and a cooler. The oil mass flow rate to the turbocharger is measured by means of a Coriolis flow meter. Lubrication inlet and outlet temperatures are measured by means of low uncertainty platinum resistance temperature detectors. Periodic samples of oil can be taken from the independent lubrication system in order to characterize oil properties such as viscosity, total acid number (TAN), total base number (TBN), density, oxidation, nitration, soot content and apparent pH. The oil inlet temperature to the turbocharger for all test carried out was regulated between 80 and 90 °C. Figure 3.2 shows the independent lubrication system used for the turbocharger.

Table 3.2: Main characteristics of turbochargers used

Turbocharger Parameter	**Thermal Characterization / Coking Tests [mm]**
Turbine wheel diameter	41
Compressor wheel diameter	49
Turbine inlet diameter	37
Compressor inlet diameter	36
Oil external diameter	8
Turbine external diameter	170.8
Bearing Housing external diameter	70
Compressor external diameter	123
Turbine external length	70
Bearing Housing external length	31
Compressor external length	32
Journal bearing radius	3
Journal bearing length	14.3
Journal bearing height	14
Minimum thrust bearing radius	5.1
Maximum thrust bearing radius	7
Mean thrust bearing radius	5.4
VGT	Yes
Water cooled	No
Type of journal bearing	fixed floating

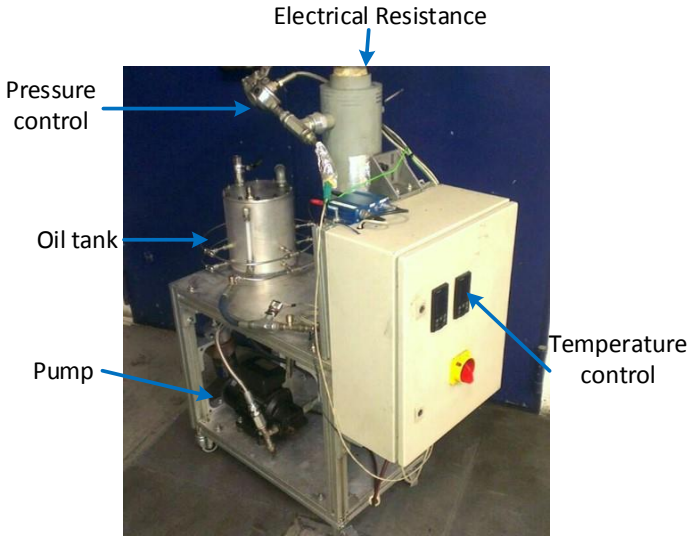

Figure 3.2: Independent lubrication system

3.3 Test description

3.3.1 Engine sensors

Temperature and pressure sensors are installed at the inlet and outlet pipes of the compressor and turbine according to supercharger testing standard [136] and turbocharger gas stand test code [137]. All thermocouple sensors are located in the external and internal surface of the turbocharger housing in order to estimate heat fluxes. For measuring the temperature in the turbocharger and in the engine, K-type thermocouples were used with an accuracy of ± 2.2 K. The turbocharger inlet, outlet and oil ducts were not insulated with the aim of study the phenomenon under most real engine driving conditions.

Piezoresistive 4260A Kistler pressure sensors were used at the inlet and outlet of the main elements of the installation. They are medium pressure transducers with ±0.05% accuracy in full scale range of 5 bar. All pressure sensors were located apart from the installation through fittings and pipes to prevent accidental vibrations or breakages. They are able to withstand temperatures up to 200 °C. The air mass flow in the engine is measured with two hot plate SIEMENS 5WK9 621 PBT-GF30 flow meters. One is located upstream of the engine and another right after this. The flow meters work through the thermal principle of a hot film anemometer. With this measuring method, the mass flow of air can be determined directly. The standard volumetric flow can also be displayed considering the normal density of gas without additional compensation of pressure or temperature.

The oil flow rate meter used is based on the principle of Coriolis. The mass flow rate of oil causes a change in the phase of oscillation between the input and output of the equipment. This delay is proportional to the mass flow, creating an amplification that corresponds to the output signal. Coriolis flow meter used for measuring the oil flow passing through the turbocharger is a KROHNE optimass 3300. The range and uncertainty of sensors are summarized in Table 3.3

Table 3.3: Transducer specifications

Variable Measured	Type	Range	Uncertainty
Temperatures	K Thermocouple	273 K to1100K	± 2.2 K
Internal Temperatures	K Thermocouple	273 K to 1100 K	± 2.2 K
Oil mass flow	Coriolis flow meter	0 to 100 kg/h	1 kg/h
Compressor/Turbine mass flow	Thermal flow meter	0 to 600 kg/h	± 2%
Pressure	Piezoresistive	0 to 500 kPa	0.05% full scale
Turbocharger speed	Inductive	0 to 400 krpm	500 rpm

For each test; the engine speed, torque, fuel temperature and turbocharger deceleration time is required. The control is carried out with two systems of acquisition one is SAMARUC and another is INCA. The latter performs the reading and control of the ECU (Engine control Unit).

3.3.2 Turbocharger sensors

The turbocharger speed has been measured with an inductive sensor placed in the compressor side. The sensor is able to measure both aluminium and titanium blades. The sensor can be mounted at a relatively large distance from the blade. Maximum distance of 2.2 mm enables reliable operation. A threaded hole is machined in the volute of compressor and the sensor is placed in such a way that the clearance between sensor surface and the compressor blades is less than 1 mm.

Temperature surface probes were adopted in the 5 planes external division of the turbocharger (three thermocouples distributed every 120 degrees on each plane). This division is taken from previous experimental works done to characterize thermal properties of tubocharger axially [58, 59]. The planes are turbine side (T), backplate turbine (H1), central housing (H2), blackplate compressor (H3) and compressor side (C) of the turbocharger. Figure 3.3 shows external and internal location of the thermocouples in turbocharger used for thermal characterization tests. The experimental characterization is performed for validation of the different subsystems that conform a full turbocharger model developed and explained in Chapter 5.

Table 3.4 summarizes the temperature sensors in the turbocharger central housing.

Table 3.4: Description turbocharger thermocouple sensors

Nº	**Internal turbocharger thermocouple Location**
01	Radial Bearing on the compressor side
02	Radial Bearing on the turbine side
04	Bearing housing, turbine side piston at 180°
05	Bearing housing, internal oil return slope
06	Bearing housing, close to oil feeding
07	Bearing housing, close pads of thrust bearing
08 to 11	Bearing housing, near sealing surface to turbine housing positions every 90°
12	Bearing housing near heat shield support

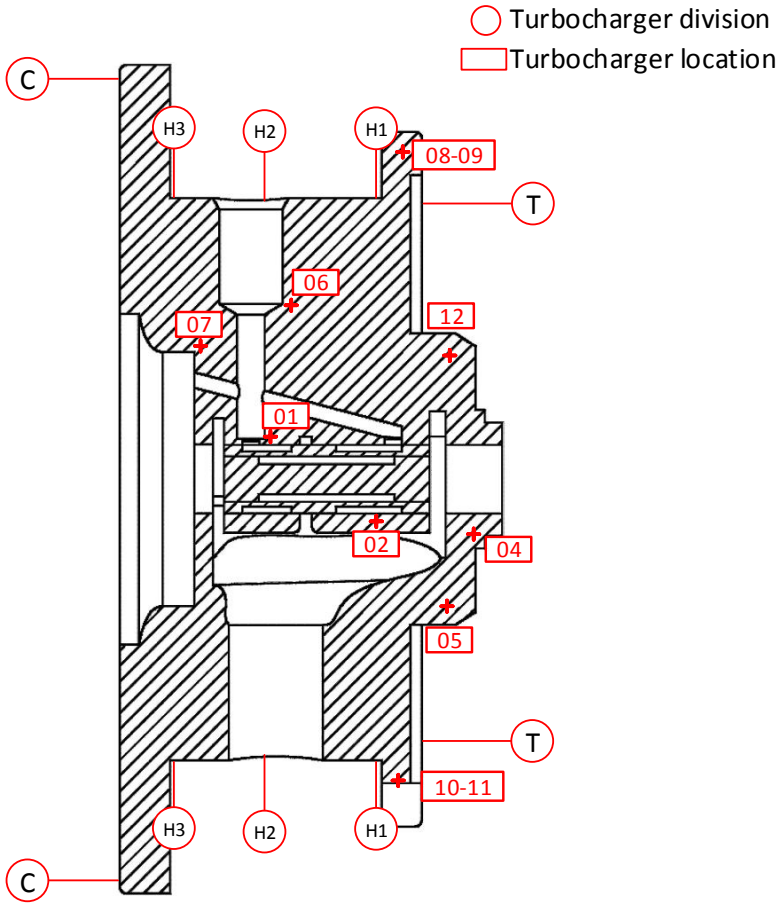

Figure 3.3: Generic turbocharger - thermocouple probes

3.3.3 Engine cycle

In this thesis, the study of oil coking problem and the heat transfer modelling validation in turbochargers will be done under an engine hot stop cycle. This engine cycle is representative of real driving conditions. Such as the case of a hot stop after driving in a highway.

These driving conditions can promote the formation of coke inside the turbocharger, due to the high temperatures reached in the oil trapped inside. Bearing temperature is primarily important because bearings are the critical links between the rotating and stationary components in a machine. Lubricant under thermal stress, can settle in the form of coke or varnish in the rotating assembly of the turbocharger. Dirt, soot, fuel, water, combustion residues, or metal abrasion can also contaminate the oil. These deposits may clog the oil

supply lines or block the turbochargers rotation. Engine manufacturers predefine these cycles in order to ensure that the studied parameters do not exceed some limits that are detrimental for the engine life. Figure 3.4 shows the engine cycle, it is divided in four main parts:

- A stabilization phase with steady state conditions (X in Figure 3.4). At the end of this phase, the temperatures in the bearing system should be constant.
- A deceleration phase (D in Figure 3.4) done with a calibrated duration according to the previous point of operation used in stabilization phase.
- A quick stop of the engine, in which circulation of water, oil and air through the turbocharger are cut for an allotted period (Y in Figure 3.4). This hot stop phase produces peak temperatures in the central housing and, thus, in the bearings sometime after stopping the engine.

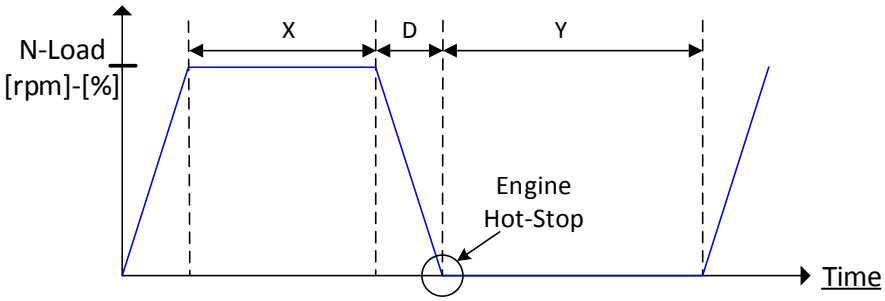

Figure 3.4: Hot stop engine cycle

The evaluation of temperature evolution at different parts of the turbocharger by using this engine cycle will be studied in the experimental and the modelling chapters.

3.4 Thermal characterization in turbochargers

The main objective is to measure the maximum level of temperature in different parts of the bearing system of the turbocharger under engine hot stop cycle (see Figure 3.4). Ensuring that during the set-up phase of the cycle, the load, as well as the time of deceleration and engine hot stop are suitable to reach the desired thermal in the central housing of the turbocharger in a relatively limited engine operating points.

This thermal characterization will help to define the conditions for the endurance test of oil coking. This includes calibration of engine speed, fuel consumption, and time needed to let the turbocharger reach thermal stabilization and maximum temperatures in the bearing system, taking into account its thermal inertia.

The main conditions for all tests are:

- Tests conducted at room temperature (ambient condition)
- No cooling air during the tests
- Additional engine water pump switched off
- No water either oil circulation during the engine hot-stop phase
- New engine oil SAE 5W-30
- Data acquisition frequency of 1 Hz

Characterization results are considered valid if the temperatures of oil, bearings and housing have been held constant at the end of stabilization phase (last 100 seconds of phase X in Figure 3.4), and if under the engine stop (phase Y in Figure 3.4), no water, air or oil is flowing through the turbocharger.

3.4.1 Experimental results of thermal characterization

Evolution of temperatures measured in the whole cycle (steady and transient conditions) are shown in Figure 3.5 for two segments of the turbocharger; one close to the radial bearing on the turbine side and another at bearing housing (drain wall), both of which are influential in the coke formation due to their high temperatures.

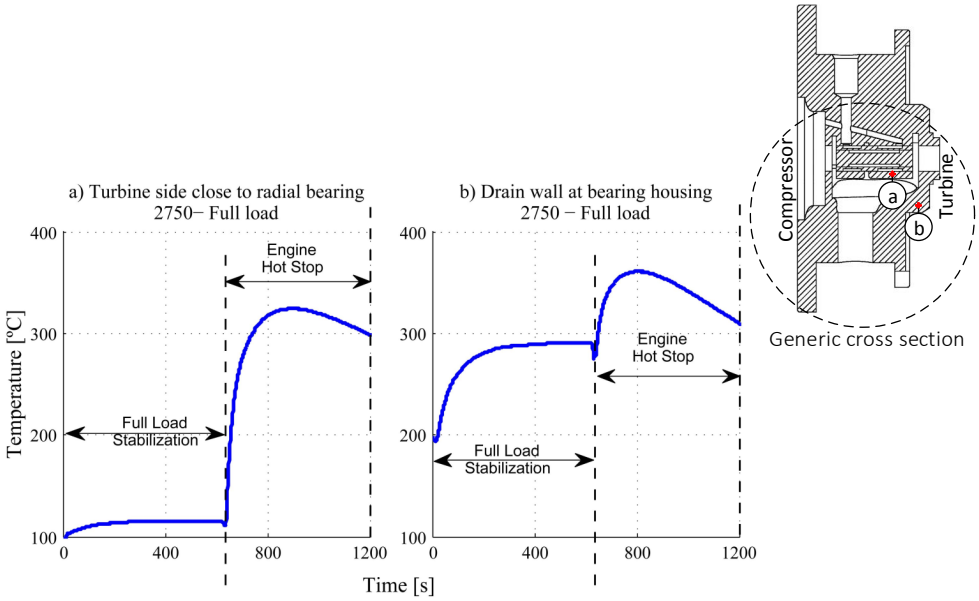

Figure 3.5: Turbocharger temperatures evolution under engine hot stop cycle

The temperature of the fluids through turbine and compressor, as well as their surface temperatures have been monitored and stabilized before engine hot stop. From the Figure 3.5 temperatures are stabilized over 10 minutes (see Figure 3.4 (engine cycle)). After, when the engine stops (phase Y in Figure 3.4), the temperature in the bearing system rises and reaches its maximum peak values in the cycle. Temperatures rise during the engine hot stop because of internal heat transfer through turbocharger bearing housing. The heat exchanges are mainly due to energy accumulated in the material and not due to the turbine gas temperature. These maximum temperatures in the bearing system must conform to the technical specifications of the component, or heat induced damage occur [138].

In total, 15 steady-state points have been tested varying several parameters to evaluate the engine hot-stop cycle. Global analysis of these points is presented. The Figure 3.6 shows the maximum wall temperature during engine hot stop (Y in Figure 3.4) for radial bearing of the turbine side (thermocouple 02 of Figure 3.3) and bearing housing - drain wall (thermocouple 05 of Figure 3.3) for the sweep of engine operating points already described in Table 3.1.

For each test, the parameters of engine speed, torque, turbine gas inlet temperature, as well as oil inlet temperature have been controlled and held constant. The input variables of pressure, temperature, mass flow and speed have been measured for the turbocharger.

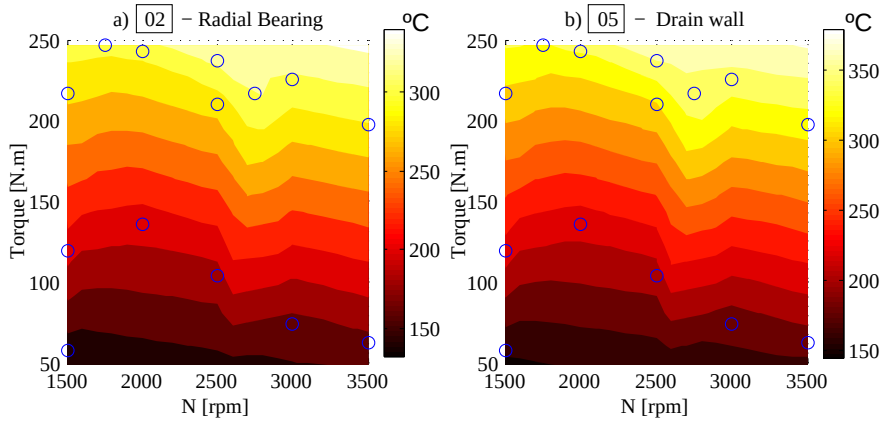

Figure 3.6: Maximum turbocharger temperatures during engine hot stop

Internal measurement analysis. The Table 3.5 shows a summary of the maximum internal temperatures in the bearing housing of a non-water cooled turbocharger after engine hot-stop for fifteen operating points shown in Table 3.1 and measured in the engine test bench. The Nº Thermocouple refers to the specific segment inside the turbocharger (refer to Figure 3.3 or Table 3.4).

With the engine hot stop the turbocharger continues running and the bearing, system reaches high temperatures. The backplate turbine side (thermocouples from 08 to 11) exchanges huge amounts of heat with the central housing as it cools down, increasing the temperature of the small amounts of oil trapped inside the turbocharger.

In lubricants, the autoignition temperature varies considerably depending on the circumstances. For example, a conventional engine synthetic lubricant will tolerate temperatures between 590 °F and 680 °F (310-360°C) [139]. In particular, synthetic engine oil SAE 5W30 used in these experiments can be ignited in a normal atmosphere without an external ignition source with temperatures above 608 °F / 320 °C [140].
Moreover, Figure 3.7 shows the safe, dangerous and critical temperatures for conventional engine oil within the bearing system. The oil burns or coke from 410 °F (210 °C). The curve represents the temperature at the turbine bearings with and without lubrication after an engine stop [138]. A high thermal load for the oil can cause burns or degradation leading to clogging of the oil passages and bearings, consequently reducing the oil mass flow. This reduction in oil flow leads

Table 3.5: Turbocharger maximum internal temperatures during engine hot-stop phase

Nº Thermocouple	01	02	04	05	06	07	08	09	10	11	12
Op. points [rpm-%]	**Turbocharger Internal temperatures [ºC]**										
1500-FL	252	285	330	316	246	240	362	350	386	347	315
1500-75FL	185	209	244	231	180	177	270	265	285	258	232
1500-33FL	134	150	173	164	131	129	191	190	200	182	165
1750-FL	272	305	352	337	266	258	389	372	409	372	336
2000-FL	272	305	351	337	266	258	391	373	410	372	336
2000-50FL	188	209	237	228	184	181	263	259	276	252	228
2500-FL	288	325	375	361	278	273	424	404	443	400	359
2500-75FL	257	**289**	331	**318**	251	244	371	360	389	351	317
2500-50FL	174	193	217	209	171	168	242	239	252	231	209
2500-25FL	133	147	166	160	131	129	186	184	193	178	160
2750-FL	289	**324**	375	**361**	279	273	414	406	446	401	358
3000-50FL	158	173	192	187	155	153	220	218	227	208	187
3000-FL	282	317	364	352	275	267	424	408	442	393	350
3500-FL	268	299	340	330	262	255	412	399	421	372	328
3500-50FL	160	174	194	190	157	154	228	227	233	212	188

to a loss of bearing load capacity and cooling performance, enabling mechanical wear and thermal damage, which may be noticed some time after it has occurred.

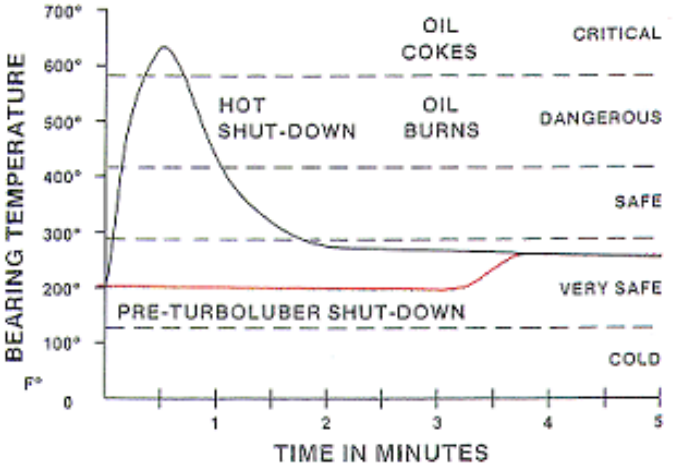

Figure 3.7: Conventional engine oil temperatures [138]

External measurement analysis. Figure 3.8 shows temperature evolution in the five external division: turbine side (T), backplate turbine (H1), central housing (H2), blackplate compressor (H3) and compressor side (C). The evolution of the temperature is shown along the engine cycle described in Figure 3.4.

The cut of oil cooling inside the turbocharger produces a notable heat exchange. The H2 plane represents the majority of central housing mass and handles the biggest part of the oil flow. The heat flow grows to a heat exchange, reaching maximum peaks of up to 287 °C for full load and regime of 2750 rpm. The compressor side (C and H3) reach maximum temperatures of 287 °C (about 33°C higher than when the engine is operating at high loads). All the external planes reach convergence temperature after 10 minutes.

In the hottest spot of the turbocharger, the turbine side reach temperatures of 697 °C followed by a drop in temperature once the engine is stopped. The turbine side (T and H1) loses heat due to external convection, while the other nodes reach their maximum temperature later.

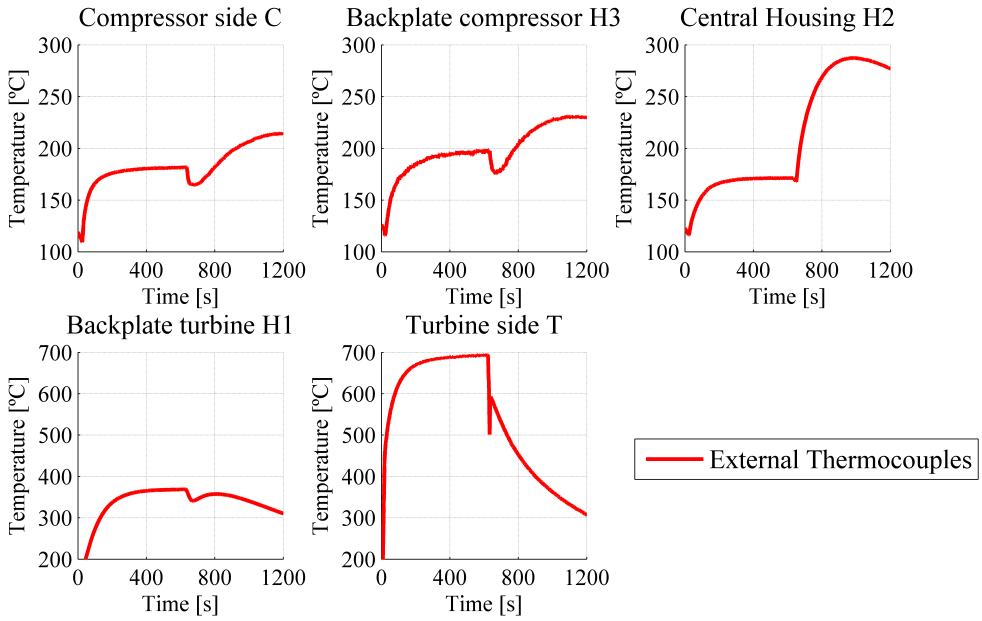

Figure 3.8: Turbocharger external temperatures evolution in the five division zone at 2750rpm/full load

Figure 3.9 shows the maximum external wall temperatures for fifteen engine operating points in the five external division.

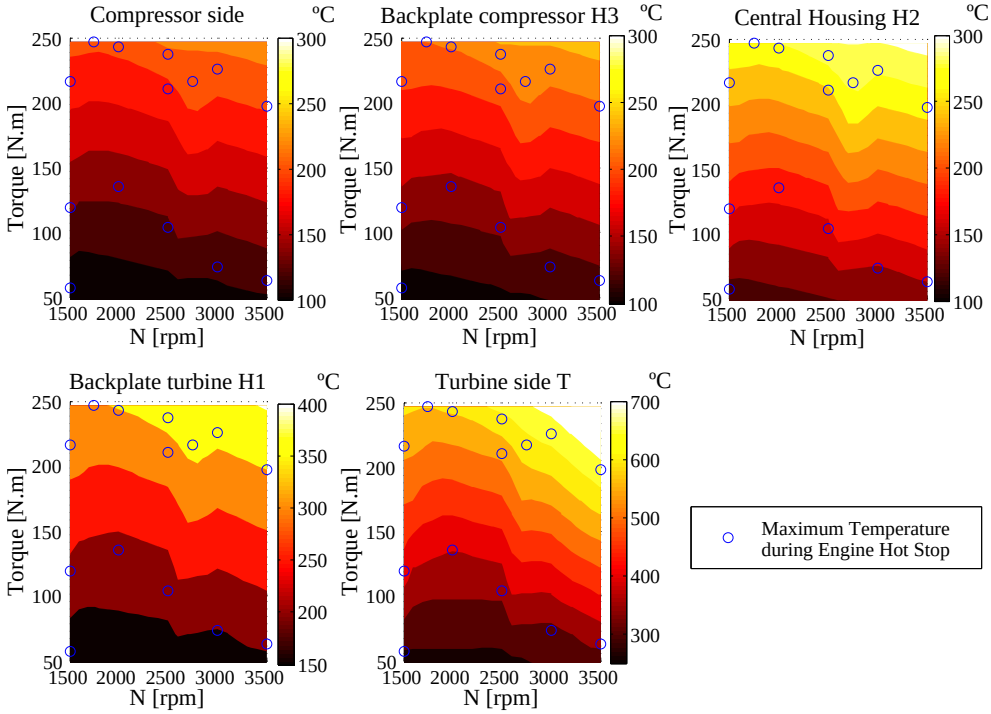

Figure 3.9: Maximum turbocharger external temperatures in the five division at engine hot stop

3.4.2 Turbine thermal decoupling

A study of the thermal sensitivity by greater or lesser thickness of wall in the turbine housing is done. The idea with thermal decoupled turbine is to radiate more heat out, by reducing the thermal bridge between turbine housing and the turbocharger central housing. Experimental tests and simulations with a 1D heat transfer model are performed.

The analysis of turbocharger heat transfer is done under the 15 engine operating points described in Table 3.1 and under engine hot stop cycle (see Figure 3.4). The test conditions and facility are the same as described in the thermal characterization (section 3.4). The Figure 3.10 shows both turbine housings used in the experiments. The “housing 1”, refers to a conventional full contact turbine without any flange and greater radial surface mostly implemented in automotive turbocharged engines and the “housing 2” refers to thermal decoupled turbine with lesser radial transfer surface to the turbocharger central housing.

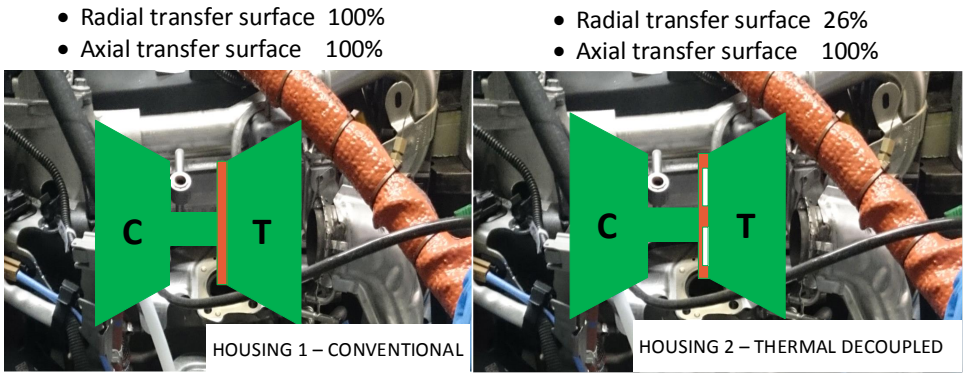

Figure 3.10: Conventional turbine housing and thermal decoupling turbine housing

The same turbocharger of thermal characterization tests is used in the thermal decoupling tests. Therefore, sensors location are the same as shown in Figure 3.3. The results are shown in 4 representative engine operating points to analyse the thermal decoupled design.

The Figure 3.11 shows the experimental results of temperatures for the five external planes of the turbocharger using conventional and thermal decoupled housings. The temperatures are sorted from the coldest to the hottest part of the turbocharger as follow: compressor side (C), blackplate compressor (H3), central housing (H2) and Turbine side (T) (see Figure 3.3). The “ST” refers to the maximum temperature reached in the stabilization phase and “HS” refers to the maximum temperature reached during the engine hot stop phase of the engine cycle already described in Figure 3.4.

In Figure 3.11 it can be seen that during the "HS" phase, the heat gradients from the compressor node (C) to the backplate turbine (H1) are slightly lower with the conventional turbine housing 1 compared to the test where thermal decoupled housing 2 was used. While in steady state "ST" for the same nodes (C to H1) no considerable differences can be observed between the both tests. Regarding the turbine side (T), the thermal decoupled solution seems to accumulate less heat.

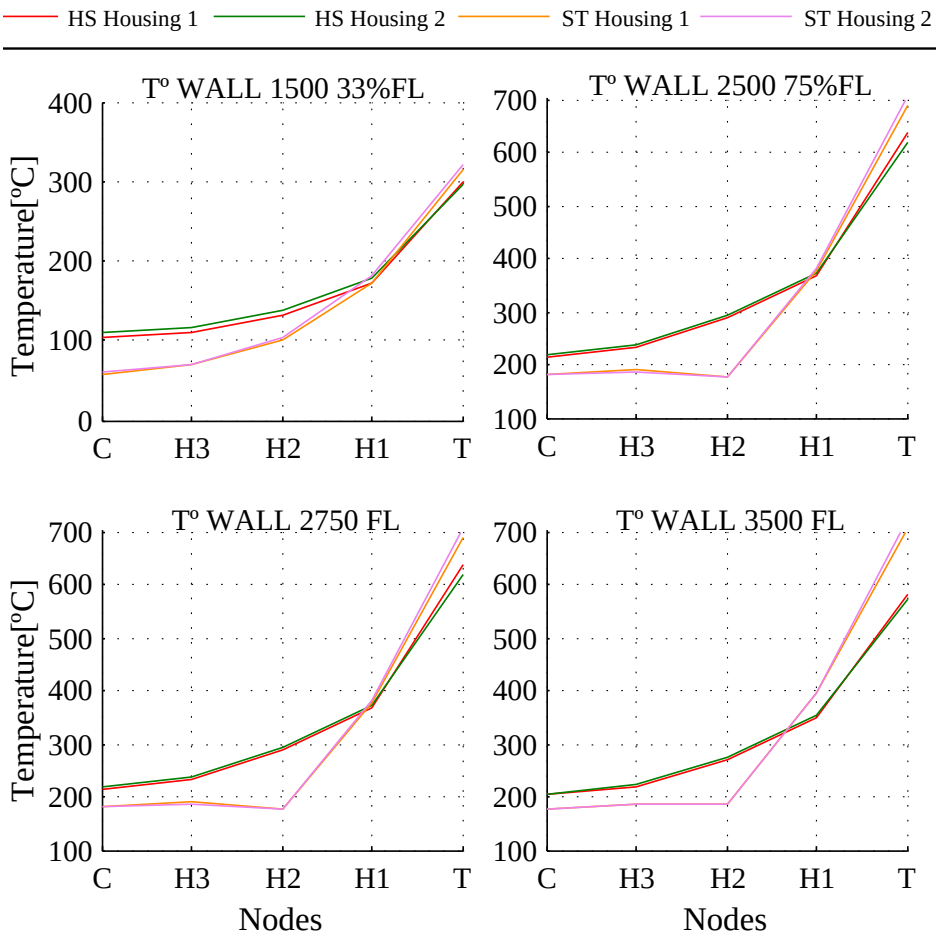

Figure 3.11: Maximum turbocharger external temperatures during engine hot-stop

Internal temperatures in the turbocharger are also analysed. Figure 3.12 shows the maximum internal wall temperatures in the central housing from the coldest to hottest sections(see Figure 3.3) under steady and hot stop phase. The thermal decoupled housing 2 produces internal temperatures slightly higher, especially in the blackplate turbine near to the sealing surface (thermocouples 08 to 11). The average of temperature is around 10 °C higher over this area for all engine-operating points measured. While by keeping a full contact surface between the central housing and turbine using conventional housing 1, the turbocharger is able to dissipate heat. The inlet temperature of the gas turbine (blue lines) Figure 3.12 has been held constant in both test, therefore, this is not a variable that influences in the differences observed in the tests.

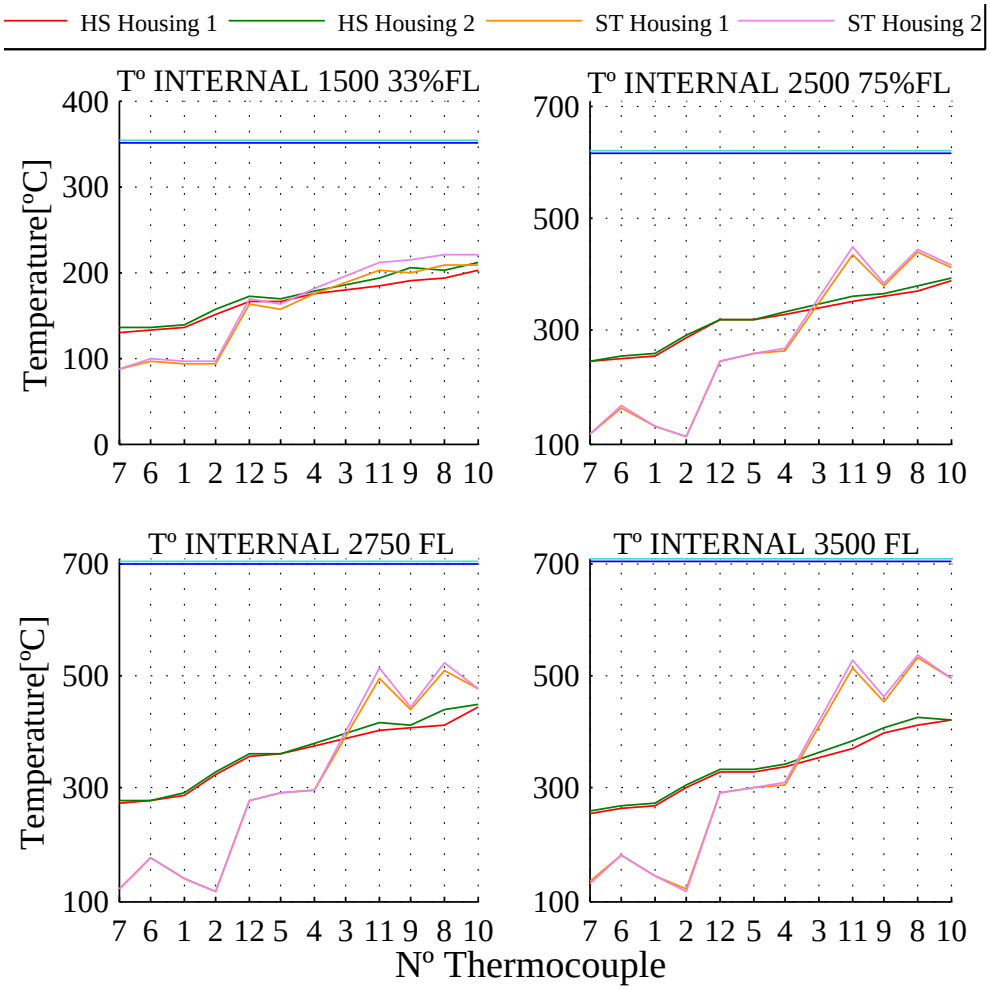

Figure 3.12: Maximum turbocharger internal temperatures during engine hot-stop

3.5 Endurance tests of oil coking in turbochargers

This section defines the procedure in engine test bench for endurance tests of cokefaction, to ensure the robustness of the technical definition retained on this type of fault. One of the critical conditions of use from the point of view of the oil coking is the engine hot stop.

During severe hot stops, the lubricant can under thermal stress, settle in the form of varnish or coke on the rotating assembly of the turbocharger. These deposits can go as far as blocking the oil supply lines or blocking the rotation of the turbocharger. The endurance tests consist in carrying out in the engine a number of critical stops to ensure the robustness of the turbocharger to coked oil.

The cycle of hot stop is characterized by:

- A phase stabilized with a high temperature of exhaust gases.
- An engine hot-stop.
- A sufficient period of time to reach the maximal internal temperatures during the hot-stop phase.

The idea of coking test thus is to reproduce many times these conditions to be representative in the most severe drivers. The tests are performed on a stationary engine test bench. During stabilized phase, the water temperature at the outlet of the engine is regulated for each operating point according to the thermal characterization of the bearing system. During phase of engine stop, the temperature of water should not be regulated and circulation of oil and water cut. The stabilized phase and engine stop corresponds to the engine cycle already described in Figure 3.4. The calibration of both phases takes 10 minutes. This period allows a steady thermal state and also lets the turbocharger reach the maximum temperatures in the bearing system after engine stops.

In order to illustrate the method, endurance tests are carried out by repeating one hundred times the engine cycle under one of the selected engine operative condition. Two steady operating points from thermal characterization (section 3.4) have been chosen for performing the endurance test and thereafter evaluate the oil coking influence in turbocharger performance.

Table 3.6 shows the working conditions chosen and maximum temperature reached in the bearing housing system during an engine hot stop. Performance parameters of the engine and turbocharger are monitored with the following operative conditions. This type of test does not require a specific instrumentation in the turbocharger. The frequency of acquisition is 10 Hz for the temperatures. The acquisition parameters (regime, load, turbine inlet temperature) helps to

Table 3.6: Temperatures in the bearing system for two engine operating conditions

Engine Speed [rpm]	Load [%]	Torque [N.m]	Radial Bearing [°C]	Drain Wall [°C]
2500	75	210.3	289	318
2750	100	216.6	324	367

ensure that the set of cycles are performed correctly in accordance with the initial set-up cycle, without any fluctuation that may affect the conclusions.

In addition, the endurance tests require provisioning of oil at different levels of aging and oxidation. Since the lubricant used can not be degraded in a totally controlled manner during the tests, oil changes are performed to study different lubricant wear conditions. This supply of oil goes through the recovery of used oil baths from other endurance tests, engine runs or artificial aged oil.

3.5.1 Test matrix

The Table 3.7 shows test matrix used for oil coking evaluation with the characteristics of each oil, the temperature that was reached in the bearing system during the thermal characterization and the operative point to perform the 100 cycles. Two different multi-grade aged oils have been used: an oil in a mean drainage interval and an oil near the maximum drainage interval. These motor oils are SAE grade 5W30 that follows the ACEA C4 quality specification and the SAE 10W40 that follows ACEA A3/B4-10 quality specifications. The oils used are referred for simplicity in this thesis with letters “A” and “C” respectively. Both oil types are contaminated at levels of 4% and 7% of soot content (impure carbon particles resulting from the incomplete combustion of hydrocarbons). Besides, these oils are oxidized by the heat to a degree reflecting the chemical condition of the oil being circulated in the engine and that carry the chemistry in its path through the turbocharger. In total 8 conditions of aged and/or oxidized oil have been used in the oil coking campaign.

For each test, the oil quantity placed in an independent lubrication system is 5 litres. In order to prevent excessive deterioration or malfunction of any component, a filter in the lubrication circuit is implemented to prevent the passage of the larger pollutant particles that could be generated along the tests and that appear in the oil circuit.

Table 3.7: Matrix for oil coking tests

Oil type	Soot content [%]	Bearing T [°C] (turbine)	Oil drain T [°C] (carter)	Engine Operating Point
A	4	324	361	2750 FL
A	4	289	318	2500 75% FL
A	7	289	318	2500 75% FL
A	7	324	361	2750 FL
C	4	289	318	2500 75% FL
C	7	289	318	2500 75% FL
C	4	324	361	2750 FL
C	7	324	361	2750 FL
A oxy	4	289	318	2500 75% FL
A oxy	7	289	318	2500 75% FL
C oxy	4	289	318	2500 75% FL
C oxy	7	289	318	2500 75% FL

After a set of 100 cycles in a turbocharger unit, the independent lubrication system is cleaned, the next corresponding oil type is replaced and a new turbocharger unit of the same model is replaced in the engine test bench.

3.5.2 Criterion Post-endurance test of cokefaction

The performance parameters of the engine and turbocharger have been monitored to study how they are influenced by formation of oil coke.

To provide a criterion for quantifying the coking level at the end of an endurance test, different inspection criteria measurements have been study. A brief description of each technique used is explained below:

Oil properties analysis. Periodic samples of oil are taken each 25 cycles from the independent lubrication system in order to characterize properties of viscosity, density, oxidation, nitration, soot content, apparent pH, total acid number (TAN) and total base number (TBN).

Oil flow monitoring. The oil cokefaction results in a reduction of passage in the flow sections. This restriction generates a diminution of flow in the central housing. Quantify the diminution of the mass flow will allow to determine the maximum level of fouling acceptable. The Equation 3.1 is used to determine a discharge coefficient for the turbocharger based on the mass flow:

$$\dot{m}_{oil} = A_G \cdot C_D \sqrt{2\rho_{oil}(\Delta p)} \tag{3.1}$$

Where A_G is the geometric area at the oil inlet port in m^2, ρ_{oil} is a correlation for five oil density samples taken at the mean temperature and Δp is the difference of pressure between the inlet and outlet ports of the central housing. The oil density ρ_{oil} is a function of the average temperature at the oil inlet and outlet as follows:

$$\rho_{oil} = f(\bar{T}_{oil}) = a_i - b_i(\bar{T}_{oil}) \tag{3.2}$$

Delta pressure is defined as:

$$\Delta_p = \mathbb{K}\frac{1}{2}\rho_{oil}\frac{\dot{m}^2}{\left(A_G\rho_{oil}\right)^2} \tag{3.3}$$

Where $\mathbb{K}$ is an unknown exponential function dependent on the Reynolds number which expresses the ratio of inertial forces to the viscous forces:

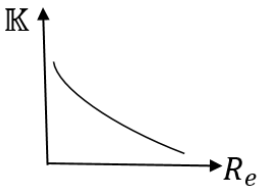

Figure 3.13: Exponential function dependent on the Reynolds number

$$R_e = \frac{uD_{oil_{in}}}{\upsilon} \tag{3.4}$$

To determine the $\mathbb{K}$ it would be necessary to do a test for many operating conditions where oil flow, oil density, Reynolds, viscosity were taken into account and then calculate u term. In this work this has not been considered. Therefore, the oil viscosity will not be explicit in the equation but through (Δ_p) it is expected to have larger delta pressure with more viscous oils.

Turbocharger efficiency. The compressor and turbocharger efficiency, the exhaust gas temperature influences, the heat fluxes and the material temperatures in the turbocharger are analyzed. The turbine efficiency can change due to changes in the heat losses for the turbine stage but also due to variations in the clearances. Depending on the turbocharger design, the exhaust gas temperature can also influence the wall temperatures in the compressor stage and consequently its efficiency. These effects are strongly size-dependent, being important for small turbochargers. The pressure losses in pipes after the compressor may be higher, resulting in a lower turbo charging efficiency. The

compressor efficiency can be calculated by the ratio of compressor isentropic work and the compressor work by using Equation 3.5.

$$\eta_c = \frac{T_{iC} \cdot \left[\left(\frac{P_{oC}}{P_{iC}} \right)^{\frac{(\gamma-1)}{\gamma}} - 1 \right]}{T_{oC} - T_{iC}} = \frac{\dot{w}_{Cs}}{w_C} \tag{3.5}$$

From Equation 3.5, P represents the pressures and T temperatures, the subscripts oC and iC mean at the outlet and inlet of the compressor respectively.

The turbocharger efficiency is calculated using Equation 3.6, where (η_T), (η_{mech}) and (η_c) are the turbine, mechanical and compressor efficiencies respectively. It is equal to the ratio between compressor and turbine isentropic power.

$$\eta_{TC} = \eta_T . \eta_{mech} . \eta_c = \frac{\dot{w}_{Cs}}{\dot{w}_{Ts}} \tag{3.6}$$

The isentropic power in the turbine side, can be calculated using Equation 3.7, where the subscripts oT and iT mean at the outlet and inlet of the turbine respectively.

$$\dot{w}_{Ts} = \dot{m}_{iT} . C_p . T_{iT} . [1 - (\frac{P_{oT}}{P_{iT}})^{\frac{(\gamma-1)}{\gamma}}] \tag{3.7}$$

Engine torque and VGT position. These parameters have been taken into account as global variables. The engine torque is monitored for seeing how flexible or how much force can be expressed in a given gear over the course of 100 engine hot stop cycles and generally to evaluate the engine performance after the whole endurance tests campaign. Likewise, the idea is to see how the ECU regulates the inflow angle and the inflow speed at turbine wheel inlet through the VGT position to compensate pumping losses and the thermal losses while maintaining a high level of efficiency in the turbocharger.

Weight of turbocharger. A criterion at the end of tests could be the mass of coked oil in the system. However, this criterion may not be transversal, if there exists difference between a family of turbocharger and another (size of the lube deposits in particular). In this case, the turbocharger units used have the same characteristics. All turbochargers are weighed before and after an endurance test of cokefaction removing the compressor housing. After 100 cycles before weighing again the turbocharger must be clean of liquid oil. Therefore, the remaining liquid is evaporated by passing the turbocharger through a special oven and only keeping the cooked oil.

Maximum static eccentricity. Measurements before and after endurance tests of the main orbital forces described by the rotating assembly are carried out on each turbocharger under the same conditions (assembly and temperature of components). The aim is to measure deflections of the rotating assembly and/or quantify the diminution of the gap induced by the coke deposits after the endurance test. The eccentricity technique is well known and is very refined thanks to previous works carried out at the CMT institute [141, 142]. This technique consists of taking a series of 41 photos to the nut positioned in front of the wheel of the compressor to determine the displacement of the axis on a fixed central point. Four photos each 45° making a force in the axis from the turbine side in direction north, south, east and west (total of 32 photos) and another nine photos turning the axis each 45° without making any force. To facilitate detection of the nut, it is painted with white and black vanes, to erase the brilliance in the photos that can cause measurement errors at the time of processing. It is also essential to have the turbocharger and the camera fixed and stable. Once the photos are taken, they are processed to make an approximation in millimetres of axis movement with the force applied in each photo. An image recording methodology and a process algorithm developed in a previous work [141] have been used, in order to estimate the maximum eccentricity. This processing consists on differentiating specific zones of the image, in order to obtain their coordinates. Two reference points have been configured on the compressor side, which help to calculate the relative position of the shaft. The aim is to superpose the displacement of the same turbocharger before and after the endurance test of oil coking, and to study this difference of shaft eccentricity.

The eccentricity can be calculated with Equation 3.8:

$$\epsilon = \sqrt{1 - \frac{(\frac{b}{2})^2}{(\frac{a}{2})^2}} \tag{3.8}$$

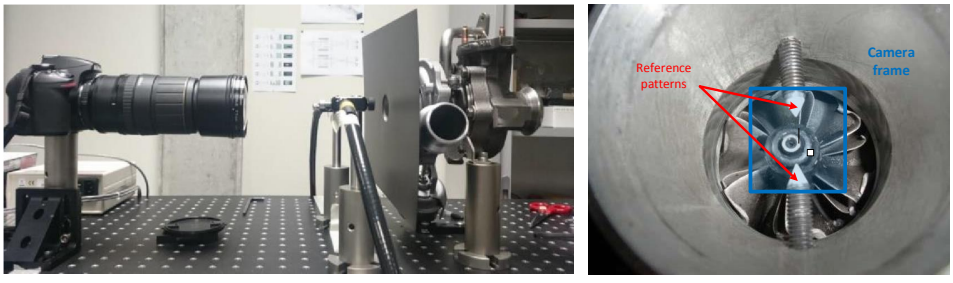

Figure 3.14: Static eccentricity assembly

Turbocharger deceleration time. The diminution of the gap may be because of the increment of resistive torque on the rotating assembly. This torque is too slow for being measured. During hot stop, the turbocharger keeps rotating on the inertia effect. The measurement of the time diminution of rotation once the engine is stopped along the tests could be a criterion of level of fouling in the bearing system for each turbocharger tested. It is important to take care of the setting up of the speed sensor.

Oil temperature monitoring. The oil delta temperature between inlet port and the carter is calculated to see the progressive trend of the friction torque in the bearing system under the influence of oil temperature during stabilization and hot stop phase.

To sum up, Table 3.8 shows the inspection criteria used to study of oil coking problem in turbochargers. The necessary instrumentation, the time interval to perform each technique, the frequency of acquisition and whether the technique requires the disassembly of the turbocharger is presented.

Table 3.8: Inspection criteria used for the study of oil coking problem in turbochargers

Measurement Technique	Instrumentation	Before ENDURANCE TESTS	During ENDURANCE TESTS	After ENDURANCE TESTS	Acquisition Frequency	Disasembling
Oil properties analysis	Oil sampling + oil lab analysis	YES	YES (1/25) cycles	YES	5 times / TURBO	NO
Oil flow monitoring	Oil mass flow & pressure sensors	NO	YES	NO	10 Hz	NO
Turbocharger Efficiency	Pressure and Temperature sensors	NO	YES	NO	10 Hz	NO
VGT and Torque	Data analysis	NO	YES	NO	10 Hz	NO
Weight of turbos	Digital weighing scale	YES	NO	YES (after thermal conditioning)	2 times/ TURBO	YES (only volutes)
Maximum eccentricity	High sensitivity camera + picture analysis software	YES	NO	YES	2 times/ TURBO	YES (compressor housing)
Turbo deceleration time	Inductive turbo speed sensor	NO	YES	NO	10 Hz	YES (compressor housing)
Oil temperature Monitoring	Thermocouples	NO	YES	NO	10 Hz	NO

3.5.3 Experimental results of coking tests

A comparison of the inspection criteria used for all test is discussed in this section.

Oil properties analysis. The impact on the oil is analysed and the results are exposed in Figure 3.15 and Figure 3.16 where multiple quantitative variables are compared. These charts allow to have a view of how the variables change with respect to the initial measurement taken and along the endurance test, which is ideal for the visualization of the impact in the oil. The results are displayed on a relative scale.

- **Soot Measurement:** The soot content has been quantified using a FT-IR spectrometer device and results have been correlated with the initial pre-sooted characterization (reference values). A remarkable reduction at the beginning of the different test has been observed. It may be possible that as a result of the storage and waiting period before the test procedure, the soot content has been decanted into the oil can.

  This situation has led to lower soot content but furthermore lower oxidation level and lower viscosity. During and after the different endurance tests of cokefaction negligible soot content variation has been observed. For oil "C", only one test has shown an abnormal beginning level probably as a consequence of cross-contamination (oil residues in the oil tank from previous test).

- **Oxidation:** Attending the measurement system used for oxidation quantification (FT-IR) it can be easily observed that higher soot content is translated in higher oxidation level. During the tests performed, a slightly increase in oxidation level has been observed in both oils, probably as consequence of the thermal stress suffered on turbocharger lubrication. The FT-IR measurements in oils oxidized with high soot content have shown no variation, due to interference of the oil condition.

- **Kinematic Viscosity (KV) @100°C:** Values reached for KV depend on fresh oil original viscosity (5W30 vs 10W40) and pre-soot level. During the tests a slightly decrease trend can be observed as a consequence of the shearing effects suffered by oil in the turbocharger. Oil "A" (5W30) has shown better performance in terms of soot handling and viscosity along the test (better formulation according analysis from oil experts at CMT department).

- **TAN/TBN and Apparent pH:** Many problems have been experienced regarding nitration measurements because of a combination of abnormally degraded samples and measurements equipment limitation.

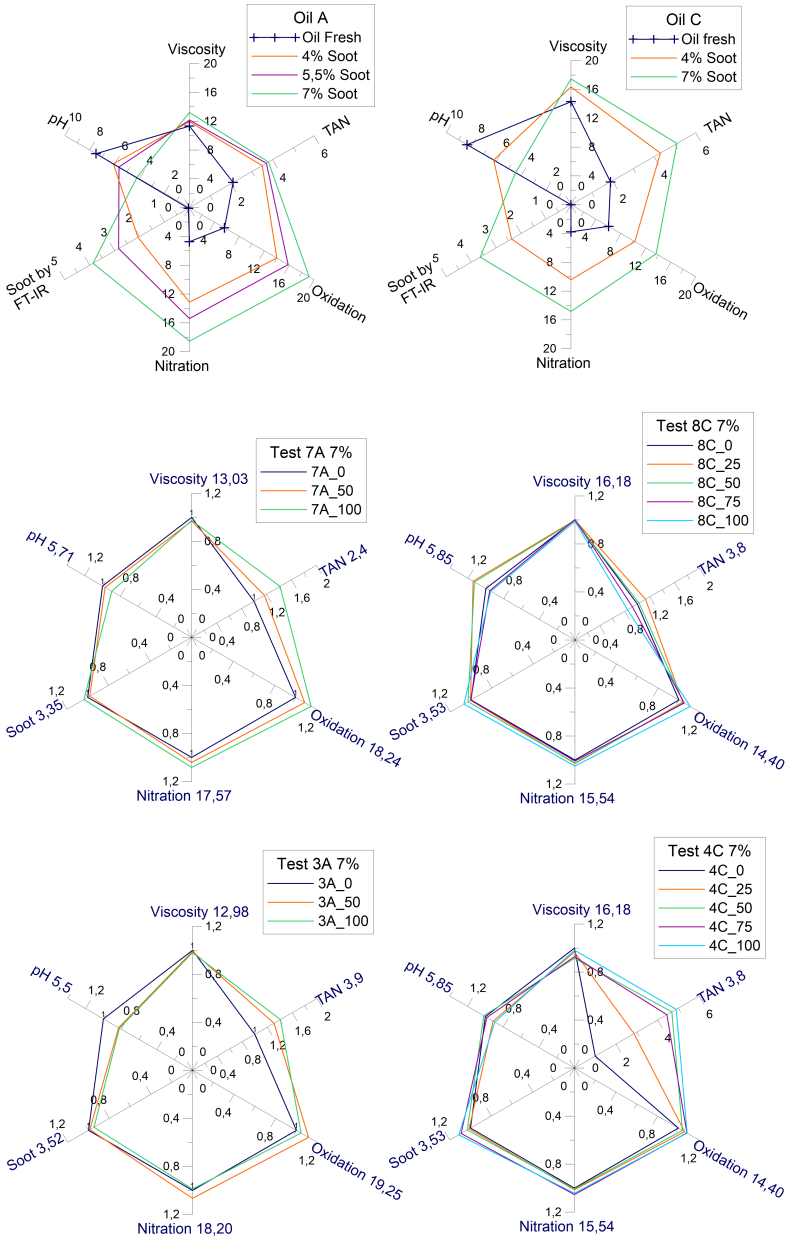

Figure 3.15: Oil properties measurements for oils “A” and “C” type

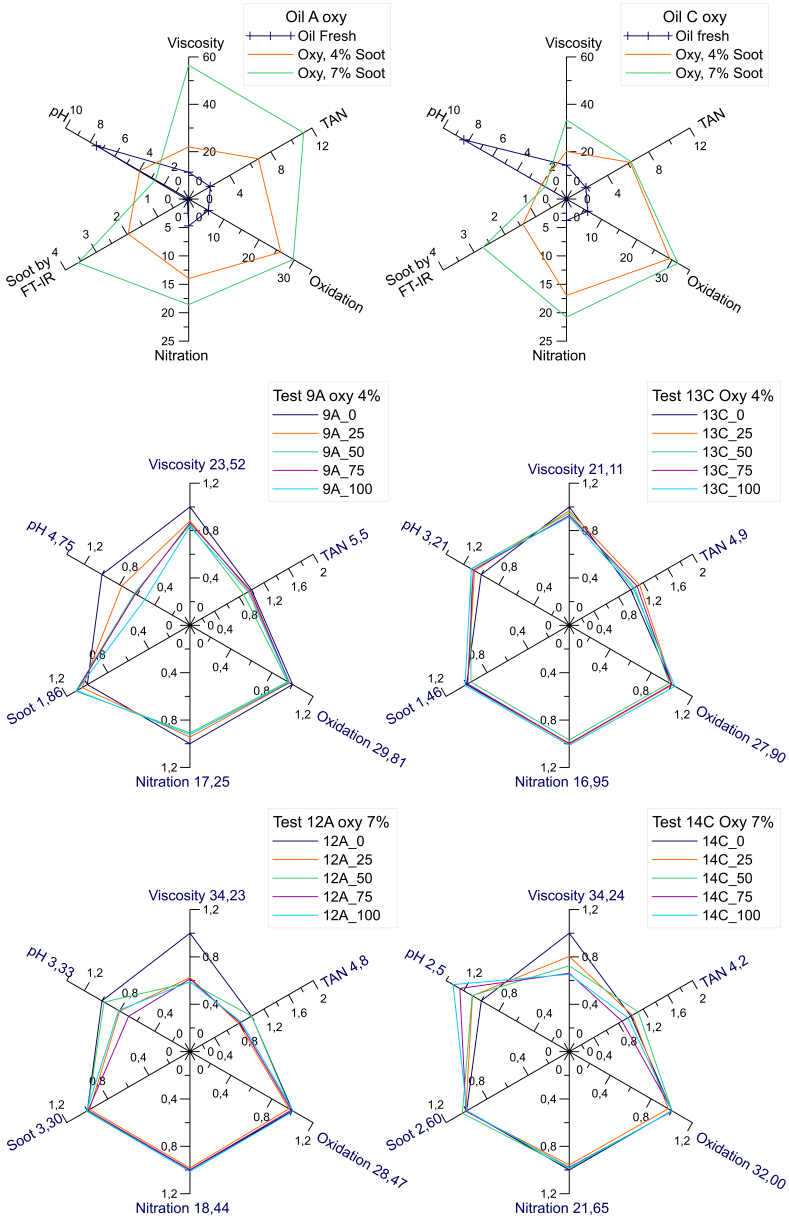

Figure 3.16: Oil properties measurements for oils “Aoxy” and “Coxy” type

Oil “A” shown a somewhat increasing trend during tests in TAN and consequently a slightly decrease in terms of apparent pH. Oil “C” performance related with those parameters can be considered erratic.

Turbocharger Performance

The engine operating point is kept constant for each cycle. During the endurance test, the acquisition parameters of the engine (speed, load, turbine inlet temperature) ensure that the set of cycles is carried out correctly without fluctuations that may affect the main conclusions of oil coking in the turbocharger.

The Figure 3.17, shows on the left hand the instantaneous data recorded for an engine cycle. On the right hand, the same engine variables are exposed as an average at the end of the stabilization phase at 600 seconds (Turquoise circle) before engine shut down for the set of hundred cycles. Turbocharger conditions such as temperatures at the inlet and outlet of the compressor and turbine side, mass flow rates, VGT position and turbocharger speed have been monitored during the experimental test campaign.

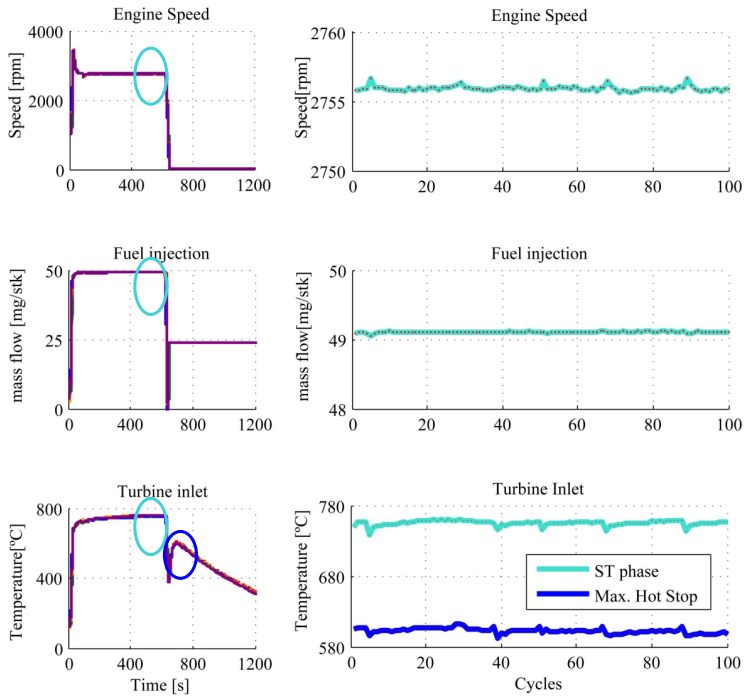

Figure 3.17: Engine control variables for endurance tests

The general procedure to measure and post-process the fundamental magnitudes involved during the whole engine operation is described in the following paragraphs. Data is obtained and processed for twelve turbocharger units.

Oil flow monitoring. Deposits of coke on bearing surfaces (internal and external) decreases the operating clearances shaft / bearing and bearing / central housing. This reduction could be quantified through the ratio of the oil mass flow rate passing through the turbocharger, which expands an identical working fluid from the same initial conditions to the same exit pressures.

Figure 3.18, shows the discharge coefficient transition along the 100 engine cycles. Dots in figures represent an average of the last phase of thermal stabilization before proceeding engine shut down. The first sub-plot a) indicates the discharge coefficient for oil types “A” and “C” both with 4% and 7% soot level at engine speed of 2750 rpm and full load; there can be seen a higher reduction of effective section in tests with oil A at 7% soot and C at 4% soot. The sub-plot b) indicates the discharge coefficient for oil types “A” and “C” and its oxidized counterpart “Aoxy” and “Coxy” oils, all of them measured with 7% of soot and at lower engine operating point (2500 rpm engine speed and 75% of full load); The “Aoxy” and “Coxy” oils suffer a bigger reduction of the oil passage through lubrication sections of the turbocharger with respect to “A” and “C” oils. Additionally in “A” and “C” oils the flow rate reduction is almost the same for both. The subplot c) shows all oxidized oils used in the endurance test of cokefaction. “Aoxy” and “Coxy” at 4% and 7% of soot concentration measured at (2500 rpm engine speed and 75% of full load). There can be observed that the reduction of the effective section is sorted by oil type, and soot content; the higher soot content, the greater reduction of the effective section. Turbochargers tested with “Coxy” oil suffer a bigger reduction in the effective section of oil passage.

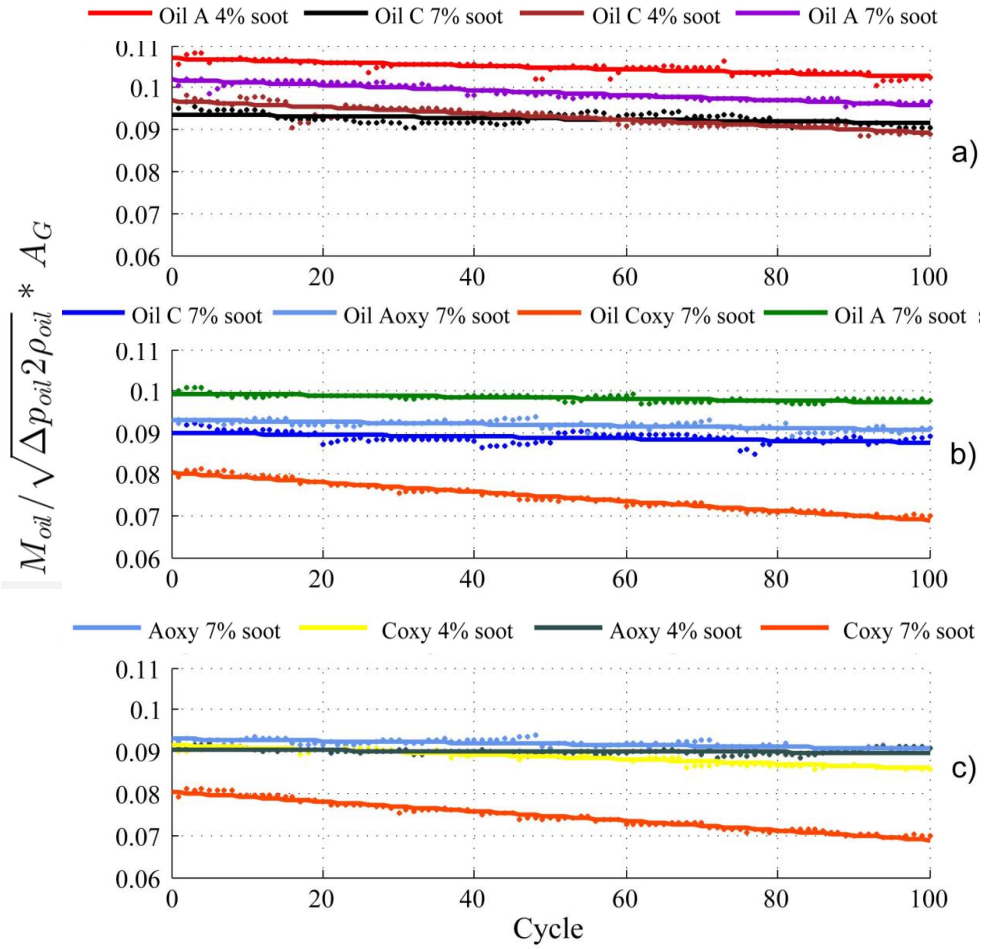

Figure 3.18: Turbocharger discharge coefficient during endurance test of oil coking

Engine torque, VGT and Turbocharger efficiencies. Before proceeding to analyse the efficiencies for each of the turbocharger unit tested, a fitted polynomial has been used to get a clearer trend pattern along the endurance test of oil coking. Figure 3.19 sub-plot a) is only one example of unfiltered and filtered lines in a turbocharger unit. The sub-plots b) and c) show the percentage of deviation in all turbochargers between unfiltered and filtered values for the compressor and turbocharger efficiencies shown in subplots c) and d) of Figure 3.20.

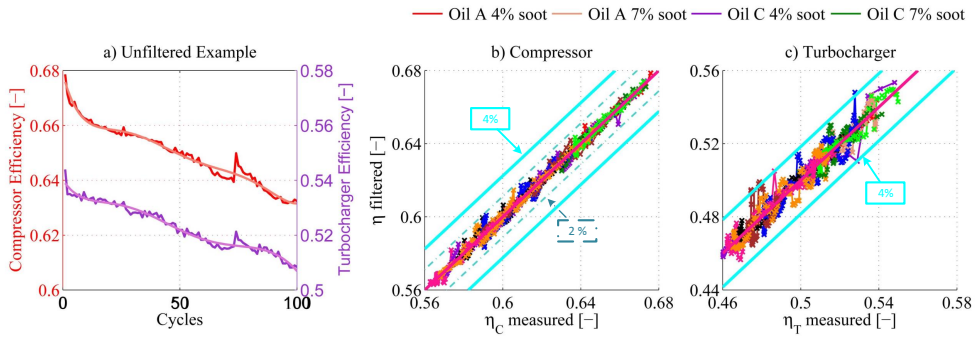

Figure 3.19: Fitted polynomial deviation in the compressor and turbocharger efficiencies

The Figure 3.20, shows the transition along the 100 cycles and the main parameters evaluated in four turbochargers at engine speed of 2750 rpm and full load. Dots in figures represent an average of the last phase of thermal stabilization before to proceed to the engine shut down. The first sub-plot a) indicates the engine torque; there can be seen a gradient of drop in the torque level that is high and similar for the four tests. Sub-plot b) indicates the vane position of the VGT vanes that are closing almost around 3% or 4% for all turbochargers. Sub-plot c) indicates the turbocharger efficiency drop, that is proportional to the level of soot either oil type “A” or “C”. The last sub-plot d) indicates the compressor efficiency that is being affected by the shaft motion or due to oil coke trapped in the bearing system producing an efficiency drop. As it can be observed in Figure 3.20, the VGT reacts to the torque level and turbocharger efficiency. The soot concentration and the oil coke deposits make the mechanical efficiency to deteriorate. The effect of soot accumulation and coke may also affect the axial position of the shaft: more closed VGT rack positions and high turbine inlet pressures due to lower mechanical efficiencies can increase the compressor tip clearance as the shaft shifts axially towards the turbine, impacting negatively its efficiency. In summary, if the mechanical and compressor efficiency drops so it does the turbocharger efficiency (according Equation 3.6). Since the control keeps the boost pressure (P2) constant, as the turbocharger efficiency drops, the VGT closes to increase the pressure ratio (π_T) as well as the turbine isentropic power ($\dot{w}_{Ts}$). As a consequence, the pressure at the turbine inlet (P3) increases and in this case, if P2 remains constant, the loss due to pumping mean effective pressure in the engine increases, therefore at constant $\dot{m}_{fuel}$ the effective torque decreases.

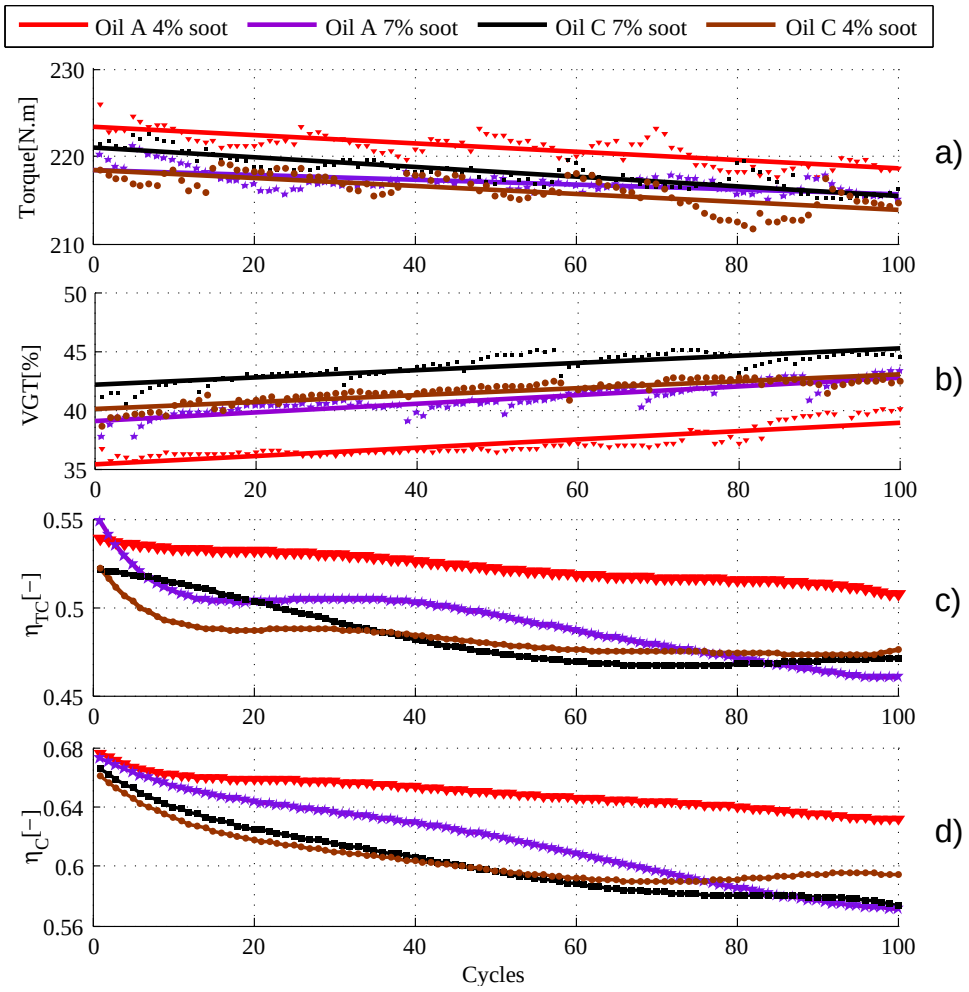

Figure 3.20: Response variables measured at 2750 rpm of engine speed and full load

Figure 3.21 shows the selected response variables for another four turbochargers measured under engine hot stop cycle at 2500 rpm and 75% of full load. In sub-plot a) the average engine torque is shown. A gradient of drop can be observed, which is grouped by the type of oil. This decrease in the engine torque level is less than tests at 2750 rpm and full load. Sub-plot b) represents the VGT vane position. The VGT vanes are closed more for oil “C”type, suffering a greater torque drop. The third sub-plot c) shows the turbocharger efficiency. In this lower engine operative condition, the drop efficiency is proportional to the level of soot either oil type “A” or “C”. In addition the higher viscosity of oil

type “C” produces greater friction and therefore a higher drop of efficiency than oil type “A”. The last sub-plot d) indicates the compressor efficiency. Higher loss of efficiency in the compressor may be attributed to the increased compressor tip clearance, as a result of shaft motion, coke deposits and increased turbine expansion ratio. An increase in the shaft motion and final axial position might generate imbalances in the compressor and even produce compressor blades damage, affecting its performance.

In Figure 3.21 it can be observed that lower engine operative conditions (lower temperature in the bearing system) produces less oil degradation. In addition, clearer differences between oil “A” and “C” quality can be observed.

To sum up, Table 3.9 shows the results of the selected response variables at the end of the endurance tests of oil coking under two engine operative conditions (high load and speed versus low load and speed). From the table, a greater and similar engine torque level drop is evidenced for the turbochargers tested at high load conditions. The loss in transient torque can be attributed to the increase in pumping mean effective pressure (PMEP), due to the increase of engine back-pressure by VGT vane position (derived through Engine Control Unit, ECU). The VGT vanes close a smaller amount for turbochargers measured at low load conditions and with less viscous oils (“A” type). The drop of turbocharger efficiency using oil type “C” is similar either at high or lower engine speed and load. The turbocharger efficiency losses are lower than the losses in the compressor side for all cases. High soot concentration is found inside the turbocharger tested at high engine speed and load using oil type “A” at 7% of soot. Greater efficiency loss is observed (bold in table); this may be attributed to stagnant carbon deposits that affects the shaft motion and consequently the performance of the turbocharger. Loss of efficiency in the turbocharger in which oil “C” with 4% of soot has been used are higher than expected since some of the compressor blades broke (see Figure 3.22). The deterioration in this turbocharger is not only due to thermal and lubrication conditions but due to aerodynamic effects. At low load and low engine speed (less temperature in the bearing system), the oil type “A” shows better response to the endurance tests than oil “C”.

Table 3.9: Results of the response variables selected after endurance tests using “A” and “C” oils

Oil type	**μ at 100°C [cSt]**	**Engine Torque drop [N.m]**		**VGT [%]**		**η_{TC} drop (Relative)**		**η_C drop (Relative)**	
		2750 rpm 100%load	**2500 rpm 75%load**	**2750 rpm 100%load**	**2500 rpm 75%load**	**2750 rpm 100%load**	**2500 rpm 75%load**	**2750 rpm 100%load**	**2500 rpm 75%load**
A 4%soot	11.49	4.2	1.7	-3.39	-0.24	0.07	0.02	0.07	0.03
A 7%soot	13.01	5	1.9	-3.73	0.3	**0.17**	0.06	**0.16**	0.07
C 4%soot	15.53	4.5	3.9	-2.86	-4.79	0.09	**0.1**	0.1	**0.12**
C 7%soot	16.18	5.1	3.7	-4.11	-3.22	0.1	0.09	0.14	0.11

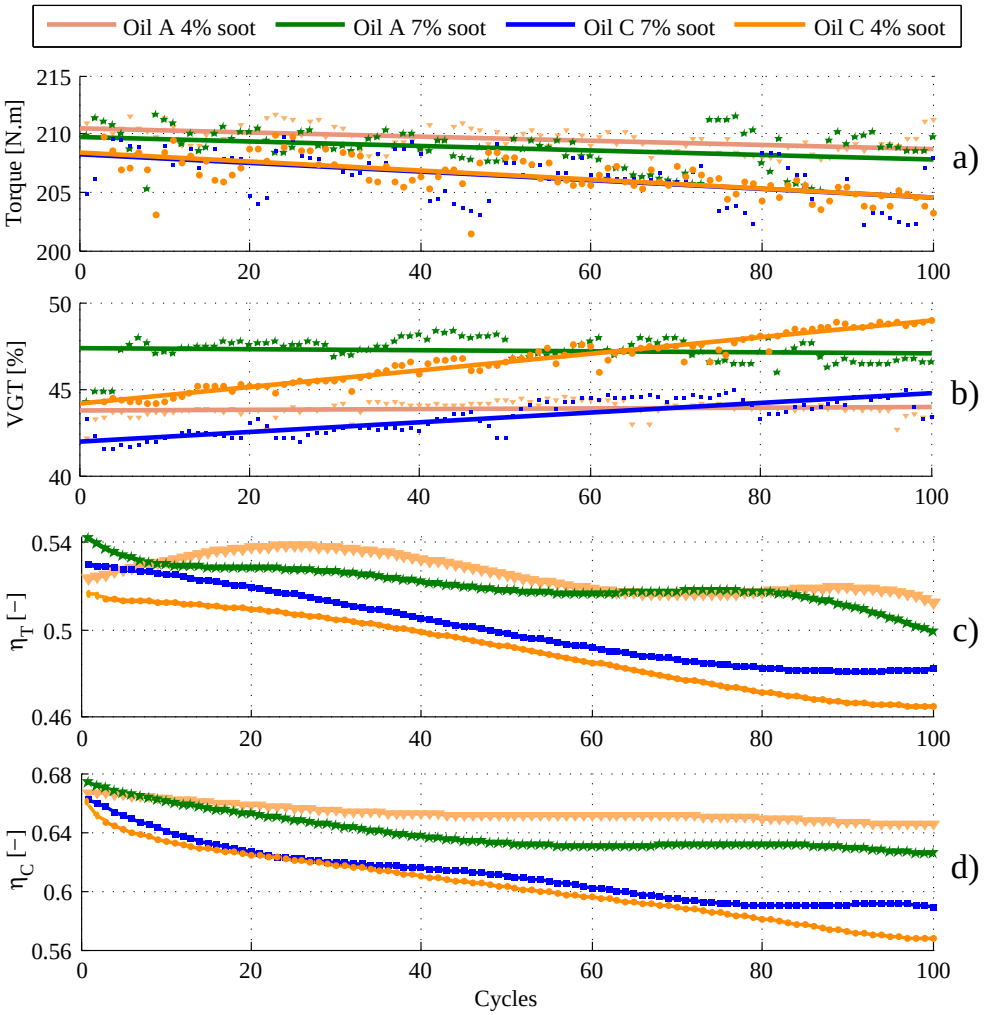

Figure 3.21: Response variables measured at 2500 rpm of engine speed and 75% of full load

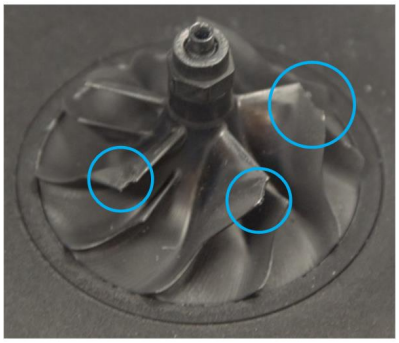

Figure 3.22: Turbocharger compressor wheel - test at 2500 rpm- 75 % full load and oil “C” 4% soot

Weight of turbochargers. In order to quantify the mass of cooked oil in the system, the turbochargers are weighed before and after the endurance test. Once the 100 engine hot-stop cycles are performed, the turbocharger is removed from the engine test bench and put to dry for one day thus all possible oil that the turbocharger can be drained. Then, a small industrial oven heated at 70 °C is used to place the turbocharger for up to 16 hours. The time and temperature are enough for not overcook the oil. Figure 3.23 shows an example of turbocharger liquid oil drying.

Figure 3.23: Turbocharger oil drain after endurance test

Subsequently weighing is carried out with the help of a high precision scale (± 0.01 gram). The difference in weight before the endurance tests and afterwards is expected to be positive; this will correspond to oil coke deposits inside the turbocharger. The weight increase for each turbocharger, the possible blocking of the floating bearing or the impediment to shaft movement is analysed and the results are shown down below.

- **"A" and "C" oils:** Table 3.10 shows the results of the weighing technique on each turbocharger for oils "A" and "C" at 4% and 7% of soot content each measured at two engine operating conditions. The weight delta between before and after the endurance tests and information of the turbocharger floating bearing after the endurance tests are shown.

Table 3.10: Weighing results of turbochargers using "A" and "C" oils

Oil type	**2750rpm - 100% load**		**2500rpm - 75%Full Load**	
	ΔWeight [g]	**Floating bearing Block?**	**Δ Weight [g]**	**Floating bearing blocked?**
A 4%	5.6	Yes	1.2	No
A 7%	15.3	Yes	4.2	No
C 4%	9.2	No	3.7	No
C 7%	**3.3**	Yes	4.6	No

For instance, the increase of weight is proportional to the amount of soot content in the oil and the engine operative condition except for the "C" oil at 7% of soot (bold in Table 3.10). At higher engine operating point, higher deposition of coke on the turbocharger is proven.

The high bearing temperature, produces greater accumulation of coke in oil type "C" compared to oil "A". As oil "C" is more viscous, more difficult the fluid circulation in the channels of turbocharger lubrication. In the mean time greater soot content causes greater coke deposits in the turbocharger.

On the other hand, the blockade of the floating bearing is qualitative. This usually occurs in the turbochargers tested at high engine speed and high load; however, this trend is not completely continuous.

- **"Aoxy" and "Coxy" oils:** The results of weight gain in the turbochargers using oxidized oils are shown in Table 3.11. These tests are carried out at lower engine speed and lower load conditions.

Table 3.11: Weighing results of turbochargers using "Aoxy" and "Coxy" oils

Oil type	**2500rpm - 75%Full Load**	
	ΔWeight [g]	**Floating bearing blocked?**
Aoxy 4%	2.7	No
Aoxy 7%	4.4	Yes
Coxy 4%	3.9	Yes
Coxy 7%	5.7	Yes

Having a previous oxidation in the oil causes a weight difference greater than with the non-oxidized oils. A higher delta weight in oxidized oils is proportional to the soot content. The higher soot content, greater turbocharger weight either wiht "Aoxy" or "Coxy" oil.

The oxidation causes an increase in the oil viscosity therefore a greater deposition of oil coke. The blocking of floating bearings in the turbocharger is presented with the use of oil oxidized type "Coxy" at both levels of soot content and in the oxidized type "Aoxy" at high level of soot (7%) as well. Non-oxidized equivalent oils used at low engine speed and load do not produce a blocking of the floating bearing on the turbocharger.

The increases in viscosity can be explained by pointing to the polymerization of products such as sludge, the non-homogeneous molecules impede the relative motion of fluid. The new compounds created from oxidation are quite different and introduce new forces of interaction between the molecules that can block the rotation of bearings.

Figure 3.24 and Figure 3.25 show a set of two images for each turbocharger at the end of each endurance test. On the left hand, the surface at the oil outlet can be observed. On the right hand, the bearing and part of the shaft can be observed. The deposits of oil coking, causes oil ducts clogging affecting not only the final turbocharger lubrication, but also its capacity to withstand high temperatures. As shown in pictures the lack of servicing and poor quality oils, results in a gradual build-up of sludge in the sump and inside the turbocharger where some of the narrowest oil ways are, some as small as 1 mm in diameter; when they become blocked failure occur.

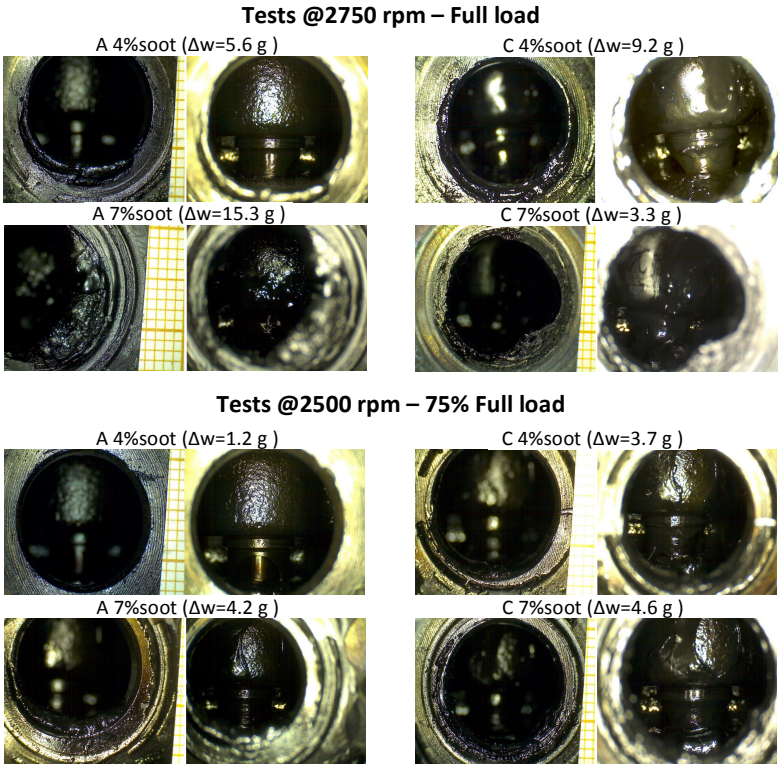

Figure 3.24: Oil coking deposits in turbochargers tested with A and C oils

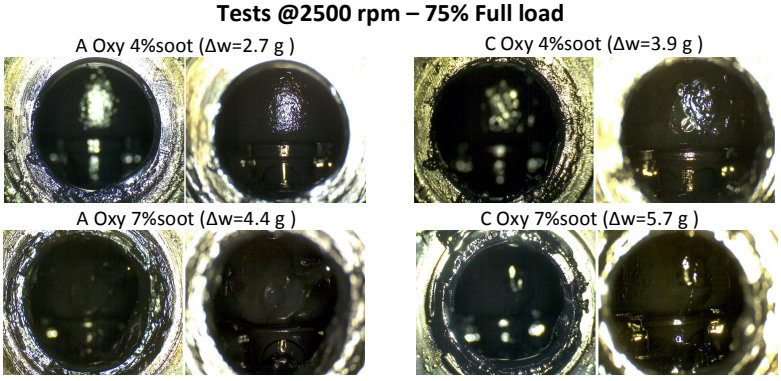

Figure 3.25: Oil coking deposits in turbochargers tested with Aoxy and Coxy oils

Maximum static eccentricity. Measurements of the deflections in the rotating assembly are analysed down below. The parameter that determines the amount by which its orbit around another body deviates from a perfect circle is the eccentricity. A value of 0 is a circular orbit, values between 0 and 1 form an elliptic orbit. In the rotating assembly of the turbocharger a positive value will indicate an axis deviation to the right from its initial centre and a negative value an axis movement to the left. Values in the eccentricity near zero indicates that the movement of the axis tends to resemble more a circumference, in the meantime a variation close to one indicates that the shape movement is described more by a line (see Equation 3.8 and the technique in Figure 3.14).

Variations of the semi-major axis (SMA) of the ellipse are also analysed, the SMA provides information with respect to the size of the ellipse. A delta SMA positive indicates that the ellipse is larger after the endurance test which can be associated with a wear of the floating bearings. On the other hand, a negative delta SMA indicates that the ellipse is smaller after the endurance test. This diminution of the gap may be associated to coke deposits that restricts the shaft movement.

The Figure 3.26 corresponds to the description of the shaft movement of a turbocharger. The sub-plot a) is the shape of the shaft rotating without applying any force, each point in the ellipse represents an angular position. The sub-plot b) are the photos taken applying force in the shaft every 45 degrees in four directions (north, south, east, west).

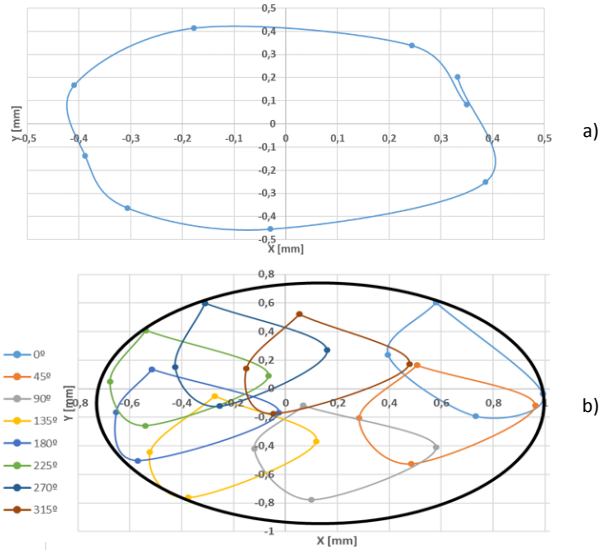

Figure 3.26: Turbocharger static eccentricity without force (a) and with external force applied every 45° (b)

Table 3.12 shows delta SMA and delta of eccentricity for turbochargers tested with “A” and “C” oils at high and lower bearing temperature and without applying any force.

Table 3.12: Turbochargers static eccentricity without force using “A” & “C” oils

Oil type	Δ SMA [mm]		Δ Eccentricity [-]	
	2750rpm 100% load	2500rpm 75%Full Load	2750rpm 100% load	2500rpm 75%Full Load
A 4%	-0.25	0.02	0.05	-0.24
A 7%	-0.075	-0.04	-0.16	-0.23
C 4%	0.03	0.025	0.33	0.31
C 7%	0.015	-0.2	-0.25	-0.13

Table 3.13 shows results of static eccentricity for the turbochargers tested with “Aoxy” and “Coxy” oils at low bearing temperature and without applying any force.

Table 3.13: Turbochargers static eccentricity without force using “Aoxy” & “Coxy” oils

Oil type	2500rpm - 75%Full Load	
	Δ SMA [mm]	Δ Eccentricity [-]
Aoxy 4%	-0.07	-0.13
Aoxy 7%	0.05	0.36
Coxy 4%	-0.01	0.04
Coxy 7%	-0.29	-0.33

The shaft motion or diminution of the gap of rotating assembly is affected in greater proportion in turbochargers tested at high bearing temperature (2750 rpm - 100% full load). In addition, tests with oils “C” suffer a delta of SMA lower than tests with “A” oils.

At lower bearing temperature (2500 rpm-75% full load) the tests with “A” and “C” oils suffer less deflections in the rotating assembly than their counterpart “Aoxy” and “Coxy”. The oxidation tends to increase the oil viscosity and deposits of varnish and sludge.

Deflections in rotating assembly are similar with “Aoxy” oil at 4% or 7%. The interference of soot content with this oil type is not observed. In tests with “Coxy”, the soot content makes a difference; at 4% the delta of SMA is almost the same that at the beginning of the endurance test while at 7% the delta of SMA is reduced to half.

Increases of the operating clearances between the shaft/bearing and bearing/central housing are small. Values between the 4% and 20% of their initial size. While diminution of the gap on bearing surfaces (internal and external) are between 20% up to 55% of the initial SMA of the ellipse.

The eccentricity tends to shift the movement of the axis more to the left. The eccentricity values are between 0.002 and no greater than 0.62, therefore, the shape of the ellipse tends mainly to be more circular than linear. Displacement of the eccentricity to the right (positive values) are small and mainly correlated with whose turbochargers that have suffered a positive delta SMA (clearance).

The Table 3.14 shows delta SMA and delta of eccentricity for turbochargers tested with "A" and "C" oils at high and lower bearing temperature and applying force to the shaft. Table 3.15 shows delta SMA and delta of eccentricity for turbochargers tested with "Aoxy" and "Coxy" oils at lower bearing temperature applying force to the shaft.

The orbital forces described by the rotating assembly applying force to the shaft, shows that almost all turbochargers have a reduction of their SMA at the end of endurance tests, this diminution of the gap is induced by coke deposits. Increases in the operating clearances shaft/bearing and bearing/central housing are presented in the turbocharger in which the blades have been broken (measured with the oil type "C" at 4%) (see Figure 3.22) and other two turbochargers measured at high engine speed and high load using oils "A" at 7% and "C" at 4%. This trend is accompanied by a drop in compressor efficiency equal or greater than 10 points as it is denoted in Table 3.9. The other nine turbocharger measured have a lower SMA and the accumulation of coke is noticeable.

Table 3.14: Turbochargers static eccentricity with force using A & C oils

	ΔSMA [mm]		**ΔEccentricity [-]**	
Oil type	**2750rpm 100% load**	**2500rpm 75%Full Load**	**2750rpm 100% load**	**2500rpm 75%Full Load**
A 4%	-0.97	-0.31	-0.51	0.41
A 7%	0.16	-0.12	-0.39	0.24
C 4%	0.14	0.23	0.48	-0.1
C 7%	-0.13	-0.21	-0.37	-0.18

Table 3.15: Turbochargers static eccentricity with force using “Aoxy” & “Coxy” oils

Oil type	**2500rpm - 75%Full Load**	
	ΔSMA [mm]	**ΔEccentricity [-]**
Aoxy 4%	-0.09	0.24
Aoxy 7%	-0.07	0.16
Coxy 4%	-0.46	-0.35
Coxy 7%	0	0.48

Turbocharger deceleration time. The time diminution of rotation along the endurance tests once the engine stops is shown in order to provide a criterion of fouling level in the bearing system for each turbocharger tested.

Figure 3.27 sub-plot a) shows the time deceleration for the turbochargers tested with oils “A” and “C” at two engine operating points; 2750 rpm-full load (high OP) and 2500 rpm-75% of full load (low OP). A higher content of soot causes a reduction in the “time to stop” in turbochargers tested with oil type “A”. While using oil “C”, the deceleration time is similar for all tests and the time rotation is reduced by half with respect to the tests performed with oil “A”. The sub-plot b) shows the “time to stop” for the turbochargers tested with oil “A” or “C” and their oxidized counterpart “Aoxy” and “Coxy”. These turbochargers are all tested at engine operating conditions of 2500rpm-75% full load. There can be observed that “Aoxy” oils take on average half time or less to stop compared with their respective counterpart not oxidized “A”. Additionally at higher soot content, lower “time to stop” of the turbocharger. For “C-type” oils neither the content of soot, nor the oxidation make a big change in the deceleration time of the turbochargers.

Table 3.16 shows a mean of the “time to stop” over the first fifty cycles for each turbocharger tested and these values have been ordered from lowest to highest. The oil quality affects the deceleration time. Turbochargers measured with more viscous (oil “C”) and oxidized oils stop faster than the less viscous oils (oil “A”), this trend is attended by the level of soot. During the first 50 cycles, with a higher content of soot the turbocharger stops before.

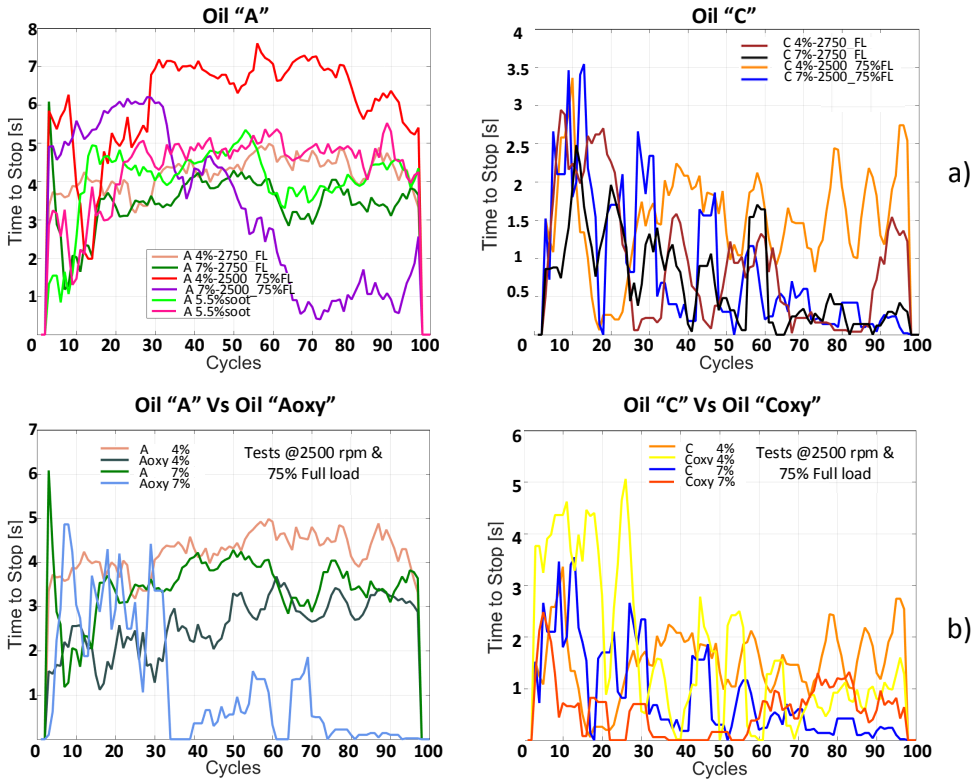

Figure 3.27: Turbocharger deceleration time

Table 3.17 shows a mean "time to stop" of the turbocharger over the last fifty cycles. In the second half of the tests, deceleration time is grouped by type of oil. The turbochargers measured with type "C" and the oxidized ones take less than 1 second to stop after the engine is shut-down. The normal rotation of the turbocharger by inertia is minimal. Regarding type "A" oils, turbochargers take between 1.5 and 6 seconds to stop once the engine is switched off. This condition depends on the content of soot and if the oil is oxidized. The turbocharger tested at low OP and using oil "C" at 4% soot (bold in table), leaves the general trend; as mentioned in previous inspection techniques, the blades of this turbocharger are broken. The thermal and aerodynamic effect can affect the oil type correlation in this case.

Table 3.16: Turbo deceleration time 0 to 50 Cycles

Oil type	Operating point	Mean time to stop (0-50 cycles) [s]
Coxy 7%	low	0.468
C 7%	high	0.9988
C 4%	high	1.224
C 7%	low	1.3472
C 4%	low	1.4168
Aoxy 7%	low	1.9068
Aoxy 4%	low	2.058
Coxy 4%	low	2.3832
A 7%	low	3.23
A 4%	low	3.812
A 7%	high	4.9072
A 4%	high	5.462

Table 3.17: Turbo deceleration time 50 to 100 Cycles

Oil type	Operating point	Mean time to stop (0-50 cycles) [s]
C 7%	low	0.3294
C 7%	high	0.342
Aoxy 7%	low	0.4353
C 4%	high	0.5765
Coxy 7%	low	0.615
Coxy 4%	low	0.8682
A 7%	high	1.44
C 4%	**low**	**1.4855**
Aoxy 4%	low	2.902
A 7%	low	3.3608
A 4%	low	4.1961
A 4%	high	6.1678

Oil temperature monitoring. The set point oil inlet temperature is regulated at 90°C through the independent lubrication system, in order to keep it constant for all endurance tests. In Figure 3.28 oil temperature monitoring for one turbocharger endurance test is shown. In the sub-plot a) on the left side, the oil inlet temperature under whole engine cycle is shown. On the left side, the blue line represents the average of temperature under steady state conditions for each cycle and the pink line represents the maximum temperature of the oil at the inlet port under hot stop phase. The sub-plot b) shows the temperatures of the turbocharger oil outlet during the different stages of the engine cycle. The blue line represents the temperature at steady state for a set of 100 cycles, the navy blue line is the maximum oil outlet peak temperature and the pink line represents the temperature at which the oil converges 10 minutes after engine stops.

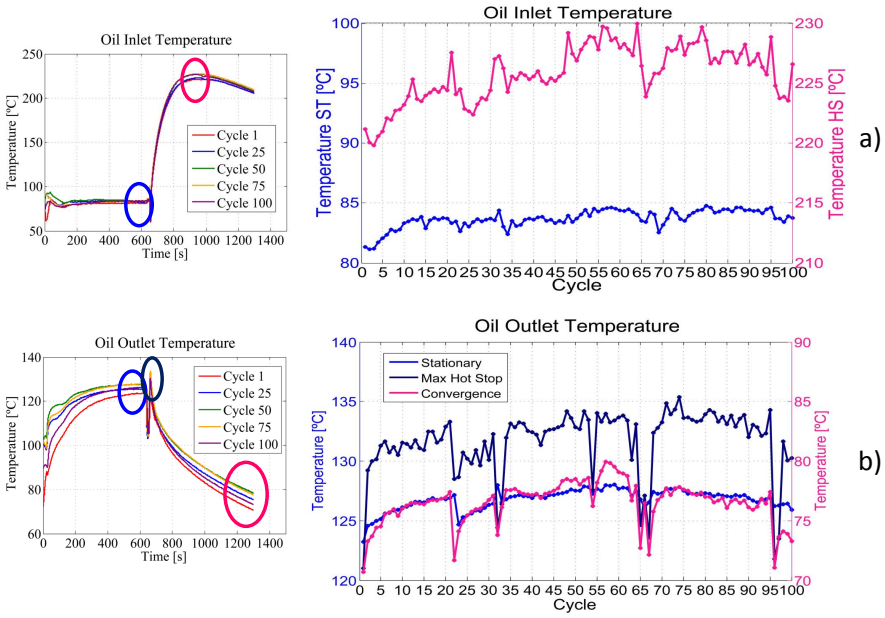

Figure 3.28: Oil temperature monitoring - control variables

Figure 3.29 represents the delta temperatures between the cycle 1 and 100. During stabilization phase (sub-plot a) the delta temperature between the inlet and outlet is small, around 10 degrees or even less. The sub-plot b) shows the delta temperature during hot stop phase (pink lines in Figure 3.28), the temperature remains almost constant, some points show a drop because of

the maximum oil inlet temperature is lower in some of the engine cycles. No significant oil temperature changes have been observed with this inspection criteria. The oil is more affected by heat losses than by friction losses.

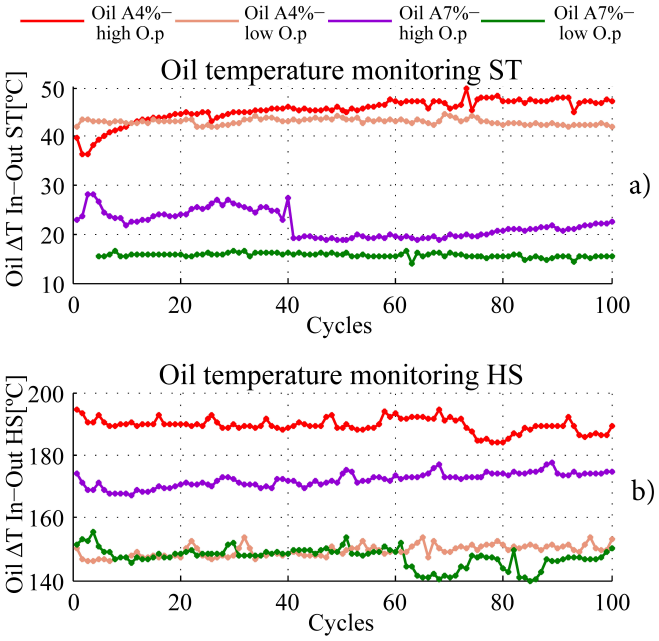

Figure 3.29: Oil temperature monitoring sample

All the results shown in this chapter come from methodologies implemented to know where is the most representative parameter. Although it is possible to assess the effect in each turbocharger according to the different characteristics of the oil, to find at the first time the resolution of a correlation is not clear. Therefore, an exhaustive statistical study is generated and applied in the next chapter.

3.6 References

[58] J R Serrano; P Olmeda; APaez; F Vidal. “An experimental procedure to determine heat transfer properties of turbochargers”. In: *Measurement Science and Technology* 21 (2010), p. 14. DOI: 10.1088/0957-0233/21/3/035109. URL: http://iopscience.iop.org/article/10.1088/0957-0233/21/3/035109/pdf (cit. on pp. 17, 64).

[59] P. Olmeda, V. Dolz, F. J. Arnau, and M. a. Reyes-Belmonte. “Determination of heat flows inside turbochargers by means of a one dimensional lumped model”. In: *Mathematical and Computer Modelling* 57 (2013), pp. 1847–1852. ISSN: 08957177. DOI: 10.1016/j.mcm.2011.11.078 (cit. on pp. 17, 64).

[136] Engine Power Test Code Committee. *Turbocharger gas stand test code (J1826 Ground Vehicle Standard)*. Tech. rep. The Engineering Society for Advancing Mobility Land Sea Air and Space, 1995. URL: https://saemobilus.sae.org/content/j1826{_}199503 (cit. on p. 63).

[137] Engine Power Test Code Committee. *Supercharger testing standard. J1723 Ground Vehicle Standard*. Tech. rep. The Engineering Society for Advancing Mobility Land Sea Air and Space, 1995, p. 9. URL: https://saemobilus.sae.org/content/j1723{_}199508 (cit. on p. 63).

[138] E. G. Ribeiro, W. B. Melo, and A. P. a. Filho. “Application of electric oil pumps on automotive systems”. In: *SAE International Journal Engines* 01.4086 (2005), pp. 1–7. DOI: 10.4271/2005-01-4086. URL: http://www.sae.org/technical/papers/2005-01-4086 (cit. on pp. 68–70, 120, 176).

[139] NHTSA. “Flammability Properties of Engine Compartment Fluids Other than Gasoline”. In: *National Highway Traffic Safety Administration* (1988). DOI: 98-3588-193 (cit. on p. 69).

[140] OSHA Hazard Communication Standard. *Formula Shell Motor Oil SAE 5W-30 Material Safety Data Sheet*. Tech. rep. 29 CFR, 2008. DOI: MSDS71135L. URL: http://ebpaving.com/wp-content/uploads/2013/09/FormulaShell-Motor-Oil-SAE-5W-30.pdf (cit. on p. 69).

[141] J. V. Pastor, J. R. Serrano, V. Dolz, M. A. Lopez, and F. Bouffaud. “Study of turbocharger shaft motion by means of non-invasive optical techniques: Application to the behaviour analysis in turbocharger lubrication failures”. In: *Mechanical Systems and Signal Processing* 32 (2012), pp. 292–305. ISSN: 08883270. DOI: 10.1016/j.ymssp.2012.04.020 (cit. on p. 81).

[142] M. A. Hidalgo Lopez. “Estudio teorico-experimental de la dinamica rotacional de turbocompresores de MCIA. Aplicacion al diagnostico de fallos.” Doctoral Thesis. Politecnic of Valencia, 2014, p. 287 (cit. on p. 81).

CHAPTER 4

Application and evaluation of heat transfer and cross analysis of oil coking

Contents

Figures

Tables

4.1 Introduction

A study of several strategies used to minimize possibilities of coke formation, an evaluation of turbine housing designs and remarks of cross analysis of oil coking test in turbochargers is presented in this chapter.

Nowadays, the working temperature of the turbo-charging system has increased, reaching values even higher than 1000 °C in the turbine side [6]. This has led turbocharger manufacturers to take into account water cooling and the incorporation of new materials [143]. A 1D heat transfer turbocharger model coupled to an engine is used to calculate the temperature of the metal, predict the mean temperatures of exhaust gas and the air flowing inside the turbocharger. The engine model used is programmed in the commercial gas dynamics 1D code GT-Power ^{TM}, it allows to model each of the most important components and processes of the engine [144, 145, 146]. The 1D turbocharger model has been used as an external plug in. The codes have been upgraded to calculate transient turbocharger thermal conditions when the engine speed is reduced to zero.

The strategies can be simulated in acceptable calculation times thanks to proposed modelling strategy. The presented methodology allows a detailed study of the temperature rise of the central housing of an automotive turbocharger after a hot-stop process, simulating several combinations of cooling strategies in order to find the optimum one in terms of minimizing extra energy consumption per K of housing temperature reduction.

The oil coking cross analysis is presented combining the results of the inspection criteria used in the experimental section 3.5. The part validated by this procedure is the turbocharger, and in particular the lubrication of its bearing system. The trends identified and correlations between parameters are shown.

4.2 Study of the delay in pump stop with GT-Power

An adaptation of a 1-D tool to study thermal transient in turbocharger bearing housing by means of a bypass system of 9 valves is done. The aim is to perform conditions of engine on and off. Thanks to this innovative modelling approach, different strategies for reducing the probability of coke formation are calculated in acceptable time. A factorial study of four variables at two different levels is presented. The optimum in terms of power consumption and extra CO_2 emissions is selected.

4.2.1 Mathematical model

A simulation campaign has been performed computing an engine cycle with some variations in operation of the oil and coolant pumps feeding the turbocharger. Those have been carried out using the GT-Power^{TM} engine simulation code. Nevertheless, in this study the turbocharger model has been implemented as an external plug-in and is able to reproduce the thermal evolution of the turbocharger. This turbocharger heat transfer model has been previously validated in steady-state and transient conditions [76, 71]. The turbocharger model is able to calculate the main performance variables of the compressor and the turbine and it has the capability of computing the main heat fluxes in the turbocharger, including the metal-to-metal heat flows, the cooling effects of the oil, the oil heating due to friction losses and the coolant and external heat flows. For the external flows, the most important heat comes from turbine external surface; external heat fluxes at housing nodes are almost negligible compared to the turbine enthalpy drop. In the compressor side, the external heat flow can absorb some heat from the ambient, especially coming from the turbine housing.

The heat transfer model is based on the axial path and the principle of similarity with an electrical circuit [147]. The Figure 4.1 shows the configuration that has been implemented, where 5 metal nodes can be seen. Each of these nodes represents a plane in the turbocharger, being part of a one-dimensional model. The heat transfer to the ambient, oil and coolant is also considered. The Table 4.1 shows the description of the nodes.

Table 4.1: Definition of external nodes on the turbocharger

Metal node	Description
T	Turbine housing node
H1	Turbine back plate node
H2	Housing central node
H3	Compressor back plate node
C	Compressor housing node

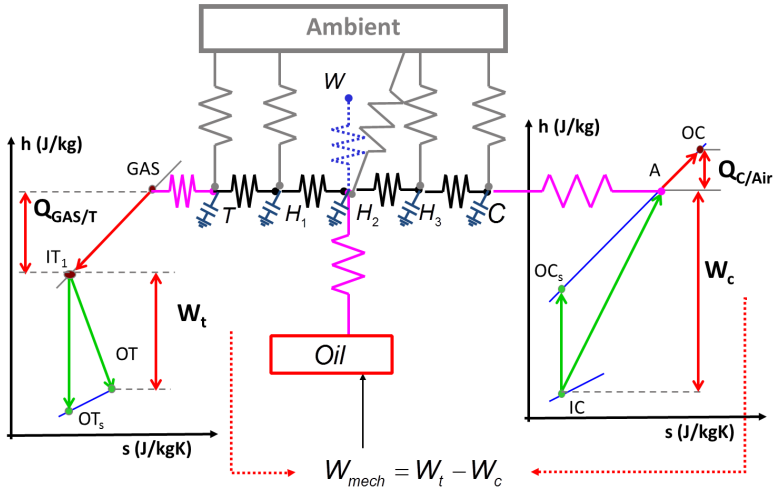

Figure 4.1: One-dimensional turbocharger heat transfer model [75]

The turbocharger heat transfer model includes as data input, the mass flow of the turbine, compressor and oil inlet, the temperatures at the compressor outlet, at the turbine inlet, in the lubrication and cooling system, the turbocharger speed, the compression and expansion ratio, the ambient velocity and ambient pressure. The method uses the engine cycle over a representative engine operating point for the analysis of temperature evolution at different parts of the turbocharger. The cycle is the same used in the experimental tests to study oil coke formation inside the turbocharger bearings, but it can also be used to study the evolution of other parameters such as temperatures and pressures in different parts of the engine. Automotive companies predefine these cycles in order to ensure that the studied parameters do not exceed some limits which are detrimental for the life of the engine and turbocharger. The Figure 4.2 shows the simulated end period of a hot stop engine cycle represented in engine power vs time.

The simulations correspond to last 700 seconds of this cycle as it is shown in Figure 4.2. The cycle has stationary and transient parts. Initially, engine temperatures are stabilized at full load and high speed, typically the speed of 3500 rpm in a Diesel engine, that takes place in the simulation for a shortened period of about 60 seconds (A to B in Figure 4.2), followed by a deceleration phase (C in Figure 4.2) as function of the operating point, a decreasing speed and load intended for reaching the engine idle conditions is done for 5 seconds (D in Figure 4.2), and finally the quick stop of the engine, where the circulation of water, oil and air through the turbocharger are cut for an allotted period of time that let the turbocharger reach maximum peaks of temperatures in each

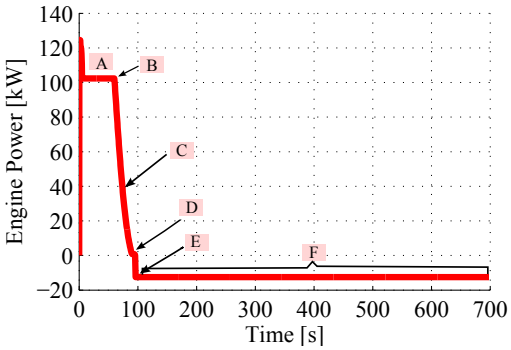

Figure 4.2: Last part of a hot stop engine cycle

section node (F in Figure 4.2). When the engine stops, a peak of temperature in the central housing is produced and thus, in the bearing system.

For this study, the adjustment of engine and turbocharger models to simulate engine hot stops is an additional task. Calculation instabilities are found when engine speed is reduced to zero. Therefore, a strategy is done by means of a bypass system of 9 valves to perform conditions of engine start/stop. In this way, the thermal evolution of the turbocharger model continues computing when the engine speed is reduced to zero. Stability problems with GT-Power ^{TM} are solved in the simulation. Figure 4.3 shows the implemented strategy of the engine-bypass system. The sub-plot a) shows when the engine is on; the turbocharger acts as a dependent element of the engine. The sub-plot b) represents the engine off; an isolation of turbine and compressor is done by closing the valves two, four, six and eight therefore, turbocharger has no contact with the engine.

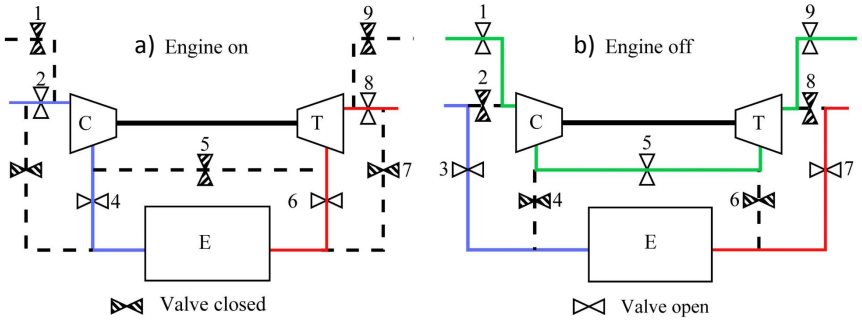

Figure 4.3: Turbocharger bypassing strategy engine on and engine off

The engine insulation strategy as well as the flow variations of the oil and/or

water mass are made to study the heat transfer under engine start/stop.

4.2.2 Model validation

The trends between the turbocharger heat transfer model (HTM) and experimental data of three engine operating conditions is evaluated. The operating points represent conditions that can be found in highway driving cycles and produce high enough turbine inlet temperatures to promote the coke formation. Figure 4.4 shows the external nodes temperature between the thermal model and the experimental data for steady state (point A to B in Figure 4.2). There can be observed that thermal model is able to adopt the temperature gradients along the turbocharger in each external section.

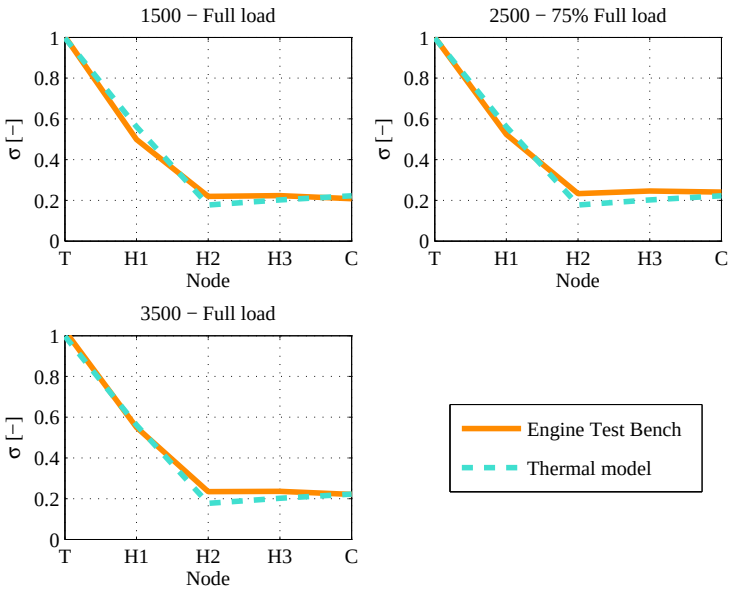

Figure 4.4: Turbocharger external nodes comparison experimental Vs 1D-model for steady state

Figure 4.5 shows the temperature comparison of the external nodes after the engine stops (point F in Figure 4.2) at approximately 400 s where the maximum temperature in central housing node is reached. On the compressor side, the measured temperatures are lower. In between, the temperatures of central housing (H2) are equivalent for both, the simulations and experimental data. On the hot end side, nodes turbine (T) and backplate turbine (H1) the temperature gradients differ from the measurements largely. A possible reason of this could be the radiation phenomenon coming from the exhaust manifold in the

experiments and that affects the turbocharger heat transfer. This phenomenon seems to have a relevant role during the engine hot-stops.

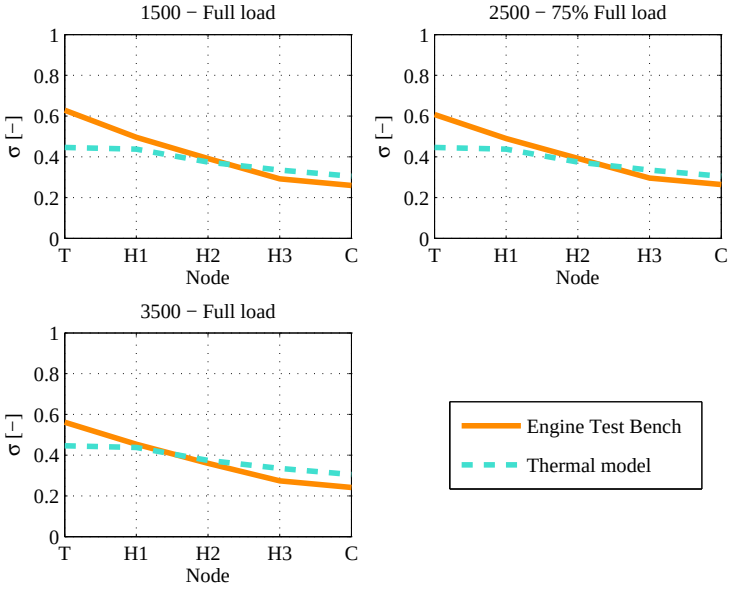

Figure 4.5: Turbocharger external nodes comparison experimental Vs 1D-model for hot stop phase

After this assessment, a simulation study of the cooling strategy has been performed using a factorial analysis with four different factors acting at two levels, leading to a total of 16 different combinations.

4.2.3 Modelling results and discusion

An important part of this work is to observe the behaviour of temperatures in the turbo-charging system once the engine is shut-off, using different cooling strategies to reduce the possibilities of coke formation. The coke formation could lead to severe turbocharger damage. This is produced at extremely high oil temperatures. The maximum oil temperature is expected to happen after the engine stops inside the bearings. The turbocharger thermal model does not have the capability of computing directly this temperature however, it is expected to be correlated with the bearing housing temperature in H1 and H2 nodes.

A factorial analysis with four different factors acting at two levels is conducted by means of GT-Power ^{TM} simulations. Two factors are the pump sizes for both the oil and coolant pumps. The pump size is used for increasing the flow

through the turbocharger. Other two factors are the use or not of auxiliary electrically driven oil and coolant pumps for the turbocharger after the engine stops. The adaptation of both the engine and turbocharger models during thermal transient hot-stop simulations were done by means of a bypassing strategy as showed in Figure 4.3. In the simulation, when engine stops the cooling system for the turbocharger is cut, and no thermosyphon effects are taken into account. There is no air, no water or oil circulation. Each of the nodes described in Table 4.1 are useful for determining the local temperature of the turbo-charging system for steady conditions and mainly during thermal transient being H2 the central node and representing the majority of bearing housing material.

The simulation matrix is shown in Table 4.2, where minus "-" symbol represents a low level, and a plus "+" represents a high level in the pump size. The $\dot{m}_{c,size}$ is pump size of the coolant, $\dot{m}_{o,size}$ is the oil pump size. 'Yes' or 'No' refers to the auxiliary pump operation after engine stops either for water or oil cooling strategy.

Table 4.2: Array of test for simulating the engine cycle

Auxiliary system				**Oil cooling**			
				Yes		No	
				$\dot{m}_{o,size}$			
Water cooling				+	-	+	-
	Yes	$\dot{m}_{c,size}$	+	case 16	case 12	case 8	case 4
			-	case 15	case 11	case 7	case 3
	No		+	case 14	case 10	case 6	case 2
			-	case 13	case 9	case 5	case 1

Table 4.3 shows the values of oil and coolant mass flow set for the different simulations carried out, and the flow value set if the auxiliary pump is used or not. Case 1 is taken as a baseline and corresponds to normal oil and coolant flow without any auxiliary pump running.

Table 4.3: Mass flow setting for simulations

	Mass flow	**Coolant [kg/s]**	**Oil [kg/s]**
Full load	+ High	0.15	0.0225
	- Low	0.1	0.015
Auxiliary pump	Yes	0.03429	0.00514
	No	0.0001	0.0001

From the baseline case simulated, a first approximation of time for the auxiliary pump is obtained. An average of H2 temperature can be obtained using Equation 4.1. Where, T_n is the temperature at time-step t_n; t_f term is the specific time where maximum temperature in the central node is reached; and t_i is the time when the engine stops.

$$T_{H2} = \sum T_n \cdot (t_n - t_{n-1}) / \left(t_f - t_i\right) \tag{4.1}$$

A hypothesis of mean temperature for oil is done according to the temperature calculated previously with the aim of maintaining the lubrication system under safe conditions. The convective conductance between the oil and H2 metal node are calculated through dimensionless numbers of Reynolds, Prandtl and Nusselt using proposed correlations in [148].

The convective heat transfer coefficient for the oil and water can be obtained with Equation 4.2, where k is the fluid conductivity and D the diameter of oil inlet port.

$$h = Nu \cdot k/D \tag{4.2}$$

Serrano et al. [149] have successfully correlated these convective coefficients. Therefore, the heat transfer to the oil or the coolant can be easily calculated. To obtain a real approximation of the mean oil temperature inside the turbocharger, oil outlet temperature needs to be recalculated having a convergence with the first approximation of temperature done in Equation 4.1.

Figure 4.6 shows the H2 and oil outlet temperatures for the baseline case 1. The oil outlet temperature in the turbocharger can be still calculated when the engine is stopped because the mass flow rate passing is not totally null; but it is a minimum value very close to zero, equivalent to the small amount of oil dripping naturally present after halting the oil pump.

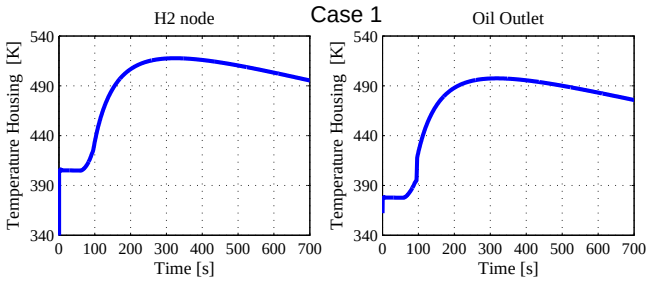

Figure 4.6: H2 node and oil outlet temperature for the baseline case

The Equation 4.3 represents the integral of heat flow already calculated, which can be used to estimate the acting time for the auxiliary pump system. The term C is the sum of all thermal capacitances of the five metal nodes of the turbocharger. The capacitance in each metal node are obtained thanks to previous experimental works [148, 149, 150]. The ΔT term is the temperature decrease from an initial case 1 that lack of any type of extra cooling after the hot-stop (refer to Table 4.2).

$$\int \dot{Q}\ dt = C \cdot \Delta T \tag{4.3}$$

To keep the oil in the bearing system under safe conditions [138], a reduction of about 25 °C in the turbocharger is needed. Therefore, the additional operating time for an auxiliary oil pump after the engine stops is approximately 2.23 minutes; the water cooling pump would need less time. For the sake of simplicity, the electric auxiliary pumping system is left acting 2 minutes for both water and oil strategies.

Once the pump operating time has been determined, the other tests from Table 4.2 have been carried out to see the thermal evolution of the turbocharger under different cooling strategies. The Figure 4.7 shows the representative simulation results for four different cases of cooling strategies used. There can be observed that the turbine node has a peak temperature of 858 K followed by a drop once the engine is stopped. The other nodes reach their maximum temperature later. The compressor node C or the H3 node backplate compressor reach maximum temperatures more than 60 K higher than when the engine is operating at high loads. Additionally, all nodes reach convergence with a temperature between 484 K and 494 K after 10 minutes that the engine is stopped.

The analysis of possible failure or loss of efficiency during hot-stop from the thermal point of view is focused on the evolution of H1 node temperature, where is the highest temperature in the central housing and in the H2 node temperature, which represents the majority of central housing mass and handles the biggest part of the oil flow.

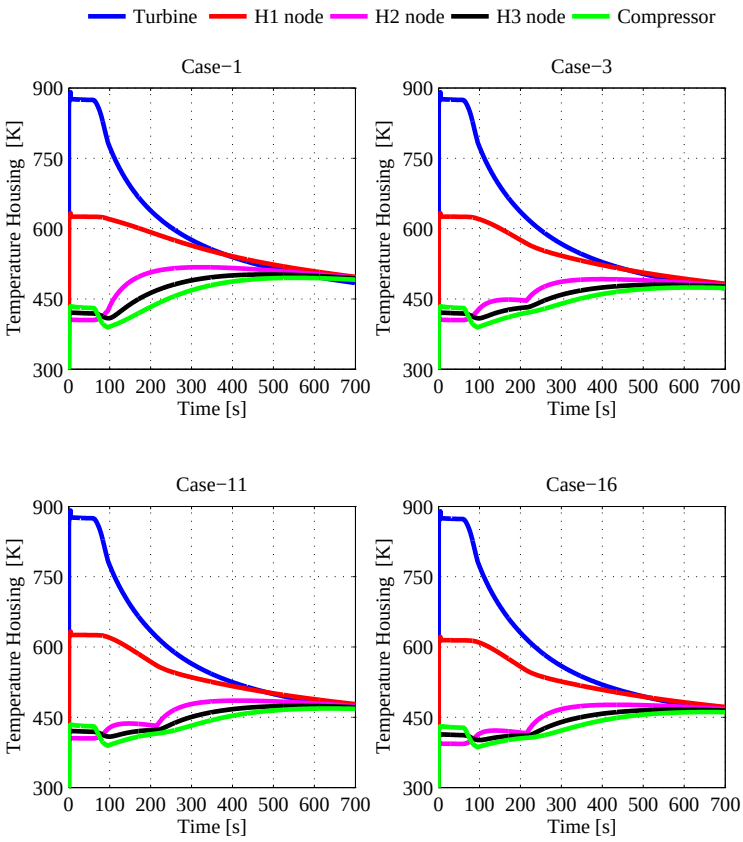

Figure 4.7: Most representative turbocharger temperatures from simulation array

During simulations, the maximum gas inlet temperature was 1100 K. The Figure 4.8 shows the evolution of temperatures in H1 metal node which is the contact node with the greatest hot spot where the hot exhaust gases are released. During the engine throttle tip-out phase, the gas temperature decreases as the amount of fuel injected decreases to zero. The variation of temperature with the different cooling strategies is not small as it is seen grouping the different cases. Clear differences in the H2 metal node behaviour with different cooling strategies is obtained. The cases 1,2,5,6 show a higher temperature than the others since no auxiliary pumps are considered and differences in maximum peak temperature and the time needed are small. For the other cases simulated, the behaviour is similar between them since the movement of water or oil is still running for about two minutes after the engine is stopped. When the cooling supply is switched off, the evolution of temperatures are rising and tend

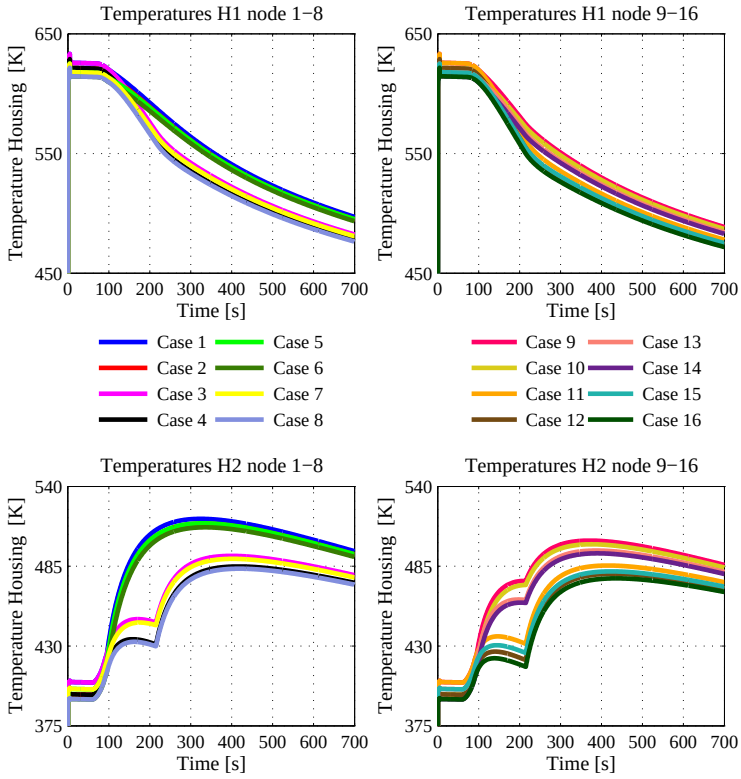

Figure 4.8: Evolution of temperatures in H1 and H2 metal nodes for all simulated cases

to be similar to those from the 1, 2, 5 and 6 group. However, the maximum temperatures from this group are never reached because of the heat loss. The water cooling strategy is more effective than oil pump. The lack of auxiliary oil pump does not affect much to the temperature control, as shown in cases 3, 4, 7, and 8.

The observed response indicates that the specific energy consumption during a whole driving and hot stop cycle by both the oil and coolant pumps can be minimized for a temperature objective by choosing a proper cooling strategy. This specific energy consumption is expressed as the amount of energy consumed by the pumps divided by the drop in maximum node H2 temperature. The case 1 is used as a baseline for comparisons. The maximum oil temperature inside the bearing system is unknown, but it should be correlated with the bearing housing temperature (as shown in Figure 4.6). A reduction in maximum H2 temperature should lead to a reduction in maximum oil temperature and thus,

the coke formation.

The results of temperature drop are shown in Table 4.4. The highest temperature drop is obtained with the combination of high flow rates of oil and coolant during normal operation of the engine and also by operating the auxiliary pumps as expected.

Table 4.4: Delta temperature decrease in H2 metal node

H2 drop [K] ΔT				Oil Cooling			
				Yes auxiliary system		No auxiliary system	
				+	-	+	-
Water Cooling	Yes	Auxiliary system	+	case 16 41	case 12 38	case 8 34	case 4 33
			-	case 15 36	case 11 32	case 7 28	case 3 26
	No		+	case 14 24	case 10 18	case 6 6	case 2 3
			-	case 13 22	case 9 15	case 5 3	case 1 0

The power consumption of the pumps is approximated by a linear correlation with the fluid flow rates, taking into account only the requirements for the turbocharger. In the case of coolant pump, the power consumption is around 25 W for typical flow rates of 0.15 kg/s, whereas for the oil pump power consumption is around 60 W for typical flow rates of 0.015 kg/s. The specific energy consumed during the simulated cycles is shown in Table 4.5. The specific CO_2 emissions are estimated for a diesel engine with an average engine efficiency of 33%. The optimum results, in terms of energy consumption per K of H2 temperature decrease are obtained with the original pumps and using an auxiliary coolant pump after the engine stops (case 3). Worse results are obtained in all the cases by using bigger oil pump, as it consumes more energy and the effect is not big. When using both auxiliary pump, (case 11) the decrease in maximum H2 temperature is higher, but the specific energy consumption rises faster than when using only the coolant pump (case 3). However, differences between the results of auxiliary pumps and the increase in CO_2 emissions are small in both cases. It is worth noting that in the case of an oil-cooled turbocharger, the auxiliary oil pump solution is expected to generate oil leakages if any new oil sealing technology is used.

Table 4.5: Extra specific consumption and emissions for sixteen simulated cases

CO_2/K				Oil Cooling			
kJ/K				Yes auxiliary system		No auxiliary system	
				+	-	+	-
Water Cooling	Yes	auxiliary system	+	1.51	0.37	1.79	0.41
				6.81	1.68	8.05	1.85
			-	1.34	0.02	1.74	0.01
				6.05	0.1	7.86	0.03
	No		+	2.6	0.79	10.46	3.96
				11.71	3.57	47.2	17.88
			-	2.22	0.04	15.61	
				10	0.17	70.4	

The calculated specific energy consumption associated with this cooling method is maximized when a normal cooling strategy in combination with a big oil pump has been modelled. The auxiliary water-cooling pump seems to produce the optimum results in terms of specific energy consumption, as it has more cooling capacity with less power consumption than the oil pump.

4.3 Analysis of turbine thermal decoupling

A frequent challenge in the turbocharger is the development of durable turbine designs. Nowadays, the engine operating temperatures are increasing which in turn impose increasing thermal loads on critical turbocharger components like turbines. This section explains thermal decoupling strategy aimed at improving conditions of temperature in the turbocharger on the hottest spots of the engine. On the basis of thermal model simulations of turbo isolated in 2D and 3D [6].

In order to check the thermal distribution proposed by turbocharger manufacturers in both turbine housings, GT-Power ^{TM} simulations were performed with a conventional turbine referred as housing 1 and the thermal decoupled turbine referred as housing 2. The heat transfer model showed in subsection 4.2.1 has been used. Thermal simulations with 3D models from manufacturers shows that decoupled turbine reduces the temperature in about 25 °C along the core of the turbocharger.

The simulations are carried out using the same hot stop cycle shown in Figure 4.2. The initialization conditions for the simulations with both turbine housings are:

- Engine speed 3500 rpm
- Fuel flow of 35 mg/cc set for stabilization phase (whitout thermal inertia in the turbocharger)
- Bypassing of turbine and compressor by means of a bypass valve system
- Oil mass flow rate of 0,0001g/s (when the engine stops)
- Increasing of the engine speed in 96,1 seconds to get out of the area in which GT-Power ^{TM} fails
- Analysis during remaining time: 10 minutes

To simulate conditions of thermal decoupling the difference in weight with the conventional turbine (housing 1) was taken into account to adjust heat transfer values of capacitance and conductance in the simulation following the same order of magnitude. In Figure 4.9 the sub-plot a) shows the temperatures results in each node for the two turbine housings. Thermal decoupling turbine allows to reduce the temperature of around 27 degrees. The sub-plot b) shows the H1 and H2 nodes and the oil outlet temperature with which the oil is correlated. According to simulations, temperatures with conventional turbine (housing 1) are higher. At the oil outlet, the maximum peak is 434 K for conventional turbine, while for the thermal decoupled turbine (housing 2) the temperature in oil is reduced to 395 K.

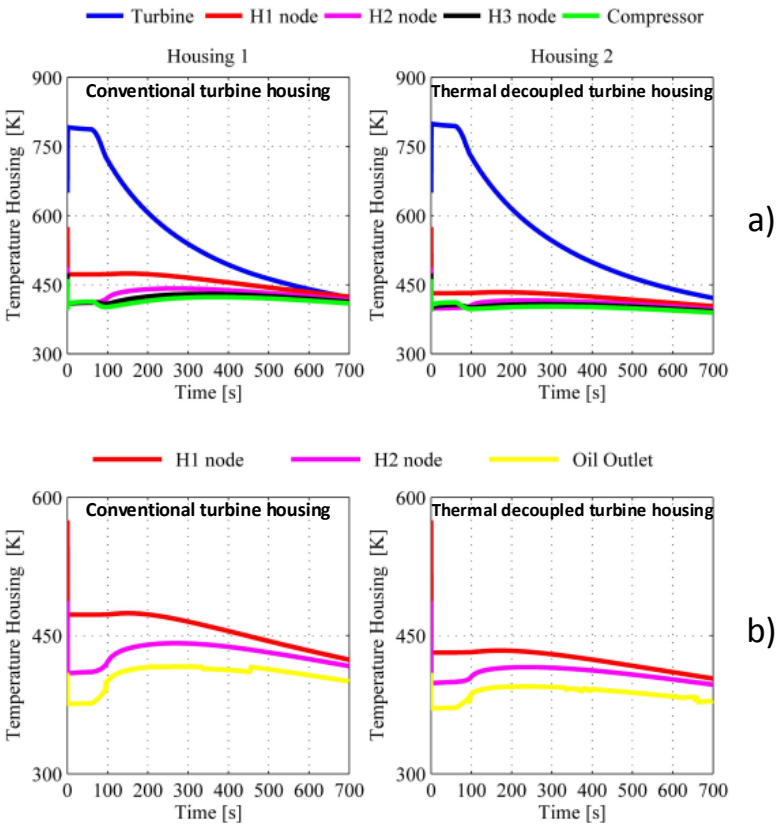

Figure 4.9: Turbocharger temperatures with conventional and thermal decoupled turbine housings

These results obtained coincide with the expected simulations with more complex 3D models. Nevertheless, experiments carried out in the engine test bench (subsection 3.4.2) show an opposite behaviour.

The idea of a thermal decoupled turbine housing is to radiate more heat out by reducing the thermal bridge between turbine housing and the backplate of the turbine. However, the heat radiated from the engine cannot be released by the core and internal temperatures in the central housing of the turbocharger are higher. Consequently, the heat transfer of radiation not only between the external ambient and the turbocharger but also between solid contact areas of the engine and turbocharger becomes important and can be exclusive of each engine-turbocharger configuration. The thermal sensitivity from the experiments showed that using the thermal decoupled housing, the temperature is approximately 10 °C higher in the turbine side (see Figure 3.11). This behaviour is evidenced at all engine operating points measured.

4.4 Cross analysis of oil coking

The objective in this part is evaluating the impact of oil coking on turbochargers and make a cross analysis with the variables explained in the experimental section 3.5. The use of this methodology is intended to quantify the damage that oil coking has in the turbocharger performance in a non-intrusive way. The analysis allows passing through the engine map of speed, in a relatively limited number of engine operating points (low, medium and high load) and therefore of tests.

4.4.1 Engine torque - VGT position

Some trends have been identified for the studied turbochargers. Figure 4.10 and Figure 4.11 show the engine torque drop and closing of the VGT as a function of engine speed and along 100 hot-stop cycles for oils type “A” and “C” respectively. For the tests at low and medium engine speed, the oil quality affects and makes a noticeable difference in the engine and turbocharger performance. The VGT vanes position close and produce reaction in a big proportion to the torque level for turbochargers tested with oil “C” while the variations in VGT and torque are small for the tests with oil type “A”.

The oil “C” at 7% of soot is degraded and aged severely with small capacity to maintain in suspension that great amount of soot. In this case, the position of VGT closes in large proportion over the hot stop cycles. An engine operating point hot or colder does not produce a significant difference with this oil condition, the VGT closes in similar proportion to increase the pressure ratio and the turbine isentropic power. For instance, in Figure 4.10 after 90 hot-stop cycles with oil “A” 4% of soot the engine torque is 210 N.m and 44% of VGT at 2500 rpm; while for the oil “A” 7% of soot and 2500 rpm there are a 208 N.m of torque and 47% of VGT.

4.4.2 Compressor efficiency - Turbocharger efficiency

Figure 4.12 and Figure 4.13 show the efficiency loss in the compressor and turbine for oil type “A” and “C” respectively as function of engine speed, hot stop cycles and soot content. The high temperature in the bearing system generates high concentration of coke inside producing a greater loss of performance in the turbocharger. Higher viscosity in oil “C” produces greater friction, and therefore higher drop in the turbocharger and compressor efficiencies.

For instance in Figure 4.12 at the beginning of the endurance test with oil “A” 4% soot and 2000 rpm, the loss of efficiency in the compressor is 0.01 points

in 27 cycles, while in Figure 4.13 with oil “C” the same loss of efficiency can be observed in only 15 cycles.

In the second half of the endurance tests, turbocharger deterioration becomes faster. Again in Figure 4.12 oil “A”4% soot taking an example from cycle 60 hereinafter lose 0.01 points of compressor efficiency take about 21 hot-stop cycles while in Figure 4.12 with oil “C” lose 0.01 points can be reduced to 9 cycles (less than half of those cycles taken by “A”oil).

Turbocharger efficiency losses are lower than losses in the compressor side for all cases. Significant reduction of compressor efficiency has been measured but no so much of turbocharger efficiency even when VGT was closed. This allows concluding that compressor efficiency deteriorates more than mechanical efficiency [151].

4.4.3 Turbocharger deceleration "time to stop"

Figure 4.14 shows the deceleration time in turbochargers as a function of bearing temperature, oil type and soot content. The oil quality affects the deceleration time, the turbochargers measured with more viscous oils and higher level of soot stop faster. The turbochargers measured with oil “C” take a time of stopping less than 1 second while turbochargers using with oil “A” take between 1.5 and 6 seconds to stop once the engine is switched off.

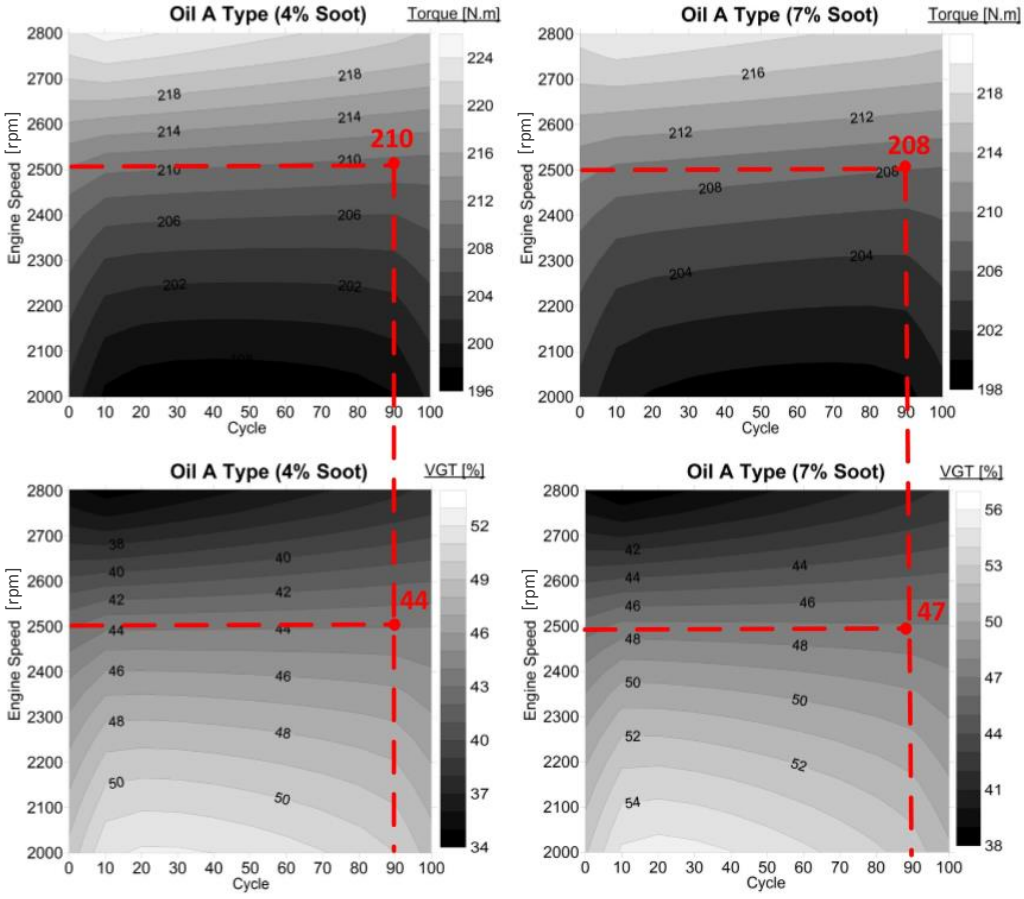

Figure 4.10: Engine torque and VGT position using oil type “A” as function of engine speed, hot stop cycles and soot content

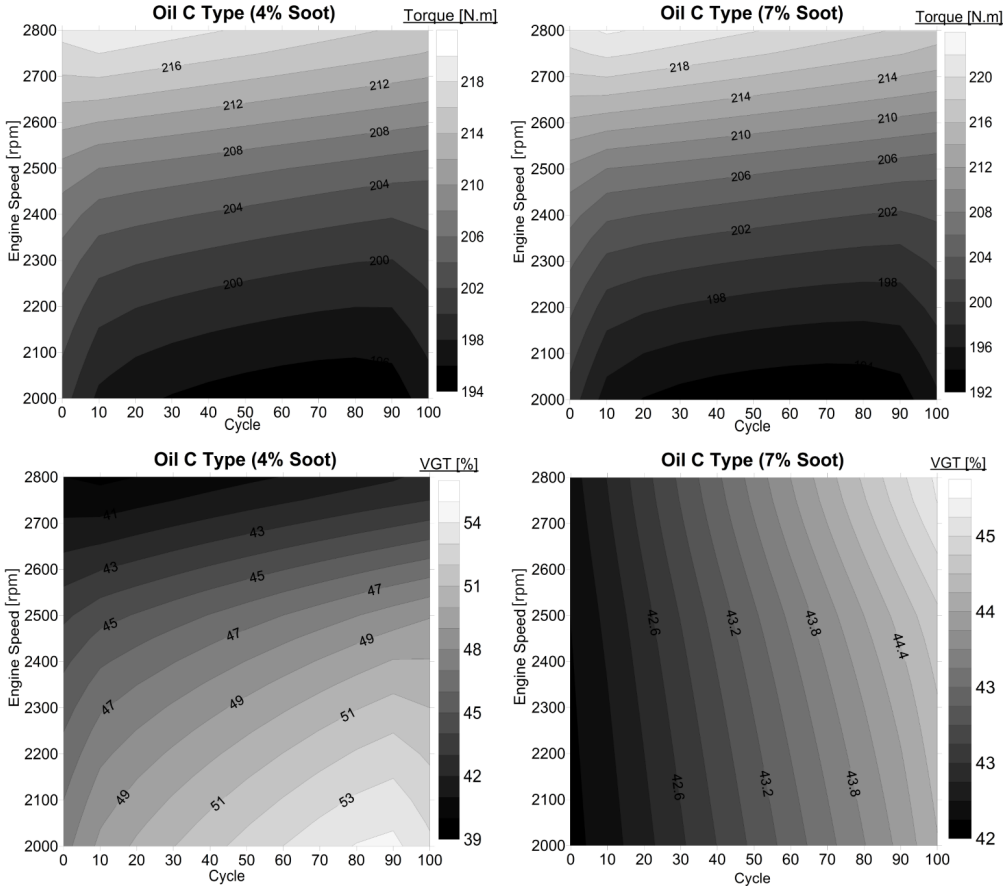

Figure 4.11: Engine torque and VGT position using oil type “C” as function of engine speed, hot stop cycles and soot content

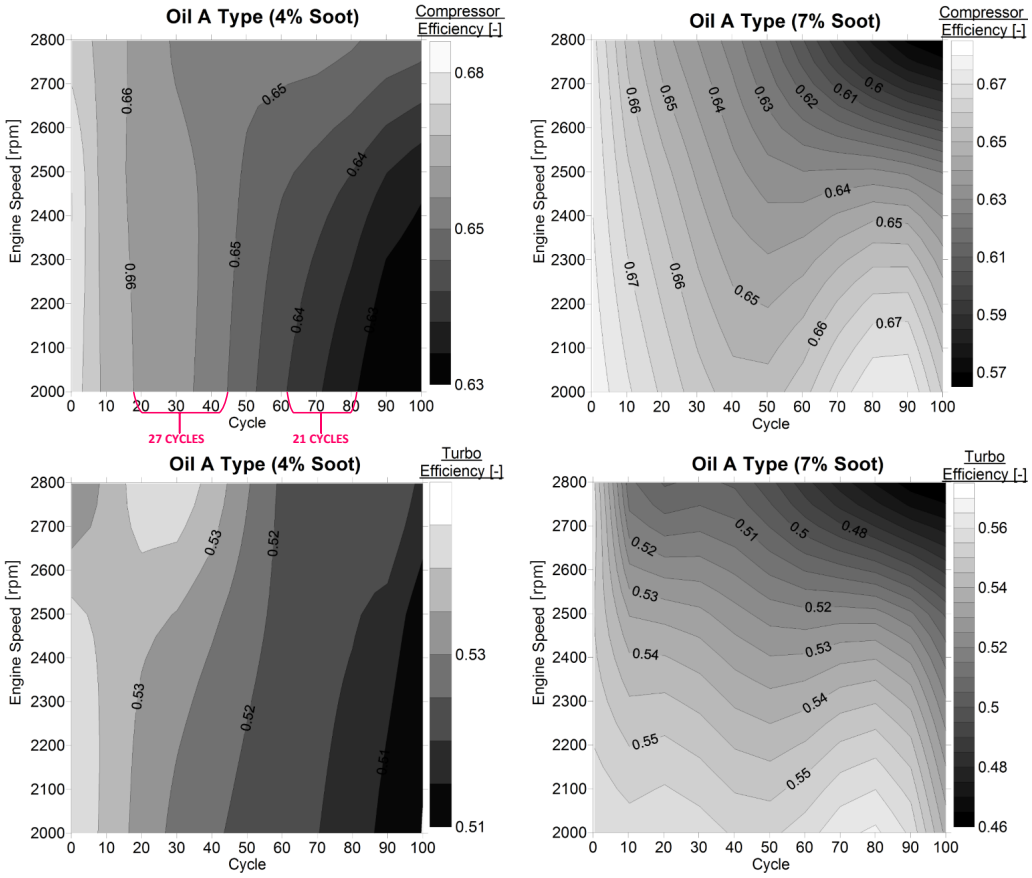

Figure 4.12: Compressor and turbine efficiencies using oil type “A”as function of engine speed, hot stop cycles and soot content

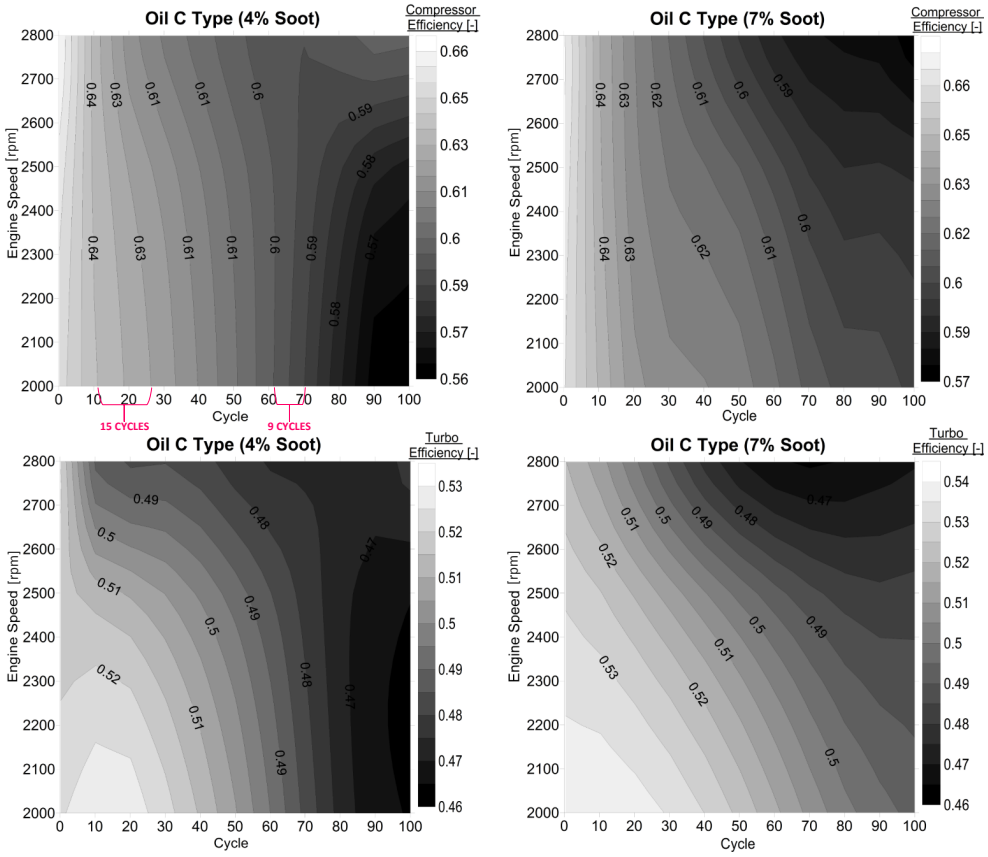

Figure 4.13: Compressor and turbine efficiencies using oil type “C”as function of engine speed, hot stop cycles and soot content

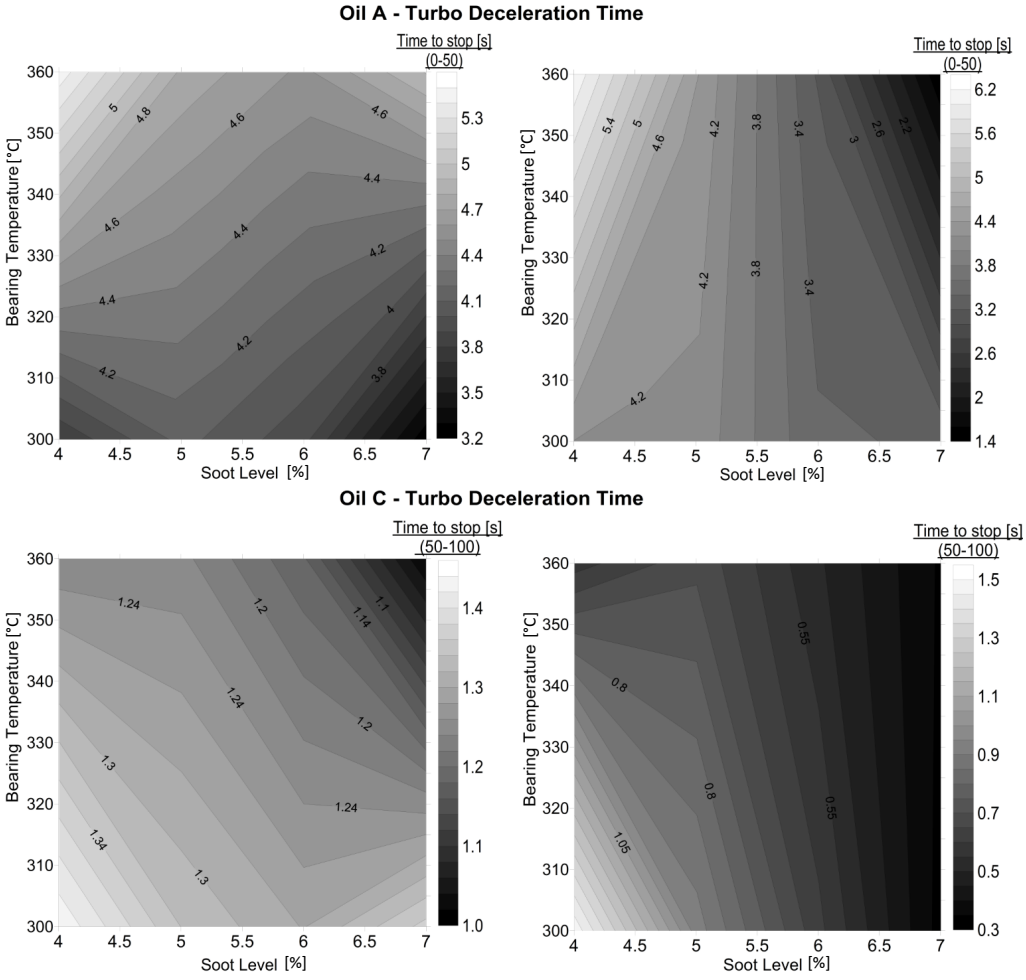

Figure 4.14: Deceleration time in turbochargers as function of bearing temperature, oil type and soot content

4.4.4 Turbocharger deceleration - Weight and Compressor efficiency

Figure 4.15 integrates the average of the "Time to stop", the weight increase in each test and the loss of compressor efficiency for turbochargers measured with oils type “A” and “C”both at 4% and 7% of soot content. The filled markers correspond to “A” oils and the empty markers to the “C” oils. The sub-plot a) is the average “time to stop” on each test for the first fifty cycles. With “A” type oils, the rotating assembly takes more in stand (greater time to stop) while with the type “C” turbochargers stop right after the engine stops.

In Figure 4.15 it can be observed that a higher operating point and using “A” oils generate a time to stop greater (red circle). In the case of oils type “C”, all the turbochargers are grouped (black and green circles); the point of operation does not influence significantly.

Weight increments after endurance tests depend on both, the operating condition and the content of soot. A high soot content and/or higher bearing temperature generate more accumulation of coke deposits in the central housing.

Figure 4.15 sub-plot b) represents the “Time to stop" moving average difference between the first and last fifty cycles. There can be observed that all the tests carried out with oil “A” have a negative delta “time to stop” (turquoise circle), hence the turbochargers take longer to stop in the second half of the endurance test. On the other hand, turbochargers measured with “C” oils stop sooner as the endurance test progress (time to stop positive values).

Figure 4.16 integrates the average of “time to stop”, the weight gain and the compressor efficiency loss for turbochargers measured with oxidized oil and its counterpart not oxidized, all measured under the same engine operating point 2500 rpm and 75% of full load. The sub-plot a) is the “time to stop” moving average for the first fifty cycles, and sub-plot b) is the "Time to stop" moving average difference between the first and last fifty cycles. Turbochargers tested with non-oxidized oil “A” suffer lower compressor efficiency drop (less than 0.7). While, turbochargers measured with oil type “C” or oxidized oils suffer a loss in compressor efficiency greater than 0.10. The carbonaceous mass is a precursor of the deposits. A weight gain greater than 4 grams is found in all turbochargers using either “A” or “C” oils at 7% soot (see red dotted line to the right side).

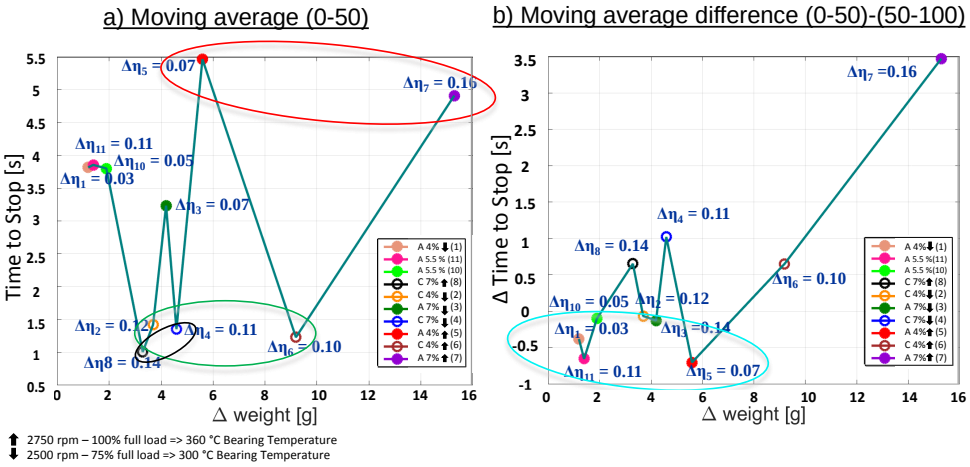

Figure 4.15: Integration of turbo deceleration, weight and compressor efficiency using “A-C” oils

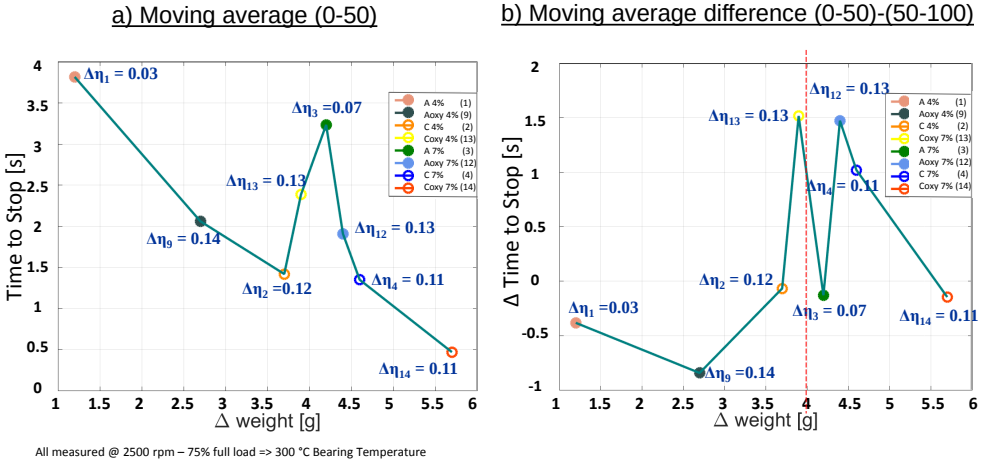

Figure 4.16: Integration of turbo deceleration, weight and compressor efficiency using “Aoxy-Coxy” oils

4.4.5 Turbocharger effective lubrication section - Weight

A reduction of the effective lubrication section is evidenced over the engine hot stop cycles. This reduction is correlated with the engine operating conditions and the oil quality. Higher discharge coefficient produces lower flow rate (effective section reduction) consequently, the permeability in the bearing system is reduced. This effective section reduction is well correlated with the delta weight results obtained.
Table 4.6 shows the slope of reduction of the effective section of lubrication in the turbocharger and the delta weight ordered from higher to lower. Some differences were observed in the study of the dispersion for the endurance test at high load and speed in which oil "A" at 7% has been used.
Figure 4.17 shows oil coking deposits found in the turbocharger tested at high engine speed and load with type "A" oil at 7 % soot. The accumulation of soot and coke produces effects on the rotation of the bearing, in fact the variations observed in the results. Additionally, the weight difference before and after the endurance test was approximately 15.3 g (bold in Table 4.6). This turbocharger has the largest efficiency drop and operating clearances shaft/bearing and bearing/central housing.

Figure 4.17: Oil coke deposits in a turbocharger tested at 2750 rpm- full load and oil "A" at 7% soot

Fluctuations in turbocharger measured with the oil "C" at 4% soot and low load question the conclusions obtained in endurance test.

Table 4.6: Discharge coefficient and weight gain after oil coking test using “A-C” oils

Oil Type	**rpm-load**	DC_{Slope}	$\Delta Weight[g]$
C 4%soot	2750-100%	-7.60E-05	9.20
A 7%soot	2750-100%	-6.07E-05	**15.30**
A 4%soot	2750-100%	-4.33E-05	5.60
C 7%soot	2500-75%	-2.32E-05	4.60
A 7%soot	2500-75%	-2.15E-05	4.20
C 7%soot	2750-100%	-2.03E-05	3.30
A 4%soot	2500-75%	-1.95E-05	1.20
C 4%soot	2500-75%	No data	3.70

Reduction of the effective section of lubrication in the turbocharger, and the delta of weight for the oxidized oils are shown in Table 4.7. Having a previous oxidation in the oil causes a weight difference greater than with their respective non-oxidized oil qualities. A higher delta weight in oxidized oils is proportional to the soot level. At higher soot greater turbocharger delta weight either for “Aoxy” or “Coxy” oils.

Table 4.7: Discharge coefficient and weight gain after the oil coking test using “Aoxy-Coxy” oils

Oil Type	**rpm-load**	DC_{Slope}	**Weight [g]**
C oxy 7%soot	2500-75%	-1.14E-04	5.70
C oxy 4%soot	2500-75%	-5.52E-05	4.40
Aoxy 7%soot	2500-75%	-2.39E-05	3.90
A oxy 4%soot	2500-75%	-6.61E-06	2.70

4.5 References

[6] V. Simon, G. Oberholz, and M. Mayer. “Exhaust gas temperature 1050 ° C An engineering challenge”. In: *BorgWarner TurboSystems Academy* (2000), pp. 1–12 (cit. on pp. 2, 112, 125).

[71] R. D. Burke. “Analysis and Modeling of the Transient Thermal Behavior of Automotive Turbochargers”. In: *Journal of Engineering for Gas Turbines and Power* 136.10 (2014). ISSN: 0742-4795. DOI: 10.1115/1.4027290. URL: http://gasturbinespower.asmedigitalcollection.asme.org/article.aspx?doi=10.1115/1.4027290 (cit. on pp. 21, 113).

[75] R. D. Burke, P. Olmeda, F. J. Arnau, and M. Reyes-Belmonte. “Modelling of turbocharger heat transfer under stationary and transient engine operating conditions”. In: *Institution of Mechanical Engineers - 11th International Conference on Turbochargers and Turbocharging*. Woodhead Publishing Limited, 2014, pp. 103–112. ISBN: 9780081000335. URL: http://www.scopus.com/inward/record.url?eid=2-s2.0-84933526285{\&}partnerID=tZOtx3y1 (cit. on pp. 21, 114, 145, 169).

[76] J. R. Serrano, P. Olmeda, F. J. Arnau, A. Dombrovsky, and L. Smith. “Analysis and Methodology to Characterize Heat Transfer Phenomena in Automotive Turbochargers”. In: *Journal of Engineering for Gas Turbines and Power* 137.GTP–14–1352 (2015), pp. 1–11. DOI: 10.1115/1.4028261 (cit. on pp. 21, 113, 145, 169).

[138] E. G. Ribeiro, W. B. Melo, and A. P. a. Filho. “Application of electric oil pumps on automotive systems”. In: *SAE International Journal Engines* 01.4086 (2005), pp. 1–7. DOI: 10.4271/2005-01-4086. URL: http://www.sae.org/technical/papers/2005-01-4086 (cit. on pp. 68–70, 120, 176).

[143] A. K. Sachdev, K. Kulkarni, Z. Z. Fang, R. Yang, and V. Girshov. “Titanium for automotive applications: Challenges and opportunities in materials and processing”. In: *Jom* 64.5 (2012), pp. 553–565. ISSN: 10474838. DOI: 10.1007/s11837-012-0310-8 (cit. on pp. 112, 165).

[144] D. Willermark and N. Smith. “Gt-Power Real-Time – Diesel engine model for Hardware in the Loop testing”. In: *GT-SUITE Conference*. Vol. 2009 (cit. on p. 112).

[145] M. Vimal, P. Abhay, and D. Sriprakash. “Study and application of predictive combustion model for parameter optimization in diesel engine”. In: *Hinduja Tech Limited GT-SUITE India Conference*. 2018 (cit. on p. 112).

[146] J. Kang, B. Lee, and D. Jung. “Evaluating the Effect of Two-Stage Turbocharger Configurations on the Perceived Vehicle Acceleration Using Numerical Simulation”. In: 2016. DOI: 10.4271/2016-01-1029. URL: http://papers.sae.org/2016-01-1029/ (cit. on p. 112).

[147] T. L. Bergman, A. S. Lavine, F. P. Incropera, and D. P. Dewitt. *Fundamentals of Heat and Mass Transfer*. Vol. 7th Editio. 1. 2011, ISBN 13 978–0470–50197–9. ISBN: 9780471457282. DOI: 10.1016/j.applthermaleng.2011.03.022. arXiv: 1105-. URL: http://www.osti.gov/energycitations/product.biblio.jsp?osti{_}id=6008324 (cit. on pp. 113, 152).

[148] J. Serrano, P. Olmeda, F. Arnau, and A. Dombrovsky. “General Procedure for the Determination of Heat Transfer Properties in Small Automotive Turbochargers”. In: *SAE International Journal of Engines* Friday, October 03, 2014 (2014), p. 12. DOI: 10.4271/2014-01-2857 (cit. on pp. 119, 120, 151).

[149] J. Serrano, P. Olmeda, F. J. Arnau, M. a. Reyes-Belmonte, and H. Tartoussi. “A study on the internal convection in small turbochargers. Proposal of heat transfer convective coefficients”. In: *Applied Thermal Engineering* 89 (2015), pp. 587–599. ISSN: 13594311. DOI: 10.1016/j.applthermaleng.2015.06.053 (cit. on pp. 119, 120, 153).

[150] M. A. Reyes Belmonte. “Contribution to the Experimental Characterization and 1-D Modelling of Turbochargers for IC Engines”. PhD thesis. University Polytechnic of Valencia, 2013 (cit. on pp. 120, 152, 169).

[151] L. M. García-Cuevas. “Experiments and Modelling of Automotive Turbochargers under Unsteady Conditions”. PhD thesis. Polytechnic University of Valencia, 2015 (cit. on p. 128).

CHAPTER 5

Fast radial and 3D turbocharger heat transfer models

Contents

Figures

Tables

5.1 Introduction

THE growing concerns about emissions in internal combustion engines, makes necessary a good prediction of the after-treatment inlet temperature in fast one-dimensional engine simulation codes. Different simple models have been developed during the last years, which improve the prediction of turbocharger heat transfer phenomena. Although these models produce good results when computing the turbine outlet temperature, those models focus on the axial heat transfer paths and lack the capability of producing detailed results about the internal thermal behaviour of the turbocharger. This chapter presents a study of the thermal characteristics in non-water cooling turbochargers by means of a radial and 3D heat transfer models. The proposed models have been developed using VBA interface and ANSYS CFX respectively.

The present chapter contains three main sections:

- section 5.2 deals with the description of the radial heat transfer model and its theoretical background. It describes the heat transfer equations that serve as base for modelling other turbochargers by modifying geometry, material, and boundary conditions with the advantage of computing the oil temperature inside the central housing and maximum level of temperature at different points in the bearing system. This model can be implemented in engine simulation codes such as GT-Power ^{TM} as an improvement of the existing axial model.

- section 5.3 focuses on the central housing 3D model. The meshing process and internal heat transfer modelling method are shown. This model is developed for understanding those physical phenomena difficult to observe by means of experimentation and also, to feed the radial heat transfer model.

- section 5.4 presents the tuning process applied for a non-water cooled turbocharger. The numerical models validation and main results are discussed in this section. The results of the models can be used to study heat exchanges occurring inside and the effects on turbocharger performance. It will allow evaluating thermal damage done to the system itself, guidance for researchers on the development of effective procedures and tools to cope with the technological exigencies in the optimum performance of the turbocharger system. As well as influences on the working fluid temperatures which leads oil coke formation, that can affect the engine performance [64].

5.2 Turbocharger heat transfer model

The model described in this chapter is a development from a previous axial turbocharger heat transfer model developed in [75, 76] and already described briefly in subsection 4.2.1. It originally consisted of an axial lumped model, which computes the temperatures and conductive heat fluxes between different parts of the turbocharger, oil, coolant, internal gases and some extra branches that compute the convective and radiative fluxes [61].

The original model was validated against experimental data, using static temperatures measured with thermocouples in both a continuous flow gas stand and an engine test bench. A thermal insulation was done to minimize axial and radial temperature variations. However, as the gas temperature remains uniform radially, several thermocouples were implemented near the turbocharger and near to the wall to have a more representative temperature and a weighted average was used, as described in [152]. The development of axial metal part of the turbocharger, is composed of a turbine node, a compressor node and three central housing nodes. Albeit being able to compute with good accuracy the compressor and turbine outlet static temperatures, this model neglected the radial fluxes inside the turbocharger. Development presented in this thesis introduces these radial heat paths, and so it provides a means for estimating the temperature in internal parts such as the bearing system.

The description of radial heat transfer model, tuning and validation for not water cooled turbocharger is shown in the next subsections.

5.2.1 Radial turbocharger model

This model discretizes the turbocharger in both the radial and axial directions, and computes the heat transfer and temperature at different parts of the machine.

The model represents the turbocharger as three cylinders maintaining the three important sections philosophy. Figure 5.1 shows the sections where (a) represents the turbine housing, (b) the central housing, and (c) the compressor housing (c). Each cylinder diameter is taken from real turbocharger geometry. For simplicity, it is assumed symmetrical about the plane containing the shaft axis. The model uses form factors to better approximate the real turbocharger geometry.

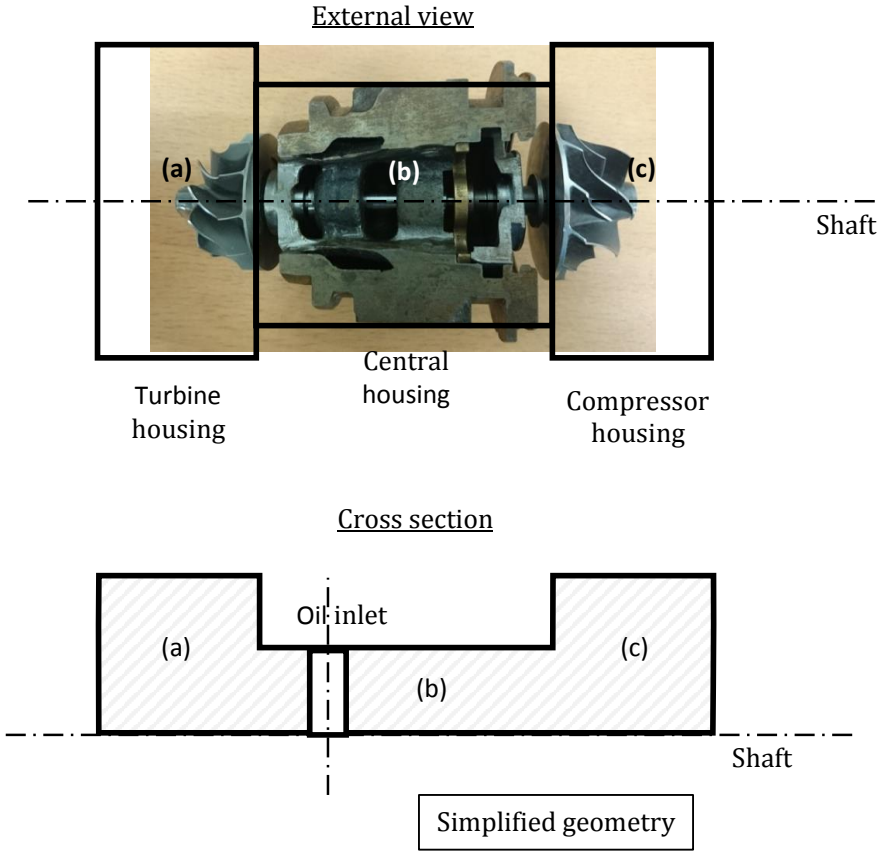

Figure 5.1: Turbocharger simplified geometry

The radial resolution of this model is obtained by adding three layers of metal nodes to the central housing (b). The five metal nodes defined previously have been used. In this radial model, nice new nodes have been added. The choice of the additional metal nodes is done taking into account the expected flow paths inside the turbocharger by analysing the actual thermal sources and taking into account the lubrication channels and bearings.

The radial model is presented in Figure 5.2. Nodes T (turbine housing), C (compressor housing) and H1, H2 and H3 (central housing, external surface) are kept, and are the easiest to measure experimentally. Nodes H4, H5 and H6 represent the internal metal nodes of the central housing, from the turbine side to the compressor side. This internal metal nodes exchange heat via convection

with the coolant, when present, and via conduction with external nodes H1, H2 and H3. Nodes denoted as H7, H8 and H9 are made of a different material depending of the turbocharger design, as they represent the bearings, and exchange heat via conduction with H4, H5 and H6 and via convection with the oil. Finally, nodes S1, S2 and S3 represent the turbocharger shaft, and exchange heat via convection with the oil and with the gases flowing through the turbine and compressor.

For the flow path, the nodes are IT and OD represent the turbine inlet gases and the compressor diffuser air, respectively. Coolant nodes are WI coolant inlet and WO coolant outlet. The heat exchange in the coolant is done at an average temperature represented in the scheme by term Wbox. Oil nodes are the oil inlet OI, the oil outlet OO, and three more intermediate points: O1, O2 and O3. Again, the convective heat transfer with the oil is done at mean temperatures, represented by Obox1, Obox2 and Obox3. The mechanical losses are represented by the term Qmech and are computed with the method described in [153]. In summary, the mechanical losses are computed with the Equation 5.1 and Equation 5.2:

$$\dot{Q}_{mech} = (e_{radial\ bearing} + e_{thrust\ bearing} \cdot e_{axial\ load}) \cdot \mu * N^2 \tag{5.1}$$

$$e_{axial\ load} = \left[\frac{\dot{m} \cdot \mu}{\Lambda_{axial}} \right]^{\frac{1}{3}} \tag{5.2}$$

where $e_{radial\ bearing}$ and $e_{thrust\ bearing}$ are constants for the radial bearing and thrust bearing effects, μ is the oil viscosity at the average temperature between O1 and O2, N is the rotational speed of the turbocharger, $\dot{m}$ is the oil flow rate and Λ_{axial} is the axial force, which can be estimated using the measured pressures at the inlet and outlet of the compressor and turbine.

The turbocharger is then considered as a thermal network consisting of a finite number of nodes, whose thermal inertia is characterized by capacitance, and linked with other nodes by means of conductances. The method for computing the phenomenon of heat transfer is presented.

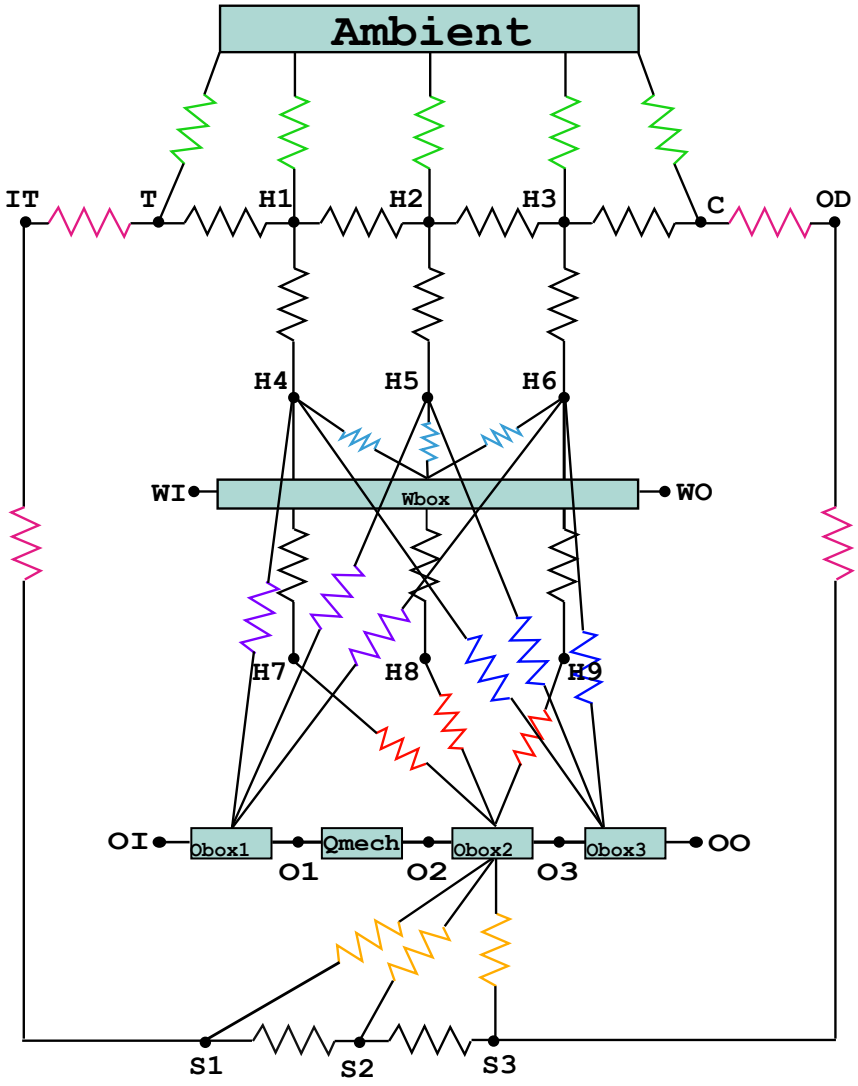

Figure 5.2: Turbocharger radial schematic model

5.2.2 Global model calculation

Once the model has been structured and divided into nodes, an energy balance is applied to each of these nodes by using Equation 5.3. The sum of heat fluxes between nodes in a time interval equals the change in the internal energy of the node:

$$\sum \dot{Q}_{Rad} + \sum \dot{Q}_{Cond} + \sum \dot{Q}_{Conv} = m_i \cdot C_{vi} \cdot \frac{\partial T_i}{\partial t} \tag{5.3}$$

From Equation 5.3 on the right hand side m denotes the mass of node i, C corresponds to its heat capacity. The term $\frac{\partial T_i}{\partial t}$ for the steady-state phase is equal to zero; and for the transient phase it can be approximated with $\frac{\Delta T}{\Delta t} = \frac{T(t)-T(t-step)}{step}$ where $\frac{1}{step}$ is the frequency of input data measurement. Heat fluxes that go in and out of the node can be calculated for each node using Equation 5.4.

$$\dot{Q}_{ij} = K_{ij} \cdot \Delta T_{ij} \tag{5.4}$$

where K_{ij} is a thermal conductance between nodes i and j and ΔT_{ij} is the temperature difference between nodes i and j. Equation 5.3 can be rewritten, when j represents the adjacent node of the i node in order to determine the heat flux between nodes as shown in Equation 5.5.

$$\begin{aligned}
\sum_i Krad_{i-j} \cdot \left(T_i - T_j\right) + Kcond_{i-j} \cdot \left(T_i - T_j\right) + Kconv_{i-j} \cdot \left(T_i - T_j\right) = 0 \\
\sum_i \left(Krad_{i-j} + Kcond_{i-j} + Kconv_{i-j}\right) \cdot \left(T_i - T_j\right) = 0 \\
T_i \cdot \sum_i \left(Krad_{ij} + Kcond_{ij} + Kconv_{ij}\right) - \sum_i \left(Krad_{ij} + Kcond_{ij} + Kconv_{ij}\right) \cdot T_j = 0
\end{aligned} \tag{5.5}$$

This system of equations is linear. Radiation terms are important for the model and cannot be neglected. External heat fluxes that come from turbine can lead up to a half of turbine enthalpy drop due to its higher temperature and its big areas [61]. External heat fluxes are about two orders of magnitude lower than heat losses from turbine node and in compressor side, heat flow can be lost or absorbed depending on the running conditions. These terms are added to estimate radiation interaction among the five-turbocharger external nodes. The system equations that represent the model are defined as an algebraic system, as shown in Equation 5.6. Assuming a boundary conditions vector T_{bc} that contains all the known temperatures and an unknowns vector T_x for all the output temperatures, the system becomes:

$$K \cdot \begin{bmatrix} T_{bc} \\ T_x \end{bmatrix} = \begin{bmatrix} T_{bc} \\ 0 \end{bmatrix} \tag{5.6}$$

where K is the conductances matrix. K is further expanded as shown in Equation 5.7:

$$K = \begin{bmatrix} I & 0 \\ C_i & M \end{bmatrix} \tag{5.7}$$

From Equation 5.7, I is the identity matrix, C contains the capacitances divided by the time step and M contains the conductance terms, added in the model for calculation in unsteady conditions. As expected, the conductances terms M are a function of the temperatures, so this system has to be solved iteratively. Matrix M is shown in Equation 5.8

$$M = (hA)_{ij} + (kA)_{ij} + (rad)_{ij} \tag{5.8}$$

The terms hA are due to convection, the terms kA are due to conduction and rad are the terms due to radiation. An element ij might be 0 if no direct heat flux path exists between nodes i and j. An element ii in the diagonal of the matrix contains all the conductivity, convection and radiation terms affecting node i. A generic element ij contains the conduction, radiation and convection terms between nodes i and j.

5.2.3 Thermal coefficients determination

Detailed information about the turbocharger internal geometry is often difficult to obtain, so the model parameters should be obtained using only basic data. An analytical method is used to obtain a first approximation of the conductance, correcting them with some form factor. Later, when experimental data is available, the model can be fine-tuned to produce more realistic results. The conductive conductance are computed taking into account the kind of connections between the different nodes: axial or radial. For axial connections, Equation 5.9 can be used, whereas Equation 5.10 can be used for radial connections.

$$(kA)_{i \to j} = \frac{\lambda}{L} \cdot A_{ij} \cdot F_{ij} \tag{5.9}$$

$$(kA)_{i \to j} = \frac{2\pi \cdot l \cdot \lambda}{\ln\left(\frac{r_e}{r_i}\right)} \cdot F_{ij} \tag{5.10}$$

Where k is the conductive conductance between the nodes, λ is the conductivity of material, A_{ij} are the contact areas between the nodes, L is the distance between nodes and r is the external or internal radius at the node. Form factors

F, take into account differences from the idealized geometry and are modified in the fine-tuned optimization process.

Equation 5.9 can be used to compute the conductances among shaft nodes, external nodes T, H1, H2, H3 and C, internal metal nodes H4 to H6 and between H7 to H9. Equation 5.10 is used to compute the conductances between nodes H1, H4 and H7, nodes H2, H5 and H8 and nodes H3, H6 and H9. In the simplified geometry, there are four different radii: one for horizontal nodes H1 to H3, another one for nodes H4 to H6 and a different, smaller radius for nodes H7 to H9 and the radius of axis that allows to calculate the conductance in the shaft. The entire radii are measured from the shaft axis.

Table 5.1 shows the calculation for each of the radial nodes of the model. For the bearing housing nodes, the values of β, γ and $1-\beta-\gamma$ are close to one third so the whole bearing housing division is distributed equitably. This axial fitting constants distribution are validated and published in [148]. Some of the nodes are located at the limit between two different materials thus, two values for the material conductivity are used.

Table 5.1: Calculation of the conductive conductance for radial nodes

Conductive conductance radial nodes	**Length [L]**	**re**	**ri**
(kA) H1→ H4	$\beta \cdot L_H$	R	r_H
(kA) H2→ H5	(1-β-γ)·L_H	R	r_H
(kA) H3→ H6	$\gamma \cdot L_H$	R	r_H
(kA) H4→ H7	β·L_H	r_H r_M	r_M r_B
(kA) H5→ H8	(1-β-γ)·L_H	r_H r_M	r_M r_B
(kA) H6→ H9	γ·L_H	r_H r_M	r_M r_B

Figure 5.3 shows some details of how lengths and radii were taken for the calculation. In blue β and γ are the longitudinal distribution of the length, the purple discontinuous lines are for the areas distribution along the turbocharger central housing, grey dots represent the nodes that radial model contains, and green dots represent the oil passage and interaction with the system.

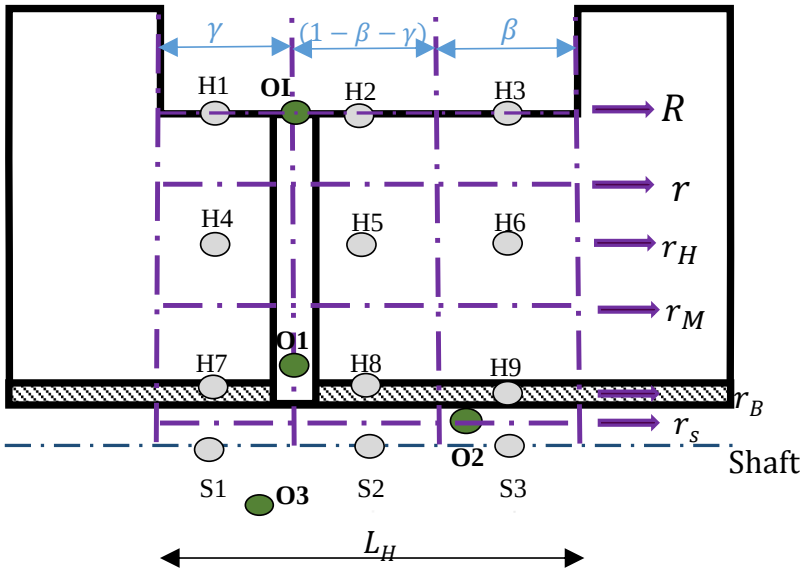

Figure 5.3: Details of the mesh used in the model, including radii and lengths

The convective conductances depend on the wetted area of the different nodes and on the turbocharger operating conditions such as fluid composition, rotational speed, mass flow and temperature. The Sieder–Tate type correlation [147] of Equation 5.11 is used in this model.

$$N_U = a \cdot {R_e}^b \cdot {P_r}^c \cdot \left(\frac{\mu_{fluid}}{\mu_{metal}}\right)^d \tag{5.11}$$

Where coefficients (a, b, c and d) must be fitted using the experimental data of heat fluxes [150]. The Reynolds number can be obtained using Equation 5.12. Where $\dot{m}$ is the mass flow, μ term is the oil viscosity and D represents the oil or water inlet port diameter of the turbocharger.

$$Re = \frac{4.\dot{m}}{\pi.\mu.D} \tag{5.12}$$

Prandtl number is related to temperature variations and can be obtained through the product of viscosity and specific heat of the oil, divided by thermal conductivity of the material, as shown in Equation 5.13.

$$Pr = \frac{\mu \cdot Cp}{k} \tag{5.13}$$

With the use of dimensionless numbers, convective conductance (Equation 4.2) can be calculated using the method described in [149] for the axial nodes T, H1, H2, H3 and C.

For all the other internal nodes, the convection is computed with a different method. Although the lack of detailed information about the complex oil flow inside the turbocharger might be compensated using a general correlation, as the ones used for the gases and the external heat transfer. Figure 5.4 shows a radial nodal scheme as a detail for a branch of the model. In steady-state operation, initially it is assumed that heat flow is going from $H1$ to $H4$ and should be equal to the sum of the heat flow going from $H4$ to the coolant, $Obox1$, $Obox3$ and $H7$. In the case studied, as the turbocharger was not water-cooled, the heat flow to the coolant is equal to zero. The energy balance is shown in Equation 5.14.

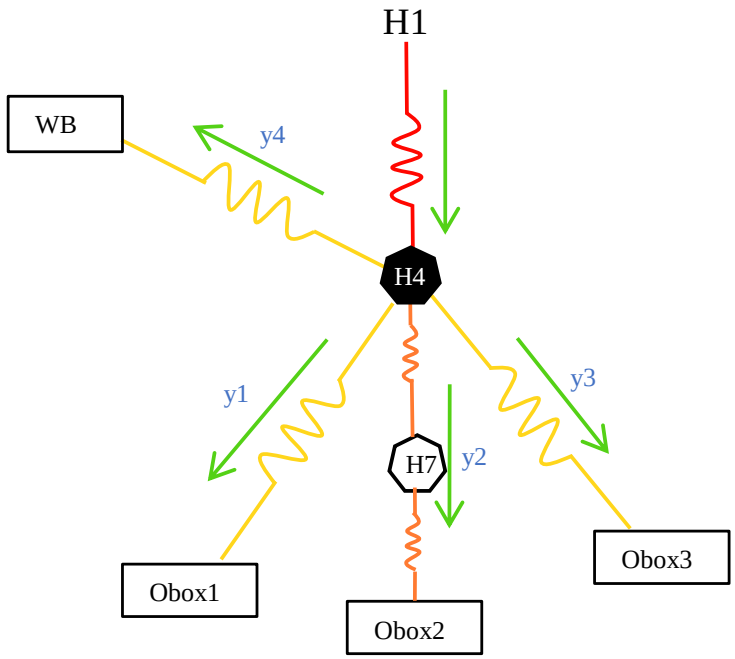

Figure 5.4: Heat flux internal distribution in first branch of the model

$$Q_{H1/H4} = Q_{H4/WB} + Q_{H4/obox1} + Q_{H4/obox3} + Q_{H4/H7} \tag{5.14}$$

The heat flows from $H4$ to $Obox1$, $Obox3$ and $H7$ are obtained as a fixed fraction of the total heat flow from $H1$ to $H4$:

$$Q_{H4/Obox1} = y_1 \cdot Q_{H1/H4} \tag{5.15}$$

$$Q_{H4/H7} = y_2 \cdot Q_{H1/H4} \tag{5.16}$$

$$Q_{H4/Obox3} = y_3 \cdot Q_{H1/H4} \tag{5.17}$$

Also, the heat flow from $H4$ to $H7$ is equal to the heat flow from $H7$ to $Obox2$ in steady-state conditions:

$$Q_{H7/Obox2} = y_2 \cdot Q_{H1/H4} \tag{5.18}$$

At first it is assumed that the heat flow $H1$ and $H4$ is the biggest thermal heat transfer in absolute value, nevertheless when the model treats a transient phase, or when input test data is not steady, the heat flux from backplate turbine ($H1$) and internal metal node ($H4$) $Q_{H1/H4}$ is not always the biggest thermal transfer. In order to avoid errors that would spread in every calculation, $y2$ is calculated as shown in Equation 5.19

$$y_2 = \frac{Min(Q_{H1/H4}; Q_{H4/H7})}{Max(Q_{H1/H4}; Q_{H4/H7})} \tag{5.19}$$

$$y_2 = \frac{Min((kA)_{H4-H7} \cdot (T_H4 - T_H7); (kA)_{H1-H4} \cdot (T_H1 - T_H4))}{Max((kA)_{H4-H7} \cdot (T_H4 - T_H7); (kA)_{H1-H4} \cdot (T_H1 - T_H4))} \tag{5.20}$$

The $y2$ term must be always inferior to the unit. The other fractions, $y1$ and $y3$, are computed as a fixed ratio of $y2$.

$$y_1 = (1 - y_2) \cdot F_{y1} \tag{5.21}$$

$$y_3 = (1 - y_2) \cdot F_{y3} \tag{5.22}$$

The selection of an appropriate value of Fy_i at this stage is arbitrary to demonstrate the impact that it could have on model accuracy.

Once this flow distribution is settled, the conductance between the $H4$ and $Obox1$ node can be calculated through Equation 5.23:

$$h_{H4-Obox1} = \frac{y1 \cdot max(Q_{H1-H4}; Q_{H4-H7})}{\Delta T_{H4-Obox1}} \tag{5.23}$$

where $Obox1$ is the average temperature between the oil inlet temperature and $O1$. The same process is used to compute the heat flow between $H4$ and

$Obox3$ and between $H7$ and $Obox2$. In addition, the same method is used for the nodes in the two extra radial planes of the model.

An empirical correlation of heat flow in a cylinder [154] is used for the convection between nodes $S1$, $S2$ and $S3$ and node $Obox2$. The radiation terms are kept same as used in the previous model [61], as they are only affecting the external nodes. The mechanical losses are computed in [132], playing role with temperatures between nodes $O1$ and $O2$.

During transient processes, metal nodes can store energy due to their associated mass. This phenomenon is taken into account in the model by means of heat capacity. The capacitance for the external nodes turbine (C_T), backplate turbine (C_{H1}), external central housing (C_{H2}), backplate compressor (C_{H3}) and compressor node (C_C) is theoretically calculated with Equation 5.24:

$$Ci = c_{material}.\rho_i.V_i.F_i \tag{5.24}$$

Where c is the massive heat capacitance of the material, ρ is the density, V_i is the volume for each node and F is a form factor considered since it is not a completely solid volume. The form factor considered, takes values between 0 and 1 since it is not a completely solid volume. There are fluid conduits where the lubrication or cooling passes inside the turbocharger. A zero value represents a hollow part and the unit will be used for a solid part.

Table 5.2 represents material properties used. It must be noted that if detailed data of turbocharger materials is available the information of Table 5.2 should not be used.

Table 5.2: Turbocharger thermodynamic properties

Part	**Material**	$k[W/mK]$	$\rho[kg/m^3]$	$c[J/kgK]$
Turbine	Cast Iron	36	7100	460
Compressor	Aluminum	205	2670	860
Housing	Cast Iron	48.4	7059	525

The heat capacity of the internal metal nodes (C_{H4}, C_{H5} and C_{H6}) and for the nodes of bearing (C_{H7}, C_{H8}, C_{H9}) will be obtained from a 3D bearing housing model. Additionally, a detailed solution of the heat fluxes by means of finite elements will be carried out making possible an optimization of the internal heat transfer prediction in this radial model. Once optimized and validated, the radial model can be coupled as an update of the existing axial model in engine simulation codes such as GT-Power ^{TM}.

5.3 3D bearing housing model

Several steps have been performed to provide general correlations for internal heat transfer calculations. The lack of information and the complex dynamics that occur inside the turbocharger make the modelling a challenging tasks. The following part focuses on the study of the thermal characteristics through a 3D bearing housing (BH) model using the commercial code ANSYS CFX.

This simplified model can be used as a diagnostic tool to study heat exchanges occurring inside and the effects on turbocharger performance. The advantage of computing the internal temperature in the central housing, lubrication channels, and maximum level of temperature at different points in the bearing system makes the reduction of experimental tasks. Additionally, the results obtained will serve to feed a faster radial thermal model previously described in subsection 5.2.1. The Figure 5.5 shows the methodology to evaluate the heat transfer in the bearing housing of the turbocharger.

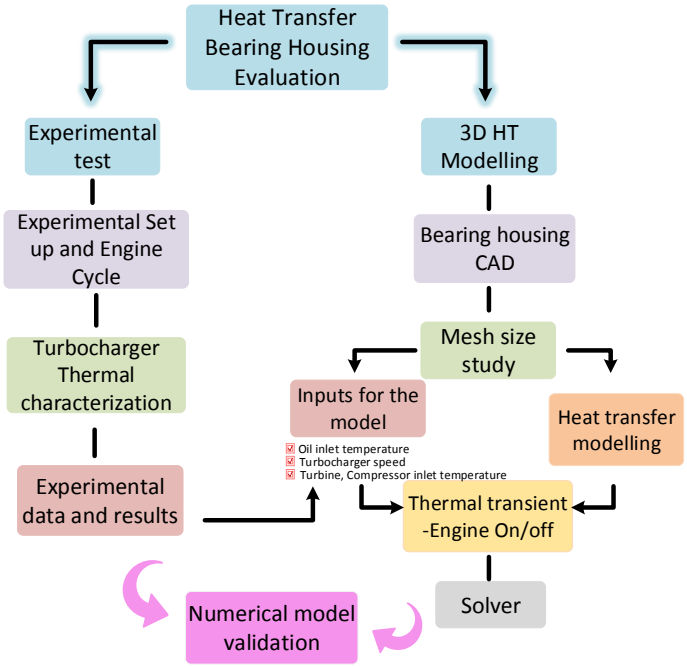

Figure 5.5: Methodology to evaluate internal temperatures in the turbocharger bearing housing

5.3.1 CAD model

A 3D BH is made taking into account a geometric simplification in order to have a model of fast calculation. It consists of the lubrication system, the bearings and shaft. The turbocharger compressor and turbine housings are excluded in order to simplify the complex 3D geometry; however, the related boundary conditions of temperature at compressor inlet, oil inlet and turbine inlet; convective film coefficients throughout the lubrication system and rotational speed of the bearings and of the shaft are imposed to get the appropriate trade off. The Figure 5.6 shows turbocharger BH and the detailed bearing system.

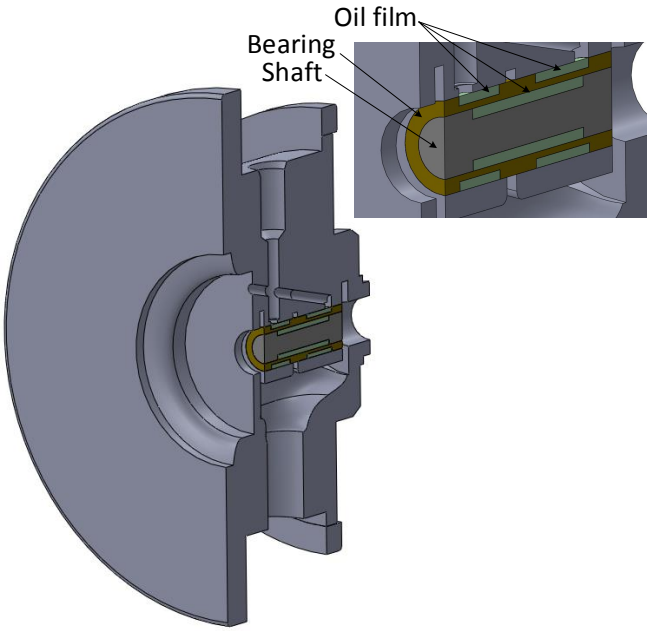

Figure 5.6: Turbocharger 3D bearing housing geometry

5.3.2 Mesh

The central housing uses a discrete element method model of the hybrid wire mesh. Discrete element methods are relatively computationally intensive, which limits the length of either a simulation or the number of particles. A numerical investigation of mesh sensitivity is done. The set-up of geometry and refinement of mesh have been studied to obtain a good extraction of results in a short calculation time. The element sizes studied were 0.002, 0.001, 0.0008 and 0.0005 m for the global mesh grid of the bearing housing in one engine operating point of high speed and load. Figure 5.7, shows the time of calculation Vs the maximum relative error between the experimental and simulations for the four

mesh sizes used. Table 5.3 details of nodes and element size of the mesh are given.

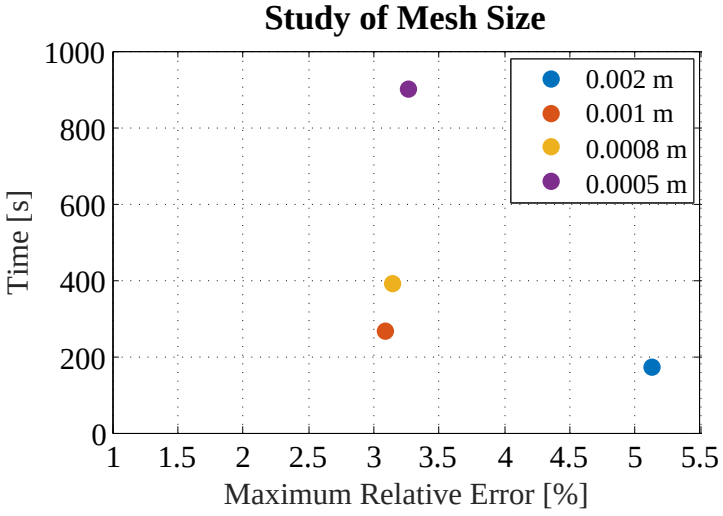

Figure 5.7: Mesh size study for CFX heat transfer simulation

Table 5.3: Meshing study - mesh size, elements, nodes and simulation time

Mesh size [m]	Elements	Nodes	Time [s]
0.002	47635	89756	170
0.001	146769	277005	266
0.0008	227143	435539	391
0.0005	632618	1233108	899

The selection of best element is systematically chosen to a size of 0,001 m. A refinement of mesh produces an increase in the computation time; besides, the relative difference error with the experiments is not very significant. In order to reduce the time of calculation without affecting the conclusions, mesh size for the compressor backplate was set to 0.005m. It is due to the low temperature of the air that compressor ingest at the inlet plus the fact that most of the temperature rise occurs in the diffuser.

5.3.3 Heat transfer modelling

In order to provide general correlations of heat transfer inside the turbocharger several steps must be performed. The lubrication system is discretized into

three sections. The Figure 5.8 shows the discretization that will be used for heat transfer coefficients determination. The lubrication system exchanges heat via convection with the bearing housing; thermal convective coefficients have been calculated in each of the discretized sections of the lubrication circuit. A mean temperature in each section of the fluid is imposed. The temperature in section 3 is obtained by taking into account the mechanical friction losses ($\dot{W}_{FL}$) and heat flux ($\dot{q}$) to the oil and calculated as a virtual source term of heat flux ($\dot{q}'$).

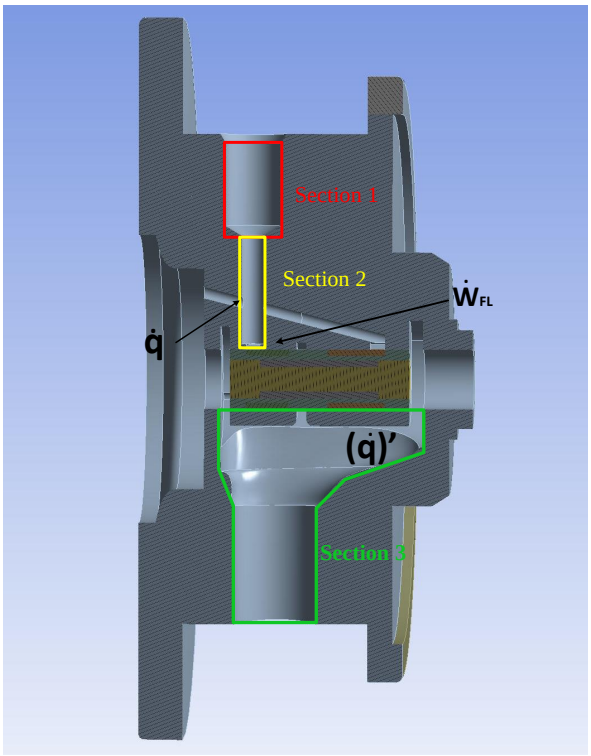

Figure 5.8: Discretization in the lubrication system of the bearing housing

The inputs of fluid physical properties have been considered on the heat transfer process. The Figure 5.9 shows the thermodynamic properties values for a 5W40 new engine oil to determine convective coefficients in the lubrication system.

From the thermodynamic properties, the next expression has been obtained and introduced in the model. The volumetric expansion coefficient (β) for this oil is equal to $7.10^{-4}/K$.

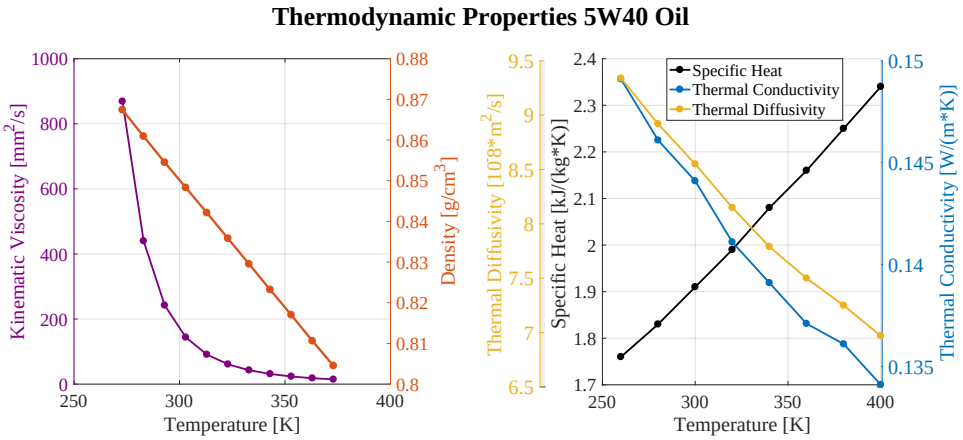

Figure 5.9: Thermodynamic properties 5W40 oil

- Kinematic Viscosity

$$\nu\ (T) = -5.478 \cdot 10^{-13} \cdot T^5 + 9.289 \cdot 10^{-10} \cdot T^4 - 6,297 \cdot 10^{-7} \cdot T^3 \ldots \\ \ldots + 2.133 \cdot 10^{-4} \cdot T^2 - 3.612 \cdot 10^{-2} \cdot T + 2.446 \left[\frac{m^2}{s} \right] \tag{5.25}$$

- Dynamic Viscosity

$$\mu\ (T) = -4.937 \cdot 10^{-10} \cdot T^5 + 8.366 \cdot 10^{-7} \cdot T^4 - 5.667 \cdot 10^{-4} \cdot T^3 \ldots \\ \ldots + 0.1918 \cdot T^2 - 32.462 \cdot T + 2196.8 \ [\ Pa \cdot s\ ] \tag{5.26}$$

- Density

$$\rho\ (T) = -0.6282 \cdot T + 1038.7 \left[\frac{kg}{m^3} \right] \tag{5.27}$$

- Thermal conductivity

$$k(T) = -4.161 \cdot 10^{-10} \cdot T^3 + 7.876 \cdot 10^{-7} \cdot T^2 - 4.886 \cdot 10^{-4} \cdot T + 2.303 \cdot 10^{-1} \left[\frac{W}{m \cdot K} \right] \tag{5.28}$$

- Specific Heat

$$C_p\ (T) = 4.167 \cdot T + 665.000 \left[\frac{J}{kg \cdot K} \right] \tag{5.29}$$

The convective conductance for the lubrication sections in the turbocharger BH need to be determined. For this purpose, dimensionless numbers of Reynolds, Prandtl and Nusselt are used. The Reynolds number can be obtained using Equation 5.12. Low Reynolds numbers are obtained with values between 91.4 and 457 for all engine-operating conditions measured. Prandtl number is related with temperature variations and it can be be obtained using Equation 5.13.

Since the flow patterns tend to be dominated by laminar flow, a heat transfer correlation based on Nusselt number [155] for laminar flow is used as shown in Equation 5.30. This equation can be used for steady state conditions in short or long tubes, forced convection and any type of fluid.

$$Nu = 3.66 + \frac{0.065\ Re\ Pr\frac{D}{L}}{1 + 0.04\ (Re\ Pr\frac{D}{L})^{2/3}} \tag{5.30}$$

The D and L terms represent the diameter and length of the tube section that interacts with the fluid. As length of the tube increases, the number of Nusselt tends to 3.66, being this the result for a wall temperature uniform when the temperature range is fully developed. The Table 5.4 shows effective diameter and length used in each of the three discretized sections of the lubrication system.

Table 5.4: Geometric data of the lubrication ducts

Lubrication	**Section 1**	**Section 2**	**Section 3**
D_{Eff} x10^{-3} [m]	9,05	4,18	13,48
L_{Eff} x10^{-3} [m]	13,51	17,7	24,78

The convective heat transfer coefficients for the lubrication sections are determined using Equation 4.2. Figure 5.10 shows the convective heat transfer coefficients obtained for the 5W40 oil under different engine operating conditions.

Heat gradients in the turbine side have been considered, since it is the hottest spot of the turbocharger. Experimental data has been used for obtaining a general expression for steady state. In Figure 5.11 the sub-plot a) shows the correlation obtained between the gas inlet temperature and the temperature of central housing turbine side. The sub-plot b) is a coefficient of adjustment (C(Op)) that considers the variations of temperature according to the engine operating condition.

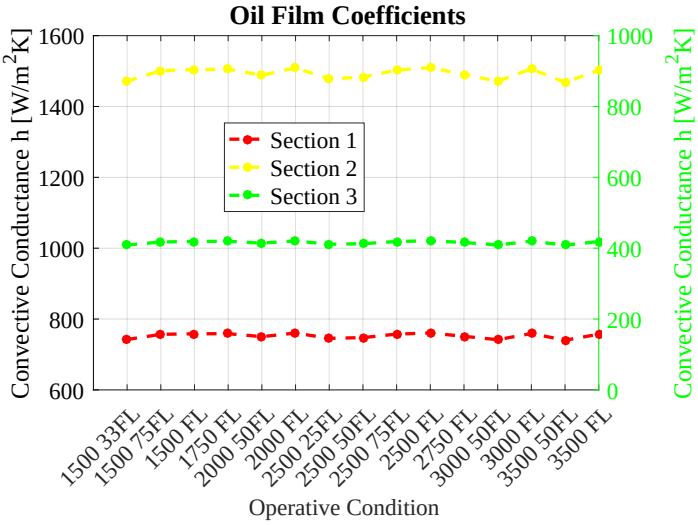

Figure 5.10: Convective coefficients for lubrication system sections of the BH

From Figure 5.11, the Equation 5.31 can be obtained for steady state conditions in the turbine side internal face.

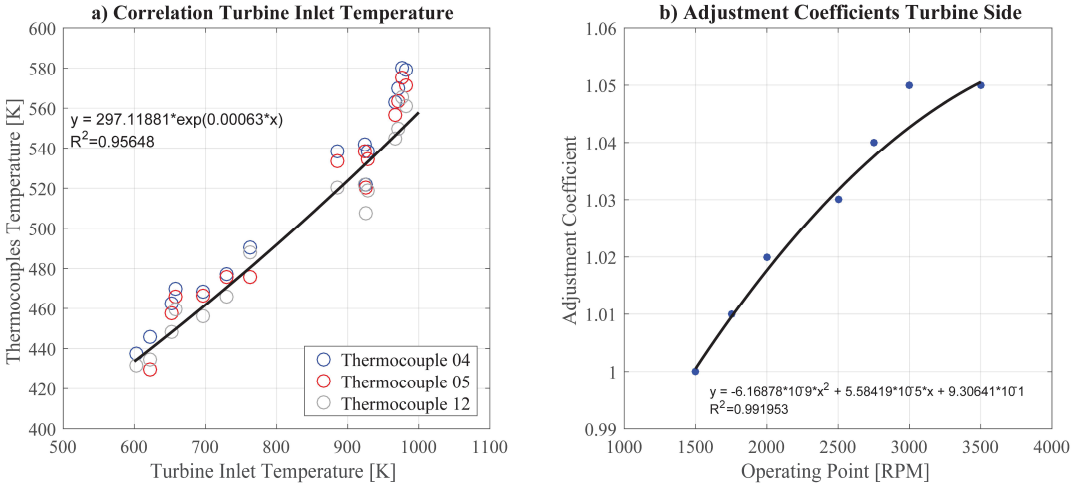

Figure 5.11: Correlations to determine temperature in the bearing housing (turbine side)

$$T_{BH\ Turbine}(T_{iT}, Op) = C(Op) \cdot 297.11881 \cdot e^{0.00063 \cdot T_{eT}} \tag{5.31}$$

Where:

$$C(Op) = -6.16878 \cdot 10^{-9} \cdot Op^2 + 5.58419 \cdot 10^{-05} \cdot Op + 9.30641 \cdot 10^{-01} \quad (5.32)$$

Thermal transient conditions – engine start/stop. Additionally, an expression has been obtained for the engine hot-stop conditions in the turbine side. Equation 5.33 correlates the temperature of turbine housing (Node T) and the turbine internal face near piston ring.

$$T_{Turb\ int}(T_{wall\ Turb}) = 1.0684 \cdot T_{wall\ Turb} - 23.099 \quad (5.33)$$

From Equation 5.33, the term $T_{wall\ turb}$ is the temperature of external node T from experimental measurements. Two random subset of experimental data have been used to evaluate these correlations. Later, the validation will be done using the whole data set.

During the engine stop, the oil stops circulating through the lubrication lines. In these ducts, lubricant stagnations may occur especially in the drain section (section 3 in Figure 5.8). Heat transfer correlation based on Nusselt number for natural convection is used to calculate the convection between metal and lubricant through Equation 5.34 [156].

$$Nu = 0.27 \cdot Ra^{1/4} \quad (5.34)$$

Where Ra is the number of Rayleigh that indicates the preponderance of heat transmission by conduction or convection in the bosom of a fluid and can be obtained through Equation 5.35.

$$Ra = Pr \cdot Gr \quad (5.35)$$

In turn, Rayleigh is dependent on the number of Grashof that expresses the ratio between buoyant forces and viscous forces. This dimensionless number can be defined as follows:

$$Gr = \frac{g\ \beta\ (T_S - T_\infty)\ L^3}{\nu^2} \quad (5.36)$$

Where g is the acceleration due to gravity, β is the coefficient of thermal expansion, T_s is the surface temperature, T_∞ is the temperature of the fluid, L is the characteristic length and ν is the kinematic viscosity.

Thermodynamic properties. The thermodynamic properties of the material BH are set. For the main central housing body the material is assumed cast iron. A study of the cast iron thermal conductivity depending on temperature can be found in [157, 158]; the thermal conductivity and specific heat is shown in Figure 5.12.

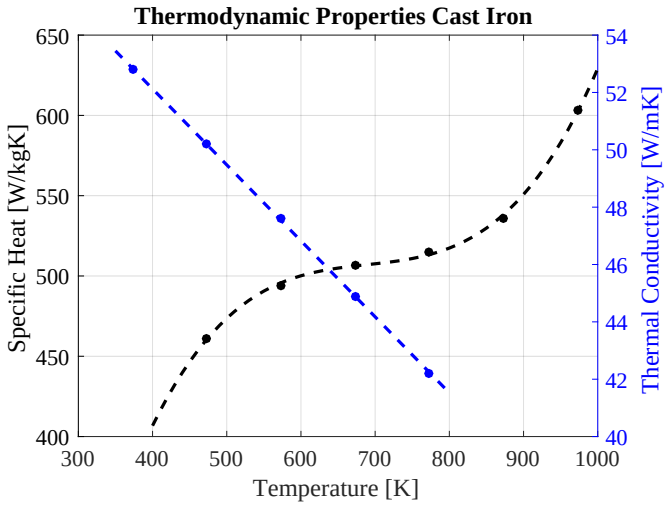

Figure 5.12: Cast iron thermodynamic properties.

From Figure 5.12, the Equation 5.37 and Equation 5.38 can be obtained and used in the central housing of the model.

$$C_p(ci) = 3.5556\ .10^{-6}.T^3 - 7.3513.10^{-3}\ T^2 + 5.1158 + T - 6.9092.10^2 \quad (5.37)$$

$$k(ci) = -0.0265\ .T + 62.725 \quad (5.38)$$

The performance and robustness in the bearings are represented in this model using as a material silicon nitride properties. The combination of thermal, dielectric, wear, and superior high-temperature mechanical properties has led to implementation of silicon nitride ball bearing [15] in most turbochargers applications. The Figure 5.13 shows the specific heat and thermal conductivity of the silicon nitride (Si3N4) [159] where Equation 5.39 and Equation 5.40 can be obtained and set for bearings in the model.

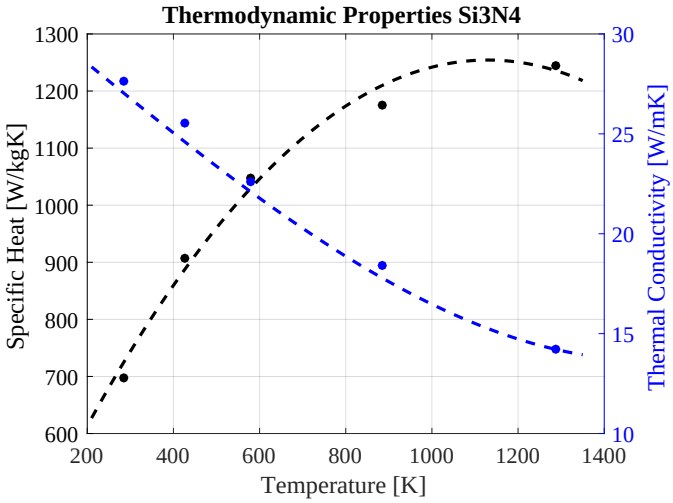

Figure 5.13: Silicon nitride S_3N_4 thermodynamic properties

$$C_p\ (Si3N4) = -7.288564\ .10^{-4}.T^2\ +\ 1.658428 + T\ +\ 3.109180.10^2 \quad (5.39)$$

$$k\ (Si3N4) = -3\ .10^{-9}.T^3 - 1\ .10^{-6}.T^2 - 0.0174.T + 32.045 \quad (5.40)$$

The gamma titanium aluminium ($\gamma - TiAl$) has been a key drive for turbocharger shaft application [143, 160, 161] and for reducing turbo lag. Its lightweight reduces rotational inertia and the power boost time. The specific heat and thermal conductivity based on gamma titanium aluminium is set in this model by using Equation 5.41 and Equation 5.42 for temperature ranges between 400 °C to 1430 °C and 25 °C to 760 °C respectively [162].

$$C_p\ \ (\gamma - TiAl) = 0.6324 + 7.44 \cdot 10^{-5} \cdot T - 2{,}07 \cdot 10^{-7} \cdot T^2 + 2.97 \cdot 10^{-10} \cdot T^3 \quad (5.41)$$

$$k\ (\gamma - TiAl)\ = 21.7959 + 8.1633 \cdot 10^{-3} \cdot T \quad (5.42)$$

The rotating conditions in the shaft and bearing are imposed. For the bearing it is adjusted to 50% of the speed rotation of the shaft [128]. The boundary conditions in the model are imposed as function of easy inputs to measure in engine test bench or known by the manufacturers of turbocharger. After the model is settled, a validation with experimental data will be carried out and the main results will discussed in the next section.

5.4 Numerical models validation and results

Experimental data has been used for model calibration and validation. The data is obtained from a 1.5 l Diesel engine and using a full instrumented non-water cooled turbocharger.

5.4.1 Radial heat transfer - model calibration

The calibration of the radial model is done using a random subset of the experimental data, while the validation is done using the whole datasets.

Experimental information was available for the 5 planes external division of turbocharger turbine (T), backplate turbine (H1), central housing (H2), backplate compressor (H3) and compressor (C), as well as for the mass flows passing through the turbocharger, the speed of the turbocharger and the temperature of several internal points within the central housing. All the temperatures were measured using standard K-type thermocouples. Specifications of the engine, transducers used in the experiments, including their expanded uncertainty are detailed in section 3.2. All thermocouples and oil outlet circuit were thermally insulated. Temperature surface probes were adopted in the 5 planes external division of turbocharger (3 thermocouples distributed every 120 degrees on each plane) to avoid the effects of the thermal boundary layer.

Internal conduction coefficients of the model are fitted minimizing the average error of the temperatures predicted by the model against experimental values, as well the maximum error. Fitting process is performed using a multi-objective MOGA-II algorithm [163]. The metal conductance, fitting parameters of the model, are allowed to change a maximum of ±5% from the values originally calculated with geometry and materials of the turbocharger. In total 12 values of conductive conductance present in the model are optimized.

The optimal solution was taken in the borders of pareto considering the best results in error minimization between the absolute maximum temperature vs. experimental average temperature for each node. New form factors can be calculated. On the other hand, thermal inertia is characterized by the heat capacity. For internal nodes of the radial model the capacitances are obtained from simulations with the 3D BH model. Table 5.5 shows the heat capacity for the external and internal nodes of the radial model.

Table 5.5: Heat capacity of the radial nodes

Radial nodes	Heat capacity [J/K]
C_T	1407.43
C_{H1}	439.48
C_{H2}	185.06
C_{H3}	529.2
C_C	1300.02
C_{H4}	36.79
C_{H5}	10.28
C_{H6}	56.51
C_{H7}	0.33
C_{H8}	0.20
C_{H9}	0.45

Additionally, the 3D BH model allows studying the heat exchanges occurring inside the turbocharger and therefore to improve the assumptions of heat flow path between branches, which are controlled by coefficients Fy1, and Fy3 in Equation 5.21 and Equation 5.22 respectively.

The Table 5.6 contains the distribution of internal heat flux obtained from the BH model simulations. It is observed that the heat flux distribution is different between radial planes H4, H5 and H6. Besides for H4 plane (close to turbine side), the Fy_i factors vary as function of the engine operating point (higher or lower turbine inlet temperature).

Table 5.6: Correlation of the internal distribution of heat flux

Internal nodes	H4		H5		H6	
Heat flux	Fy1	Fy3	Fy1	Fy3	Fy1	Fy3
TIT>800 K	0.01	0.99	0.7	0.3	0.99	0.01
TIT<800 K	0.2	0.8	0.7	0.3	0.99	0.01

5.4.2 Radial heat transfer - model validation

The same parameters obtained in the fitting procedure are used in the radial model validation. The experimental data of temperature is obtained for nodes T, H1, H2, H3, C and OI, as well in points close to nodes H4, H5, H6, H7, H8 and H9. The input data of the radial model are: Turbine mass flow, compressor mass flow and oil mass flow, the turbine inlet temperature, compressor outlet temperature and oil inlet temperature, ambient air temperature, turbocharger speed, compression and expansion ratio, ambient pressure and air velocity, the

geometry of the turbine, the bearing housing and the compressor (diameters and lengths) and their materials.

Table 5.7 shows the boundary conditions of mass flow and turbocharger speed for three of the operating points validated.Two of them correspond to engine operating points that influence the formation of oil coking in the turbocharger due to high temperatures.

Table 5.7: Boundary conditions of the radial model

Engine Speed [rpm]	Load [%]	Mass flow [kg/s]			Turbocharger Speed [rpm]
		Turbine	Compressor	Oil	
2000	50	0.05	0.05	0.016	150645
2500	75	0.08	0.08	0.02	215000
2750	100	0.09	0.09	0.0160	230125

The input data are set in a programmed interface that uses an iterative method. For each time unit, the interface checks a test cycle array, and calls, either steady (ST) or transient (TR) functions. Both functions work the same way: they use the input data to calculate coefficients in a matrix and obtain the results for each node during the iterative process. Once all the input data has been reviewed, the program ends and the output data with the results are generated.

Figure 5.14 shows the results of the radial model under steady state for three selected engine operating points. As regards external temperatures, Node T and H1 show the main error. This seems to affect in a lesser degree the errors in predictions for other nodes, which might indicate a bigger than expected experimental uncertainty for those nodes, which should be investigated in future works. Maximum deviation corresponds to the temperature in H2-H3 nodes at 2000rpm@50%FL, with values lower than 5%. The remainder external temperatures are modelled with a difference less than 4%. Regarding internal temperatures, nodes H4, H5, H8 and O2 are shown. As described in the model, node O2 is a virtual node used to represent the variation of oil temperature due to mechanical losses and after a first heat exchange. Some thermocouples were located close to the oil film before and after passing through the bearings, average temperature was computed and quite good agreement is seen between experimental and modelled results. The maximum deviation for internal temperatures corresponds to H5 node, with a value of 4.12% at 2750rpm@FL. The remainder temperatures of the system are calculated with less difference between the experiments and the model.

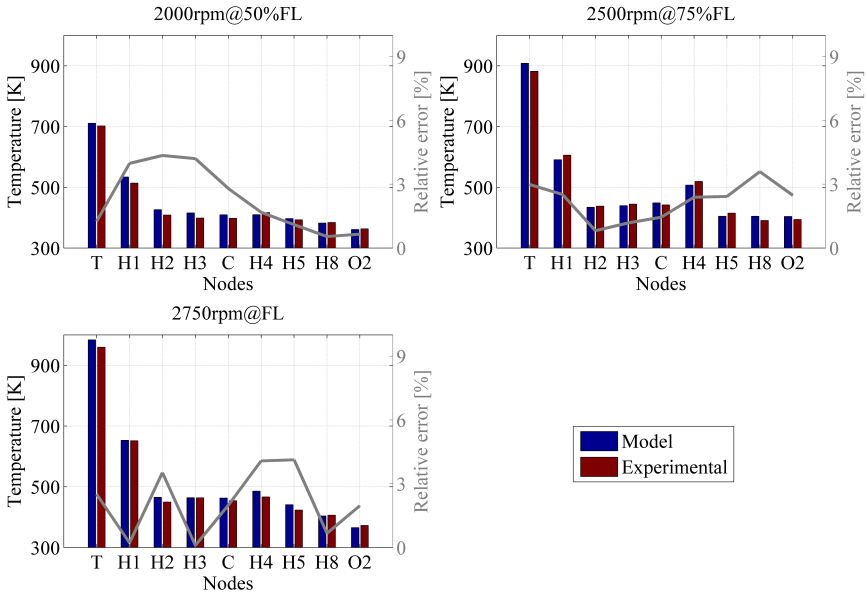

Figure 5.14: Radial model temperatures - steady state

Following the analysis, Table 5.8 shows the deviation between model and measured data as delta temperature in kelvin. The negative values are due to the fact that calculated temperatures are lower than experimental data.
For steady state conditions the difference in temperature between nodes H2, H5 and H8 is small and the heat flux becomes predominantly axial. This explains the good results obtained with the previous 1D axial model [76, 150], which only exchanged heat with the oil through node H2 [75]. Some variances still exist; the differences are bigger between nodes H1 and H4. The axial heat flow hypothesis is less robust in that zone, and this proposed model should improve the results when temperature in the bearings close to turbine is required. This is interesting when investigating oil thermal damage such as that produced with engine hot stops.

During engine hot-stops, the lack of oil flow inside the turbocharger makes trapped oil in the bearings while turbine housing exchanges heat with the central housing. In the thermal model, when engine stops mechanical losses disappear, the mass flow of the oil and compressor, as well as the speed of turbocharger stop abruptly changing to zero.

Table 5.8: Deviation of temperature between the modelled and measured

Nodes	**2000rpm @50%FL**	**2500rpm @75%FL**	**2750rpm @FL**
T	8.8	26.4	24.0
H1	20.4	-15.3	1.4
H2	17.8	-3.6	15.8
H3	16.8	-5.2	0.4
C	11.2	6.4	9.0
H4	-7.0	-12.4	19.0
H5	4.3	-10.0	17.5
H8	-2.1	14.0	-2.7
O2	-2.4	9.8	-7.3

Figure 5.15 to Figure 5.17 show the transient results during an engine hot stop cycle as the shown in Figure 3.4. In the model the temperature of external nodes (T, H1, H3 and C) is slightly over predicted and underestimated for external node H2. On turbine side the heat flux correction avoids an overestimation of turbine power output. The biggest error in temperature is found in H2 node with 4.14% of relative error at 2750 rpm engine speed and full load.

For the internal nodes the model follows experimental trends, the overestimated thermal resistances of the convective heat transfer at a nearly analogous energy balance of radial model leads to higher solid temperatures mainly. The virtual oil node O2 represents the biggest difference with a relative error of 5.35% at 2000rpm and 50% of full load. The heat transfer mechanism between the oil and solid elements can be improved.

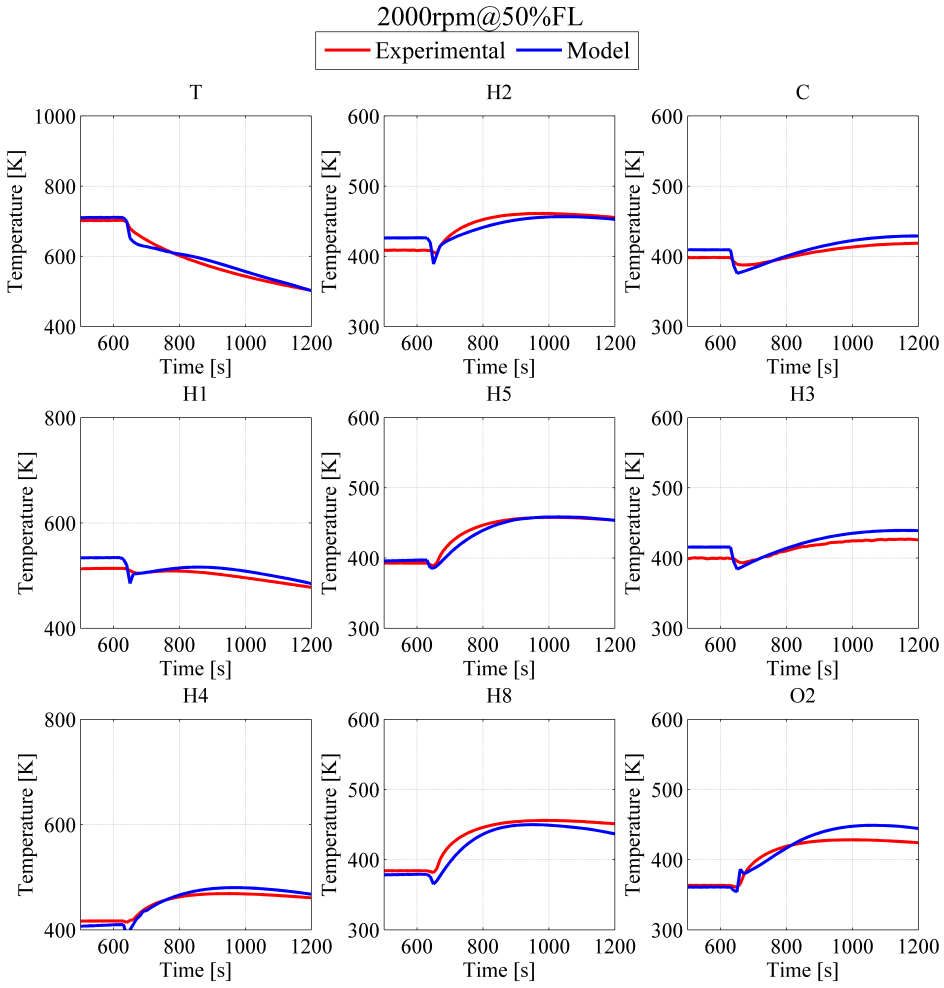

Figure 5.15: Radial model temperatures - transient at 2000-50%FL

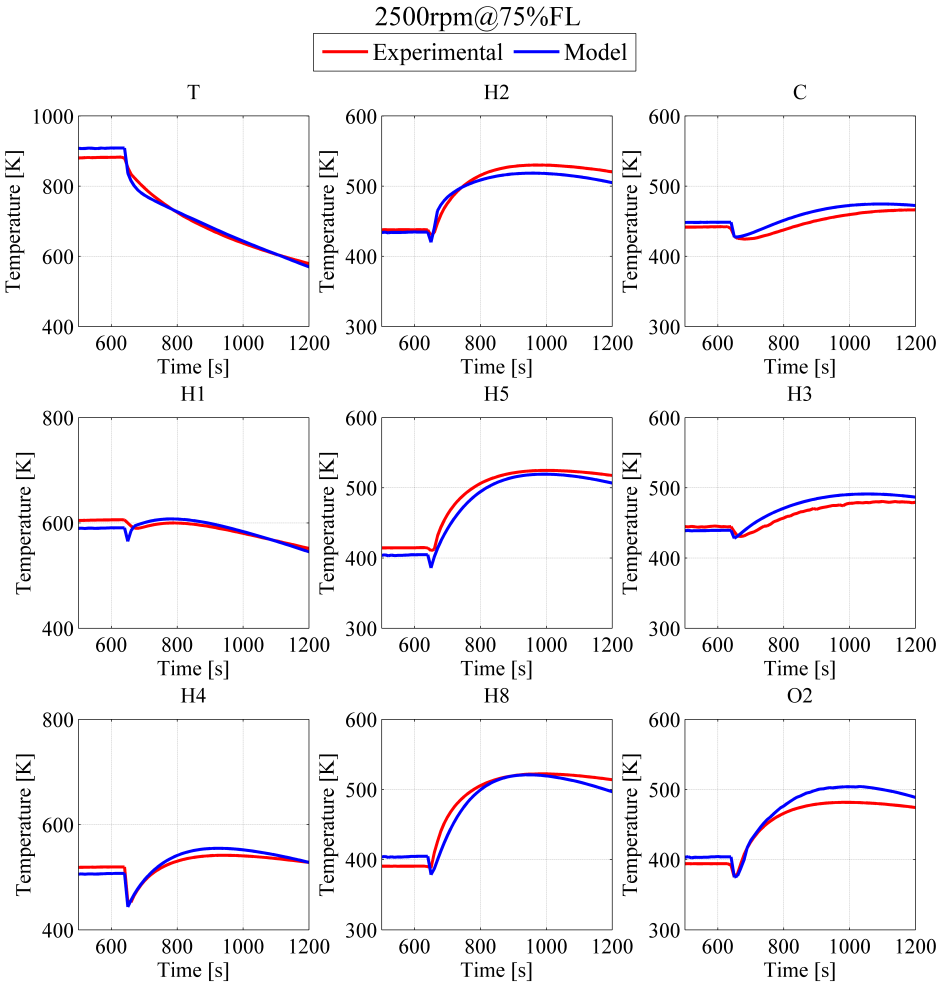

Figure 5.16: Radial model temperatures - transient at 2500-75%FL

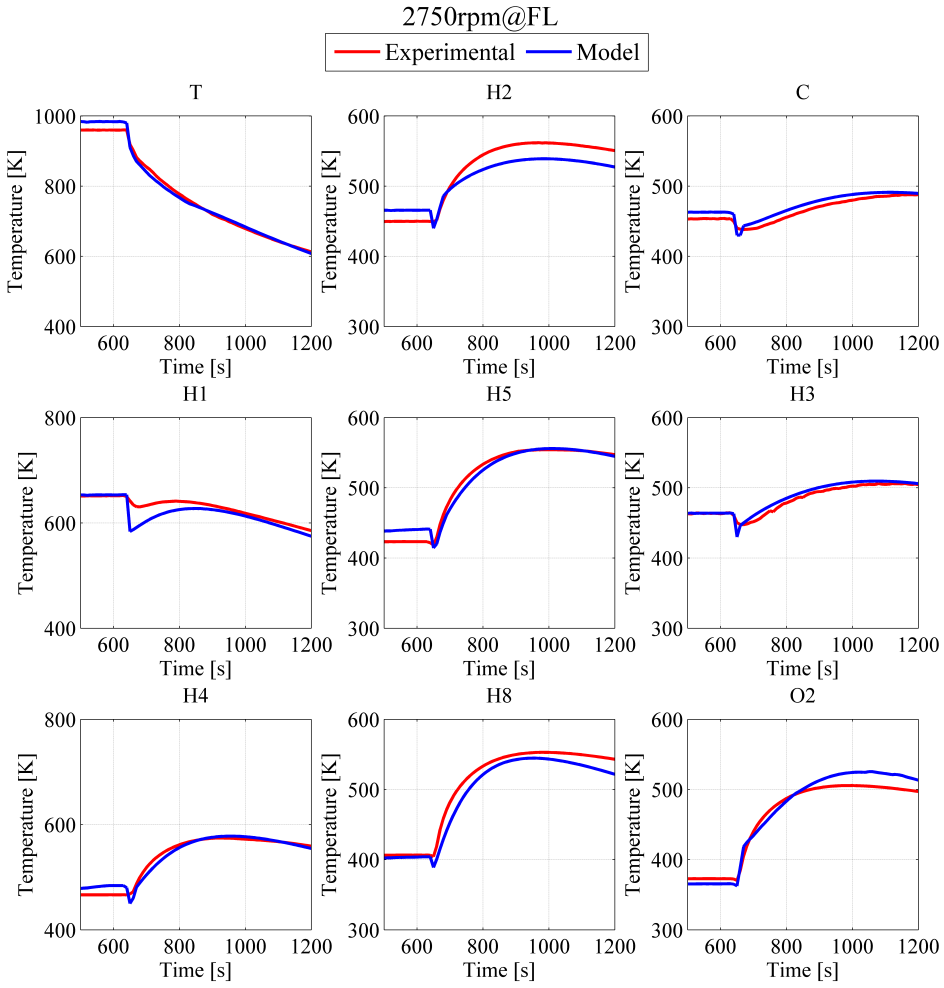

Figure 5.17: Radial model temperatures - transient at 2750-FL

The relative errors for external and internal nodes are calculated with Equation 5.43 and plotted in Figure 5.18 for the three operating points of previous results. On the left side relative error for external nodes is plotted and on the right side for the internal nodes. Black horizontal lines are ±5% relative error reference. The energy stored during transient process by the metal nodes due to their associated mass is well predicted with the radial model. Figure 5.19 shows the maximum temperature reached during engine hot stop cycle for each node compared with experimental data.

$$\delta = \frac{x_i - x_j}{xj}.100\% \tag{5.43}$$

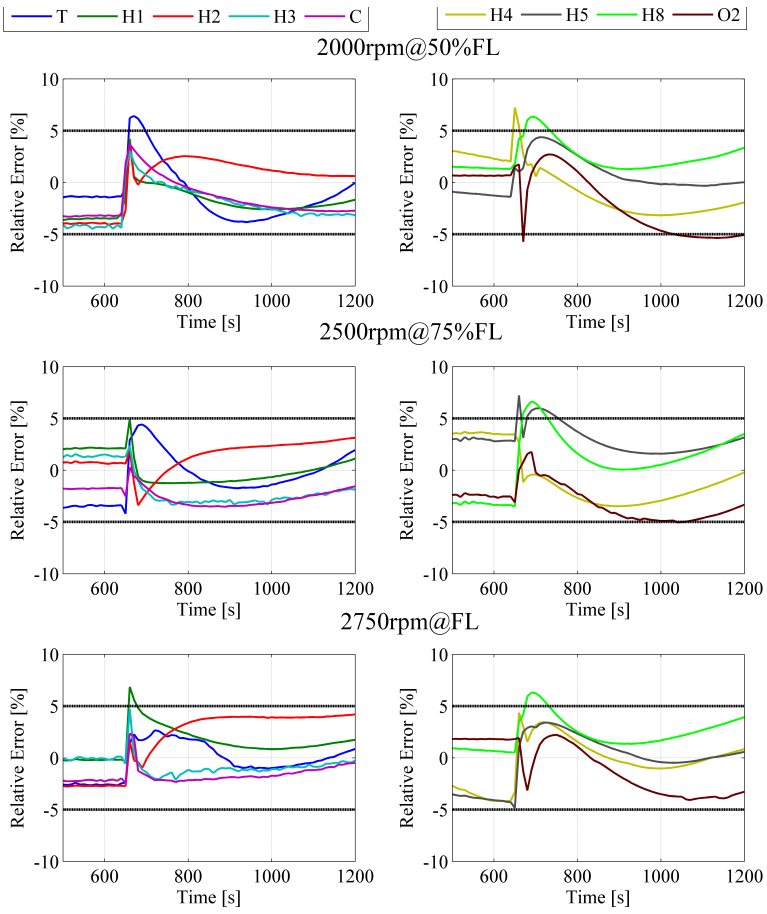

Figure 5.18: Relative error radial model at 2000-50%FL and 2500-75%FL

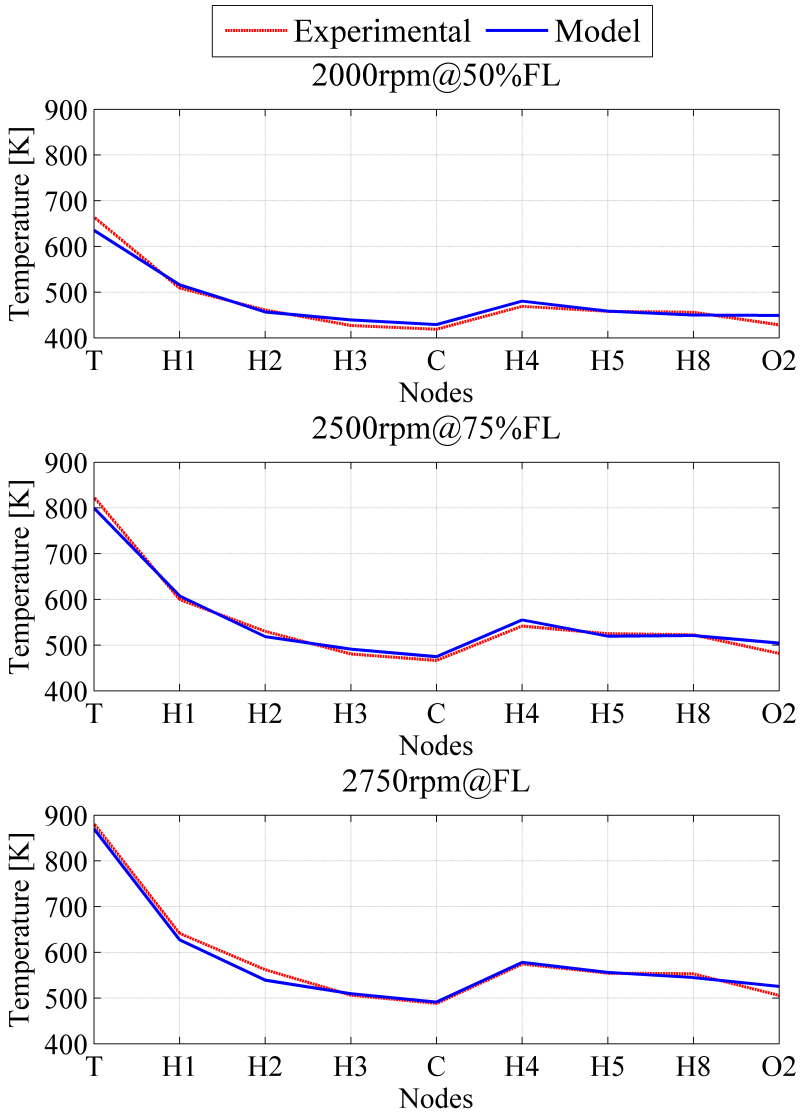

Figure 5.19: Radial model maximum temperatures under engine hot-stop

The model is even able to produce results for the temperature distribution along the shaft however, as no experimental data was available in those points, it was not possible to make a direct comparison. A detailed solution of heat fluxes in the bearing system is performed by means of finite elements.

5.4.3 Bearing housing - model validation

The results presented in this study aim to show the internal heat transfer over the bearing housing surface of the turbocharger, including the shaft. Experimental temperature data is available in 27 internal and external locations of the turbocharger. The surface temperature probes are adopted in the vicinity of the oil path, radial bearings and thrust bearing. All the experimental tests were carried out at constant oil inlet temperature of 90 °C and shaft speeds ranging from 65000 to 230000 rpm. The validation is done using different set of experimental data from the thermal characterization of section 3.4.

The purpose is to set boundary conditions known by turbocharger manufacturers or easy to measure in engine test benches to generalize the process and to determine thermal behaviour inside the turbocharger at any engine operating condition. The numerical solution is made using finite volume discretization. The backplate turbine has been discretized in two regions since the exhaust manifold has a greater influence over one section of the backplate turbine. Rotational speed of the bearing is adjusted to 50% of the speed rotation of the shaft [128]. The Table 5.9 shows input parameters imposed for three engine operating points. The results presented corresponds to the most representative engine

Table 5.9: Boundary conditions of the BH model

OP	Engine Speed [rpm]	Load [%]	Temperature [K]			Turbocharger Speed [r/min]	Oil film coefficients [W/m^2K]		
			Turbine	Compressor	Oil Inlet		Section 1	Section 2	Section 3
1	2000	50	730.3	332.7	356.6	150645	1509	760.5	420.6
2	2500	75	886.2	333.2	361.4	215000	1482.7	747.6	412.7
3	2750	100	970.8	337.4	360.9	230125	1490.8	751.2	416

operating conditions in terms of bearing temperature. A high temperature engine operating point where the oil can burn (1) and two additional points (2,3) where the oil coke may occur[138].

Figure 5.20 shows the model validation in each particular internal location of the turbocharger central housing. The thermocouple sensor location is shown in Figure 3.3. The maximum temperature deviation corresponds to the thermocouple 06 close to oil feeding at high bearing temperature OP (3) bold in Table 5.10. The model overpredicts the temperature at this point, with a difference of 10 K above the experimental test. Other internal temperatures of the bearing housing are modelled with a deviation less than 2%.

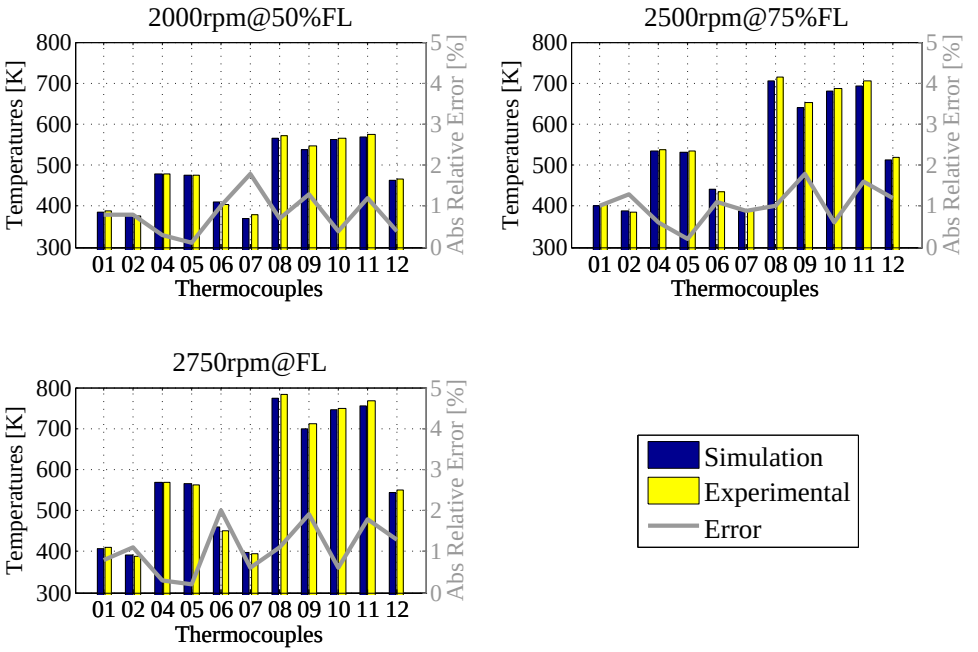

Figure 5.20: BH model Vs experimental temperatures - steady state

Table 5.10 presents the model outputs for the three engine operating points selected. In every point three columns appear, the first “CFX” column, corresponds to simulation results, "Exp", is the experimental data and the third "δ " is the relative error. Temperatures are given in K and error in %.

Table 5.10: Outputs of the BH model

Thermocouple	**2000@50%FL OP(1)**			**2500@75%FL OP(2)**			**2750@FL OP(3)**		
Nº	CFX [K]	Exp [K]	δ [%]	CFX [K]	Exp [K]	δ [%]	CFX [K]	Exp [K]	δ [%]
01	384.4	387.4	-0.8	400.1	404	-1	407.2	410.6	-0.8
02	378.3	375.4	0.8	389.4	384.4	1.3	392.9	388.5	1.2
04	478.8	477.2	0.3	535.5	538.5	-0.6	568	569.8	-0.3
05	476.6	475.9	0.1	532.7	533.5	-0.2	564.7	563.5	0.2
06	408.8	404.8	1	441.3	436.5	1.1	**458.5**	**449.3**	**2**
07	371.4	378.1	-1.8	387.1	390.4	-0.9	396.9	394.4	0.6
08	566.2	570.4	-0.7	705.8	713.2	-1	772.5	781.4	-1.1
09	538.4	545.6	-1.3	641.1	652.6	-1.8	697.9	711.8	-1.9
10	562	564.4	-0.4	681.7	685.6	-0.6	744.3	749	-0.6
11	568.9	575.9	-1.2	693.9	705.4	-1.6	755.2	768.8	-1.8
12	463.6	465.7	-0.4	514.1	520.2	-1.2	542.7	549.7	-1.3

Figure 5.21 shows the temperature distribution predicted by the BH model under this three engine operating conditions under steady state. There can be observed that temperature difference in backplate compressor is small; the

heat flux in the central housing at low engine operating conditions becomes predominantly axial as shown in Figure 5.21 sub-plot 1). However, variances exist in the turbine side especially at engine operating points of high load and engine speed as seen in Figure 5.21 sub-plot 2) and 3). The heat exchanges are bigger between the external backplate turbine and the internal surface, the axial heat flow hypothesis is less robust in the turbine side and the bearing system zones. The BH model improves the results when temperature of the bearings, shaft and close to the turbine is required.

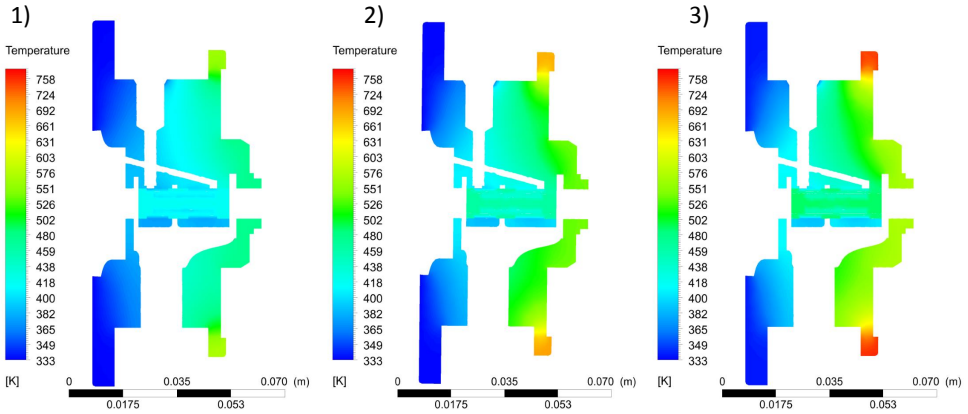

Figure 5.21: BH model internal temperatures - steady state

Thermal behaviour in the turbocharger when engine speed is reduce to zero is also evaluated. The results will be shown for the same three engine operating points selected 2000rpm@50%FL (1), 2500rpm@75%FL (2) and 2750rpm@FL (3). The heat transfer between oil and solid elements will be analysed in the vicinity of the bearings where heat transfer increases.

Figure 5.22 to Figure 5.24 show the temperature evolution within the turbocharger when the engine stops. The temperature in the radial bearing turbine side **02** is underestimated in the BH model, the maximum deviation is 15.7 K (exp-mod) at engine OP 3. The radial bearing on the compressor side **01**, bearing housing turbine side piston at 180 ° **04** and bearing housing internal oil return slope **05** are well predicted by the BH model.

Figure 5.25 to Figure 5.27 show the temperature in three bearing housing solid areas. At higher temperature (engine OP 3) the element close to oil feeding **06** delivers up to 17 K higher temperature than the experiments. Sensors close pads of thrust bearing **07** and near heat shield support **12** are predicted with a deviation less than 3%.

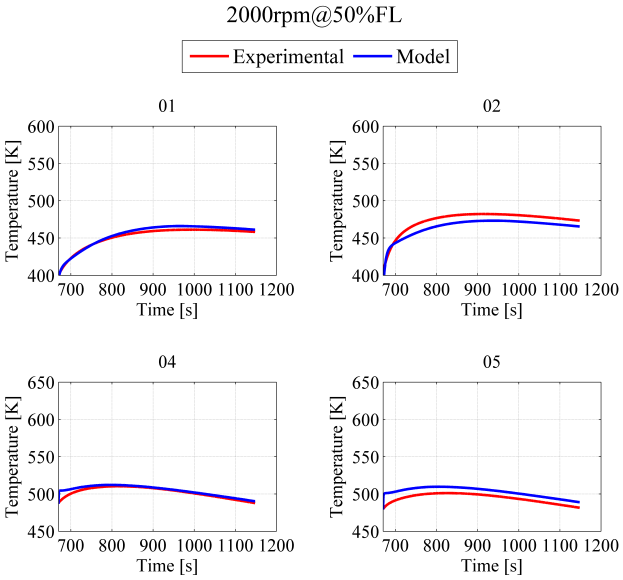

Figure 5.22: BH temperatures near to shaft at 2000 rpm and 50%FL

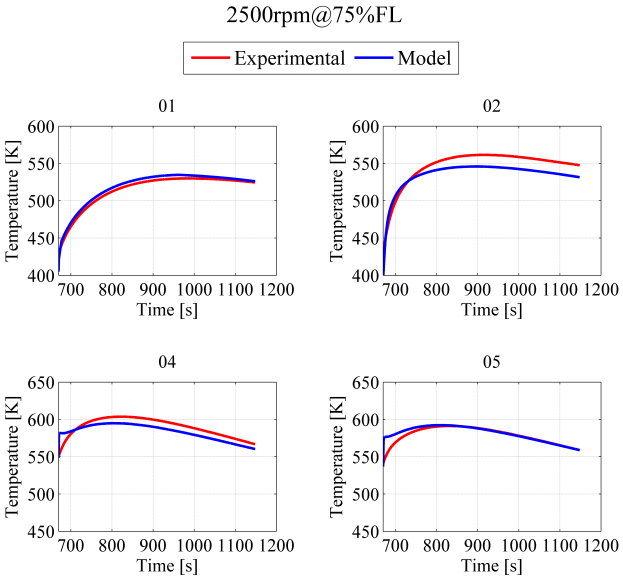

Figure 5.23: BH temperatures near to shaft at 2500 rpm and 75%FL

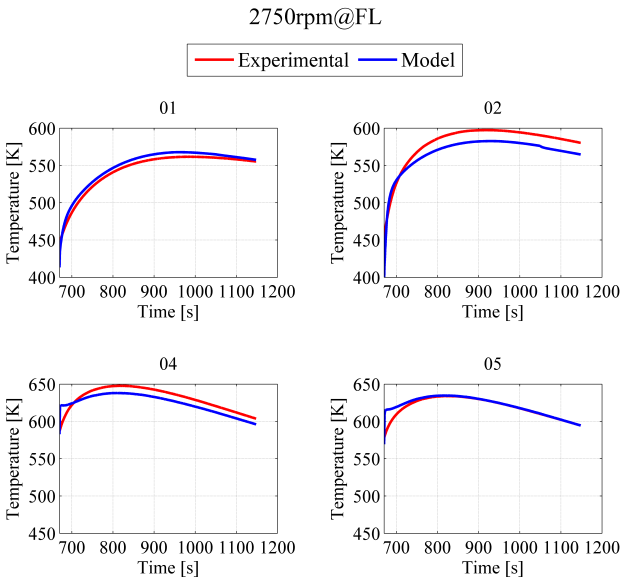

Figure 5.24: BH temperatures near to shaft at 2750 rpm and FL

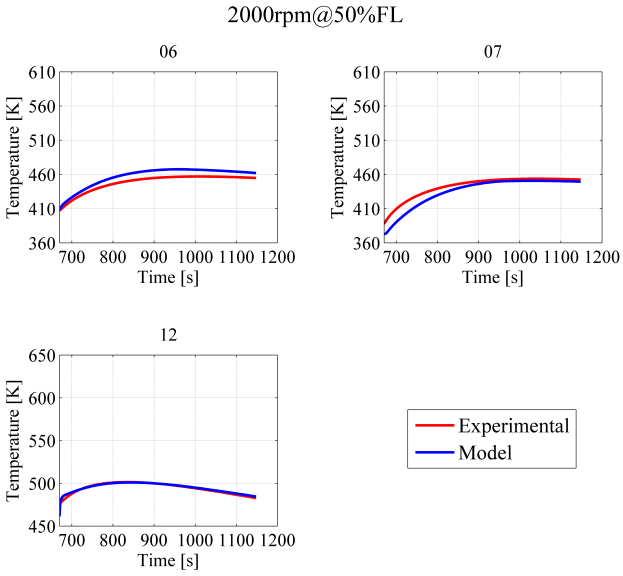

Figure 5.25: BH internal wall temperatures at 2000 rpm and 50%FL

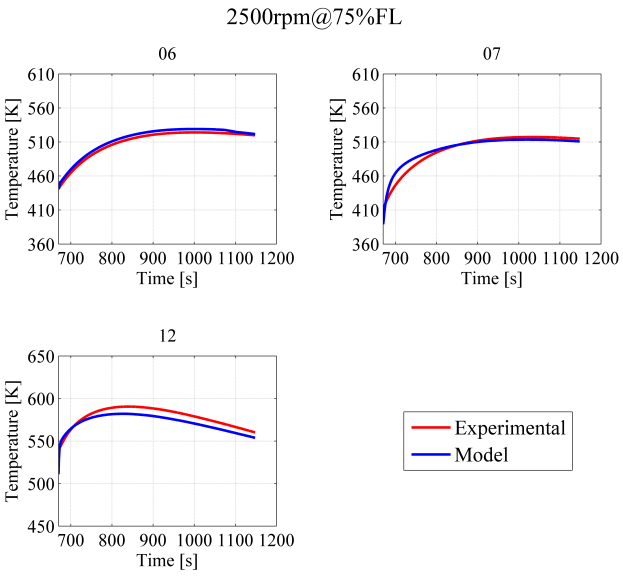

Figure 5.26: BH internal wall temperatures at 2500 rpm and 75%FL

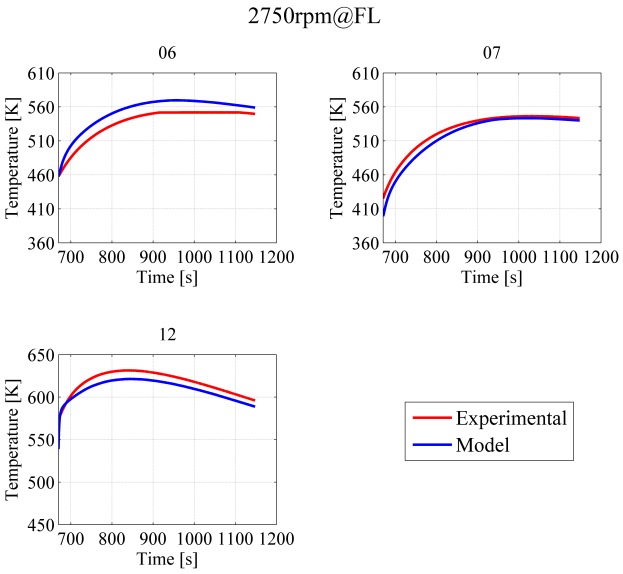

Figure 5.27: BH internal wall temperatures at 2750 rpm and FL

Figure 5.28 shows the relative errors in the BH for the three engine operating conditions previously shown from Figure 5.25 to Figure 5.27. The BH model predicts temperatures with a difference less than 5% all over internal surface. This trend is shared for all points of operation leading to a conclusion that heat transfer set-up in the model have been properly established. The comparison of both experimental and simulated results, reveals that the model delivers up to 3.6% higher temperature especially for the bearing housing (**06** close to oil feeding) what is emphases in Figure 5.28 at 2750 rpm engine speed and full load.

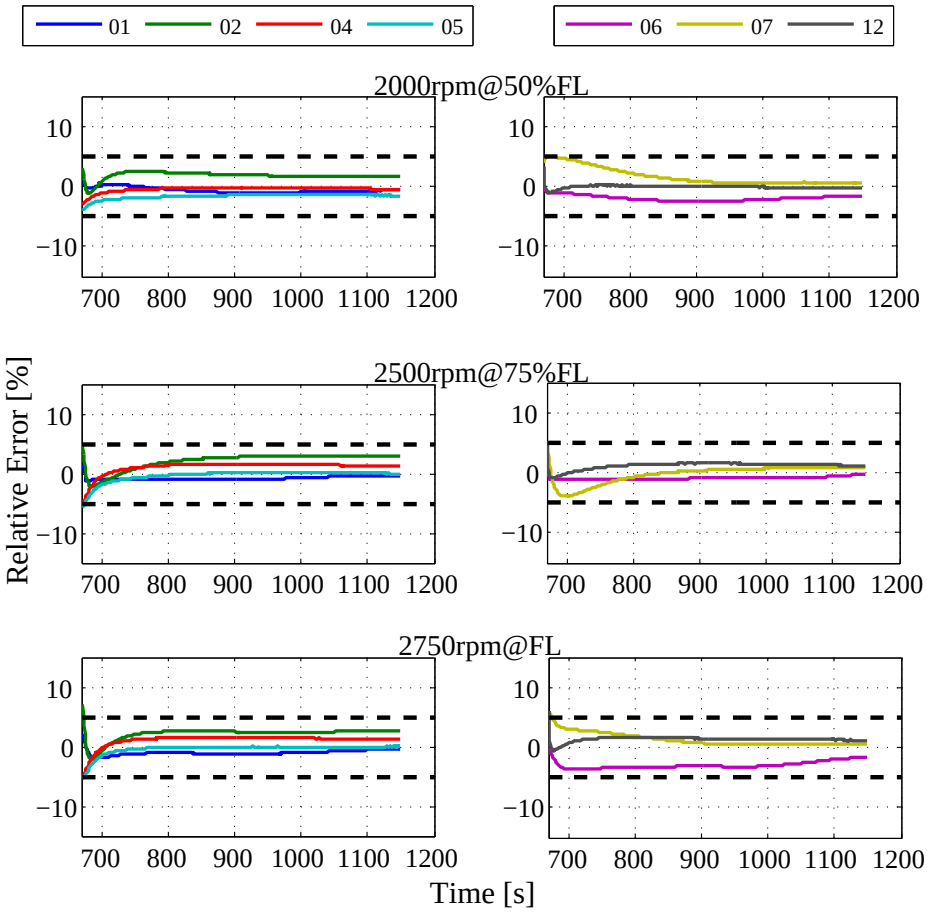

Figure 5.28: BH relative error internal temperatures

A variation of temperatures between the internal surface of the turbocharger is observed during the engine hot stop. The three components of the heat transfer contribute to increase the temperature in the turbocharger bearing housing:

The heat conduction between adjacent turbine and the bearing housing, as well as the compressor and bearing housing; the heat convection directly from the hot turbine side to the lubricating oil and the heat transfer by radiation mainly coming from the exhaust turbine and from the engine depending on the proximity of the installation of the turbocharger and the exhaust manifold to the main engine block. The Figure 5.29 shows the temperature rise over all internal surface of the turbocharger predicted by the BH model. The high temperatures occur in the bearing housing section next to the turbine segment (**04** Bearing housing, turbine side piston at 180 °) which reaches temperatures higher than 630 K (357 °C). The segments on the turbine side (05 and 12) reach very high temperatures during the engine hot-stop and are also strongly influential in coke formation.

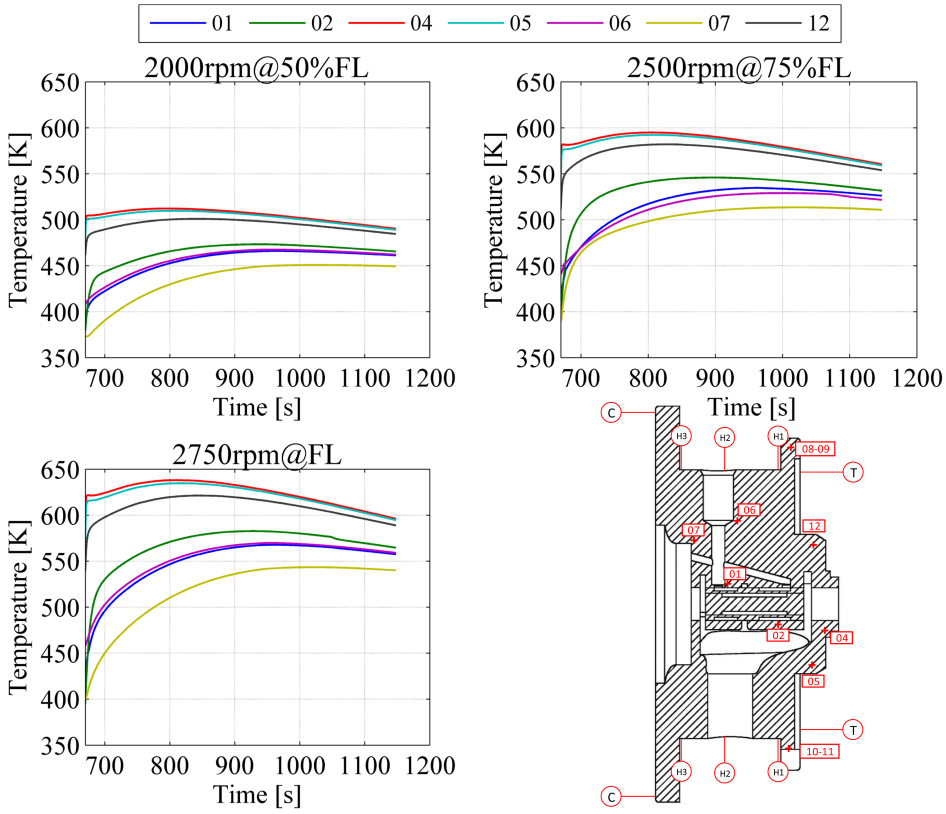

Figure 5.29: Modelled BH internal temperatures

Following the analysis, thermal studies show that coking in fresh oils starts at 300 °C and oil degradation at a temperature of 280°C [64]. Simulations show that during hot-stops internal temperatures in the central housing are higher

than the coking start temperature. For instance, oil carbon slowly builds up on bearing surfaces, internal oil channels, seal clearances as shown in Figure 5.30 [64].

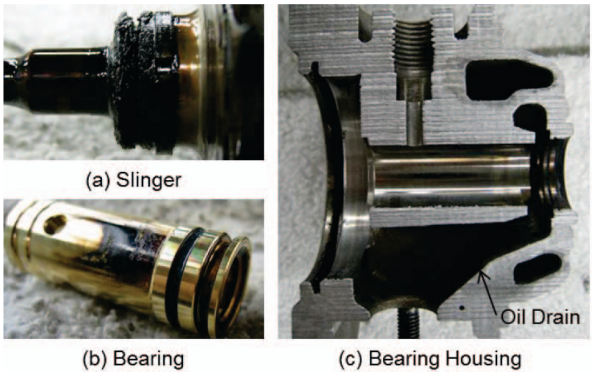

Figure 5.30: Turbocharger parts after coking test [64]

In addition, during hot-stops the turbine side transfers significant levels of heat to the bearing housing. Figure 5.31 shows the contour temperature of just after an engine hot-stop.

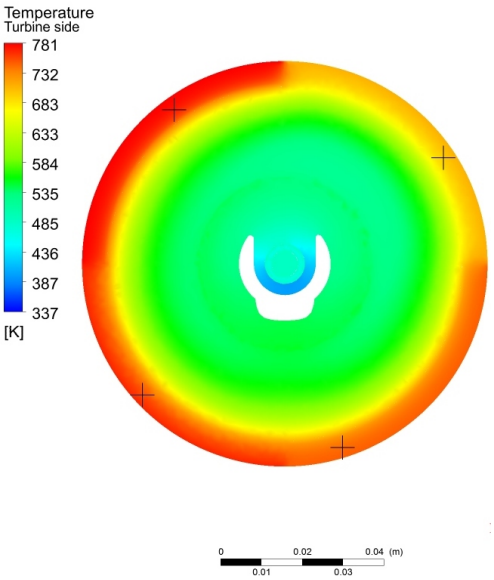

Figure 5.31: Temperature backplate turbine after engine hot-stop @ 2750 rpm and full load

Temperature variation around the back plate of the turbine shown in Figure 5.31 comes directly from the experimental data. At the moment the BH model does not predict the radiation coming from the exhaust manifold. Although it is possible to see that the obtained results of the model are reliable, it would be interesting to study the radiation heat transfer phenomena between the turbocharger and exhaust manifold. Quantifying this radiation can be exclusive of each engine-turbocharger configuration.

5.5 References

[15] D. Zeppei, S. Koch, and A. Rohi. “Ball Bearing Technology for Passenger Car Turbochargers”. In: *Motortechnische Zeitschrift - Springer* 77.11/2016 (2016), pp. 26–31 (cit. on pp. 4, 29, 164).

[61] F. Payri, P. Olmeda, F. J. Arnau, A. Dombrovsky, and L. Smith. “External heat losses in small turbochargers: Model and experiments”. In: *Energy* 71 (2014), pp. 534–546. ISSN: 03605442. DOI: 10.1016/j.energy.2014.04.096 (cit. on pp. 17, 145, 149, 155).

[64] I. Miyata, S. Hirano, M. Tanada, and K. Fujimoto. “Mechanism of Turbocharger Coking in Gasoline Engines”. In: *SAE International* JSAE 20159223 (2015), pp. 1–15. DOI: 10.4271/2015-01-2029 (cit. on pp. 18, 36, 144, 183, 184).

[75] R. D. Burke, P. Olmeda, F. J. Arnau, and M. Reyes-Belmonte. “Modelling of turbocharger heat transfer under stationary and transient engine operating conditions”. In: *Institution of Mechanical Engineers - 11th International Conference on Turbochargers and Turbocharging*. Woodhead Publishing Limited, 2014, pp. 103–112. ISBN: 9780081000335. URL: http://www.scopus.com/inward/record.url?eid=2-s2.0-84933526285{\&}partnerID=tZOtx3y1 (cit. on pp. 21, 114, 145, 169).

[76] J. R. Serrano, P. Olmeda, F. J. Arnau, A. Dombrovsky, and L. Smith. “Analysis and Methodology to Characterize Heat Transfer Phenomena in Automotive Turbochargers”. In: *Journal of Engineering for Gas Turbines and Power* 137.GTP–14–1352 (2015), pp. 1–11. DOI: 10.1115/1.4028261 (cit. on pp. 21, 113, 145, 169).

[128] D Deng, F. Shi, L. Begin, I Du, and General Motors. “The Effect of Oil Debris in Turbocharger Journal Bearings on SubSynchronous NVH”. In: *SAE International* 2015-01-12.April (2015). DOI: 10.4271/2015-01-1285 (cit. on pp. 36, 38, 165, 176).

[132] J. R. Serrano, P. Olmeda, A. Tiseira, L. M. Garcia-Cuevas, and A. Lefebvre. “Theoretical and experimental study of mechanical losses inautomotive turbochargers”. In: *Energy* 55 (2013), pp. 888–898. ISSN: 03605442. DOI: 10.1016/j.energy.2013.04.042. URL: http://dx.doi.org/10.1016/j.energy.2013.04.042 (cit. on pp. 37, 38, 155).

[138] E. G. Ribeiro, W. B. Melo, and A. P. a. Filho. “Application of electric oil pumps on automotive systems”. In: *SAE International Journal Engines* 01.4086 (2005), pp. 1–7. DOI: 10.4271/2005-01-4086. URL: http://www.sae.org/technical/papers/2005-01-4086 (cit. on pp. 68–70, 120, 176).

[143] A. K. Sachdev, K. Kulkarni, Z. Z. Fang, R. Yang, and V. Girshov. “Titanium for automotive applications: Challenges and opportunities in materials and processing”. In: *Jom* 64.5 (2012), pp. 553–565. ISSN: 10474838. DOI: 10.1007/s11837-012-0310-8 (cit. on pp. 112, 165).

[147] T. L. Bergman, A. S. Lavine, F. P. Incropera, and D. P. Dewitt. *Fundamentals of Heat and Mass Transfer*. Vol. 7th Editio. 1. 2011, ISBN 13 978–0470–50197–9. ISBN: 9780471457282. DOI: 10.1016/j.applthermaleng.2011.03.022. arXiv: 1105-. URL: http://www.osti.gov/energycitations/product.biblio.jsp?osti{_}id=6008324 (cit. on pp. 113, 152).

[148] J. Serrano, P. Olmeda, F. Arnau, and A. Dombrovsky. “General Procedure for the Determination of Heat Transfer Properties in Small Automotive Turbochargers”. In: *SAE International Journal of Engines* Friday, October 03, 2014 (2014), p. 12. DOI: 10.4271/2014-01-2857 (cit. on pp. 119, 120, 151).

[149] J. Serrano, P. Olmeda, F. J. Arnau, M. a. Reyes-Belmonte, and H. Tartoussi. “A study on the internal convection in small turbochargers. Proposal of heat transfer convective coefficients”. In: *Applied Thermal Engineering* 89 (2015), pp. 587–599. ISSN: 13594311. DOI: 10.1016/j.applthermaleng.2015.06.053 (cit. on pp. 119, 120, 153).

[150] M. A. Reyes Belmonte. “Contribution to the Experimental Characterization and 1-D Modelling of Turbochargers for IC Engines”. PhD thesis. University Polytechnic of Valencia, 2013 (cit. on pp. 120, 152, 169).

[152] J. Serrano, P. Olmeda, F. J. Arnau, A. Dombrovsky, and L. Smith. “Turbocharger heat transfer and mechanical losses influence in predicting engines performance by using one-dimensional simulation codes”. In: *Energy* 86 (2015), pp. 204–218. ISSN: 03605442. DOI: 10.1016/j.energy.2015.03.130 (cit. on p. 145).

[153] J. R. Serrano, P. Olmeda, A. Tiseira, L. M. García-Cuevas, and A. Lefebvre. “Importance of Mechanical Losses Modeling in the Performance Prediction of Radial Turbochargers under Pulsating Flow Conditions”. In: *SAE paper 2013-01-0577* (2013). ISSN: 19463936. DOI: 10.4271/2013-01-0577. URL: http://www.sae.org/technical/papers/2013-01-0577 (cit. on p. 147).

[154] S. K. S. Boetcher. *Natural Convection from Circular Cylinders*. Ed. by Francis A. Kulacki. 2014. Daytona: Springer, 2014, p. 48. ISBN: 2193-2530. DOI: 10.1007/978-3-319-08132-8. URL: https://link.springer.com/content/pdf/10.1007/978-3-319-08132-8.pdf (cit. on p. 155).

[155] R. S. Subramanian. “Heat transfer to or from a fluid flowing through a tube”. In: (). URL: http://web2.clarkson.edu/projects/subramanian/ch330/notes/HeatTransferinFlowThroughConduits.pdf (cit. on p. 161).

[156] T. L. Bergman, T. L. Bergman, A. Lavine, F. P. Incropera, and D. P. DeWitt. *Introduction to heat transfer*. Ed. by R. Linda. 6th Edition. United Sates of America: John Wiley & Sons Inc., 2011, p. 960. ISBN: 9780470501962 (cit. on p. 163).

[157] S. M Shelton. “Thermal conductivity of irons and steels over the temperature tange 100 to 500c”. In: *Part of Bureau of standards journal of research* 12.5 (1934), pp. 619–620. ISSN: 00160032. DOI: 10.1016/S0016-0032(34)90359-8 (cit. on p. 164).

[158] BCIRA. “Specific heat capacity of cast irons”. In: *British Cast Iron Research Association Broadsheet 203-7* (1985) (cit. on p. 164).

[159] D. de Faoite, D. J. Browne, F. R. Chang-Diaz, and K. T. Stanton. “A review of the processing, composition, and temperature-dependent mechanical and thermal properties of dielectric technical ceramics”. In: *Journal of Materials Science* 47.10 (2012), pp. 4211–4235. ISSN: 0022-2461. DOI: 10.1007/s10853-011-6140-1. URL: http://link.springer.com/10.1007/s10853-011-6140-1 (cit. on p. 164).

[160] T. Tetsui. “Development of a TiAl turbocharger for passenger vehicles”. In: *Materials Science and Engineering A329–* 331.2016 (2002), pp. 582–588. URL: www.elsevier.com/locate/msea (cit. on p. 165).

[161] X. Wu. “Review of alloy and process development of TiAl alloys”. In: *Intermetallics* 14.10-11 (2006), pp. 1114–1122. ISSN: 0966-9795. DOI: 10.1016/J.INTERMET.2005.10.019. URL: https://www.sciencedirect.com/science/article/pii/S0966979506000823 (cit. on p. 165).

[162] F. Appel, J. D. Paul, and M. Oehring. *Gamma titanium aluminide alloys: science and technology*. John Wiley & Sons, 2011, p. 745. ISBN: 3527636218 (cit. on p. 165).

[163] C. Poloni. “Hybrid GA for multi objective aerodynamic shape optimization”. In: *Genetic algorithms in engineering and computer science 33* (1998), pp. 397–415 (cit. on p. 166).

CHAPTER 6

Conclusions and future works

Contents

6.1 Introduction

DURING the present work, extensive experimental tests were conducted to study the oil coking in the bearing system. The coking influence on turbocharger performance, during steady state and transient operation were analysed. This is of great interest for the automotive industry that increasingly adopts “start/stop” engine operation to save fuel.

The extended study includes the impact of soot-contaminated oil on turbocharger and engine performance, which is also relevant to the automotive industry that might have overlooked this potentially critical issue when diesel or gasoline particulate filter is adopted to address the exhaust pipe soot emission.

The methodology employed throughout the document is based on:

- Experimental tests
- Analysis of heat transfer phenomena and oil coking
- Simulation models and numerical validation

In the first part, the achievements made by the experimental tests are presented in steady-state and transient operating conditions. The second part presents a study of several strategies used to minimize possibilities of coke formation, the evaluation of turbine housing designs and the cross analysis of oil coking tests. The third part is focused in mathematical models developed using VBA and ANSYS CFX software and the numerical validation. The last part suggest the future working plan regarding the heat transfer analysis in the turbocharger and influences on the working fluid temperatures which leads oil coke formation that can affect the performance of IC engines.

6.2 Main conclusions

6.2.1 Experimental tests

In order to study the impact that degraded oils have on turbocharger performance and on the bearing system, an experimental installation with a turbocharged diesel engine is used.

Thermal characterization A thermal characterization procedure has been done with a non water cooled turbocharger properly set up to measure the internal and external wall temperatures under engine hot stop conditions. The data information obtained were used to calibrate and validate the heat transfer models presented in this thesis. The thermal characterization showed that:

- Close to bearing system the temperature can reach peaks up to 325°C when the engine stops. During sudden hot stops, lubricant may under thermal condition precipitate in the form of a varnish or coke on the rotating parts of the turbocharger affecting its performance.

- In the turbocharger, the big amounts of heat exchanged between the backplate turbine side and the central housing as it cools down increases the temperature of the small amounts of oil trapped inside the turbocharger. The temperatures inside are found to be higher than the autoignition temperature of the engine oils.

- An evaluation of turbine housings designs are carried out. The results show that less heat comes to the turbocharger by using the conventional full contact turbine rather than a thermal decoupled turbine housing. While may be true the idea that thermal decoupled design radiates more heat out by reducing the thermal bridge between turbine housing and the backplate turbine; the heat radiated from the engine cannot be released by the core. The heat transfer of radiation between solid contact areas of the engine and turbocharger becomes important and can be exclusive of each engine-turbocharger configuration. Internal temperatures are approximately 10 °C less above the turbocharger external surface using a full contact turbine housing.

Oil coking test The experimental test of oil coking has been carried out under two engine operating conditions; one at high bearing temperature (2750 rpm @ 100% full load) and another with lower bearing temperature (2500 rpm @ 75% of full load). Two oil qualities have been used; one SAE grade 5W30 (referred in this work as “A”) and another SAE 10W40 (referred in this work as “C”). Both

oil types are contaminated at levels of 4% and 7% of soot content. Additionally oxidized oils with the same properties described above have been used.

Different non-intrusive inspection criteria for oil coking tests have been used. The global engine variables have been held constant ensuring that endurance tests were performed properly without any fluctuation that may affect in the main oil coking conclusions. The following results have been obtained based on critical hot stops:

- The oil mass flow rate passing through the turbocharger is reduced along the endurance tests of oil coking. This reduction depends of the bearing temperature but also of the oil soot content. Oxidized oil and non-oxidized oils with 7% of soot have the greatest slope of reduction.

- At high bearing temperature, the engine torque level drops more, higher deposition of coke on the turbocharger is evidenced. The high bearing temperature, produces greater accumulation of coke in oil type "C" oil compared with oil "A".

- The oxidation causes an increase in the oil viscosity therefore a greater deposition of oil coke. The blocking of floating bearing in the turbocharger occurs with the use of oil oxidized type "Coxy" at both levels of soot content and in the oxidized type "Aoxy" at high level of soot (7%) as well. Non-oxidized equivalent oils used at low engine speed and load do not produce a blocking of the floating bearing on the turbocharger.

- At lower bearing temperature the tests with "A" and "C" oils suffer less deflections in the rotating assembly than their counterpart "Aoxy" and "Coxy".

- The increase of operating clearances between the shaft/bearing and bearing/central housing are between the 4% and 20% of their initial size. The diminution of gap on the bearing surfaces (internal and external) are from 20% up to 55% of the initial SMA of an ellipse. The diminution of gap is induced by coke deposits. In general, the orbital forces described by the rotating assembly applying force to the shaft shows that almost all turbochargers have a reduction of their SMA at the end of an endurance test.

- A higher content of soot causes a reduction in the "time to stop" in turbochargers for the tests with oil "A". Tests with the oil "C" have a deceleration time similar between them, the level of soot content does not influence significantly. The "time to stop" in the turbocharger using oils "C" is reduced by half with respect to the tests carried out with type "A" oil.

- Oxidized oils “A” take, on average half time or less to stop compared with their respective counterpart not oxidized.

- The shaft motion or diminution of the gap of the rotating assembly is affected in greater proportion in turbochargers tested at high bearing temperature (2750 rpm @ 100% full load).

6.2.2 Application and evaluation of the heat transfer

Study with Gt-Power Different cooling strategies have been simulated in order to minimize the possibility of thermal damage and coke formation inside the bearing housing of the turbocharger under hot-stop engine cycle while keeping the associated fuel consumption to this cooling strategies as low as possible. The heat transfer model is coupled to a full engine simulation code in GT-Power. According to the simulations performed, the results are summarized in the following points:

- The sudden stop of cooling power will cause an important increase of bearing housing temperature due to its internally accumulated energy that cannot be released.

- Thermal transient study shows good overall results in the turbocharger metal nodes temperatures. Peaks of temperature in the central bearing housing (H2 node) seems to be relatively insensitive to pump size when there are no auxiliary pumps. The calculated specific energy consumption is associated with this cooling method thoroughly when a normal cooling strategy in combination with a big oil pump has been modelled. The improvement in H2 temperature drop is produced with a big energy consumption and CO_2 production when compared with the results of normal-sized pumps.

- The auxiliary water cooling pump seems to produce the optimum results in terms of specific energy consumption as it has more cooling capacity with less power consumption than the oil pump. The operation of auxiliary pump not only reduces the peak of temperature in H2 node, but also delays that peak one or two minutes later.

Turbine thermal decoupling A thermal decoupling strategy is simulated with the 1D engine simulation tool. The simulation results show that:

- As the simulations proposed by manufacturers of turbochargers, the reduction of thermal bridge between the turbine housing and the central housing improves conditions of temperature in around 27 °C. However

more work is needed to perform a full validation of this strategy since these results diverge from experimental results obtained.

It would be interesting to study the radiation heat transfer phenomena between the turbocharger and engine. However, quantifying this radiation can be exclusive of the proximity between turbocharger and the main engine block.

Cross analysis of oil coking tests A cross analysis of the different inspection criteria to evaluate the impact that degraded oils have on turbocharger performance and on the bearing system has been done. The following results have been obtained:

- As coke accumulates inside the bearings, turbocharger efficiency drops and the VGT vanes need to close for achieving the same boost pressure, making an increase in the pumping losses and thus lowering the engine torque.
- Turbocharger efficiency losses are lower than losses in the compressor side. Significant reduction of compressor efficiency has been measured but not much of turbocharger efficiency even if VGT was closed. This allows concluding that compressor efficiency deteriorates more than mechanical efficiency.
- The effective section reduction is affected by the engine operating condition and oil quality. Higher discharge coefficient, lower flow passage consequently the loss in permeability bearing system is reduced. This effective section reduction is well correlated with the turbocharger weight increase after coking test.
- At lower bearing temperature (2500 rpm @ 75% load), the bearings are not clogged and the weight is less than 5 grams. At higher operating condition, the bearings may be blocked in some cases and the weight is greater than 5 grams.
- Fluctuations in the endurance tests using oil “C” at 4% and low load question the conclusions obtained. The deterioration in this turbocharger is not only due to thermal and lubrication conditions but due to aerodynamic effects.
- Either at high or lower bearing temperature the oil type “C” shows a similar response in turbocharger efficiency drop and deceleration time. With “C” type oils neither the soot content nor the oxidation cause a big change in the deceleration times of the turbochargers.

- Attending results obtained, oil “A” seems to have higher dispersancy capacity than oil “C”. Detergent and dispersant additives are used to keep the engine’s metal surfaces clean, prevent the formation of deposits and to neutralize the harmful effects of corrosive acids that are formed by the combustion of diesel and gasoline fuels. The oil type “A” shows better response to the endurance tests than oil “C”.
- The antioxidant capability (as a combination of base quality) can be higher for oil “A” oil than for oil “C” considering that both oils have suffered the same oxidation process.

6.2.3 Simulation models

Heat transfer modelling The presented models allow a detailed study of the heat transfer during stationary and transient phase. The models are focused in calculating turbocharger thermal transients when the engine speed is reduced to zero. The developed heat transfer approach is successfully applied to non-water cooled turbochargers. The development and validation are summarized in the following points:

- A 2D lumped model discretizes the turbocharger in both the radial and axial directions, and computes the heat transfer and temperature at different parts of the machine. Aiming for a low computational cost, it was designed to be compatible with fast one-dimensional engine simulations as a replacement of previous model.
- The radial model is based on electric-thermodynamic analogy and is validated with experimental data under steady and transient conditions. The description of the heat transfer equations serve as base for modelling other turbochargers by modifying geometry, material, and boundary conditions.
- A detailed solution of heat fluxes in the turbocharger is performed by means of finite elements. A 3D BH model is developed for this purpose. The design of compressor and turbine housings are excluded to optimize the calculation time but the related boundary conditions are imposed to get an appropriate trade off.
- The 3D BH housing model uses a discrete element method of wire mesh with size of 0,001 m for the main body and 0,005 m for the compressor side. The element sizes were systematically chosen and are enough to observe the dynamic associated with the temperatures in the turbocharger.
- A turbine side correlations have been obtained as function of gas inlet temperature from the experiments. The correlations are used to validate the model under steady and transient conditions.

Model capabilities - numerical validation The models results can be used practically to study heat exchanges occurring inside and the effects on the turbocharger performance. They are a powerful tool for today's engine development needs. The models will help to evaluate thermal damage done to the system itself, guidance for researchers on the development of effective procedures and tools to cope with the technological exigencies in the optimum performance of the turbo-charging system. As well as influences on the working fluid temperatures which leads to oil coke formation, that can affect the performance of the engine.

- The 2D radial model calibration is obtained thanks to data available from the 3D BH model. A dynamic response in radial model prediction becomes more accurate with a heat flux correction. The BH model allows to extract information for improving the heat fluxes hypothesis in the radial model. In the compressor side, the heat flux becomes predominantly axial. While in the turbine side heat exchanges are bigger.

- The hypothesis made in the radial model shows good agreement between experimental and modelled results. The temperature of external nodes (T, H1, H3 and C) is slightly over predicted in the model and underestimated for external node H2. On turbine side the heat flux correction avoids an overestimation of turbine power output. The biggest error in temperature is found in the central housing H2 node with 4.14% of relative error at 2750 rpm engine speed and full load.

- The accuracy level of the lumped mass approach seems to be sufficient for thermodynamic purpose. Regarding the internal radial nodes, the virtual oil node 02 represents the biggest difference with a relative error of 5.35% under hot stop conditions. Other internal nodes, are modelled with relative error less than 5%.

- The radial model has proven to be a robust method to improve current equivalent one-dimensional model with a very low computational costs.

- The 3D BH model improves the results when temperature of the bearings, shaft is required. The heat transfer balance shows sufficient agreement between the experiments and BH model approach. Correlations adopted as input condition shows a good prediction in all operating conditions simulated. The internal temperatures predicted by the BH model in solid areas show a deviation in the radial bearing turbine side (thermocouple 02) of 15.7 K (exp-mod) at 2750 rpm and full load engine operating point. Besides, the temperature predicted by the model in the turbine side near heat shield are predicted with differences less than 3%.

- Thermal properties such as heat capacity and thermal conductivity in the internal sections of the turbocharger can be obtained through the 3D BH model. Experimental tasks in the thermo-hydraulic test bench for the estimation of metal conductances and capacities [164] can be reduced. More validation will be necessary using other geometries of turbochargers.
- The development processes of heat transfer by radiation between solid elements needs more attention.

6.3 Future works

Further research is needed to continue improving the turbocharger system in terms of compactness and reliability. The following aspects should be studied:

Experimental future works

- Experimental evaluation of heat sources in the engine can be carried out. The radiation between the turbocharger and the engine main block should be possible.
- Larger experimental database will help to refine the fitting parameters used in the radial model.
- New experimental tests will have to be carried out using water-cooled turbochargers to understand the potential of all heat sources.
- Some extra measurements with other turbochargers units should be tested in the future to obtain more data about internal heat transfer. Those measurements will help to evaluate the results obtained with the 3D heat transfer model.

Theoretical future works

- Integration of radial model into a 1-D engine simulation code like GT-Power should be done in order to simulate accurately turbocharger performance taking into account all physical phenomena.
- For now the heat transfer by water convection remains unresolved in the radial model. The convection in the water box is zero. Therefore, it is proposed to study water-cooled turbochargers, to continue with the development of the model.
- Viewing factors of radiation for each single node to the rest of external nodes should be calculated. Calculations of this radiation may be exclusive of every engine-turbocharger configuration.
- More CFD studies should be addressed to have high-fidelity simulations. A full turbocharger simulation using turbulent models between the gas and the turbine could be coupled to the BH model to observe the effects of heat transfer to the lubrication circuit and the bearing system.

6.4 References

[164] A. Dombrovsky. “Synthesis of the 1D modelling of turbochargers and its effects on engine performance prediction”. PhD thesis. University Polytechnic of Valencia, 2016, pp. 1–238. DOI: 10.4995/Thesis/10251/82307 (cit. on p. 197).

Bibliography

[1] **Serrano, J. R., Tiseira, A., García-Cuevas, L. M., Rodriguez Usaquen, T., and Mijotte, G.**
"Fast 2-D Heat Transfer Model for Computing Internal Temperatures in Automotive Turbochargers"
in: *SAE World Congress WCX 17* 2017-01-0513 (2017). ISSN: 01487191. DOI: 10.4271/2017-01-0513.Copyright (cit. on p. vii)

[2] **Serrano, J. R., Tiseira, A., García-Cuevas, L. M., and Rodríguez Usaquen, T.**
"Adaptation of a 1-D tool to study transient thermal in turbocharger bearing housing"
in: *Applied Thermal Engineering* 134 (2018), pp. 564–575. ISSN: 1359-4311. DOI: 10.1016/J.APPLTHERMALENG.2018.01.085. URL: https://www.sciencedirect.com/science/article/pii/S1359431118305039 (cit. on p. vii)

[3] **Serrano, J. R., Tiseira, A., García-Cuevas, L. M., Rodriguez Usaquen, T., and Mijotte, G.**
"A methodology to study oil-coking problem in small turbochargers"
in: *International J of Engine Research* (2018), pp. 1–12. DOI: 10.1177/1468087418803197 (cit. on p. vii)

[4] **Gil, A., García-Cuevas, L. M., Tiseira, A., and Rodriguez Usaquen, T.**
"Fast 3-D heat transfer model for computing internal temperatures in the bearing housing of automotive turbochargers"
in: *International J of Engine Research* (2018), pp. 1–12. DOI: 10.1177/1468087418803197 (cit. on p. vii)

[5] **National Research Council (U.S.)**
Assessment of fuel economy technologies for light-duty vehicles
ed. by Improving Light-Duty Vehicle Fuel Economy., C. on the Assessment of Technologies for. National Academies Press 2011, p. 217. ISBN: 9780309156073 (cit. on p. 2)

[6] **Simon, V., Oberholz, G., and Mayer, M.**
"Exhaust gas temperature 1050 ° C An engineering challenge"
in: *BorgWarner TurboSystems Academy* (2000), pp. 1–12
(cit. on pp. 2, 112, 125)

[7] **Matsumoto, K., Jinnai, Y., Tojo, M., Hayashi, N., and Ibaraki, S.**
Development of Compact and High-performance Turbocharger for 1050°C Exhaust Gas
tech. rep. September. Mitsubishi Heavy Industries, Ltd. Technical Review 2008, pp. 1–5 (cit. on pp. 2, 23)

[8] **Comerais, M., Chesse, P., and Hetet, J.-F.**
"Turbocharger Heat Transfer Modeling Under Steady and Transient Conditions"
in: *International Journal of Thermodynamics* 12.4 (2009), pp. 193–202. URL: http://dergipark.ulakbim.gov.tr/eoguijt/article/view/1034000257/1034000237 (cit. on pp. 2, 17, 19, 21)

[9] **Addison, J. and Needelman, W.**
"Diesel Engine Lubricant Contamination and Wear"
in: *Pall Corporation Engwear* (1986), p. 12 (cit. on p. 3)

[10] **Stark, M., Wilkinson, J., Lee, P., Lindsay Smith, J., Taylor, R., and Chung, S.**
"The Degradation of Lubricants in Gasoline Engines: Lubricant Flow and Degradation in the Piston Assembly"
in: *Tribology and Interface Engineering Series* 48 (2005), pp. 779–786. ISSN: 1572-3364. DOI: 10.1016/S0167-8922(05)80079-3. URL: https://www.sciencedirect.com/science/article/pii/S0167892205800793 (cit. on p. 3)

[11] **Plumley, M. J., Wong, V., and Martins, T.**
"Oil Degradation in a Diesel Engine with Dual-Loop Lubricating System"
in: *Tribology Transactions* 61.4 (2018), pp. 596–603. ISSN: 1040-2004. DOI: 10.1080/10402004.2017.1378396. URL: https://www.tandfonline.com/doi/full/10.1080/10402004.2017.1378396
(cit. on p. 3)

[12] **Selby, T. W.**
"Turbocharger Deposits and Engine Deposits – A Duality : Correlative Bench Test Studies of Turbocharger Deposits Shut-down"
in: *TAE Esslingen Conference* (2010), pp. 1–12 (cit. on p. 4)

[13] **Galindo, J, Serrano, J. R., Dolz, V, and Lopez, M. A.**
"Behavior of an IC Engine Turbocharger in Critical Condition of Lubrication"

in: *SAE International Journal Engines* 6.2 (2013), pp. 797–805. ISSN: 19463936. DOI: 10.4271/2013-01-0921 (cit. on pp. 4, 14, 38)

[14] **Mitchell, C., Schaefer, C., Graf-Goller, O., Solfrank, P., and Scheidt, M.**
"Rolling Bearings in Turbochargers A Real Bargain with Regard to CO2 Emissions"
in: *10th Schaeffler Symposium - Solving the Powertrain Puzzle*. USA: Schaeffler Technologies AG & Co. KG 2014, pp. 1–10 (cit. on p. 4)

[15] **Zeppei, D., Koch, S., and Rohi, A.**
"Ball Bearing Technology for Passenger Car Turbochargers"
in: *Motortechnische Zeitschrift - Springer* 77.11/2016 (2016), pp. 26–31 (cit. on pp. 4, 29, 164)

[16] **Burkinshaw, M and Blacker, D**
The high temperature tribological performance of turbocharger wastegate materials
tech. rep. 2014, pp. 289–298. DOI: 10.1016/B978-0-081000-33-5.50024-X. URL: https://ac.els-cdn.com/B978008100033550024X/3-s2.0-B978008100033550024X-main.pdf?{_}tid=1fea6f38-770e-48f5-91f1-0b794611d337{\&}acdnat=1537525468{_}9d68c108414b330d1f43f88a121f9ffc (cit. on p. 4)

[17] **Zhang, F., Zhu, Q., Li, D., He, Y., and Xu, X.**
"Semi-solid moulding technology in making automotive turbocharge compressor wheels"
in: *International Journal of Computational Materials Science and Surface Engineering* 6.3/4 (2016), p. 204. ISSN: 1753-3465. DOI: 10.1504/IJCMSSE.2016.081684. URL: http://www.inderscience.com/link.php?id=81684 (cit. on p. 4)

[18] **Chinchilla, A., Burkinshaw, M., Lindsay, M., Proprentner, D., and Shollock, B.**
The tribological performance of coated and non-coated materials in high temperature environments
tech. rep. 2018 (cit. on p. 4)

[19] **Schmitt, M., Frouzakis Tomboulides, C. E., Ananias, G., Wright, Y. M., and Boulouchos, K.**
"Direct numerical simulation of multiple cycles in a valve/piston assembly"
in: *Physics of Fluids* 26.3 (2014). ISSN: 10897666. DOI: 10.1063/1.4868279 (cit. on p. 5)

[20] **Vinuesa, R., Negi, P. S., Atzori, M., Hanifi, A., Henningson, D. S., and Schlatter, P.**
"Turbulent boundary layers around wing sections up to Rec=1,000,000"
in: *International Journal of Heat and Fluid Flow* 72.April (2018), pp. 86–99. ISSN: 0142727X. DOI: 10.1016/j.ijheatfluidflow.2018.04.017 (cit. on p. 5)

[21] **European Commission**
Reducing CO2 emissions from passenger cars | Climate Action
2018. URL: https://ec.europa.eu/clima/policies/transport/vehicles/cars{_}en (cit. on p. 13)

[22] **Stock, J. H.**
"The Renewable Fuel Standard: A Path Forward"
in: *Center On Global Energy Policy | Columbia Sipa* (2015). URL: https://scholar.harvard.edu/files/stock/files/renewable{_}fuel{_}standard.pdf (cit. on p. 13)

[23] **The European Parliament and The Council of the European Union**
"Amending Regulation (EC) No 443/2009 to define the modalities for reaching the 2020 target to reduce CO2 emissions from new passenger cars"
in: *Official Journal of the European Union* (2014). URL: http://eur-lex.europa.eu/legal-content/EN/TXT/?uri=uriserv:OJ.L{_}.2014.103.01.0015.01.ENG (cit. on p. 13)

[24] **Watson, N and Janota, M. S**
Turbocharging the Internal Combustion Engine
1st edition. London and Basingstoke: The macmillan press LTD 1982, p. 595. ISBN: 978-1-349-04024-7. DOI: 10.1007/978-1-349-04024-7. URL: https://link.springer.com/content/pdf/bfm{\%}3A978-1-349-04024-7{\%}2F1.pdf (cit. on p. 13)

[25] **Grissom, T.**
"Turbocharging for Improved Engine Performance & Reduced CO2 Emissions Turbocharging for Improved Engine"
in: *BWTS* (2013) (cit. on p. 13)

[26] **Padhiyar, B. and Sharma, P**
"Application of hybrid turbocharger to improve performance of engine"
in: *IJEET* 1 (Apr. 2014), pp. 1–2014 (cit. on p. 13)

[27] **Williams Martin and Minjares Ray**
"A technical summary of Euro 6/VI vehicle emission standards"
in: *The international council on clean transportation* (2016), p. 12. URL: https://www.theicct.org/sites/default/files/publications/ICCT{_}Euro6-VI{_}briefing{_}june2016.pdf (cit. on p. 13)

[28] **United States Environmental Protection Agency**
Tier 3 Evap/OBD - Epa, Us of Transportation Office and Quality Air Division Compliance
2016. URL: https://www.epa.gov/sites/production/files/2016-12/documents/tier3-evap-obd-summary.pdf (cit. on p. 13)

[29] **United States Environmental Protection Agency**
Renewable Fuel Standard Program: Standards for 2018 and Biomass-Based Diesel Volume for 2019, 40 CFR Part 80
2017. URL: https://www.gpo.gov/fdsys/pkg/FR-2017-12-12/pdf/2017-26426.pdf (cit. on p. 13)

[30] **Global Market Insights Inc.**
Automotive Turbochargers Market Size, Growth Potential, Price Trends, Competitive Market Share and Forecast, 2017 – 2024
tech. rep. Delaware: Global Market Insights 2018, p. 300. DOI: GMI2463. URL: https://www.gminsights.com/methodology/detail/automotive-turbocharger-market (cit. on p. 13)

[31] **Feneley, A. J., Pesiridis, A., and Andwari, A. M.**
"Variable Geometry Turbocharger Technologies for Exhaust Energy Recovery and Boosting A Review"
in: *Renewable and Sustainable Energy Reviews* 71 (2017), pp. 959–975. ISSN: 1364-0321. DOI: 10.1016/J.RSER.2016.12.125. URL: https://www.sciencedirect.com/science/article/pii/S1364032116311807 (cit. on p. 13)

[32] **Knecht, W.**
"Diesel engine development in view of reduced emission standards"
in: *Energy* 33.2 (2008), pp. 264–271. ISSN: 03605442. DOI: 10.1016/j.energy.2007.10.003 (cit. on p. 13)

[33] **Watel, E., Pagot, A., Pacaud, P., and Schmitt, J.-c.**
"Matching and Evaluating Methods for Euro 6 and Efficient Two-stage Turbocharging Diesel Engine"
in: *SAE Technical Paper* (2010). DOI: 10.4271/2010-01-1229. URL: http://dx.doi.org/10.4271/2010-01-1229 (cit. on p. 14)

[34] **Serrano, J., Tormos, B., Gargar, K., and Bouffaud, F.**
"Study of the Effects on Turbocharger Performance Generated by the Presence of Foreign Objects at the Compressor Intake"
in: *Experimental Techniques* 37.2 (2013), pp. 30–40. ISSN: 07328818. DOI: 10.1111/j.1747-1567.2011.00795.x. URL: http://doi.wiley.com/10.1111/j.1747-1567.2011.00795.x (cit. on p. 14)

[35] **Payri, F., Serrano, J. R., Olmeda, P., Paez, A., and Vidal, F.**
"Experimental Methodology to Characterize Mechanical Losses in Small Turbochargers"
in: *Volume 5: Industrial and Cogeneration; Microturbines and Small Turbomachinery; Oil and Gas Applications; Wind Turbine Technology*. ASME 2010, pp. 413–423. ISBN: 978-0-7918-4400-7. DOI: 10.1115/GT2010-22815. URL: http://proceedings.asmedigitalcollection.asme.org/proceeding.aspx?articleid=1609171 (cit. on p. 14)

[36] **Deligant, M., Podevin, P., and Descombes, G.**
"CFD model for turbocharger journal bearing performances"
in: *Applied Thermal Engineering* 31.5 (2011), pp. 811–819. ISSN: 13594311. DOI: 10.1016/j.applthermaleng.2010.10.030
(cit. on pp. 14, 26, 37)

[37] **Sim, K., Lee, Y.-B., and Kim, T. H.**
"Effects of Mechanical Preload and Bearing Clearance on Rotordynamic Performance of Lobed Gas Foil Bearings for Oil-Free Turbochargers"
in: *Tribology Transactions* 56.2 (2013), pp. 224–235. ISSN: 1040-2004. DOI: 10.1080/10402004.2012.737502. URL: http://www.tandfonline.com/doi/abs/10.1080/10402004.2012.737502 (cit. on p. 14)

[38] **Polichronis, D., Evaggelos, R., Alcibiades, G., Elias, G., and Apostolos, P.**
"Turbocharger Lubrication - Lubricant Behavior and Factors That Cause Turbocharger Failure"
in: *International Journal of Automotive Engineering and Technologies* 2.1 (2013), pp. 40–54 (cit. on pp. 14, 18, 38)

[39] **Bloch, H. P. and Budris, A. R.**
Pump user's handbook : life extension
2nd ed. Fairmont Press 2006, p. 477. ISBN: 0849391792
(cit. on pp. 14, 39)

[40] **Bloch, H. P.**
"Bearing Isolators: An Expert Guide"
in: *AESSEAL* (). URL: http://www.aesseal.com/en/resources/academy/bearing-isolators (cit. on pp. 14, 18, 39)

[41] **Aghaali, H.**
"On-Engine Turbocharger Performance Considering Heat Transfer"
PhD thesis. KTH Royal Institute of Technology 2012. ISBN: 978-91-7501-332-9. URL: http://kth.diva-portal.org/smash/get/diva2:524801/FULLTEXT01 (cit. on pp. 15, 20)

[42] **Galindo, J, Lujan, J. M., Guardiola, C, and Lapuente, G. S.**
"A method for data consistency checking in compressor and variable-geometry turbine maps"
in: *Proceedings of the Institution of Mechanical Engineers, Part D: Journal of Automobile Engineering* 220.10 (2006), pp. 1465–1473. ISSN: 0954-4070. DOI: 10.1243/09544070JAUTO82. URL: http://sdj.sagepub.com/lookup/10.1243/09544070JAUTO82 (cit. on p. 16)

[43] **Serrano, J. R., Arnau, F. J., Dolz, V, and Piqueras, P**
"Methodology for characterisation and simulation of turbocharged diesel engines combustion during transient operation. Part 1: Data acquisition and post-processing"
in: *Applied Thermal Engineering* 29 (2008), pp. 142–149. DOI: 10.1016/j.applthermaleng.2008.02.011. URL: http://ac.els-cdn.com/S135943110800077X/1-s2.0-S135943110800077X-main.pdf?{_}tid=57560138-4473-11e7-9693-00000aab0f26{\&}acdnat=1496064963{_}d2bc76947168411d6499a0e925e0ea77 (cit. on p. 16)

[44] **Szymko, S., Martinez-Botas, R. F., and Pullen, K. R.**
"Experimental Evaluation of Turbocharger Turbine Performance Under Pulsating Flow Conditions"
in: *Volume 6: Turbo Expo 2005, Parts A and B*. ASME 2005, pp. 1447–1457. ISBN: 0-7918-4730-6. DOI: 10.1115/GT2005-68878. URL: http://proceedings.asmedigitalcollection.asme.org/proceeding.aspx?articleid=1585493 (cit. on p. 16)

[45] **Jung, M., Ford, R. G., Glover, K., Collings, N., Christen, U., and Watts, M. J.**
"Parameterization and Transient Validation of a Variable Geometry Turbocharger for Mean-Value Modeling at Low and Medium Speed-Load Points"
in: 2002. DOI: 10.4271/2002-01-2729. URL: http://papers.sae.org/2002-01-2729/ (cit. on p. 16)

[46] **Cormerais, M., Hetet, J. F., Chesse, P., and Maiboom, A.**
"Heat Transfer Analysis in a Turbocharger Compressor: Modeling and Experiments"
in: 2006. DOI: 10.4271/2006-01-0023. URL: http://papers.sae.org/2006-01-0023/ (cit. on p. 16)

[47] **Serrano, J, Guardiola, C, Dolz, V, Tiseira, A., and Cervelló, C**
"Experimental Study of the Turbine Inlet Gas Temperature Influence on Turbocharger Performance"
in: *SAE World Congress & Exhibition* Apr. 2007 (cit. on p. 16)

[48] **Romagnoli, A. and Ricardo, M.-B.**
"Heat Transfer on a Turbocharger Under Constant Load Points"
in: *ASME Turbo Expo 2009: Power for Land, Sea, and Air* Jan. 2009
(cit. on p. 16)

[49] **Chesse, P., Chalet, D., and Tauzia, X.**
"Impact of the Heat Transfer on the Performance Calculations of Automotive Turbocharger Compressor"
in: *Oil & Gas Science and Technology* 66 (Sept. 2011), pp.791–800
(cit. on p. 16)

[50] **Baines, N., Wygant, K. D., and Dris, A.**
"The Analysis of Heat Transfer in Automotive Turbochargers"
in: *Journal of Engineering for Gas Turbines and Power* 132.4 (2010), p. 042301. ISSN: 07424795. DOI: 10.1115/1.3204586. URL: http://gasturbinespower.asmedigitalcollection.asme.org/article.aspx?articleid=1474996 (cit. on p. 16)

[51] **Casey, M. V. and Fesich, T. M.**
"The Efficiency of Turbocharger Compressors With Diabatic Flows"
in: *Journal of Engineering for Gas Turbines and Power* 132.7 (2010), p. 072302. ISSN: 07424795. DOI: 10.1115/1.4000300. URL: http://gasturbinespower.asmedigitalcollection.asme.org/article.aspx?articleid=1428499 (cit. on p. 17)

[52] **Sidorow, A. and Isermann, R.**
"Physical and experimental modeling of turbochargers with thermodynamic approach for calculation of virtual sensors"
in: *The International Federation of Automatic Control Rueil-Malmaison* (2012). DOI: 10.3182/20121023-3-FR-4025.00064 (cit. on p. 17)

[53] **Shaaban, S. and Seume, J.**
"Impact of Turbocharger Non-Adiabatic Operation on Engine Volumetric Efficiency and Turbo Lag"
in: *International Journal of Rotating Machinery* 2012 (2012), pp. 1–11. ISSN: 1023-621X. DOI: 10.1155/2012/625453 (cit. on p. 17)

[54] **Romagnoli, A and Martinez-Botas, R**
"Heat Transfer Analysis in a Turbocharger Turbine: An Experimental And Computational Evaluation"
in: *Applied Thermal Engineering* 38.May 2012 (2012), pp. 58–77
(cit. on pp. 17, 19, 20)

[55] **Tanda, G., Marelli, S., Marmorato, G., and Capobianco, M.**
"An experimental investigation of internal heat transfer in an automotive turbocharger compressor"

in: *Applied Energy* 193 (2017), pp. 531–539. ISSN: 0306-2619. DOI: 10.1016/J.APENERGY.2017.02.053. URL: https://www.sciencedirect.com/science/article/pii/S0306261917301812?via{\%}3Dihub (cit. on p. 17)

[56] **Marelli, S., Marmorato, G., and Capobianco, M.**
"Evaluation of heat transfer effects in small turbochargers by theoretical model and its experimental validation"
in: *Energy* 112 (2016), pp. 264–272. ISSN: 03605442. DOI: 10.1016/j.energy.2016.06.067. URL: http://linkinghub.elsevier.com/retrieve/pii/S0360544216308416 (cit. on p. 17)

[57] **Marelli, S., Gandolfi, S., and Capobianco, M.**
"Heat Transfer Effect on Performance Map of a Turbocharger Turbine for Automotive Application"
in: *SAE international United States* 2017. DOI: 10.4271/2017-01-1036. URL: http://papers.sae.org/2017-01-1036/ (cit. on p. 17)

[58] **J R Serrano; P Olmeda; APaez; F Vidal**
"An experimental procedure to determine heat transfer properties of turbochargers"
in: *Measurement Science and Technology* 21 (2010), p. 14. DOI: 10.1088/0957-0233/21/3/035109. URL: http://iopscience.iop.org/article/10.1088/0957-0233/21/3/035109/pdf (cit. on pp. 17, 64)

[59] **Olmeda, P., Dolz, V., Arnau, F. J., and Reyes-Belmonte, M. a.**
"Determination of heat flows inside turbochargers by means of a one dimensional lumped model"
in: *Mathematical and Computer Modelling* 57 (2013), pp. 1847–1852. ISSN: 08957177. DOI: 10.1016/j.mcm.2011.11.078 (cit. on pp. 17, 64)

[60] **Serrano, J., Olmeda, P., Arnau, F., Reyes-Belmonte, M., and Lefebvre, A.**
"Importance of Heat Transfer Phenomena in Small Turbochargers for Passenger Car Applications"
in: *SAE International Journal of Engines* 6 (2013), pp. 716–728. ISSN: 19463936. DOI: 10.4271/2013-01-0576. URL: http://www.scopus.com/inward/record.url?eid=2-s2.0-84878797944{\&}partnerID=tZOtx3y1 (cit. on p. 17)

[61] **Payri, F., Olmeda, P., Arnau, F. J., Dombrovsky, A., and Smith, L.**
"External heat losses in small turbochargers: Model and experiments"
in: *Energy* 71 (2014), pp. 534–546. ISSN: 03605442. DOI: 10.1016/j.energy.2014.04.096 (cit. on pp. 17, 145, 149, 155)

[62] **Aghaali, H., Angstrom, H.-E., and Serrano, J. R.**
"Evaluation of different heat transfer conditions on an automotive turbocharger"
in: *International J of Engine Research* 16.2 (2015), pp. 137–151. DOI: 10.1177/1468087414524755 (cit. on pp. 17, 21)

[63] **Sirakov, B. and Casey, M.**
"Evaluation of Heat Transfer Effects on Turbocharger Performance"
in: *Journal of Turbomachinery* 135.2 (2012), p. 021011. ISSN: 0889-504X. DOI: 10.1115/1.4006608. URL: http://turbomachinery.asmedigitalcollection.asme.org/article.aspx?doi=10.1115/1.4006608 (cit. on p. 18)

[64] **Miyata, I., Hirano, S., Tanada, M., and Fujimoto, K.**
"Mechanism of Turbocharger Coking in Gasoline Engines"
in: *SAE International* JSAE 20159223 (2015), pp. 1–15. DOI: 10.4271/2015-01-2029 (cit. on pp. 18, 36, 144, 183, 184)

[65] **Osborne, S., Kopinsky, J., Norton, S., Sutherland, A., Lancaster, D., Nielsen, E., Isenstadt, A., and German, J.**
"Automotive Thermal Management Technology"
in: *The international council on clean transportation* (2016), p. 16. URL: https://www3.epa.gov/otaq/climate/regs-light-duty.htm{\#}2017-2025. (cit. on p. 19)

[66] **Galindo, J., Lujan, J., Serrano, J., Dolz, V., and Guilain, S.**
"Description of a heat transfer model suitable to calculate transient processes of turbocharged diesel engines with one-dimensional gas-dynamic codes"
in: *Applied Thermal Engineering* 26.1 (2006), pp. 66–76. ISSN: 13594311. DOI: 10.1016/j.applthermaleng.2005.04.010 (cit. on p. 19)

[67] **Shaaban, S, Seume, J., Berndt, R, Pucher, H, and Linnhoff, H.**
"Part-load Performance Prediction of Turbocharged Engines"
in: *8th International Conference on Turbochargers and Turbocharging* (Dec. 2006), pp. 131–144. DOI: 10.1016/B978-1-84569-174-5.50013-0 (cit. on p. 19)

[68] **Luddecke, B., Filsinger, D., and Bargende, M.**
"On wide mapping of a mixed flow turbine with regard to compressor heat flows during turbocharger testing"
in: *10th International Conference on Turbochargers and Turbocharging*. International Conference on Turbochargers and Turbocharging, 10. Oxford: Elsevier 2012, pp. 185–202. ISBN: 978-085-709-209-0. DOI: 10.1533/9780857096135.4a.185. URL: http://linkinghub.elsevier.com/retrieve/pii/B9780857092090500157 (cit. on p. 20)

[69] **Aghaali, H. and Angstrom, H.-E.**
"Improving Turbocharged Engine Simulation by Including Heat Transfer in the Turbocharger"
in: *SAE 2012 World Congress & Exhibition*. SAE International 2012. DOI: 10.4271/2012-01-0703. URL: http://papers.sae.org/2012-01-0703/ (cit. on p. 21)

[70] **Aghaali, H. and Angstrom, H.-E.**
"Temperature Estimation of Turbocharger Working Fluids and Walls under Different Engine Loads and Heat Transfer Conditions"
in: *11th International Conference on Engines & Vehicles*. SAE Internationa 2013. DOI: 10.4271/2013-24-0123. URL: http://papers.sae.org/2013-24-0123/ (cit. on p. 21)

[71] **Burke, R. D.**
"Analysis and Modeling of the Transient Thermal Behavior of Automotive Turbochargers"
in: *Journal of Engineering for Gas Turbines and Power* 136.10 (2014). ISSN: 0742-4795. DOI: 10.1115/1.4027290. URL: http://gasturbinespower.asmedigitalcollection.asme.org/article.aspx?doi=10.1115/1.4027290 (cit. on pp. 21, 113)

[72] **Burke, R., Vagg, C., Chalet, D., and Chesse, P.**
"Heat transfer in turbocharger turbines under steady, pulsating and transient conditions"
in: *International Journal of Heat and Fluid Flow* 52 (2015), pp. 185–197. ISSN: 0142727X. DOI: 10.1016/j.ijheatfluidflow.2015.01.004 (cit. on p. 21)

[73] **Schinnerl, M., Seume, J., Ehrhard, J., and Bogner, M.**
"Heat Transfer Correction Methods for Turbocharger Performance Measurements"
in: *Journal of Engineering for Gas Turbines and Power* 139.2 (2016), p. 022602. ISSN: 0742-4795. DOI: 10.1115/1.4034234. URL: http://gasturbinespower.asmedigitalcollection.asme.org/article.aspx?doi=10.1115/1.4034234 (cit. on p. 21)

[74] **Serrano, J. R., Arnau, F. J., Novella, R., and Reyes-belmonte, M. Á.**
"A Procedure to Achieve 1D Predictive Modeling of Turbochargers under Hot and Pulsating Flow Conditions at the Turbine Inlet"
in: *SAE Technical Paper* 2014-01-10.February 2016 (2014). ISSN: 0148-7191. DOI: 10.4271/2014-01-1080 (cit. on p. 21)

[75] **Burke, R. D., Olmeda, P., Arnau, F. J., and Reyes-Belmonte, M.**
"Modelling of turbocharger heat transfer under stationary and transient engine operating conditions"
in: *Institution of Mechanical Engineers - 11th International Conference on Turbochargers and Turbocharging*. Woodhead Publishing Limited 2014, pp. 103–112. ISBN: 9780081000335. URL: http://www.scopus.com/inward/record.url?eid=2-s2.0-84933526285{\&}partnerID=tZOtx3y1 (cit. on pp. 21, 114, 145, 169)

[76] **Serrano, J. R., Olmeda, P., Arnau, F. J., Dombrovsky, A., and Smith, L.**
"Analysis and Methodology to Characterize Heat Transfer Phenomena in Automotive Turbochargers"
in: *Journal of Engineering for Gas Turbines and Power* 137.GTP–14–1352 (2015), pp. 1–11. DOI: 10.1115/1.4028261
(cit. on pp. 21, 113, 145, 169)

[77] **Porzig, D., Raetz, H., Schwarze, H., and Seume, J.**
"Thermal analysis of small high-speed floating-ring journal bearings"
in: *11th International Conference on Turbochargers and Turbocharging* (2014), pp. 421–436. DOI: 10.1533/9780081000342.421. URL: http://linkinghub.elsevier.com/retrieve/pii/B9780081000335500342
(cit. on p. 22)

[78] **San Andrés, L and Kerth, J**
"Thermal effects on the performance of floating ring bearings for turbochargers"
in: *Proceedings of the Institution of Mechanical Engineers, Part J: Journal of Engineering Tribology* 218.5 (2004), pp. 437–450. ISSN: 1350-6501. DOI: 10.1243/1350650042128067. URL: http://pij.sagepub.com/lookup/doi/10.1243/1350650042128067 (cit. on p. 22)

[79] **Mohd, I. A., Rajoo, S, and Darus, A. N.**
"Heat Distribution Study on Turbocharger Turbine's Volute"
in: *Jurnal Mekanikal* 35 (2012), pp. 63–81. URL: http://mech.utm.my/wp-content/uploads/2017/01/6-Heat-Distribution-Study-onTurbocharger-Turbines-Volute{_}revised{_}version.pdf
(cit. on p. 22)

[80] **Drewczynski, M and Rzadkowski, R**
"A stress analysis of a compressor blade in partially blocked inlet condition"
in: *Proceedings of the Institution of Mechanical Engineers, Part G: Journal of Aerospace Engineering* 230.5 (2016), pp. 934–952. DOI: 10.1177/0

954410015601149. URL: http://journals.sagepub.com/doi/10.1177/0954410015601149 (cit. on p. 22)

[81] **Filsinger, D., Szwedowicz, J., and Schafer, O.**
"Approach to Unidirectional Coupled CFD–FEM Analysis of Axial Turbocharger Turbine Blades"
in: *Journal of Turbomachinery* 124.1 (2002), p. 125. ISSN: 0889504X. DOI: 10.1115/1.1415035. URL: http://turbomachinery.asmedigitalcollection.asme.org/article.aspx?articleid=1466279 (cit. on p. 22)

[82] **Shafi, S. M., Ramakrishna, V, and Rajasekhar, S**
"Thermal Analysis of Turbocharger by Varying Materials"
in: *International Journal and Magazne of engineering, technology, management and research* 2 (2015), pp. 1840–1844. ISSN: 2348-4845. URL: http://www.ijmetmr.com/oldecember2015/ShaikMohammedShafi-VVRamakrishna-SRajasekhar-A-111.pdf (cit. on p. 23)

[83] **Bet, F. and Sieder, G.**
"Dynamic Simulating Systems - Multi-disciplinary design exploration unleashing simulation"
in: *Computational Thermal Management of Transient Turbocharger Operation* (), pp. 1–56. URL: www.cd-adapco.com/magazine (cit. on pp. 23, 24)

[84] **Zheng, X., Jin, L., Du, T., Gan, B., Liu, F., and Qian, H.**
"Effect of temperature on the strength of a centrifugal compressor impeller for a turbocharger"
in: *Proceedings of the Institution of Mechanical Engineers, Part C: Journal of Mechanical Engineering Science* 227.5 (2013), pp. 896–904. ISSN: 09544062. DOI: 10.1177/0954406212454966 (cit. on pp. 24, 25)

[85] **Zheng, X. and Ding, C.**
"Effect of temperature and pressure on stress of impeller in axial-centrifugal combined compressor"
in: *Advances in Mechanical Engineering* 8.6 (2016), pp. 1–11. ISSN: 16878140. DOI: 10.1177/1687814016653547 (cit. on p. 25)

[86] **Burke, R., Copeland, C., and Duda, T.**
"Investigation into the Assumptions for Lumped Capacitance Modelling of Turbocharger Heat Transfer"
in: *University of Bath* (2014) (cit. on p. 26)

[87] **Burke, R. D., Copeland, C. D., Duda, T., and Rayes-Belmote, M. A.**
"Lumped Capacitance and Three-Dimensional Computational Fluid Dynamics Conjugate Heat Transfer Modeling of an Automotive Turbocharger"

in: *Journal of Engineering for Gas Turbines and Power* 138.9 (2016), p. 092602. ISSN: 0742-4795. DOI: 10.1115/1.4032663. URL: http://gasturbinespower.asmedigitalcollection.asme.org/article.aspx?doi=10.1115/1.4032663 (cit. on p. 26)

[88] **Roclawski, H., Oberste-brandenburg, C., and Böhle, M.**
"Conjugate Heat Transfer Analysis of a Centrifugal Compressor for Turbocharger Applications"
in: *International Symposium on Transport Phenomena and Dynamics of Rotating Machinery*. Hawaii, Honolulu 2016, pp. 1–7 (cit. on p. 26)

[89] **De Vos, S., Haehndel, K., Frank, T., Christel, F., and Abanteriba, S.**
"The Development of Turbine Volute Surface Temperature Models for 3D CFD Vehicle Thermal Management Simulations: Part 3: Exhaust Radial Turbine Volute Systems"
in: *SAE International Journal of Passenger Cars - Mechanical Systems* 7.2 (2014), pp. 2014–01–0648. ISSN: 1946-4002. DOI: 10.4271/2014-01-0648. URL: http://papers.sae.org/2014-01-0648/ (cit. on p. 26)

[90] **Tomm, U., Weiske, S., Coksen, A., Rafaa, Y., and Münz, S.**
"Validation of a Heat Transfer Prediction Approach Inside Turbochargers and its Application on Turbocharged Engine Performance Analysis"
in: *Volume 8: Microturbines, Turbochargers and Small Turbomachines; Steam Turbines*. Charlotte: ASME 2017, V008T26A003. ISBN: 978-0-7918-5095-4. DOI: 10.1115/GT2017-63195 (cit. on p. 26)

[91] **Song, Y. and Gu, C.-w.**
"Development and Validation of a Three-Dimensional Computational Fluid Dynamics Analysis for Journal Bearings Considering Cavitation and Conjugate Heat Transfer"
in: *Journal of Engineering for Gas Turbines and Power* 137.12 (2015), p. 122502. ISSN: 0742-4795. DOI: 10.1115/1.4030633. URL: http://gasturbinespower.asmedigitalcollection.asme.org/article.aspx?doi=10.1115/1.4030633 (cit. on p. 26)

[92] **Li, Y., Liang, F., Zhou, Y., Ding, S., Du, F., Zhou, M., Bi, J., and Cai, Y.**
"Numerical and experimental investigation on thermohydrodynamic performance of turbocharger rotor-bearing system"
in: *Applied Thermal Engineering* 121 (2017), pp. 27–38. ISSN: 1359-4311. DOI: 10.1016/J.APPLTHERMALENG.2017.04.041. URL: https://www.sciencedirect.com/science/article/pii/S1359431117323724 (cit. on pp. 27, 28)

[93] **Bukovnik, S, Offner, G, Diemath, A, and Smolik, L**
"Turbocharger Dynamic Analysis: Advanced Design Simulation in Time Domain Using CFD Predicted Thermal Boundary Conditions"
in: *Technische Mechanik* 37 (2017), pp. 2–5. DOI: 10.24352/UB.OVGU-2017-117. URL: http://www.uni-magdeburg.de/ifme/zeitschrift{_}tm/2017{_}Heft2{_}5/32{_}Bukovnik.pdf (cit. on p. 28)

[94] **Karpuschewski, B., Welzel, F., Risse, K., Schorgel, M., Kreter, S., and Putz, M.**
"Potentials for Improving Efficiency of Combustion Engines due to Cylinder Liner Surface Engineering"
in: *Procedia CIRP* 46 (2016), pp. 258–265. ISSN: 2212-8271. DOI: 10.1016/j.procir.2016.04.025. URL: www.sciencedirect.com (cit. on p. 29)

[95] **Wong, V. W. and Tung, S. C.**
"Overview of automotive engine friction and reduction trends–Effects of surface, material, and lubricant-additive technologies"
in: *Friction* 4.1 (2016), pp. 1–28. DOI: 10.1007/s40544-016-0107-9. URL: http://link.springer.com/10.1007/s40544-016-0107-9 (cit. on p. 29)

[96] **Ahmed Ali, M. and Xianjun, H.**
"Improving the tribological behavior of internal combustion engines via the addition of nanoparticles to engine oils"
in: 4 (2015), 347–358 (cit. on p. 29)

[97] **Milojevic, S., Pesic, R., and Taranovic, D.**
"Determination of Losses Related to Friction within the Reciprocating Compressors – Influences of Tribological Optimization of Piston and Cylinder"
in: *13th International Conference on Accomplishments in Mechanical and Industrial Engineering DEMI*. Banja Luka 2017, pp. 1–6 (cit. on p. 29)

[98] **Morris, N. J., Rahmani, R., and Rahnejat, H.**
"A hydrodynamic flow analysis for optimal positioning of surface textures"
in: *Proceedings of the Institution of Mechanical Engineers, Part J: Journal of Engineering Tribology* 231.9 (2017), pp. 1140–1150. DOI: 10.1177/1350650117709672. URL: http://journals.sagepub.com/doi/10.1177/1350650117709672 (cit. on p. 29)

[99] **Burkinshawa, M and Blackerb, D**
"The high temperature tribological performance of turbocharger wastegate materials"
in: *11th International Conference on Turbochargers and Turbocharging:*

13-14 May 2014: 13-14 May 2014. Vol. 1384. Elsevier 2014, p. 289 (cit. on p. 29)

[100] **Bobzin, K. and Brogelmann, T.**
"Minimizing Frictional Losses in Crankshaft Bearings of Automobile Powertrain by Diamond-like Carbon Coatings under Elasto-hydrodynamic Lubrication"
in: *Surface and Coatings Technology* 290 (2016), pp. 100–109. ISSN: 0257-8972. DOI: 10.1016/J.SURFCOAT.2015.08.064. URL: https://www.sciencedirect.com/science/article/pii/S0257897215302383 (cit. on p. 29)

[101] **Stachowiak, G. W. and Batchelor, A. W.**
Engineering tribology
3rd ed. Elsevier Butterworth-Heinemann 2006, p. 832. ISBN: 978-0-7506-7836-0. DOI: https://doi.org/10.1016/B978-0-7506-7836-0.X5000-7 (cit. on p. 29)

[102] **Taylor, C. M.**
Engine tribology
Elsevier 1993, p. 301. ISBN: 9780080875903 (cit. on pp. 30, 31)

[103] **Frene, J., Nicolas, D., Degueurce, B., Berthe, D., and Godet, M.**
Hydrodynamic lubrication : bearings and thrust bearings
Elsevier 1997, p. 470. ISBN: 9780080534312 (cit. on p. 30)

[104] **Roslan, A., Ibrahem, A. S., and Hadi, A.**
"Metal additives composition and its effect on lubricant characteristic"
in: *AIP Conference Proceedings*. Vol. 1774. 040001. American Institute of Physics 2016. DOI: 10.1063/1.4965083. URL: https://doi.org/10.1063/1.4965083https://doi.org/10.1063/1.4965083 (cit. on p. 30)

[105] **Maru, M. M. and Tanaka, D. K.**
"Consideration of Stribeck Diagram Parameters in the Investigation on Consideration of Stribeck Diagram Parameters in the Investigation on Wear and Friction Behavior in Lubricated Sliding"
in: *Journal of the Brazilian Society of Mechanical Science & Eng.* XXIX.1 (2007), p. 8. DOI: 10.1590/S1678-58782007000100009. URL: http://www.scielo.br/pdf/jbsmse/v29n1/a09v29n1 (cit. on p. 30)

[106] **Caines, A. J., Haycock, R. F., and Hillier, J. E.**
Automotive lubricants reference book
Second edition. Pennsylvania: Professional Engineering Pub 2004, p. 737. ISBN: 9781860584718 (cit. on p. 31)

[107] **Blau, P. J.**
"The significance and use of the friction coefficient"
in: *Tribology International* 34.9 (2001), pp. 585–591. DOI: 10.1016/S0301-679X(01)00050-0. URL: https://www.sciencedirect.com/science/article/pii/S0301679X01000500 (cit. on p. 31)

[108] **Ichiro, M.**
"Molecular Science of Lubricant Additives"
in: *Applied Sciences* 7.April (2017). DOI: 10.3390 (cit. on p. 31)

[109] **Laad, M. and Jatti, V. K. S.**
"Titanium oxide nanoparticles as additives in engine oil"
in: *Journal of King Saud University - Engineering Sciences* 30.2 (2018), pp. 116–122. DOI: 10.1016/J.JKSUES.2016.01.008. URL: https://www.sciencedirect.com/science/article/pii/S101836391600012X (cit. on p. 31)

[110] **Andersson, P., Tamminen, J., and Sandstrom, C.-E.**
Piston ring tribology A literature survey
ed. by Maini Manninen. Espoo, Finland 2002, p. 108. ISBN: 951–38–6107–4. URL: https://www.vtt.fi/inf/pdf/tiedotteet/2002/T2178.pdf (cit. on p. 31)

[111] **James, C. J.**
"Analysis of parasitic losses in heavy duty diesel engines"
PhD thesis. Massachusetts Institute of Technology 2012, p. 131. DOI: 1721.1/74921. URL: https://dspace.mit.edu/handle/1721.1/74921 (cit. on p. 31)

[112] **American Petroleum Institute**
Annex E—Api Base Oil Interchangeability Guidelines For Passenger Car Motor Oils And Diesel Engine Oils E.1 General
2015. URL: http://www.api.org/{~}/media/files/certification/engine-oil-diesel/publications/anne-rev-03-25-15.pdf?la=en (cit. on p. 32)

[113] **Noria Corporation**
Understanding the Differences in Base Oil Groups
tech. rep. Machinery Lubrication 2012. URL: https://www.machinerylubrication.com/Read/29113/base-oil-groups (visited on 07/02/2018) (cit. on p. 32)

[114] **Viswanath, D. S.**
Viscosity of liquids : theory, estimation, experiment, and data
Springer 2007, p. 660. ISBN: 1402054815 (cit. on p. 33)

[115] **Shayler, P. J., Allen, A. J., Leong, D. K. W., Pegg, I, Brown, A. J., and Dumenil, J.-C.**
"Characterising Lubricating Oil Viscosity to Describe Effects on Engine Friction"
in: *JSAE/SAE International Fuels & Lubricants Meeting*. United States: SAE international 2007. DOI: 10.4271/2007-01-1984. URL: http://papers.sae.org/2007-01-1984/ (cit. on p. 33)

[116] **ASTM International**
"Standard Test Method for Density, Relative Density, or API Gravity of Crude Petroleum and Liquid Petroleum Products by Hydrometer Method"
in: *ASTM* D1298.July (2017). DOI: 10.1520/D1298-12BR17. URL: https://compass.astm.org/download/D1298.11799.pdf (cit. on p. 33)

[117] **ASTM International**
"Standard Test Method for Pour Point of Petroleum Products"
in: *ASTM* D97.December (2017). DOI: 10.1520/D0097-17B. URL: https://compass.astm.org/download/D97.4665.pdf (cit. on p. 33)

[118] **ASTM International**
"Standard Test Method for Cloud Point of Petroleum Products and Liquid Fuels"
in: *ASTM* D2500.January 2018 (2017). DOI: 10.1520/D2500-17A. URL: https://compass.astm.org/download/D2500.35295.pdf (cit. on p. 33)

[119] **ASTM International**
"Standard Test Methods for Flash Point by Pensky-Martens Closed Cup Tester"
in: *ASTM* D93 (2016). DOI: 10.1520/D0093-16A. URL: https://compass.astm.org/download/D93.36165.pdf (cit. on p. 34)

[120] **ASTM International**
"Standard Test Method for Flash and Fire Points by Clevelenad Open Cup Tester"
in: *ASTM* D92 (2016). DOI: 10.1520/D0092-16B. URL: https://compass.astm.org/download/D92.4457.pdf (cit. on p. 34)

[121] **ASTM International**
"Standard Test Method for Acid Number of Petroleum Products by Potentiometric Titration"
in: *ASTM* D664.December (2017). DOI: 10.1520/D0664-17A. URL: https://compass.astm.org/download/D664.20424.pdf (cit. on p. 34)

[122] **ASTM International**
"Standard Test Method for Base Number of Petroleum Products by Potentiometric Perchloric Acid Titration 1"
in: *ASTM* D2896.December (2015). DOI: 10.1520/D2896-15. URL: https://compass.astm.org/download/D2896.31866.pdf
(cit. on p. 34)

[123] **SAE Standard**
Engine Oil Viscosity Classification (J300 Ground Vehicle Standard)
tech. rep. USA: SAE 2015. URL: https://saemobilus.sae.org/content/J300{_}201501/{\#}datasets (cit. on p. 34)

[124] **ACEA Oil Sequences**
Service Fill Engine Oils For Gasoline &Amp; Light Duty Diesel Engines (A/B Categories), Gasoline &Amp; Light Duty Diesel Engines With Exhaust Aftertreatment Devices (C Categories), And Heavy Duty Diesel Engines (E Categories)
tech. rep. ACEA 2016, p. 14. URL: https://www.acea.be/uploads/news{_}documents/ACEA{_}European{_}oil{_}sequences{_}2016{_}update.pdf (cit. on p. 35)

[125] **Sharma, P. and Jayaswal, P.**
"Wear Rate Measurement (Ic Engine) Using Lubricant Oil Testing Method"
in: *IJREAS International Journal of Research in Engineering & Applied Sciences* 2.22 (2012). ISSN: 2249-3905. URL: http://www.euroasiapub.org (cit. on p. 35)

[126] **Jun, H. B., Kiritsis, D., Gambera, M., and Xirouchakis, P.**
"Predictive algorithm to determine the suitable time to change automotive engine oil"
in: *Computers and Industrial Engineering* 51.4 (2006), pp. 671–683. ISSN: 03608352. DOI: 10.1016/j.cie.2006.06.017 (cit. on p. 36)

[127] **Jun, H.-B., Conte, F. L., Kiritsis, D., and Xirouchakis, P.**
"A Predictive Algorithm for Estimating the Quality of Vehicle Engine Oil"
in: *International Journal of Industrial Engineering* 15.4 (2008), pp. 386–396 (cit. on p. 36)

[128] **Deng, D, Shi, F., Begin, L., Du, I, and General Motors**
"The Effect of Oil Debris in Turbocharger Journal Bearings on SubSynchronous NVH"
in: *SAE International* 2015-01-12.April (2015). DOI: 10.4271/2015-01-1285 (cit. on pp. 36, 38, 165, 176)

[129] **Siddaiah, A., Khan, Z., Ramachandran, R., and Menezes, P.**
"Performance Analysis of Retrofitted Tribo-Corrosion Test Rig for Monitoring In Situ Oil Conditions"
in: *Materials* 10.10 (2017), p. 1145. DOI: 10.3390/ma10101145. URL: http://www.mdpi.com/1996-1944/10/10/1145 (cit. on p. 36)

[130] **Black, J, Eastwood, P. G., Tufail, K, Winstanley, T, Hardalupas, Y, and Taylor, A. M. K. P.**
"The Effect of VGT Vane Control on Pumping Losses during Full-Load Transient Operation of a Common-Rail Diesel Engine"
in: *SAE Naples Section* 2007-24-0063 (2007). DOI: 10.4271/2007-24-0063 (cit. on p. 36)

[131] **Ghazikhani, M., Davarpanah, M., and Shaegh, S. A. M.**
"An experimental study on the effects of different opening ranges of waste-gate on the exhaust soot emission of a turbo-charged DI diesel engine"
in: *Energy Conversion and Management* 49.10 (2008), pp. 2563–2569. ISSN: 01968904. DOI: 10.1016/j.enconman.2008.05.012 (cit. on p. 36)

[132] **Serrano, J. R., Olmeda, P., Tiseira, A., Garcia-Cuevas, L. M., and Lefebvre, A.**
"Theoretical and experimental study of mechanical losses inautomotive turbochargers"
in: *Energy* 55 (2013), pp. 888–898. ISSN: 03605442. DOI: 10.1016/j.energy.2013.04.042. URL: http://dx.doi.org/10.1016/j.energy.2013.04.042 (cit. on pp. 37, 38, 155)

[133] **Owrang, F., Mattsson, H., Olsson, J., and Pedersen, J.**
"Investigation of oxidation of a mineral and a synthetic engine oil"
in: *Thermochimica Acta* 413.1-2 (2004), pp. 241–248. ISSN: 00406031. DOI: 10.1016/j.tca.2003.09.016 (cit. on p. 37)

[134] **Yang, K., Fletcher, K. A., Styer, J. P., Lam, W. Y., and Guinther, G. H.**
"Engine Oil Components Effects on Turbocharger Protection and the Relevance of the TEOST 33C Test for Gasoline Turbocharger Deposit Protection"
in: *SAE International Journal of Fuels and Lubricants* 10.3 (2017), pp. 2017–01–2341. DOI: 10.4271/2017-01-2341. URL: http://papers.sae.org/2017-01-2341/ (cit. on p. 37)

[135] **Moreira, M. F.**
"Failure analysis in aluminium turbocharger wheels"
in: *Engineering Failure Analysis* 61 (2016), pp. 108–118. ISSN: 13506307.

DOI: 10.1016/j.engfailanal.2015.11.024. URL: http://dx.doi.org/10.1016/j.engfailanal.2015.11.024 (cit. on p. 38)

[136] **Engine Power Test Code Committee**
Turbocharger gas stand test code (J1826 Ground Vehicle Standard)
tech. rep. The Engineering Society for Advancing Mobility Land Sea Air and Space 1995. URL: https://saemobilus.sae.org/content/j1826{_}199503 (cit. on p. 63)

[137] **Engine Power Test Code Committee**
Supercharger testing standard. J1723 Ground Vehicle Standard
tech. rep. The Engineering Society for Advancing Mobility Land Sea Air and Space 1995, p. 9. URL: https://saemobilus.sae.org/content/j1723{_}199508 (cit. on p. 63)

[138] **Ribeiro, E. G., Melo, W. B., and Filho, A. P. a.**
"Application of electric oil pumps on automotive systems"
in: *SAE International Journal Engines* 01.4086 (2005), pp. 1–7. DOI: 10.4271/2005-01-4086. URL: http://www.sae.org/technical/papers/2005-01-4086 (cit. on pp. 68–70, 120, 176)

[139] **NHTSA**
"Flammability Properties of Engine Compartment Fluids Other than Gasoline"
in: *National Highway Traffic Safety Administration* (1988). DOI: 98-358 8-193 (cit. on p. 69)

[140] **OSHA Hazard Communication Standard**
Formula Shell Motor Oil SAE 5W-30 Material Safety Data Sheet
tech. rep. 29 CFR 2008. DOI: MSDS71135L. URL: http://ebpaving.com/wp-content/uploads/2013/09/FormulaShell-Motor-Oil-SAE-5W-30.pdf (cit. on p. 69)

[141] **Pastor, J. V., Serrano, J. R., Dolz, V., Lopez, M. A., and Bouffaud, F.**
"Study of turbocharger shaft motion by means of non-invasive optical techniques: Application to the behaviour analysis in turbocharger lubrication failures"
in: *Mechanical Systems and Signal Processing* 32 (2012), pp. 292–305. ISSN: 08883270. DOI: 10.1016/j.ymssp.2012.04.020 (cit. on p. 81)

[142] **Hidalgo Lopez, M. A.**
"Estudio teorico-experimental de la dinamica rotacional de turbocompresores de MCIA. Aplicacion al diagnostico de fallos."
Doctoral Thesis. Politecnic of Valencia 2014, p. 287 (cit. on p. 81)

[143] **Sachdev, A. K., Kulkarni, K., Fang, Z. Z., Yang, R., and Girshov, V.**
"Titanium for automotive applications: Challenges and opportunities in materials and processing"
in: *Jom* 64.5 (2012), pp. 553–565. ISSN: 10474838. DOI: 10.1007/s11837-012-0310-8 (cit. on pp. 112, 165)

[144] **Willermark, D. and Smith, N.**
"Gt-Power Real-Time – Diesel engine model for Hardware in the Loop testing"
in: *GT-SUITE Conference*. Vol. 2009 (cit. on p. 112)

[145] **Vimal, M., Abhay, P., and Sriprakash, D.**
"Study and application of predictive combustion model for parameter optimization in diesel engine"
in: *Hinduja Tech Limited GT-SUITE India Conference* 2018 (cit. on p. 112)

[146] **Kang, J., Lee, B., and Jung, D.**
"Evaluating the Effect of Two-Stage Turbocharger Configurations on the Perceived Vehicle Acceleration Using Numerical Simulation"
in: 2016. DOI: 10.4271/2016-01-1029. URL: http://papers.sae.org/2016-01-1029/ (cit. on p. 112)

[147] **Bergman, T. L., Lavine, A. S., Incropera, F. P., and Dewitt, D. P.**
Fundamentals of Heat and Mass Transfer
vol. 7th Editio. 1 2011, ISBN 13 978–0470–50197–9. ISBN: 9780471457282. DOI: 10.1016/j.applthermaleng.2011.03.022. arXiv: 1105-. URL: http://www.osti.gov/energycitations/product.biblio.jsp?osti{_}id=6008324 (cit. on pp. 113, 152)

[148] **Serrano, J., Olmeda, P., Arnau, F., and Dombrovsky, A.**
"General Procedure for the Determination of Heat Transfer Properties in Small Automotive Turbochargers"
in: *SAE International Journal of Engines* Friday, October 03, 2014 (2014), p. 12. DOI: 10.4271/2014-01-2857 (cit. on pp. 119, 120, 151)

[149] **Serrano, J., Olmeda, P., Arnau, F. J., Reyes-Belmonte, M. a., and Tartoussi, H.**
"A study on the internal convection in small turbochargers. Proposal of heat transfer convective coefficients"
in: *Applied Thermal Engineering* 89 (2015), pp. 587–599. ISSN: 13594311. DOI: 10.1016/j.applthermaleng.2015.06.053 (cit. on pp. 119, 120, 153)

[150] **Reyes Belmonte, M. A.**
"Contribution to the Experimental Characterization and 1-D Modelling of Turbochargers for IC Engines"
PhD thesis. University Polytechnic of Valencia 2013
(cit. on pp. 120, 152, 169)

[151] **García-Cuevas, L. M.**
"Experiments and Modelling of Automotive Turbochargers under Unsteady Conditions"
PhD thesis. Polytechnic University of Valencia 2015 (cit. on p. 128)

[152] **Serrano, J., Olmeda, P., Arnau, F. J., Dombrovsky, A., and Smith, L.**
"Turbocharger heat transfer and mechanical losses influence in predicting engines performance by using one-dimensional simulation codes"
in: *Energy* 86 (2015), pp. 204–218. ISSN: 03605442. DOI: 10.1016/j.energy.2015.03.130 (cit. on p. 145)

[153] **Serrano, J. R., Olmeda, P., Tiseira, A., García-Cuevas, L. M., and Lefebvre, A.**
"Importance of Mechanical Losses Modeling in the Performance Prediction of Radial Turbochargers under Pulsating Flow Conditions"
in: *SAE paper 2013-01-0577* (2013). ISSN: 19463936. DOI: 10.4271/2013-01-0577. URL: http://www.sae.org/technical/papers/2013-01-0577 (cit. on p. 147)

[154] **Boetcher, S. K. S.**
Natural Convection from Circular Cylinders
ed. by Francis A. Kulacki. 2014. Daytona: Springer 2014, p. 48. ISBN: 2193-2530. DOI: 10.1007/978-3-319-08132-8. URL: https://link.springer.com/content/pdf/10.1007/978-3-319-08132-8.pdf
(cit. on p. 155)

[155] **Subramanian, R. S.**
"Heat transfer to or from a fluid flowing through a tube"
in: (). URL: http://web2.clarkson.edu/projects/subramanian/ch330/notes/HeatTransferinFlowThroughConduits.pdf
(cit. on p. 161)

[156] **Bergman, T. L., Bergman, T. L., Lavine, A., Incropera, F. P., and DeWitt, D. P.**
Introduction to heat transfer
ed. by Linda, R. 6th Edition. United Sates of America: John Wiley & Sons Inc. 2011, p. 960. ISBN: 9780470501962 (cit. on p. 163)

[157] **S. M Shelton**
"Thermal conductivity of irons and steels over the temperature tange 100 to 500c"
in: *Part of Bureau of standards journal of research* 12.5 (1934), pp. 619–620. ISSN: 00160032. DOI: 10.1016/S0016-0032(34)90359-8 (cit. on p. 164)

[158] **BCIRA**
"Specific heat capacity of cast irons"
in: *British Cast Iron Research Association Broadsheet 203-7* (1985) (cit. on p. 164)

[159] **Faoite, D. de, Browne, D. J., Chang-Diaz, F. R., and Stanton, K. T.**
"A review of the processing, composition, and temperature-dependent mechanical and thermal properties of dielectric technical ceramics"
in: *Journal of Materials Science* 47.10 (2012), pp. 4211–4235. ISSN: 0022-2461. DOI: 10.1007/s10853-011-6140-1. URL: http://link.springer.com/10.1007/s10853-011-6140-1 (cit. on p. 164)

[160] **Tetsui, T.**
"Development of a TiAl turbocharger for passenger vehicles"
in: *Materials Science and Engineering A329–* 331.2016 (2002), pp. 582–588. URL: www.elsevier.com/locate/msea (cit. on p. 165)

[161] **Wu, X.**
"Review of alloy and process development of TiAl alloys"
in: *Intermetallics* 14.10-11 (2006), pp. 1114–1122. ISSN: 0966-9795. DOI: 10.1016/J.INTERMET.2005.10.019. URL: https://www.sciencedirect.com/science/article/pii/S0966979506000823 (cit. on p. 165)

[162] **Appel, F., Paul, J. D., and Oehring, M.**
Gamma titanium aluminide alloys: science and technology
John Wiley & Sons 2011, p. 745. ISBN: 3527636218 (cit. on p. 165)

[163] **Poloni, C.**
"Hybrid GA for multi objective aerodynamic shape optimization"
in: *Genetic algorithms in engineering and computer science 33* (1998), pp. 397–415 (cit. on p. 166)

[164] **Dombrovsky, A.**
"Synthesis of the 1D modelling of turbochargers and its effects on engine performance prediction"
PhD thesis. University Polytechnic of Valencia 2016, pp. 1–238. DOI: 10.4995/Thesis/10251/82307 (cit. on p. 197)